# The dynamics of category-specific perception in ventral temporal cortex

Kai Joshua Miller

A dissertation
submitted in partial fulfillment of the
requirements for the degree of

Doctor of Philosophy

University of Washington
2014

Reading Committee:

Rajesh P.N. Rao, Chair
Jeffrey G. Ojemann
Elizabeth A. Buffalo

Program Authorized to Offer Degree:

Neurobiology & Behavior

University of Washington

## Abstract

The dynamics of category-specific perception in ventral temporal cortex

Kai Joshua Miller

Chair of the Supervisory Committee:

Rajesh P.N. Rao

Computer Science and Engineering

My thesis investigates the relationship between the ventral temporal cortex and perception of different categories of visual stimuli, in humans. Under the guidance of my scientific and clinical mentors, we performed a set of visual perception experiments with human patients who had been implanted with arrays of subdural electrocorticography (ECoG) electrodes on the ventral temporal brain surface. In order to understand these experiments and what they teach us about brain function, my evolving thought process throughout graduate school was guided by a series of central questions:

**What are the relevant portions of the ECoG signal needed to understand ventral temporal physiology?** The text begins with a general discussion of category-selective regions in the ventral temporal brain and introduces some of the principles of ECoG measurement. The ECoG signal reflects multiple aspects of population-scale neurophysiology, and these are carefully explored and illustrated specifically in the ventral visual stream.

"Broadband" changes in the ECoG voltage power spectrum are decoupled from intermingled oscillatory motifs, and shown to be a generic correlate of local cortical function across a variety of brain areas and behavioral tasks. Continuous approximations of this broadband track behavior at approximately the 20-50ms timescale, making it the optimal setting to explore visual processing, perception, and decision making on the same timescales that these phenomena occur.

Likewise, the rhythmic gamma oscillation has been proposed to be a key marker of visual perception and attention. We find that robust gamma oscillations can indeed be generated with specific visual stimuli, such as luminance gratings, but are not a prerequisite for perception, as they are not seen with noise patterns, nor with most easily identifiable natural images. However, many brain rhythms are more than just passive phenomena in visual cortex. By examining how broadband spectral change is entrained on the phase low frequency oscillations (δ, θ, α, β, and γ), we were able to show that brain rhythms selectively couple to the average population activity in a task-dependent manner. This entrainment mechanism dynamically engages and releases cortical areas on a second-to-second basis during visual processing. Because this rhythmic influence in the α and β ranges is selectively decreased in early visual areas during visual task engagement, we propose a "suppression by synchronization" hypothesis, where widespread populations of cortical neurons are synchronized and phase-coupled to the rhythm to impose a cortically suppressed (disengaged) state.

*These rhythmic changes, like the stimulus-triggered averaged potentials (ERPs), are idiosyncratic to specific cortical loci, and not generic across brain regions. Broadband spectral changes, in contrast, are a generic correlate of local activity in each cortical region.*

**How robust are the neuronal population responses that we measure?** In order to quantify how reliable the ECoG response is to individual types of stimuli in ventral temporal cortex, we showed subjects simple grayscale pictures of faces and houses. Robust category-specific responses to each type of stimulus were found, where face-picture selective sites were consistently found on the fusiform gyrus and house-selective sites were found on the lingual and parahippocampal gyri. A novel method was

developed, where averaged ECoG response templates (both broadband and ERP) from a training period were projected into a testing period. Our initial decoding allowed for pre-designated stimulus timing, and 97% of stimuli could be accurately classified as face or house. Real world experience, however, is spontaneous, and to this end, we attempted to simultaneously predict the occurrence, timing, and type of visual stimuli from the spontaneous ECoG stream. In this setting, 96% of all stimuli were captured spontaneously, with ~20ms timing error (only 4% of the spontaneous predictions were incorrect; 4% of the stimuli were missed).

*This examination of the spatiotemporal distributions of category-selective cortical sites reveals that activity highly delineated and can be classified robustly, and activity temporally is sufficient to construct a simple visual stream from the ECoG array, at the timescales of perception.*

**Do these ventral temporal neuronal populations reflect perceptual context?** Even in a series of randomly interleaved grayscale faces and houses, there is perceptual context. A face following a prior face is viewed in a different context than a face that follows a house, and we isolated face- and house-selective ventral temporal loci to see if this sequence-context might be reflected in the single-trial broadband responses. Approximately half of the category-selective sites showed greater total broadband activity for novel than for repeated stimulus class. In approximately half of the face-selective sites (and none of the house-selective sites), latency to peak activity was faster for novel than repeat stimuli (with no correlation between the total activity and latency effects). These observations suggest that aspects of ventral temporal cortical physiology are especially tuned to sequential context, with an emphasis on novelty during perception.

*The unexpected finding that novel stimuli are processed faster suggests that ventral temporal cortex is optimized for perceiving changing context.*

**Is ventral temporal cortex is an active locus of visual object perception?** A face and house picture decision task was performed, where visual evidence was parametrically degraded, and responses were

measured from category-selective loci. Robust neurometric functions revealed decreasing neuronal population activity as image noise increased, with shape preserved whether subjects correctly reported the stimulus or not. A basic face-house template-projection classifier was built on a simple, choice-free, localizer experiment, and then applied to the decision task where visual evidence was parametrically degraded. At low levels of stimulus noise, predicted stimulus type was correlated more closely with the stimulus than subjects' perception. The converse was true at high noise level, where predicted stimulus type was more correlated with the subjects' choice than stimulus type.

*With decreasing stimulus (increasing noise) the influence of higher order cognition is revealed. Ventral temporal cortex must therefore be an active locus of perception, where bottom-up and top-down information converge.*

# Dedicated to Dora and Max

She said: I'll never let you out of my sight again. I'm going to keep on watching you and never stop.'

And after a pause: 'I get scared when my eye blinks. Scared that during that second when my gaze goes out, a snake or a rat or another man could slip into your place.'

He tried to raise himself a little to touch her with his lips.

She shook her head: 'No, I just want to watch you'.

And then: 'I'm going to leave the lamp on all night. Every night'.

# The dynamics of category-specific perception in ventral temporal cortex

## Table of contents

# Chapter 1: Introduction

Evolution has shaped the functional architecture of the human cortex with a mixture of organizational strategies. In one respect, functional specialization has been attained through distributed networks which span across lobes and hemispheres, and there is currently a paradigm shift within systems neuroscience to emphasize this. In another respect, functional specialization has been attained by regional specialization, where specific loci in the brain correspond with specific aspects of human perception and behavior (Figure 1). This thesis focuses on regional specialization in the brain, focusing on the ventral temporal cortex during category specific perception.

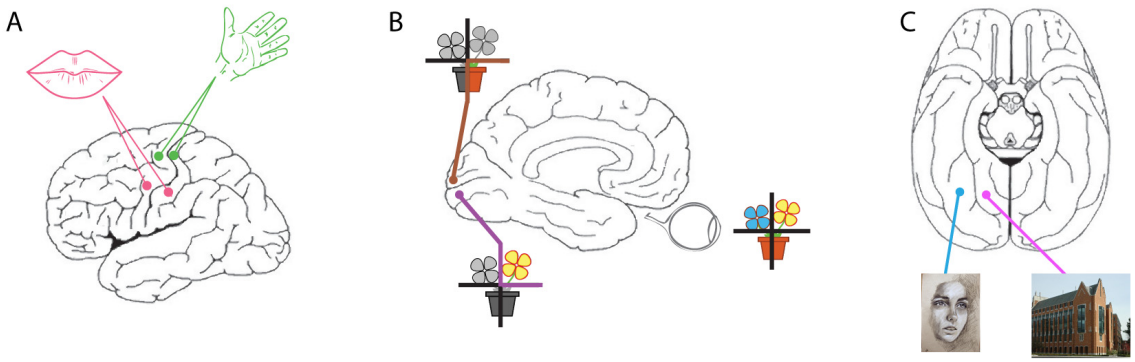


**Figure 1: Regional specialization in the brain** (A) In pre- and post-central cortex there is "motortopy" and "somatotopy": a part of the brain represents a part of the body. (B) In pericalcarine cortex there is "retinotopy": a part of the brain represents a part of the visual field. (C) In the ventral temporal cortex, different adjacent regions represent different categories of objects represented in the world. There is no simple correlation with a physical property of the world. This thesis asks the question: "Do these areas represent 'high-level' semantic perception, or rather do they represent 'low-level' accumulating evidence for an object belonging to a particular class of stimulus?".

Anatomically distinct loci within pre- and post-central cortex represent sensory inputs and motor outputs from distinct parts of the body. Similarly, distinct regions in auditory cortex represent distinct tones and distinct regions in early visual cortex represent distinct sub-areas of the visual field. The inferior temporal cortex, however, is different: distinct regions appear to represent different categories of objects encountered in the outside world. The relationship is not a physical correspondence, but rather a conceptual correspondence. It implies a complex process of putting together simple visual features into a larger construct that can be related to a general concept encountered in the external environment: perception. Throughout my time as a graduate student, I studied how ventral temporal cortex encodes low-level, “bottom-up,” representation of visual stimuli, as well as high-level, “top-down,” assignment of this representation to a general concept encountered in the outside world.

The neurosurgeon Wilder Penfield was able to produce hallucinations of faces, the interior of rooms, and topographical scenes, by stimulation of the fusiform and parahippocampal gyri (Penfield and Perot, 1963). Since then, category specific areas in the human temporal lobe have been established unambiguously at the several millimeter to centimeter scale, using functional

imaging (Joseph, 2001), and field potentials (Allison et al., 1999). They have also been demonstrated at the single unit level in epileptic human patients (Kreiman et al., 2000) and non-human primates (Kiani et al., 2007). This thesis describes a series of electrocorticographic studies focused on the dynamics of category-specific perception in ventral temporal cortex (the anatomy of which is delineated in figure 2).

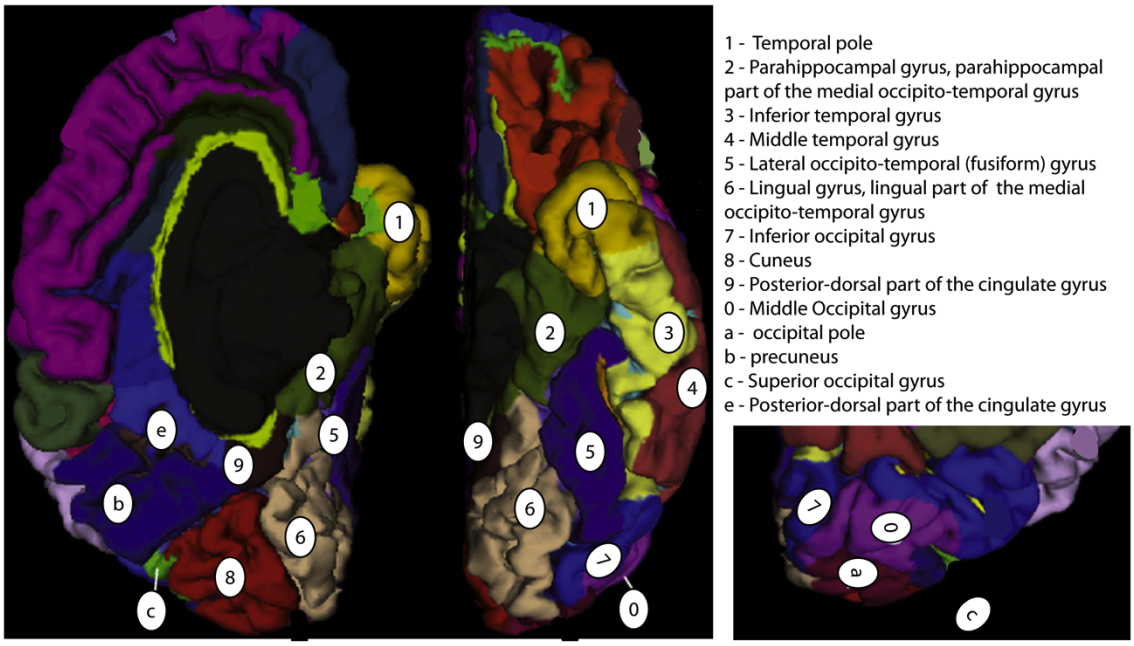


**Figure 2: The inferior temporal (and some occipital) anatomy examined in this thesis.** Electrodes were considered ventral temporal if they were localized to one of the following gyri: Temporal pole, Parahippocampal portion of the medial occipito-temporal gyrus, Inferior temporal gyrus, Middle temporal gyrus, Fusiform gyrus (Lateral occipito-temporal gyrus), Lingual portion of the medial occipito-temporal gyrus, Inferior occipital gyrus. Figure modified from (Destrieux et al., 2010).

## Known properties of category specific regions in inferotemporal cortex

### Lesion studies

Lesions of fusiform area may induce the inability to recognize faces, a condition known as "prosopagnosia" (Meadows, 1974, Damasio et al., 1982). These face recognition deficits are particularly associated with right sided lesions (Landis et al., 1986, Sergent and Villemure, 1989).

More recent studies have shown that lesions of the right fusiform area can impair the basic perception of facial configuration, not just with the association of a basic configuration of shapes with the concept of a face (Barton et al., 2002).

For example, there is the case of a boy who sustained brain damage at 1 day of age, resulting in bilateral congenital lesions of the fusiform gyri. Throughout development, he continued to have the classic lesions and behavioral profile of adult-acquired prosopagnosia (Farah et al., 2000). He had a category-selective deficit, with severely impaired face recognition, with relative sparing of object recognition. This implies that experience with these categories is not necessary for their functional delineation and differential brain localization, and therefore they must be genetically determined – "hard wired" during neurodevelopment. While the anatomic connection between the fusiform gyrus and general face-recognition is hard-wired, the ability to segregate similar faces of different individuals (based upon more subtle cues) is a specialized skill that is related to experience. Infants lose the ability to discriminate between faces of non-human primates at 6-9 months of age, unless they are specifically trained to retain this capability (Pascalis et al., 2005).

## Studies of evoked potentials (ERPs)

Intracranial recordings have shown that the "N200" face response, a characteristic deflection in the raw potential obtained after averaging (also known as an event-related potential – "ERP"), is seen in sub-temporal areas specifically following presentations of faces, but not other stimuli (Allison et al., 1994a, Allison et al., 1994b). The same group demonstrated that this robust phenomenon was found to have some, but not strict, overlap with face-specific fMRI identified areas (Puce et al., 1997). In a 98 subject, 3 manuscript, study of epileptic patients (with the same type of implanted strips that we examine), Allison, Puce, Belger, and McCarthy characterized many of the subtleties of the N200 (Allison et al., 1999, McCarthy et al., 1999, Puce et al., 1999). They found that it was multiphasic, that it didn't vary by gender, whether the stimulus was in color or black-and-white, or

whether or not it was in the same hemisphere as the epileptic focus. They also found characteristic ERPs in response to non-face stimuli, and, based upon the fact that these were at distinct electrode sites from the face specific N200, they postulated that the "ventral object recognition system was divided into functionally distinct areas". Using blurred and line-drawn faces, they found that the latency of the N200 was increased with increased blurring or addition of an edge filter (to create line-drawn faces), but that the amplitude was not significantly changed across the population. fusiform N200 sites showed the characteristic ERP with presentations of size-scaled, scrambled, inverted, and upside-down faces, as well as fragments of faces, but the amplitude of the ERP was diminished, and the latency of the ERP was extended, to varying degree (as also demonstrated in figure 8). Direction of gaze in the face did not affect the magnitude of the ERP, but rotation of the head did diminish the magnitude and extend the latency of the ERP, with degree dependent upon the amount of rotation.

Recordings of scalp potentials (electroencephalogram, EEG) have shown a robust, strong N170 response (scalp equivalent of N200) for faces. This response behaves qualitatively different for regular or inverted faces (Itier and Taylor, 2004). The face specificity of the N170 was a subject of some contention, since it was claimed (Thierry et al., 2007) – and subsequently refuted (Bentin et al., 2007) – that the N170 was simply an artifact of uncontrolled interstimulus perceptual (physical) variance. That is, that face stimuli are all more like each other than separate stimuli from different classes, and thus induce a more reliable N170 from the scalp. More recent EEG studies by the Sajda group have quantitatively calculated a single trial (not ERP averaging), and they found, interestingly, that the N170 was not the most relevant part of the signal, but rather a later component, ~130ms later, was more important for accurate classification of face cues (Philiastides et al., 2006, Philiastides and Sajda, 2006). In general, ERP averaging approaches to cortical, face-specific, field potentials suffer because they are parameterized by a large set of variables (P150, N200, P350, N700; each with variable amplitude, latency, etc) and the connection to direct

population level activity is difficult to establish (which we address directly in chapter 5). In fact, some have hypothesized that a change in overall neural activity isn't even required, just a change in synchrony of underlying sources (Makeig et al., 2002).

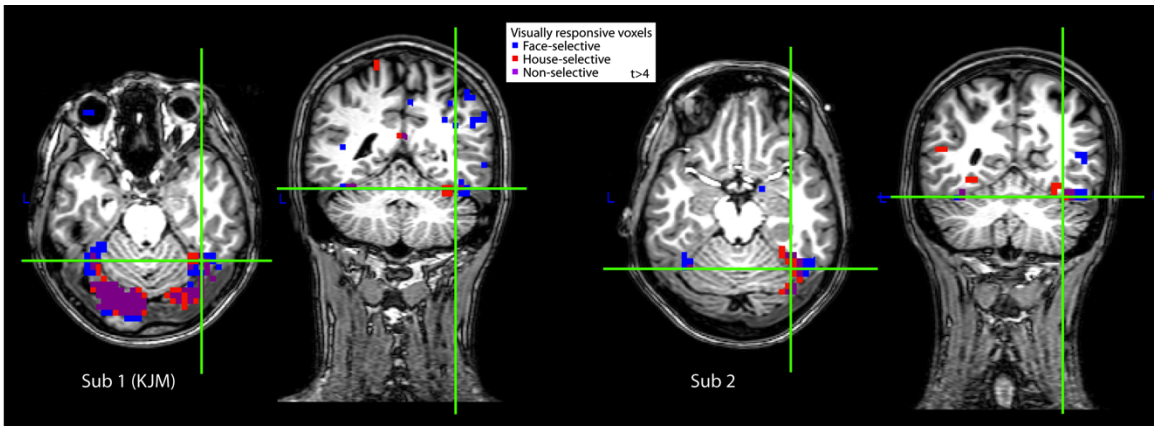


**Figure 3: fMRI distribution of activity in a simple block design task in 2 subjects.** Face-selective responses are reliably localized to the bilaterally fusiform gyri on the inferotemporal surface of single subjects (subject 1 is the author). House-selective responses are reliably found medial to face-selective sites on the lingual and parahippocampal portions of the medial occipitotemporal gyrus. (Experiment performed while at the Ramsey Lab in Utrecht, Netherlands).

## Functional imaging studies

As illustrated in figure 3, ventral temporal BOLD signal changes are robust and anatomically distinct for different classes of stimuli. Beginning in the late 1990s, the functional organization of ventral temporal cortex in humans has been characterized primarily using functional imaging (Kanwisher et al., 1997, Aguirre et al., 1998, Epstein and Kanwisher, 1998). One such study demonstrated differential organization of 3 classes of stimuli, houses – faces – chairs, located, in order, medially to laterally on subtemporal cortical surface (Ishai et al., 1999). In a follow-up study, they found that both faces and non-faces involved distributed networks, but that faces were more confined to a local cortical area (Ishai et al., 2000).

It is a topic of active discussion whether the fusiform gyrus was specific for faces, or is rather related to discrimination within tasks of expertise (Gauthier et al., 1997, Tarr and Gauthier,

2000, Gauthier et al., 2005, McGugin et al., 2012). However, Grill-Spector et al, found that the fusiform gyrus did not show differential activation during discrimination tasks of non-face objects in experts (Grill-Spector et al., 2004). For example, car experts did not show increased activity in FFA while discriminating between cars, but other extra-striate areas did. Also, while having individuals distinguish between objects within the same category, fusiform cortex did not show differential activity (unless the category was faces). A similar face-specific, rather than expertise-specific, role for the characteristic ERP (in MEG – "M170") was demonstrated by comparing car experts to non-expert controls (Xu et al., 2005).

### Interfering with perception

Electrical stimulation of inferotemporal cortex can influence perception and bias face recognition in humans non-humans primates. In monkeys performing a 'face'/'non-face' categorization task, stimulation of face-selective neurons in the temporal cortex biased the monkeys' decisions in favor of the face category (Afraz et al., 2006). In humans performing a face detection task with different levels of noise, stimulation of face-seletive electrodes could interfere with the perception of faces (Chong et al., 2013).

### Neurophysiologic context

Category-specific processing has been demonstrated at the single unit level in epileptic human patients (Kreiman et al., 2000) and non-human primates (Kiani et al., 2007). At a larger scale, previous MEG and EEG studies have characterized specific components of the event-triggered that relate to the recognition of objects. An MEG study showed that category differences between faces and houses could be distinguished already around 100 ms (at the M100 component), while face identification could only be distinguished around 170 ms (in the later M170) (Liu et al., 2002). EEG studies showed faces and cars with different levels of noise and investigated the relation between different components in the event related potentials (ERPs) and detection performance. They found two ERP components that correlated with detection performance, one at 170 ms (N170) and a later

one at 300 ms (Philiastides et al., 2006, Philiastides and Sajda, 2006). The timing of the early component did not change much, and was not related to the amount of noise in the stimulus. The later component did show shifts in time that matched with the detection performance. They argued that the earlier component may reflect lower level features and that the later component is more related to the recognition event and the decision.

## Semantically "non-specific" areas[1]

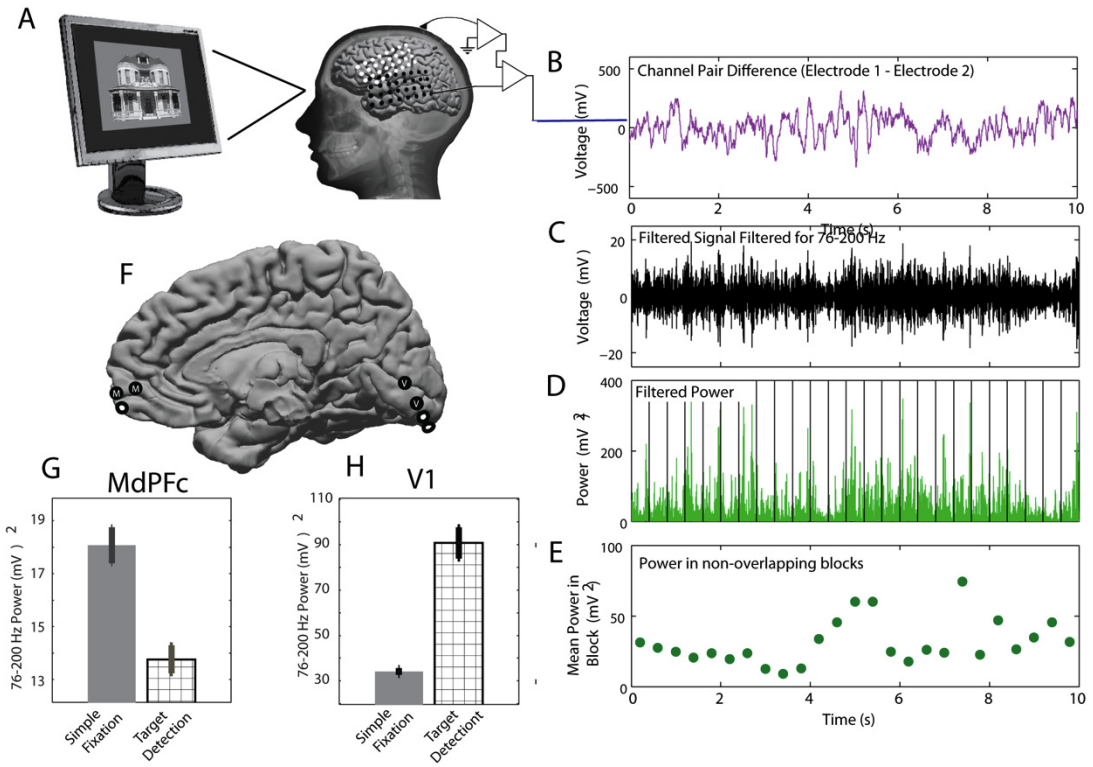


**Figure 4: Default regions are inactivated with engagement of early visual cortex in a face-house viewing task. (A)** Subdural electrode arrays were placed on the cortical surface, and the patient performed a simple target detection task, with pictures of houses and faces, with 3 vocally reported targets (of 300 total pictures). A 3-minute fixation task served as the 'resting state'. **(B-E)** *Signal Processing* - Nearest neighbor electrode potential pair difference channels were used to isolate the most local cortical activity A band-pass filter for 76-200Hz (χ-band(Miller et al., 2007a)) was applied, and the signal was then element-wise squared and summed to obtain the power in non-overlapping 400ms blocks. The distribution resting (fixation) and visually engaged blocks were compared using an unpaired t-test, and the resulting p-value from each electrode pair was Bonferroni corrected for the total number of medial pairs. **(F-H)** This χ-band signal was compared between resting fixation (solid grey bars) and the visual task (hatched). Corresponding locations of electrode pairs are shown in schematic, with coverage of medial prefrontal cortex ("M") and early visual cortex ("V"). Error bars indicate the standard error, both differences significant ($p<0.001$). Figure from (Miller et al., 2009c)**.**

[1] Excerpted from: Miller KJ, Weaver KE, Ojemann JG (Direct electrophysiological measurement of human default network areas. Proceedings of the National Academy of Sciences 106:12174.2009c).

Unlike regions of cortical specialization (figure 1), there are brain areas that appear to be specifically non-specialized, and active only when someone is not actively engaged with their environment, "default regions" are disengaged. We explicitly identified and measured these regions during ECoG measurement. As shown in figure 4, electrode pairs in early visual cortex illustrate significant increase in activity associated with visual task engagement. A medial prefrontal electrode pair, however, shows the exact opposite: neural activity is diminished from resting state. This finding was the first direct cortical measurement of changes in the amplitude of population-scale neurophysiology associated with human default network regions, and reveal that high levels of electrical brain activity persist specifically in the absence of outside stimulation. This conjugate on/off pattern of ECoG activation, which was consistent during visual perception, speech production, and motor behavior, parallels a vast literature of fMRI inquiry linking default network activity to cognition and behavior (Niessing et al., 2005, Weissman et al., 2006, Buckner et al., 2008, Clare Kelly et al., 2008, Luhmann et al., 2008). These results reveal a neural signature of stimulus independent activity, refuting alternative hypotheses which attribute resting state BOLD changes in default regions to non-neuronal artifact (Kannurpatti and Biswal, 2004, Wise et al., 2004). The hypothesis put forth by many functional imaging studies that neural activity in MdPFc is specifically increased during rest was concretely validated by this measurement.

## Electrocorticography in inferior (ventral) temporal cortex

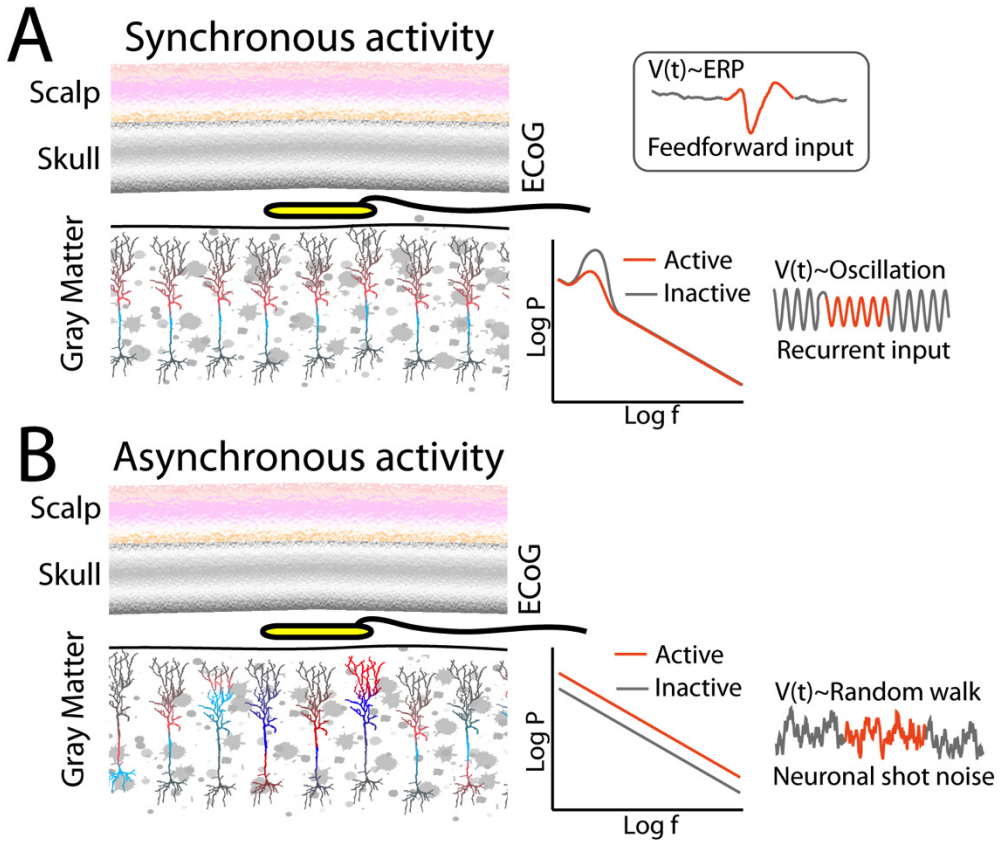


**Figure 5: How synaptic input to a neuronal population might be reflected in the ECoG potential timeseries (V(t)).** (A) Synchronized activity, feedforward input revealed by a transient, multiphasic, event-related potential (ERP) changes, or recurrent feedback oscillatory inputs revealed by changes in peaked aspects of the power (P) vs. frequency (f) spectrum. (B) Asynchronous, local activity, revealed by broadband spectral changes.

### Different types of physiology of the ECoG measurement[2]

For many years, the electroencephalogram (EEG) has been thought to reflect synchronized neuronal populations. Because of the large perpendicular distance of the EEG electrode from the cortical surface (~2cm for the scalp and skull), the EEG necessarily averages across large areas of the

[2] Originally written by KJM for: Ritaccio A, Brunner P, Crone NE, Gunduz A, Hirsch LJ, Kanwisher N, Litt B, Miller K, Moran D, Parvizi J, Ramsey N, Richner TJ, Tandon N, Williams J, Schalk G (Proceedings of the Fourth International Workshop on Advances in Electrocorticography. Epilepsy Behav 29:259-268.2013).

cortical surface. Therefore, aspects of neuronal populations that are not synchronized are largely lost to spatial averaging in the EEG measurement. Macroscale potentials from electrodes which lie directly on the cortical surface, electrocorticography (ECoG), measures neuronal population activity on a much more local scale than those from the scalp, at same spatial scale as the exposed electrode surface.

Based upon the work of Nunez and predecessors, it is understood that current dipoles between cortical lamina produce macroscale field potentials (Nunez and Cutillo, 1995). Properties of the physiology underlying the current source density (CSD) in different cortical lamina were established experimentally in the late 1970s and early 1980s (Mitzdorf, 1985). Propagating action potentials in axons and axon terminals do not contribute strongly to the CSD at spatial scales of ~50-300 μm or above, e.g. the scales where CSD varies, LFPs pool from, or macroscale ECoG potentials average over. Instead, dendritic synaptic current influx and efflux modulate the CSD and, by extension, the LFP and the ECoG-scale potential. This has recently been substantiated by emerging in-vivo, simultaneous, recording of the intracellular potential and the LFP, showing that they are tightly coupled temporally, independent of the spiking pattern of the neuron (Okun et al., 2009). As such, one might directly infer properties about the underlying neuronal statistics from the shape of the changes in the electric potential (Miller et al., 2009b, Miller et al., 2010a).

A way to think about populations of neurons is the degree to which they receive synaptic input in concert, synchronized across the neuronal population, compared to the asynchronous pattern of complex local inputs between actively computing neurons in a population (see figure 5). The asynchronous inputs will, when averaged over to the point that they are apparent in the ECoG potential, appear as a type of random walk in time. Changes in the way local neurons interact with one another will appear as a "speeding up" of the random walk, difficult to see when looking at the raw potential, but apparent as broadband, power-law, changes when looking in the frequency domain (Miller et al., 2009b). Synchronized changes, by contrast, can be visually apparent in the raw

tracing – even if the synchronization is relatively weak, averaging augments the synchronized portion, while the other aspects are diminished. If the synchronization is tied to an oscillatory feedback process of some kind (such as a cortico – basal ganglial – thalamic loop), then a "rhythm" will emerge, and the synchronization and de-synchronization of the rhythmic process will be revealed as changing amplitude of a sinusoid in the timeseries, and a peak in the frequency domain. If the synchronization is tied to a feedforward process, such as thalamic input to V1 following a visual stimulus, the timeseries may reflect a multi-phasic, time-locked response – the "event-related potential", where the different portions of the event-locked timeseries likely reflect initial input to cortical pyramidal neurons from thalamus, and then synchronized lateral inhibition. The measured ECoG voltage timeseries will be then be a mixture of random-walk like changes reflecting asynchronous local cortical processing, sinusoidal changes reflecting synchronized oscillatory feedback, and event-locked multiphasic characteristic deflections reflecting feedforward synchronized volleys tied to a specific input event.

## Broadband spectral change[3]

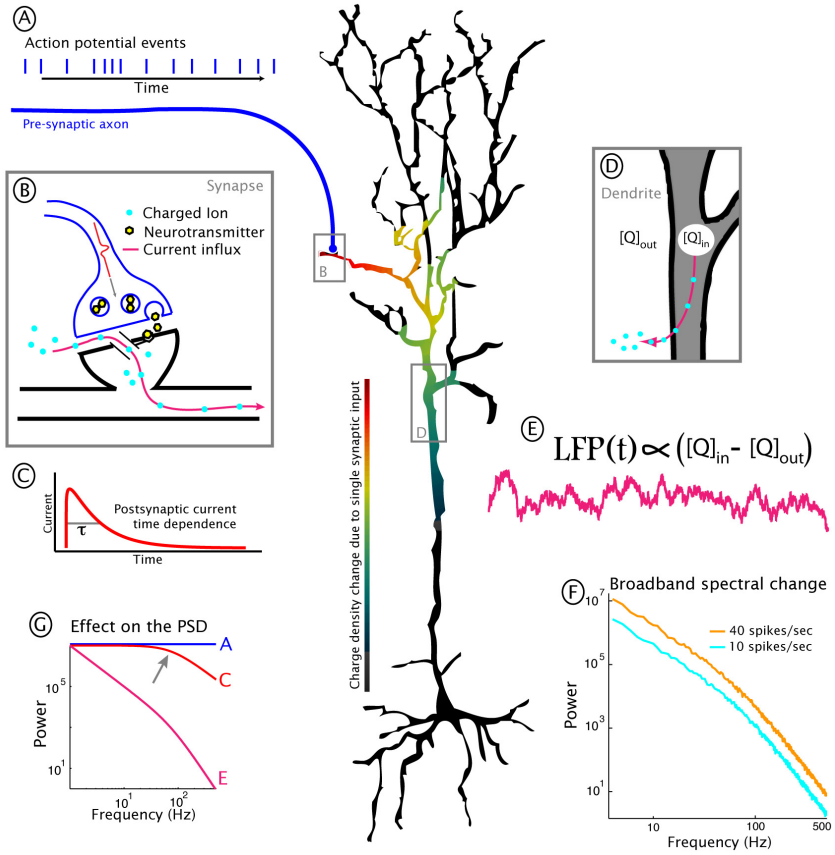


**Figure 6: A heuristic model for how broadband spectral increases might emerge from increases in pre-synaptic action potential (AP) firing rate.** (A) Poisson-distributed pre-synaptic APs arrive at a neighboring neuron. The power spectral density (PSD) of these AP events over time has a flat, frequency-independent, form (i.e. a "white noise" shape, with spikes coming with equal probability at every frequency, blue trace in G). (B) At the synapse between the two neurons, each arriving AP triggers release of neurotransmitter, and post-synaptic current influx. As shown in the central schematic neuron, this results in a gradient of charge density within the dendritic arbor. (C) The temporal shape of the post-synaptic current smears out the PSD, giving it a $1/f^2$ form, with a "kink" at a particular frequency determined by the decay time, τ, of the post-synaptic current (here ~70Hz), shown with a gray arrow in G. (D) In this model, the inputs from 6000 such synaptic currents are integrated over time and space, simulating time-dependent change in transmembrane charge concentration. The associated transmembrane potential produces time-dependent current across the dendritic membrane. (E) The combined effect of synaptic and trans-dendritic current influx/efflux induces a gradient of current-source density in the surrounding medium. The time-dependence of transmembrane potentials are mimicked by the local field potential (LFP) (Okun et al., 2009), and likely the macroscale (ECoG) potential as well. (F) The PSD shifts associated with changes in mean firing rate from pre-synaptic inputs are broadband in nature (spread across all frequencies), with a characteristic $P \sim 1/f^{\chi}$ form (i.e. the power in the PSD falls off with increasing frequency according to the exponent, χ). (G) The $P \sim 1/f^{\chi}$ PSD structure might emerge from the combinations of 3 simple processes. The first is Poisson distributed input spikes). The second is a characteristic post-synaptic current with exponential decay, which produces a $1/f^2$ form following a "kink" (gray arrow) at a frequency determined by the decay time at the synapse. The last process to shape the PSD is the integration of inward currents over time in the dendrite (as in D+E). This model demonstrates how the relationship between firing rate and broadband change might arise. Model adopted from (Bedard et al., 2006, Miller et al., 2009b). Figure originally in (Miller et al., 2010a).

[3] Excerpted from: Miller KJ, Schalk G, Fetz EE, Den Nijs M, Ojemann JG, Rao RPN (Cortical activity during motor execution, motor imagery, and imagery-based online feedback. Proceedings of the National Academy of Sciences 108:4430-4435.2010b).

In 1972, Brindley and Craggs measured the electric potential from the surface of the baboon brain using a 1mm diameter electrode (Brindley and Craggs, 1972). They found that the power in the 80-250 Hz frequency range of the electric potential timeseries was dynamically increased in motor areas during movement. Sites 2mm apart from one another were specific for different movements of the same limb. This observation, that power in the high frequency portion of the brain surface electric potential was specific for local cortical activity, was again demonstrated in electrocorticography (ECoG) by Crone and colleagues in 1998, for different functions in distant regions of the human brain (Crone et al., 1998a). Both groups proposed that this high frequency power was a correlate of specific cortical activity, but it was unclear what this power increase meant at the neuronal level. More recently, Miller and colleagues proposed and demonstrated that these observed high-frequency power changes actually reflected "broadband" power spectral change, across all frequencies. The low frequency portion of these broadband changes was often obscured at lower frequencies by coincident changes in rhythmic phenomena ($\alpha$, $\beta$, etc), so that only the high frequency portion of the broadband change was observed. These broadband changes have a particular form (a power-law in the frequency domain, as shown in Figure 6), and capture functionally-specific cortical activity with a temporal precision of tens of milliseconds (Miller et al., 2009b, Miller et al., 2009d).

A recent manuscript by Manning and colleagues directly shed light on the neurophysiologic nature of these broadband changes by measuring what aspects of the power spectral density (PSD) of the local field potential (LFP) correspond with single neuron firing rates measured at the same cortical site (Manning et al., 2009). The firing rate was then compared with various spectral features using a regression approach, and an associated significance level was estimated by resampling. The best predictor of firing rate was the broadband feature of the PSD, and close examination revealed that there is a clear relation between increased firing rate and increased broadband power in the LFP. This relation was robust, significant, and reproduced across a large number of individuals and

brain sites. Other recent manuscripts have shown that 30-100 Hz aspects of the LFP are significant predictors of multi-neuron firing rate (Whittingstall and Logothetis, 2009); it is likely that this high frequency change reflects broadband change, and represents a secondary confirmation of the finding by Manning and colleagues. The electrical potential from both studies was measured at the spatial scale of the LFP, which has recently been demonstrated to reflect neuronal activity within ~250μm of the recording electrode (Katzner et al., 2009). Because this broadband spectral change is correlated with action potential rate at the LFP scale, broadband electric potential spectral changes may generically represent mean firing rate at larger scales as well. If true at larger scales, then the spatial scale that the recording electrode reflects would then dictate the size of the neuronal population that the firing rate is being averaged over. Seen in this light, the manuscript by Manning and colleagues provides empirical evidence that broadband (or associated high-frequency) changes observed at larger spatial scales, in ECoG, are a correlate of the mean firing rate of the neuronal population beneath each recording electrode.

How might the reader gain intuition for the measured correlation in terms of neurophysiology? From a modeling perspective, heuristics for the relationship between changes in action potential rate and broadband, power-law, changes can be constructed relatively simply. Properties of the physiology underlying the current source density (CSD) in different cortical lamina were established experimentally in the late 1970s and early 1980s (Mitzdorf, 1985): Propagating action potentials in axons and axon terminals do not contribute strongly to the CSD at spatial scales of ~50-300 μm or above, e.g. the scales where CSD varies, LFPs pool from, or macroscale ECoG potentials average over. Instead, dendritic synaptic current influx and efflux modulate the CSD and, by extension, the LFP and the ECoG-scale potential. Emerging in-vivo, simultaneous, recording of intracellular potential and LFP by Okun, Naim, and Lampl show that the LFP and single-neuron transmembrane potential are tightly coupled temporally, independent of the spiking pattern of the neuron (Okun et al., 2009). A very simple model to produce broadband spectral changes from

changes in firing rate can be illustrated to provide intuition for this correlation, and also to illustrate why Manning and colleagues' experimental finding provides evidence for a macroscale correlate in population firing rate. A model based upon an original by Bedard and colleagues (Bedard et al., 2006) (later extended in (Miller et al., 2009b)) shows how the timecourse of the intracellular dendritic charge concentration results from spatiotemporal summation of postsynaptic current influxes from each arriving AP (Figure 6). The broadband in the PSD results from the noise-like distribution of AP arrival times, and its 1/f falloff with frequency results from the shape of the synaptic current decay and the effect of temporal integration in the dendritic arbor.

## Structure of thesis

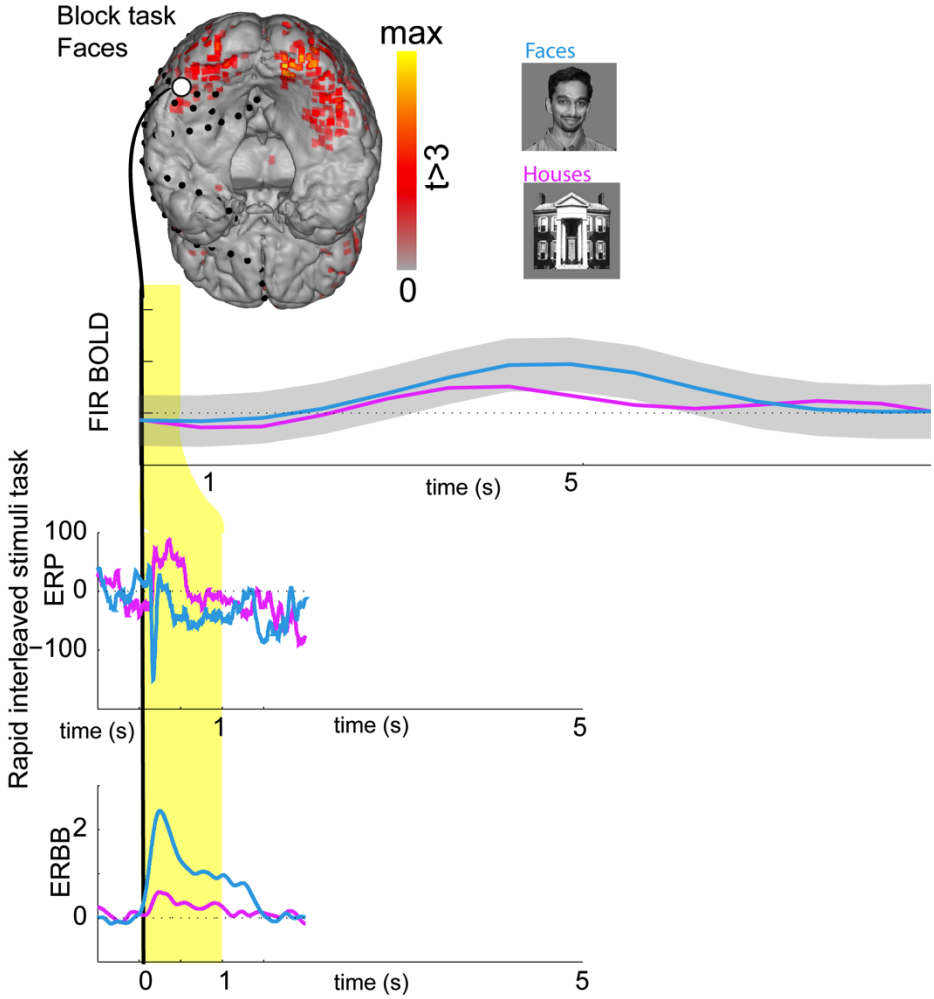


**Figure 7:** The timecourse of the fMRI BOLD response is far more drawn out than that of the electrophysiologic ECoG response in the event related broadband or the event related potential

### The timecourse of broadband spectral changes

In the second chapter of this thesis we illustrate, in the setting of inferior temporal recordings, how broadband spectral changes can be extracted from the electrical potential timeseries using a principal component approach. Broadband shifts are shown to be a ubiquitous marker of local cortical activity in five different settings: first (and most importantly) in face and house visual responses (inferotemporal cortex), visual search (peri-Calcarine cortex), speech production (peri-Sylvian and peri-Rolandic cortex), and finger tapping (peri-Rolandic cortex). In each setting,

spatially focal shifts in broadband power are observed in a task-selective manner. We then illustrate how broadband power shifts may appear to be band-limited in certain contexts due to contamination by amplifier noise at high frequencies and masking due to the general anticorrelation of low frequency rhythm power. Furthermore, broadband spectral change mimics the spatial distribution of fMRI bold changes (Hermes et al., 2012), but has much faster timecourse (figure 7).

### Gamma oscillations

Gamma oscillations have been postulated to be important for all aspects of visual cortical computation, modulating basic processing of stimuli (Gray et al., 1989, Bosman et al., 2012), interactions between brain areas (Gray and Singer, 1989, Fries, 2005), conscious perception (Melloni et al., 2007), and decision making (Siegel et al., 2011). Because this thesis is concerned with precisely these functions, we specifically examined the gamma oscillation in the visual system in the third chapter. We show that gamma oscillations are an idiosyncrasy of visual processing that result from low-level features of the stimulus. Specifically, only grating stimuli reliably generate gamma oscillations while most other stimuli do not. Instead, spatial noise patterns and many images of faces and houses, show strong broadband spectral change and an absence the gamma rhythm changes.

### Low frequency rhythms and rhythmic entrainment[4]

While gamma oscillations are not a general property of visual cortex, there are a multitude of other, low-frequency, rhythms in inferior temporal and early visual cortical regions. We might therefore question whether these rhythms are important for understanding the dynamics of category-specific perception in inferotemporal cortical processing. Viewpoints are changing concerning the functional role of rhythmic brain activity. There is increasing evidence that low-frequency (2-25 Hz) neural oscillations are not simply epiphenomena, but in some cases reflect an essential mechanism for coordinating brain function. A leading mechanistic hypothesis for how rhythms might directly

[4] Portions of this text excerpted from: Miller KJ, Foster BL, Honey CJ (Does rhythmic entrainment represent a generalized mechanism for organizing computation in the brain? Front Comput Neurosci 6:85.2012a).

influence neural circuit function is by synchronously modulating the membrane potentials of many neurons such that mutual dendritic input between members of this population is more likely to induce action potentials at specific times (Volgushev et al., 1998, Miller et al., 2012b). This proposed pathway of influence matches the observation that, across numerous cortical sites and behaviors, single cell and population spiking is selectively enhanced at specific phases of ongoing narrow-band oscillations in the field potential (Murthy and Fetz, 1992, O'Keefe and Recce, 1993).

Given that coherent electrical fields sum spatially, the same distributed rhythmic brain process can be observed across multiple scales of measurement. The large-scale relationship between aggregate spike timing and these widespread rhythms has not been fully explored, because spiking behavior has generally been measured at the scale of the single neuron. However, as shown in chapter 2, it has been recently established that increases and decreases in local firing rate are accompanied by upward and downward broadband shifts in the power spectrum of the cortical surface potential. In human electrocorticographic (ECoG) measurements, this broadband signal component, reflecting aggregate firing rate, is modulated by the phase of narrow band brain rhythms, so-called "phase-amplitude coupling" (PAC) (Miller et al., 2010b, Miller et al., 2012b, Hermes et al., 2014).

We explore this rhythmic entrainment in chapter 4. We find that (in general terms) low-frequency oscillations appear to be specialized more for homeostatic, organizational brain processes, rather than for actively controlling spatiotemporally precise local computations as they occur. One reason for this is that the 40-500ms timescales corresponding to each full rhythmic cycle (2-25 Hz) are slower than many of the timescales of perception and action. Secondly, low frequency oscillations are coherent across centimeters of the cortical surface, and thus can exert a similar influence on local circuits that implement dramatically different computations. Thirdly, the modulation of population firing by low-frequency rhythms is usually greater during rest conditions than during visual engagement (or motor/language/perceptual tasks), when rhythms are often

suppressed (desynchronized) – such that rhythmic entrainment is most pronounced during disengaged cortical states (Hermes et al., 2010, Miller et al., 2010b, Miller et al., 2012b, Hermes et al., 2014). Thus, the amplitude and phase of a spatially coherent rhythm can provide a general constraint on the computational state of local circuits. When rhythms are strong, circuits exhibit more regulated spiking patterns that are likely associated with processes such as inter-regional communication or priming before computation; when rhythms are weak, then circuits are freed from a restricted periodic regime to engage in more of the specialized computations specific to local wiring. Notwithstanding these general observations, the specific role of rhythmic entrainment upon spiking activity in local circuit computations is in need of mechanistic elucidation. Simple heuristic model that reproduces experimental patterns of phase entrainment can be developed, based on the assumption that cortical rhythms arise from the reciprocal interaction of inhibitory and excitatory neurons, and one such model is illustrated in chapter 4.

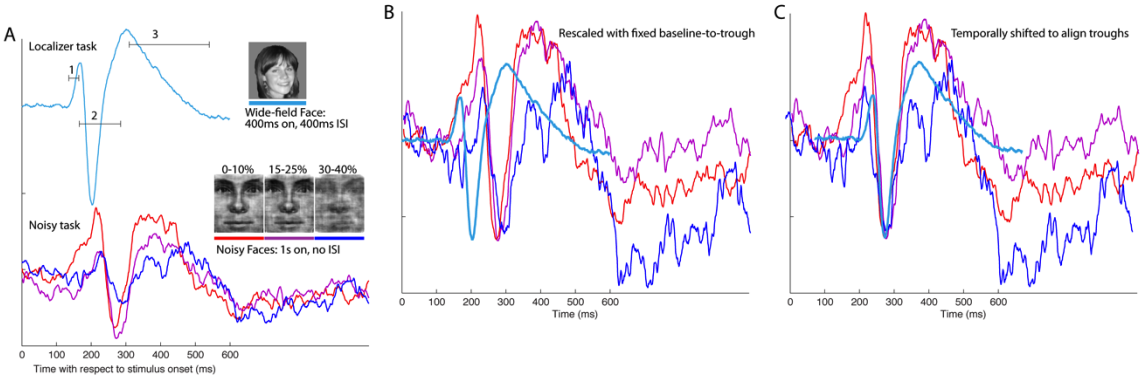


**Figure 8: ERPs retain their general shape in response to the same category of stimulus** (e.g. a face) even when the low level properties of the stimulus are degraded by noise, but the individual components change independent of one another, depending on the task type and the amount of noise. Responses are from a fusiform gyral site in subject ZT. **(A)** See chapter 7 for task details. Three epochs are identified in the top ERP. **(B)** The ERPs are scaled in magnitude so that they each have a fixed baseline-to-trough magnitude. **(C)** The ERPs are shifted in time to align the troughs. Examination of epoch 1 reveals that begins at the same post-stimulus time, but is prolonged for the noisy stimuli descrimination task (even at low noise levels), and is prolonged with increasing noise. Epochs 2 and 3 are smaller with increasing noise, but have grossly the same duration, regardless of task or noise.

## The Dynamics of Category-specific Perception in Inferotemporal Cortex: Decoding the inferior temporal cortex at the speed of perception

As detailed above, we found that gamma oscillations are an idiosyncrasy visual processing that result from low-level features of the stimulus and that other low frequency oscillations generally reflect less engaged cortical. Therefore, we primarily disregarded cortical oscillations for further study of categorical processing states in inferotemporal cortex.Instead, we focused on broadband spectral change to understand neuronal population dynamics on a single trial basis. The interpretation of this signal as population-averaged firing rate is straightforward. We also examined event-locked polyphasic responses throughout inferotemporal as well as pericalcarine regions, the so-called "event-related potential" – ERP. As shown in the first figure of chapter 5, face- or house-specific ERPs are highly polymorphic, even when in cortical sites 1cm away from one another. This suggests sophisticated underlying physiology, that is a generic within a local neuronal population (such that the timing is synchronized across the population of cells), but can be very different in character for different cortical regions – even if these regions appear to serve similar functions and have similar semantic category specificity.

Unlike gamma oscillations, which represent low-level features in the data, ERPs retain their same general shape in response to the same general type of stimulus (e.g. a face) even when the low level properties of the stimulus are degraded by noise (as illustrated in figure 8). Their interpretations are not straightforward, and different individual components change independent of one another, depending on the task type and the amount of noise. The varied morphologies of the ERPs in different cortical patches can present technical difficulties for their use as experimental tools. The literature contains a myriad of approaches to addresses this, many of which require special attention to specific epochs of specific ERPs, in response to specific stimuli, in specific cortical regions. In the set of our inferotemporal studies, our goal when examining ERPs was generally to describe or predict the state of several cortical regions simultaneously, in such a way that we could use a generic approach. Rather than manually define a set of handpicked, expected,

stimulus specific responses in each cortical region, we let the data from a training period or separate (localizer) experiment define template responses (the ERPs themselves). Then, templates could be projected into the data, and the magnitude of these projections could be directly compared between different cortical sites and stimuli, with straightforward interpretation.

A similar approach could be taken for the broadband timecourse, although the shape of the event-triggered broadband (ERBB) templates generally has a simple rising epoch followed by a decline that is slower than the rise (see figure 1 in chapter 5). This template projection technique was used to generate feature spaces in which the general "brain state" (as measured with the ECoG array) could be measure to decode the timing and type of single visual stimuli with unprecented accuracy.

## The Dynamics of Category-specific Perception in Inferotemporal Cortex: Context immediately influences the physiology of perception

There is an interesting property in the dynamics of inferotemporal areas, termed "repetition suppression". Subtle examination of the fMRI hemodynamic responses in these regions shows that repeated presentation of the same visual stimulus is associated with less metabolic expenditure during processing. This effect is also present when stimuli from within the same class are presented in repetition. The changes reflected by the blood-oxygen-level-dependent (BOLD) contrast signal measured by fMRI are intrinsically smeared over metabolic timescales of order one second or more (figure 7). However, the speeds of perception, decision, and action are all faster than this. What are the mechanisms that underlie repetition suppression? Does inferior temporal processing happen slower for repeat processing of the same type? Is the magnitude of neural population response not as strong? Or is it just as strong, but shorter? On what timescales are these repetition adaptations happening? As described in chapter 6, we measured the dynamics of the fusiform "face area" and the medial occipitotemporal "place area" (parahippocampal/lingual), while serially presenting simple pictures of faces and houses. Subjects were first presented with simple, grayscale, pictures of whole-field faces and houses that were displayed in random order for 400ms each, with 400ms inter-

stimulus interval (blank screen) between. We found that approximately half of the category-selective sites showed greater total activity for novel than for repeated stimulus class. In ~1/2 of the face-selective sites (and none of the house-selective sites), latency to peak activity was faster for novel stimuli.

## The Dynamics of Category-specific Perception in Inferotemporal Cortex: Visual perception and semantic perception meet in the inferior temporal cortex

As described, we can decode the timing and semantic category of visual stimuli from inferior temporal cortex with high temporal fidelity (chapter 6), but we also found that context influences the dynamics of the response. In the setting of these observations we might ask whether inferotemporal cortex is primarily specialized for semantic perception (as suggested by the category specific cortical organization), without representation of the quality of the stimulus. Although fMRI studies have found a graded response with increasing stimulus noise (Heekeren et al., 2004), and single unit studies in inferotemporal cortex have found the same, the poor temporal resolution of fMRI and the stochastic nature of single unit firing have not allowed for direct interpretation of increased noise in visual stimuli. ECoG is uniquely suited to address the nature of the response to single stimuli: the direct electrophysiologic measurement results in fine temporal resolution, and the fact that the electrical changes represent an average over the whole neuronal population results in robust single trial responses.

Some of the subjects who performed the "localizer" task above also performed a face-identification task with 1s presentation of phase-scrambled close-up pictures of faces and houses. Stimuli ranged from 0 to 100% noise in 5% increments, and subjects pressed a key when they believed a face was shown. From inferotemporal sites, we found robust neurometric curves, where increased stimulus noise resulted in decreased neural activity, even with isolated responses from correctly identified stimuli at low noise levels. A classifier, trained on the localizer task (which did not have a category choice component), but used on the noisy stimuli task was used to decode brain state. At high levels of noise, where subjects perform at chance level, predicted stimulus type is

correlated with the subjects' choice rather than the stimulus type. At low levels of noise, predicted stimulus type is correlated more closely with the stimulus that the subjects' choice. Collectively, these findings suggest that, in addition to semantic category (face or house), low-level features such as stimulus noise, as well as high-level features such as semantic perception, are represented in the same neuronal population in inferotemporal cortex.

A

Normalized Mutual information is used to co-register the pre-impant MRI and the post-implant CT

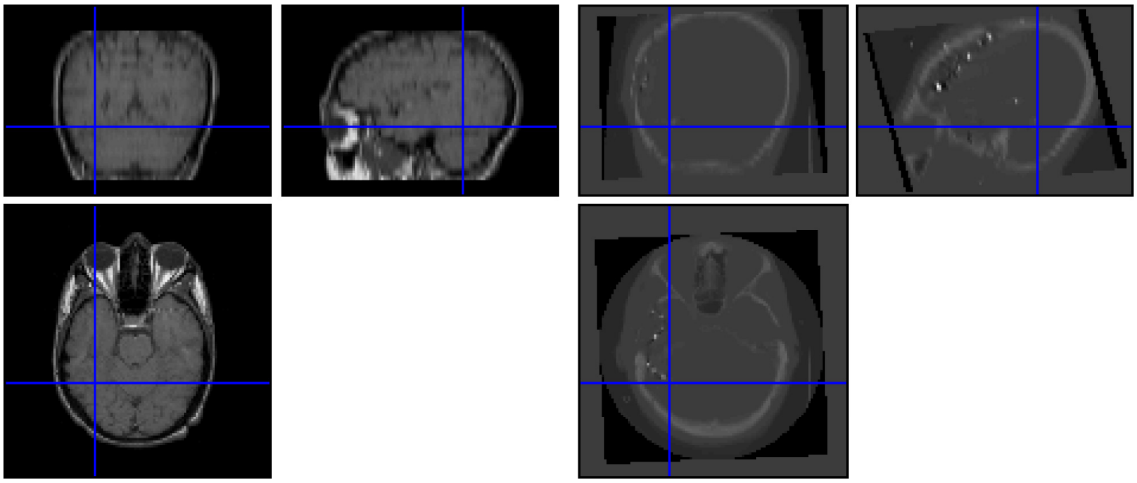

B

The CT is re-sliced into the space of the thickly-cut MRI, and then electrode positions from the CT are directly associated with locations on an MRI axial slice.

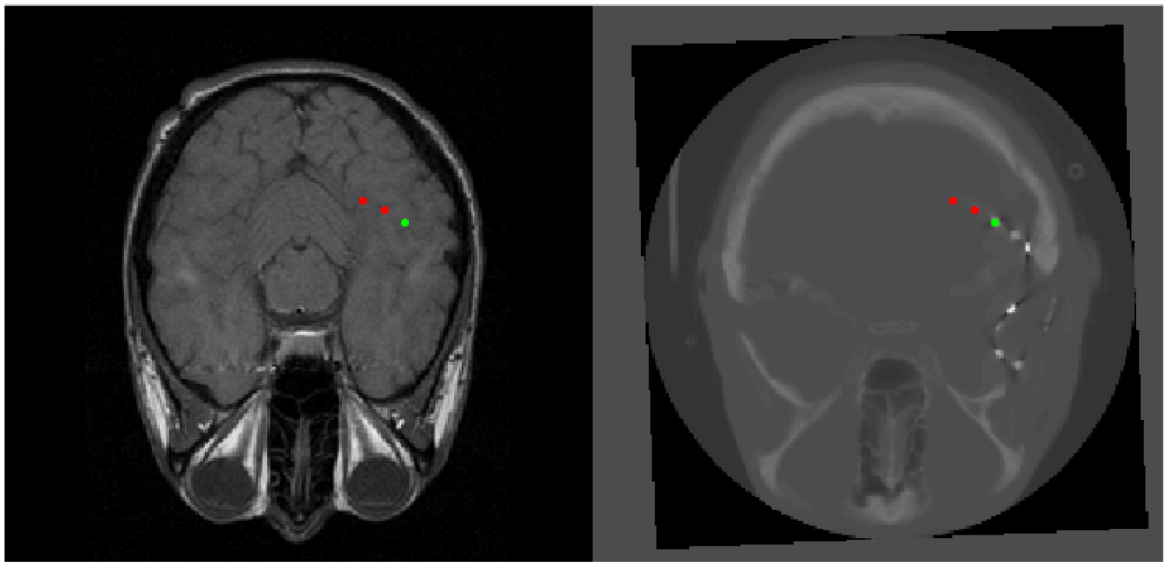

**Figure 9: Illustration of the electrode localization throughout the manuscript.** The MRI slice thickness used most often with the subjects studied were by clinical protocol, and 5mm. This is generally not sufficient to render surfaces and co-register electrodes by the standard methods used in lateral fronto-parietal cortical studies (Hermes et al., 2010). However, the clinical protocol axial T1 used most often does generate slices that are approximately parallel to the brain surface in the inferior temporal surface, a few centimeters anterior to the occipital pole. Therefore, electrode location relative to gyral surface anatomy was determined by projection of the post-implant CT to the pre-operative axial T1 in the following manner: CT is co-registered to T1 Axial MRI using normalized mutual information in SPM (SPM 5). CT is then interpolated and resliced into the T1 axial MRI. Electrodes are then identified in this mutual space on each slice so that their position is known with respect to gyral anatomy. Because of the tentorium cerebelli, there is little to no brain sag to distort the comparison of electrode position from post-op CT with the pre-operative MRI, so none of the standard correction techniques are necessary.

# Chapter 2: Broadband changes track functionally diverse neuronal populations[5]

We illustrate a general principal of electrical potential measurements from the surface of the cerebral cortex, by revisiting and reanalyzing experimental work from the visual, language and motor systems. A naïve decomposition technique of electrocorticographic power spectral measurements reveals that broadband spectral changes reliably track task engagement. These broadband changes are shown to be a generic correlate of local cortical function across a variety of brain areas and behavioral tasks. Furthermore, they fit a power-law form that is consistent with simple models of the dendritic integration of asynchronous local population firing. Because broadband spectral changes covary with diverse perceptual and behavioral states on the timescale of 20-50ms, they provide a powerful and widely applicable experimental tool.

[5] This chapter appeared originally as a manuscript in NeuroImage: Miller KJ, Honey CJ, Hermes D, Rao RPN, denNijs M, Ojemann JG (2014). Broadband changes in the cortical surface potential track activation of functionally diverse neuronal populations. *NeuroImage*,15, 711-20.

## Introduction

When examining the extracellular voltage power spectrum of occipital or rolandic cortex, the shift from rest to task is strongly associated with an increase in power at high frequencies (greater than ~50Hz), and often accompanied by a decrease in power at low frequencies (less than ~30Hz) (Crone et al., 1998a, Crone et al., 1998b, Aoki et al., 1999, Crone et al., 2001, Miller et al., 2007b, Hermes et al., 2010). When we first investigated these signals, our interpretation was that there would be different high-frequency oscillations specific to each cortical region and function. However, in each case that we examined the high-frequency spectral changes lacked a definitive upper bound, and appeared to extend to the highest frequencies resolvable with our sampling rate and noise floor.

This presented a pair of questions. First, might the high-frequency spectral changes reflect a broadband change in the power spectrum? Second, might this broadband change track asynchronous processes in the underlying neuronal dynamics? In this paper, we review and reanalyze data supporting the claim that that broadband shifts are indeed a generic marker of circuit activation in the neocortex (Manning et al., 2009, Miller et al., 2009b, Miller et al., 2009d, Whittingstall and Logothetis, 2009, Miller et al., 2010a, Ray and Maunsell, 2011). Moreover, we discuss how broadband spectral change can be obscured by rhythmic phenomena at lower (e.g. α, β) frequencies, and we illustrate how the changes in high frequencies are different in kind from changes in the canonical lower-frequency rhythms.

Before describing the details of the broadband power shifts, it is important to distinguish rhythmic and non-rhythmic neural processes and their manifestations in the field potential. Rhythmic processes (such as the occipital αand peri-central motor βrhythms) exhibit band-limited spectral peaks, reflective of a characteristic oscillatory time-scale (Jasper and Andrews, 1938, Miller et al., 1940, Jasper, 1941, Jasper and Penfield, 1949, Bates, 1951, Penfield, 1954, Crone et al., 1998b, Pfurtscheller, 1999, Miller et al., 2007b). Non-rhythmic processes do not have an oscillatory

timescale and do not produce isolated peaks in the power spectrum. Nonetheless, a non-rhythmic process may exhibit a distinctive spectral profile, and changes in its amplitude will produce changes in the spectrum of the electrical field (Bullock et al., 2003).

We have proposed (Miller et al., 2009b) that the broadband "1/f" background, ubiquitous in neocortical field spectra, reflects a non-rhythmic underlying process with an intuitive connection to neuronal population activity. In particular, the approximately power-law profile of the broadband component can be understood as the signature of the summation of asynchronously arriving synaptic inputs in the dendrites of pyramidal neurons (Bedard et al., 2006, Miller et al., 2009b). The dendritic summation model predicts a particular form of power-law in the spectrum above 80 Hz, and this prediction matches the empirical spectral profile to >500 Hz (once one corrects for gain-modulation in amplifier hardware).

Regardless of the details of the biophysics that produce the broadband 1/f component, it is clear that (i) the underlying process is not rhythmic and (ii) the process is strongly associated with the activation of local circuits. Behavior-locked increases in the broadband component have been demonstrated in peri-Rolandic cortex (during finger tapping) and in the occipital lobe (during visual search) via intracranial recordings from the surface of the human neocortex (Miller et al., 2009c, Miller et al., 2010b). More generally, task-locked power increases in the "high gamma" band of the power spectrum (~80-200 Hz) are widely observed in mammalian cortical electrophysiology (Crone et al., 1998a, Crone et al., 2001, Sederberg et al., 2003, Canolty et al., 2007, Miller et al., 2007b, Jacobs and Kahana, 2009, Swann et al., 2009, Edwards et al., 2010, Vidal et al., 2010, Gunduz et al., 2011, Pei et al., 2011, Foster et al., 2012, Hermes et al., 2012, Mesgarani and Chang, 2012). In many cases, these wide-band power shifts are probably reflective of an underlying broadband shift, especially when there is no band-limited peak observed above 80 Hz.

Direct support for the broadband model was provided by simultaneous measurements of unit activity and field potentials. Based on 2030 identified units across numerous human

neocortical sites, Manning et al (Manning et al., 2009) demonstrated a positive relationship between the average firing rate of the units and the amplitude of the broadband component. Recent work in macaque visual cortex found a robust relationship between broadband high-frequency power increases and single unit activity, and was also able to separate the (non-rhythmic) high-frequency broadband effect from those attributable to (rhythmic) visual gamma (Ray and Maunsell, 2011).

Because rhythmic (band-limited) and non-rhythmic (broadband) components of the power spectrum have distinct frequency profiles and exhibit distinct task-related changes, they can be decoupled from one another (Miller et al., 2009d) (Figure 1). Once decoupling is performed, the spectrum of the electrical field can be expressed as a composite of rhythmic and non-rhythmic components (Figures 1-5). A broadband shift can then be understood as a change in the amplitude of a non-rhythmic, stochastic, process, which reflects the dendritic integration of asynchronous inputs.

In this review, we begin by demonstrating that broadband shifts are a ubiquitous marker of local cortical activity, we present data from five different settings: face and house detection (inferotemporal cortex, Figure 2), visual search (peri-Calcarine cortex, Figure 3), speech production (peri-Sylvian and peri-Rolandic cortex, Figure 4), and finger tapping (peri-Rolandic cortex, Figure 5). In each setting, spatially focal shifts in broadband power are observed in a task-selective manner. We then illustrate how broadband power shifts may appear to be band-limited in certain contexts due to contamination by amplifier noise at high frequencies and masking due to the general anticorrelation of alpha and beta rhythm power at low frequencies (Figure 6).

# Methods

## Human subjects

Five patients participated in the study, one patient each is reflected in Figures 1-5. All were patients at Harborview Hospital in Seattle, WA, USA, with sub-dural electrocorticographic (ECoG) grids placed for extended clinical monitoring and localization of seizure foci, in the course of the treatment for medically-refractory epilepsy. All patients participated in a purely voluntary manner, after providing informed written consent, under a protocol approved by the Institutional Review Board of the University of Washington.

## Electrocorticographic recording

The platinum electrode arrays (Ad-Tech, Racine, WI) were configured as combinations of "grid" (4×8, 8×8) and strip arrays. The electrode pads had 4 mm diameter (2.3 mm exposed), 1 cm inter-electrode distance, and were embedded in silastic. These arrays were surgically placed on the sub-dural brain surface during the treatment for epilepsy. ECoG signals were split into two identical sets. One set was fed into the clinical EEG system (XLTEK, Oakville, Ontario, Canada) and the other set was recorded with Synamps2 (Neuroscan, El Paso, TX) biosignal amplifiers at 1kHz with an instrumental bandpass-filter from 0.3 Hz to 200 Hz. ECoG signals were acquired from the experimental amplifiers using the general-purpose BCI2000 software (Schalk et al., 2004), which was also used for visual stimulus presentation. Audio was recorded using a Logitech USB desktop microphone at 11 kHz, and synchronized with a trigger in the BCI2000 program (Figure 4). Finger position was recorded using a sensor dataglove (5DT, Irvine, CA, Figure 5).

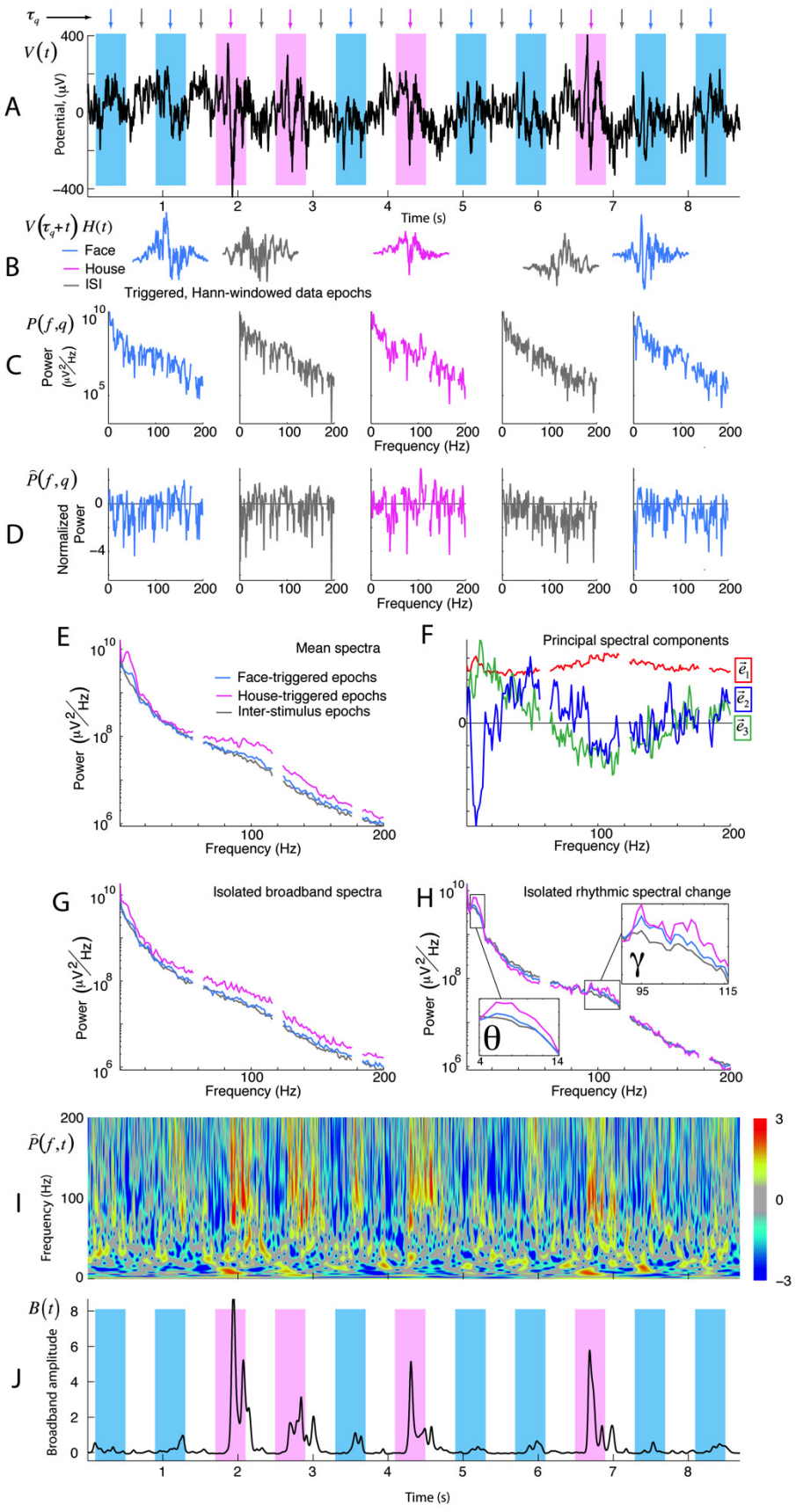
A
B
C
D
E
F
G
H
I
J
Face
House
ISI
Triggered, Hann-windowed data epochs
Mean spectra
Face-triggered epochs
House-triggered epochs
Inter-stimulus epochs
Principal spectral components
Isolated broadband spectra
Isolated rhythmic spectral change
Potential, (μV)
Time (s)
Power (μV²/Hz)
Normalized Power
Frequency (Hz)
Broadband amplitude

**Figure 1: Decoupling the cortical spectrum to reveal broadband spectral change.** Simple black-and-white pictures of faces and houses were presented to a patient while recording from an ECoG electrode on the parahippocampal gyrus. **(A)** Raw potential, $V$, with time triggers, $\tau_q$, in the middle of each stimulus ($q$) and ISI period (noted with arrows, 400ms each). Times of face presentation are shown with pink background, with house presentations in blue. The gray triggers are the middle of ISI periods. **(B)** 1-s epochs of raw potential. centered at each time $\tau_q$, are extracted and Hann-windowed: $V(\tau_q + t)H(t)$. **(C)** The power spectral density (PSD) of each of these epochs is calculated: $P(f,q)$. **(D)** Each spectrum is normalized with respect to the mean spectrum across trials of all types, and the log is taken, to produce the transformed PSD: $\hat{P}(f,q)$. **(E)** The average power spectrum is shown for all face/house/ISI presentations in pink/blue/gray. **(F)** Principal spectral components, $\vec{e}_1, \vec{e}_2, \vec{e}_3$ (in red, blue, and green; "PSCs") of the normalized spectra (as in D) are identified, and reveal motifs of change in the power spectrum. The first is primarily broadband increase across all frequencies, whereas the 2nd to 4th typically capture changes in rhythmic, peaked phenomena of power spectral change. **(G)** Isolated broadband spectra for each stimulus type – the 2nd to 4th PSCs have been removed and the power spectra are reconstructed, and broadband increase across all frequencies is revealed during presentation of house stimuli. **(H)** Reconstructed power spectra of the 2nd to 4th PSCs only. Selective increase during house stimuli in the theta and high gamma range are extracted from the raw spectra and observed here. **(I)** The dynamic power spectral density after dividing by the average across all time, then taking the log: similar to D, but where the power spectrum is estimated at each point in time, using 7-cycle Morlet wavelets: $\hat{P}(f,t)$. **(J)** The dynamic spectrum, $\hat{P}(f,t)$, is projected into the 1st PSC, $\vec{e}_1$, smoothed, z-scored, and exponentiated to obtain the timecourse of broadband spectral change, $B(t)$. Comparison with stimuli reveals that the cortex beneath this electrode is involved in visual processing of both face and house stimuli, but house stimuli more dramatically than face stimuli.

## Cortical rendering and electrode localization

The relationship between electrode position and gyral anatomy was determined by first rendering the cortical surface from a pre-operative MRI, using either the freesurfer (Dale et al., 1999) or spm5 (Friston et al., 1995, Ashburner and Friston, 2005) environment. Then, electrode positions were calculated with respect to this pre-operative MRI from post-operative computed tomography (CT) using the CTMR package of Hermes, et. al., 2010 (Hermes et al., 2010), demonstrated to accurately localize the electrode positions within an error of ~4mm (the same as the size of the electrodes).

## Spectral Analysis and Decomposition (Figure 1)

After rejection of artifactual or epileptiform electrodes, scalp-referenced ECoG potentials were re-referenced with respect to the common average reference across all remaining electrodes. From

each electrode, samples of power spectral density (PSD; $P\left(f,\tau_q\right)$) as a function of frequency ( $f$ ) were calculated from 1 second epochs centered at the midpoint of each "events" (different for each task), $\tau_q$, where a Hann taper was applied, the Fourier transform was implemented, and the resulting quantity was multiplied by it's complex conjugate. These samples of power spectral density were then decomposed using a principal-component type approach to obtain "principal spectral components" (PSCs), as illustrated in Figure 1 and described in the associated caption. Reconstruction of the PSDs from a subset of all of the PSCs differentiates underlying motifs, and the 2nd-4th PSCs were first removed, and then examined in isolation in Figures 1-5.

Continuous time-frequency approximations (dynamic spectra) were calculated using a wavelet approach, and projected onto the 1st PSC. After smoothing (by filtering with a Gaussian window of width σ=50ms), z-scoring, and exponentiating, a "broadband time series", $B(t)$, is obtained. There is a power law in the cortical PSD of the form $P(f,t) \sim A(t) f^{-\chi}$, which is revealed by broadband fluctuations in the PSD across all frequencies (separate from the classic θ, α, β, and γ rhythmic motifs) (Miller et al., 2009b, Miller et al., 2009d), and appears to directly correlate with local neuronal population firing rate (Manning et al., 2009, Miller et al., 2010a). The exponent $\chi$ is addressed in the discussion. We have proposed that $B(t)$ approximates multiplicative scaling in the timecourse of $A(t)$, and may be directly correlated with multiplicative factor in the average neuronal firing rate of neuronal populations. This manuscript demonstrates that $B(t)$ is highly correlated to task-specific dynamics at very short timescales, and is a general property across many brain areas.

## Tasks

*Face-house picture task* (Figures 1 and 2): Pictures of simple, luminance and contrast matched, grayscale faces and houses (10cm by 10cm at 1m distance) were displayed in random order for

400ms each, with 400ms inter-stimulus interval between. Patients were asked to report a simple target (a single upside-down house). "Event times," $\tau_q$, were denoted at midpoint of picture presentation or each blank screen in between stimuli. Figure 2 results also quantified in (Miller et al., 2009a)

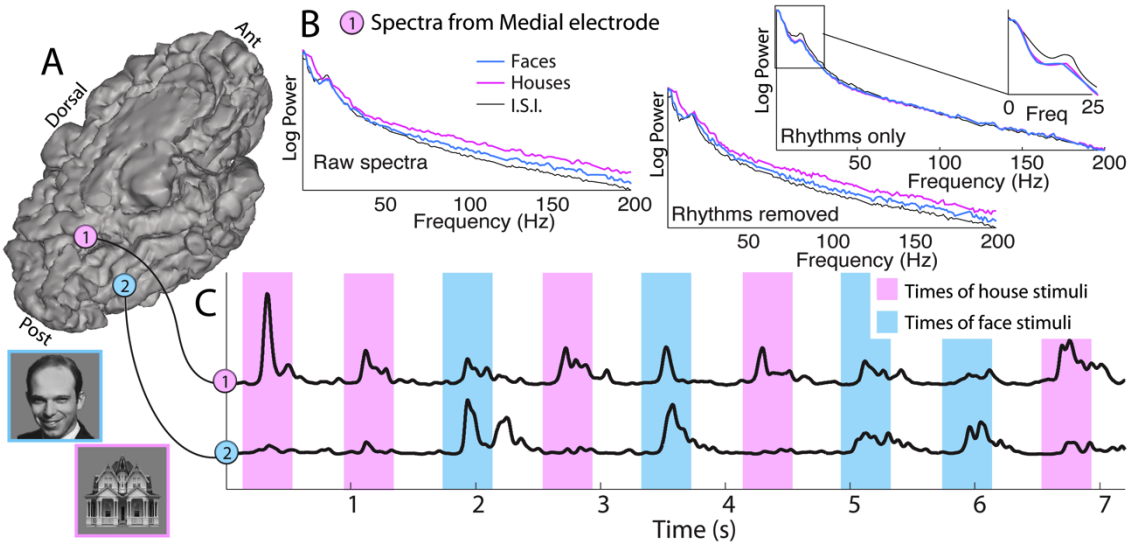


**Figure 2: Inferotemporal category-specific response. (A)** A medial ("1") and a lateral ("2") inferotemporal electrode are shown in situ. **(B)** The raw power spectral density ("Raw spectra") from site "1" in (A) is decomposed as illustrated in Figure 1. **(C)** The broadband time series from each site. Note that the lateral electrode shows selective increase during face pictures, and the medial electrode shows significant response during both face and house stimuli, but with larger response for house picture stimuli. Of the 300 presentations of face and house pictures, all 300 correctly identified from the spontaneous stream of data (with 22 false positives, (Miller et al., 2009a)). The correct face or house label could be identified with 95% accuracy, with 23ms precision (23ms standard deviation).

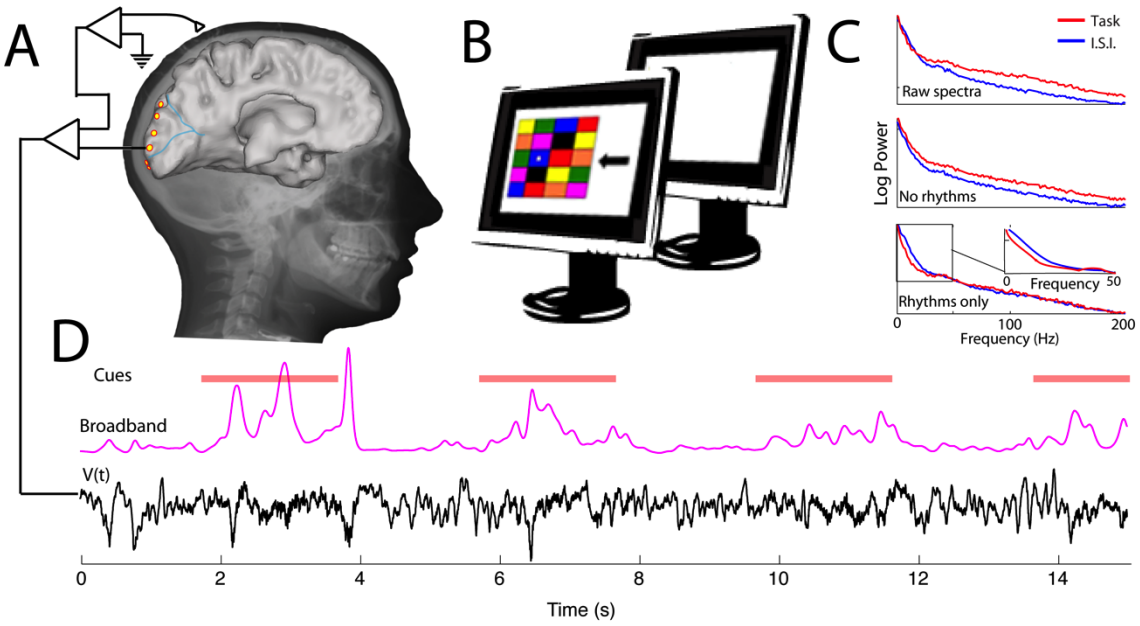


**Figure 3: Peri-calcarine broadband response during a visual search task. (A)** The ECoG potential is measured from occipital lobe brain surface sites during participation in a visual search task, and decomposed as in Figure 1. **(B)** The visual search task consists of a 4-by-5 array of colored squares. Each cue consists of a star in one of the boxes (in this case a blue box), and an arrow. The patient states the color of the box in the direction of the arrow from the star ("green" would be the appropriate response in this case). Visual search cues are shown for 2 seconds, with blank inter-stimulus-interval (ISI) cues shown for intervening 2 seconds. **(C)** As illustrated previously, power spectral changes during different portions of the experiment (top panel) may be appreciated and naively decoupled into broadband changes (middle panel, $2^{nd}$-$4^{th}$ PSCs omitted) and changes in brain rhythms (bottom panel, $2^{nd}$-$4^{th}$ PSCs only, with prominent theta and alpha range changes). **(D)** Broadband increases are observed during the various saccades required for processing of each cue. Figure modified from (Miller et al., 2010b).

*Visual search task* (Figure 3): The patient surveyed an array of colored squares (free to saccade, without a fixation cross), on each trial stating the color of a box that was in a particular direction adjacent to a starred box. "Event times," $\tau_q$, were denoted at midpoint of box array presentation or blank screen in between. For a full description, see (Miller et al., 2010b).

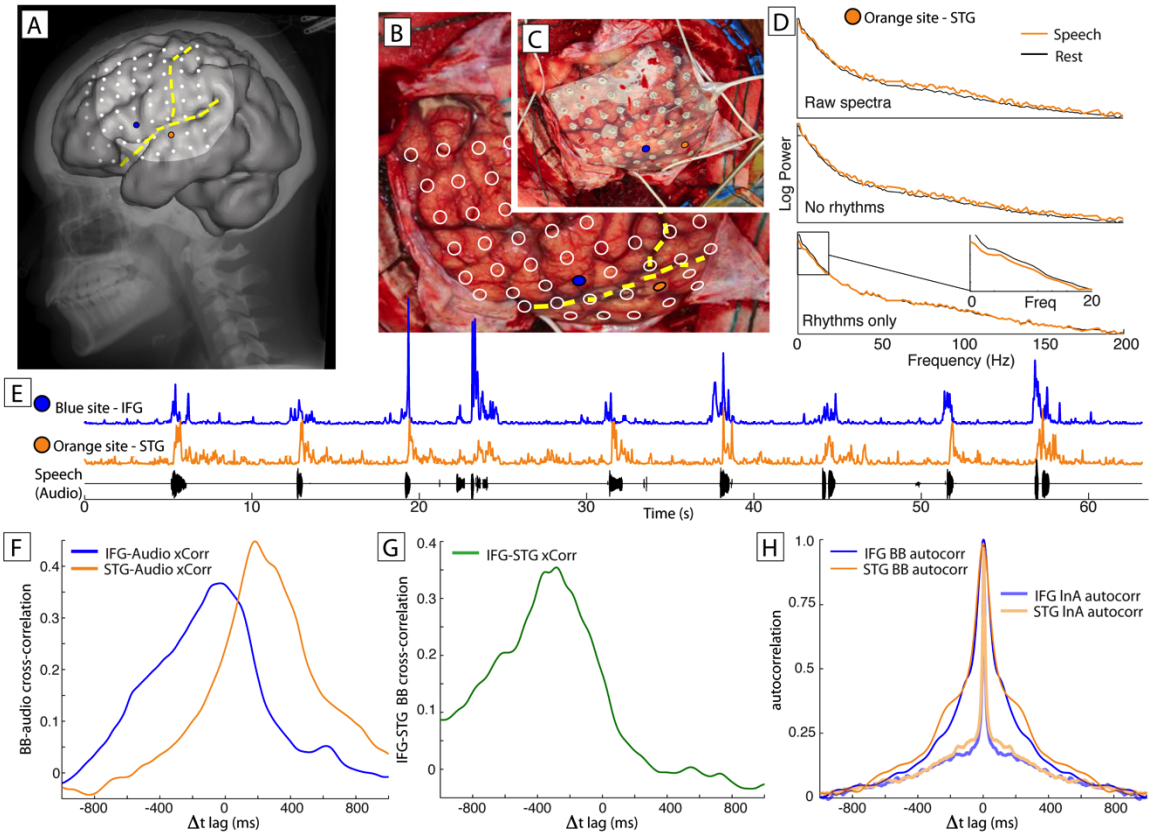


**Figure 4: Language and auditory area activity during verb generation. (A)** The cortical anatomy is shown, with the non-shaded region representing the area of the exposed craniotomy, as seen in panels B and C. Yellow lines indicate the Sylvian fissure and the central sulcus. The blue dot is an electrode site in the inferior frontal gyrus (IFG) - Broca area (Brodmann area 44). The orange dot is an electrode site on the superior temporal gyrus (STG - Brodmann area 22). The white dots are the locations of the remainder of the electrode sites. **(B)** The locations of the electrodes are shown on the exposed brain surface, and the craniotomy with the grid in situ is also shown **(C)**. **(D)** As illustrated previously, power spectral changes during different portions of the experiment (top panel) may be appreciated and naively decoupled into broadband (BB) changes (middle panel, 2nd-4th PSCs omitted) and changes in brain rhythms (bottom panel, 2nd-4th PSCs only). **(E)** BB timecourses from IFG (blue trace) and STG (orange trace). Simultaneous audio recording is also shown (black trace). **(F)** The lagged cross-correlation between BB from the two ECoG channels and the envelope of the audio trace (absolute value of the Hilbert transformed signal) shows that IFG activity (Blue site) precedes speech by 30ms, while STG activity (Orange site) follows speech by 180ms. **(G)** Similar comparison of cross-correlation between the IFG and STG sites shows that IFG activity leads STG activity by 280ms. **(H)** The temporal fidelity and the ability of the varying BB can be estimated by examining the auto-correlations of the BB from the two sites. As would be expected, the unsmoothed lnA autocorrelation falls off much faster. Panels A-C modified from (Miller et al., 2011).

*Verb generation task* (Figure 4): Patients stated verbs that were connected to written nouns on a screen. "Event times," $\tau_q$, were denoted at times of speech onset or silent periods in between. For a full description of the task, see (Miller et al., 2011). The data have been analyzed differently in this manuscript from the original.

*Finger movement task* (Figure 5): Patients performed self-paced movements of individual fingers in response to simple visual cues. "Event times," $\tau_q$, were denoted at times of peak finger displacements or points of rest. For a full description, see(Miller et al., 2012b) and (Miller et al., 2009d).

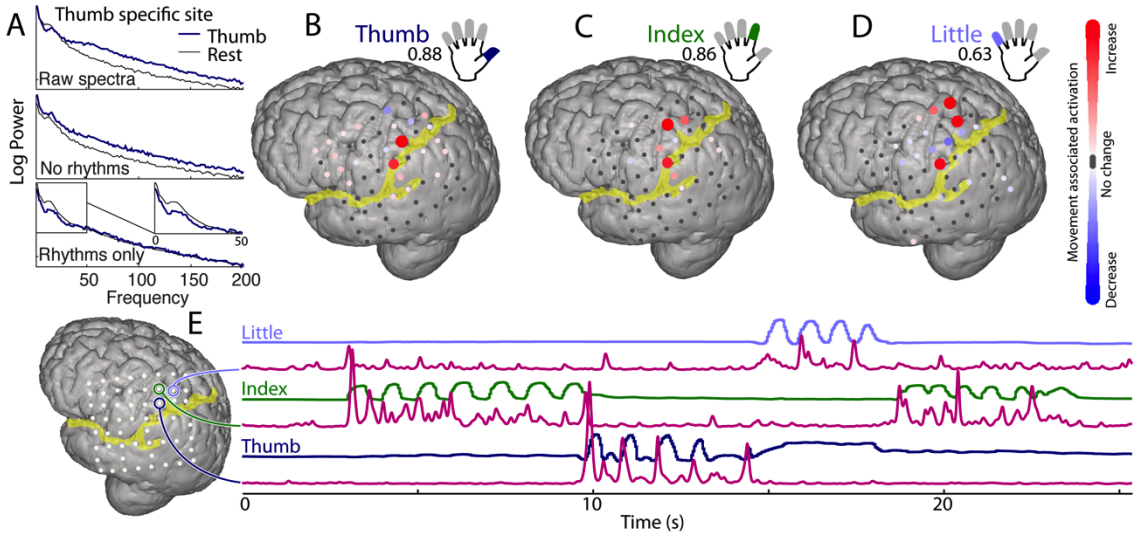


**Figure 5: ECoG broadband power resolves somatotopic representation of fingers.(A)** Power spectral changes, raw and decoupled, during thumb movement and rest. **(B-D)** Changes in broadband at different cortical sites for movement of thumb, index, and little finger, are each compared with rest. Colors denote a signed $r^2$ measurement of increases and decreases in power with movement relative to rest (individually scaled with maximum noted below each label). **(C)** Traces of thumb (dark blue), index (green), and little finger (light blue) flexion, with corresponding timecourse of broadband spectral change (pink) for 3 pre-central cortical sites. Note that broadband timecourse from each site is remarkably specific for the flexion of only one finger. Figure partially modified from the supplement of (Miller et al., 2012b).

# Results and Discussion

## Decoupling the cortical power spectrum to reveal broadband spectral changes

The decoupling approach illustrated in Figure 1 is used to identify which spectral components covary as the PSD changes over time. The covarying frequency components are referred to as motifs. The strength of the linear spectral decomposition is that it makes few assumptions regarding the underlying structure of the motifs, except that they are orthogonal. The most robust phenomenon in the PSD, seen in every motif decomposition and across five different tasks, is a broadband increase that is roughly even in magnitude across frequencies when plotted in log space (Figures 1-5). In addition, there are task-related changes in the amplitude of low frequency rhythms (usually but not always decreases), with a center frequency that varies across cortical locations.

Because the low frequency rhythms do not completely decohere during tasks, there is typically residual amplitude in the peaked portions of the PSD during task engagement. The naïve mechanism used in this manuscript does not assume the form for the underlying spectral motifs, and the underlying rhythms are frequently present in the background shape of the "broadband" decoupled.

We include an illustration and description of the decoupling technique so that the reader may gain an intuitive understanding for how a broadband motif in spectral changes emerges naively. This method is important from a conceptual viewpoint because it illustrates that a 'band-independent' motif across many frequencies is specific for the dynamics of functionally diverse neuronal populations in different brain areas and across different tasks. From a practical viewpoint, filtering for a "high frequency band" (HFB) may capture a majority of the variance in broadband spectral change. Although the extracted broadband was demonstrated to vary with behavior more closely than with HFB changes ((Miller et al., 2009c), Supplemental material), the decoupling process is more analytically burdensome. For practical purposes, isolating HFB changes is a

reasonable and appropriate approximation of the broadband change. For example, HFB power in the 76-100 Hz range approximated the broadband component of intracranial peri-Rolandic recordings ((Miller et al., 2009d), Supplemental Figure 15). However, we emphasize the specific HFB frequency range will vary depending on sites and recording systems, and should always be selected after inspecting the power spectrum for peaked rhythms and signal-to-noise characteristics. In conclusion, when interpreting HFB changes, it is essential to make the distinction between asynchronous broadband change (reflecting a population-averaged stochastic process) and synchronized rhythmic change (reflecting some coherent property of cortical microcircuitry).

## Linking behavior to asynchronous broadband activity across tasks and brain regions

As shown in Figures 1-5, broadband spectral change reflects selective activation of local cortical circuits across many tasks and brain areas. In Figures 1 and 2 we see that, broadband responses within the fusiform and parahippocampal gyri track the presentation of visual stimuli (such as faces and houses) on a single stimulus basis with high temporal fidelity. Furthermore, the category-specific nature of these inferotemporal loci is sufficiently robust that the stimulus category can be classified on individual trials by simple inspection of the response trace. Of the 300 presentations of face and house pictures for the patient in Figure 2, all 300 were correctly identified from the spontaneous stream of data (with 22 false positives, (Miller et al., 2009a)). The correct face or house label could be identified with 95% accuracy, with 23ms precision (23ms standard deviation).

In peri-calcarine cortex (Figure 3) the broadband time series reveals an activated dynamical state during visual search, but not while resting or staring at a blank screen. Within each cue period, there are broadband fluctuations that presumably reflect individual saccades associated with gaze shifts required for the individual elements of task performance – finding the target box, making a saccade to the arrow, returning to the target, and then identifying the appropriate color.

Broadband changes also reveal the fine temporal dynamics of speech and language in frontal and temporal areas (Figure 4). An intracranial recording from Broca's area shows broadband activity that immediately precedes speech during verb generation. Conversely, recording from a superior temporal gyral auditory site shows broadband increase following the onset of speech production. Examining the temporal cross-correlations of broadband spectral change and the speech envelope, we see that inferior frontal gyrus (IFG) activity precedes speech by 30ms, while superior temporal gyral (STG) activity follows speech by 180ms. Cross-correlation between activity from the IFG and STG sites shows that IFG leads STG activity by 280ms. The fact that 30+180<280 demonstrates that simplified cross-correlations cannot take into account complex temporal dynamics, and serve only as a first pass for interaction times between cortical areas and behavioral parameters. The cortical activity during speech at each of these cortical sites is sustained for multiple seconds (panel 4E), this 70ms discrepancy is likely explained by more complex within-trial dynamics. The falloff of the autocorrelation functions in Figure 4H suggest meaningful broadband signal change happens at well under 100ms.

Finally, as seen in the hand region of dorsal pre-central cortex, adjacent sites are highly specific for the movements of individual fingers, with minimal overlap, and robustly capture the dynamics of each individual finger flexion (Figure 5, from a larger study, detailed in (Miller et al., 2012b)). Close examination of the timing between motor cortex activity and movement onset of approximately 85ms (±39ms SD) (Miller et al., 2009d).

These data demonstrate, across five behavioral tasks and multiple cortical regions, that broadband power spectral change can be used to track local cortical activity, with meaningful resolution, at approximately the 20-50ms timescale. This suggests that broadband power changes in the ECoG potential are a generic marker of activation for populations of cortical neurons. Future studies will be required to demonstrate that broadband shifts are directly related to changes in population

firing rate throughout the cerebral cortex. However, in light of the conserved geometry of superficial pyramidal neurons, this relationship is likely to extend well beyond the occipital (Ray and Maunsell, 2011), temporal (Manning et al., 2009), and somatomotor (Mollazadeh et al., 2009) areas where it has been directly confirmed.

## The significance of the power law form of the broadband spectral change

As demonstrated previously, the ECoG cortical power spectral density has a power law form at high frequency, fitting tightly to $P(f) \sim 1/f^{\chi}$, with $\chi$=4 (Miller et al., 2009b). If low frequency oscillations are avoided, either by selecting cortical sites where they are absent, or removing them using a principle component approach, a two-Lorentzian form is revealed. A single Lorentzian form indicates the presence of stochastic activity with a particular biophysical timescale (Miller et al., 2009b); a double Lorentzian indicates the presence of two biophysical timescales within the circuit that generates the cortical surface potential. With behavior, there is a proportional increase at each frequency, e.g. $P(f,t) \sim A(t)P(f)$. This structure is important, because these two-Lorentzian forms can emerge generically from noise-like processes that have two simple correlation times (Sigeti and Horsthemke, 1987). Transmitted action potentials between neurons are approximately Poisson-distributed in time, and appear as a pure noise-like, Lorentzian, process when averaged over many neurons (Dayan and Abbott, 2001b). Laminar recordings, measured alongside the surface potential, suggest that the current source densities (CSD) in different cortical lamina are due to synaptic currents and ensuing current dipoles in the dendritic tree (Mitzdorf, 1985). In contrast, propagating action potentials in axons and axon terminals do not contribute strongly to the CSD at spatial scales of ~50-300 μm, the scale where CSD varies, setting up the dipole currents which the LFPs (and by extension ECoG potentials) measure. The *overall magnitude*, $A(t)$, of the measured power spectrum results from the averaging of many *input* action potentials to the population of neurons in the vicinity of a recording electrode. The *shape* of the power spectrum results from the combination

of two simple known neuronal processes (each with a characteristic correlation time and resulting Lorentzian form), such as: temporal integration in dendrites or soma, exponentially decaying membrane currents, low-pass RC filtering by tissue, or local network connectivity which, when modeled, produces precisely the measured form. The integer exponent of 2 in each $1/f^2$ term indicates an underlying stochastic process, suggesting that the ECoG signal does not resolve self-organized critical processes (which would be associated with non-integer exponents).

A simple single-neuron model for the generation of the cortical potential may provide insight into the two-Lorentzian form (Bedard et al., 2006, Miller et al., 2009b, Miller et al., 2010a). Two biophysical processes determine the spectral form: one process is the exponentially decaying post-synaptic current of fast-synapses (decay timescale 2.3ms (Sabatini and Regehr, 1996)), and the other process is the temporal integration and leakage of polysynaptic input in the dendritic tree (leakage timescale 100ms (Koch et al., 1996)). This is only one of many models that are consistent with the measured form, but it is parsimonious and empirically grounded. Our model suggests that broadband spectral shifts generically reflect changes in the input firing rate to a local neuronal population. It may be that inputs to more superficial lamina dominate, or that pyramidal neurons have a larger contribution than interneurons, or that, in some contexts, specific frequency ranges dominate because of peculiarities of local circuitry (Cunningham et al., 2003, Buzsaki and Draguhn, 2004, Rotstein et al., 2005, Steriade, 2006, Tiesinga et al., 2008, Sohal et al., 2009). Additionally, inter-spike temporal correlations will be important at smaller spatial scales. However, the internal correlations between neuronal events are likely to be lost by averaging over large spatial areas, and the spectral changes that we measure using subdural macro-electrodes generically inform us about the overall number of events taking place in the neuronal population.

This hypothesis was tested explicitly by comparing spiking rate to both band-limited and broadband power spectral changes in human microelectrode recordings (Manning et al., 2009). The best predictor of firing rate was the broadband feature of the PSD. This relation was robust,

significant, and reproduced across a large number of individuals and brain sites. Several years later, this was reproduced in non-human primates, with similar results (Ray and Maunsell, 2011), and in a setting where the broadband component was concretely distinguished from the narrow-band occipital gamma rhythm.

When extracted, this broadband spectral change then likely reflects mean firing rate, spatially averaged over the neuronal population beneath. If the size of the electrode is made smaller, then fewer neurons are being averaged over. The resolution of cortical representation is directly tied to the electrode size and density of spacing. By intrinsically averaging over many stochastic synaptic inputs, broadband spectral change reveals a robust correlate of local cortical activity on the single trial basis, with high temporal fidelity.

## Examples of genuinely rhythmic high-frequency activity

We have emphasized the ubiquity and significance of broadband power shifts, and have suggested that (apparently) band-limited spectral changes in the high-gamma range may in many cases actually reflect a broadband shift. However, there are also functionally critical processes, such as hippocampal sharp wave ripples (Okeefe and Nadel, 1979, Buzsaki et al., 1983, Ylinen et al., 1995), that have genuine high-frequency oscillatory signatures. Other examples include the gamma rhythm in the occipital lobe, which can be observed at frequencies as high as 90 Hz (Figure 1H) (Womelsdorf et al., 2006, Ray and Maunsell, 2011) and which appear to be related to the intrinsic timescales of interneuronal activity (Traub et al., 2001).

Rhythmic and non-rhythmic processes in the high-frequency range may co-occur, if, for example, synchronization of one subpopulation co-occurs with asynchronous firing in another subpopulation of neurons. Therefore the development of tools for separating synchronous and asynchronous processes is crucial. A separation method based on power spectral covariance was illustrated in Figure 1, and other tools based on signal coarse-graining (Yamamoto and Hughson, 1993) have also been employed. It is crucial to test the performance of these methods in cases

where the asynchronous broadband component deviates from its expected form (e.g. if it does not precisely follow a power law).

The implication of broadband power shifts will also vary as a function of the spatial geometry of the electrode. When recording with penetrating electrodes, sharp edges in the field potential (due, e.g., to individual action potentials) may introduce wide-band energy into the spectrum. Depending on their spectral profile, these edge-induced bursts may be difficult to distinguish from the asynchronous broadband shifts that reflect population activity (Scheffer-Teixeira et al., 2013). However, when recording with surface electrodes as in the examples shown here (Figures 1-5), the possibility of spike contamination is dramatically reduced, as the signal is aggregated across hundreds of thousands of neurons, and is dominated by currents in proximal apical dendrites (Mitzdorf, 1985).

It has been shown in a variety of behavioral settings that the amplitude of this broadband spectral change is modulated by the phase of low-frequency rhythms — a specific instance of "phase amplitude coupling" (PAC) (Miller et al., 2010b, Miller et al., 2012b). As such, this modulation likely reflects a macroscopic index of well-known spike-field interaction (Traub et al., 2001, Buzsaki and Draguhn, 2004, Mollazadeh et al., 2009, Okun et al., 2009), and provides evidence that averaged spiking activity in widespread cortical circuits, reflected by this broadband, can be entrained with the phase of underlying rhythms.

## How broadband changes have gained attention

More than 40 years ago, Brindley and Craggs observed that the power in the 80–250 Hz frequency range of the electric potential time series from motor cortex was dynamically and somatotopically increased in adjacent motor areas during movement (Brindley and Craggs, 1972). This finding lay obscure and dormant for more than 25 years, until Nathan Crone and colleagues independently re-discovered that the high-frequency (~75-100 Hz) portion of the human ECoG potential was highly specific for the dynamics of different motor functions (Crone et al., 1998a). Although both groups

proposed that this high-frequency power was a correlate of specific cortical activity, the nature and relationship to underlying physiology was unknown. Crone's group has more clearly postulated that very local populations of neurons were selectively synchronized with one another at multiple fast timescales, in a spatially-overlapping tableau of microdomains, with the spatial scale of coherence falling off with increasing frequency, producing a $1/f$ shape in the PSD (Crone et al., 2011).

However, the lack of a clear upper bound in the difference between active and inactive spectra in motor cortex led to the hypothesis (Miller et al., 2007b), and later demonstration (Miller et al., 2009b, Miller et al., 2009d) that some behavior-related changes in the cortical spectrum do not correspond to synchronized populations of neurons, but are rather asynchronous and broadband in nature. As illustrated in Figure 6, these broadband spectral changes are often mistaken for band-limited changes. The broadband is obscured at lower frequencies by intersection with classic area-specific oscillations such as the α and β rhythms in visual and motor cortices ($J_0$ in Figure 6 (Miller et al., 2008)). At high frequencies, the power in the cortically generated electrical potential falls off rapidly as $P \sim 1/f^4$. Because all amplifiers have an intrinsic noise floor, the brain signal becomes lost in the instrument noise at an upper bound ($J_N$ in Figure 8 (Miller et al., 2009b)). When researchers observing only the $1/f$ correlate of local brain activity between $J_0$ and $J_N$, they may mistakenly refer to it as a band-limited "high-gamma power".

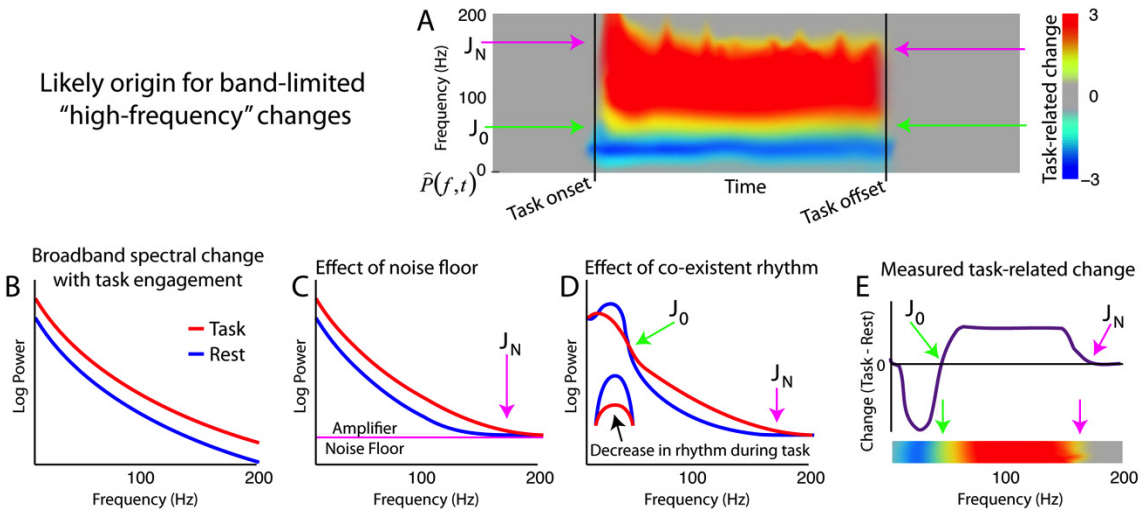


**Figure 6: Why "band-limited, high frequency" features may be seen in experimental data. (A)** Stereotypical time-frequency plot, with task-associated power increases observed in a wide frequency range, beginning at $f = J_0$, extending to $f = J_N$. **(B)** Shows idealized time-averaged broadband power-law spectra seen during task. **(C)** At high frequencies, the size of the amplifier noise floor drowns out the power in the electric potential due to cortical activity (we denote the frequency where this becomes relevant as $J_N$). **(D)** At lower frequencies, the presence of co-existent synchronous rhythms obscures changes in the asynchronous broadband, and there is a crossover in power between the task and rest spectra ($J_0$). **(E)** When the difference between task and rest spectra shown in (D) are plotted, it becomes clear why spectrograms have band-limited, task-associated, high frequency power changes: They are bound on the low end by $J_0$ and the high end by $J_N$.

Focusing on changes in particular frequency bands is practical and computationally expedient, but we suggest caution in interpreting spectral changes (especially those above 60 Hz) as changes in cortical oscillations. The oscillatory interpretation is most plausible when the high-frequency spectral shift is large and tightly band-limited, conditions which are rarely met in extra-cortical recordings. We propose that the first interpretation of a high-frequency change in the spectrum should be in terms of broadband spectral shifts. These broadband shifts, which can be characterized using the methods described above, are the signature of changes in asynchronous firing rate within local population, and they are therefore both expected and observed (Figures 1-5) in wide-ranging experimental settings. An advantage of this approach is that once a broadband shift is isolated, concurrent changes in the θ, α, β, and γ rhythms can be more readily and precisely observed.

## Conclusion

Having surveyed a variety of experimental settings, we reiterate the claim that the popular ‘‘high-gamma’’ range of the cortical electrical potential is widely misunderstood. In most cases, changes in spectral power in this band do not reflect changes in synchronous, rhythmic, actionpotentials in underlying cortex. We propose that, especially for recordings outside the cortex, spectral changes in this band most often reflect changesin asynchronous activity, which has a power-law spectral signature. This power-law process, observable via broadband spectral changes during behavior, likely correlates with the mean neuronal population activity. The data indicate that this broadband spectral signature is robustly linked to function across cortical areas and behaviors, thereby generically tracking the activation of cortical populations with high temporal fidelity.

# Chapter 3: Rhythmic entrainment of local population activity is dynamically modulated with task in visual cortex[6]

Brain rhythms are more than just passive phenomena in visual cortex. For the first time, we show that the physiology underlying brain rhythms actively suppresses and releases cortical areas on a second-to-second basis during visual processing. Furthermore, their influence is specific at the scale of individual gyri. We quantified the interaction between broadband spectral change and brain rhythms on a second-to-second basis in electrocorticographic (ECoG) measurement of brain surface potentials in five human subjects during a visual search task. Comparison of visual search epochs with a blank screen baseline revealed changes in the raw potential, the amplitude of rhythmic activity, and in the decoupled broadband spectral amplitude. We present new methods to characterize the intensity and preferred phase of coupling between broadband power and band-limited rhythms, and to estimate the magnitude of rhythm-to-broadband modulation on a trial-by-trial basis. These tools revealed numerous coupling motifs between the phase of low frequency (δ, θ, α, β, and γ band) rhythms and the amplitude of broadband spectral change. In the θ and β ranges, the coupling of phase to broadband change is dynamic during visual processing, decreasing in some occipital areas and increasing in others, in a gyrally specific pattern. Finally, we demonstrate that the rhythms interact with one another across frequency ranges, and across cortical sites.

[6] This chapter originally appeared as a manuscript in Frontiers of Human Neuroscience. Miller KJ, Hermes D, Honey CJ, Sharma M, Rao RP, den Nijs M, Fetz EE, Sejnowski TJ, Hebb AO, Ojemann JG, Makeig S, Leuthardt EC (2010). Dynamic modulation of local population activity by rhythm phase in human occipital cortex during a visual search task.*Front. Hum. Neurosci.* 4:197.

## Introduction

Recent electrocorticographic (ECoG) and local field potential (LFP) measurements have revealed a link between neuronal population activity and changes in broadband spectral power in the brain surface electric potential (Manning et al., 2009, Miller et al., 2009b, Whittingstall and Logothetis, 2009). This broadband change has been studied primarily by examining power at higher frequencies, where underlying brain rhythms (δ, θ, α, β, and low-γ) do not obscure behaviorally-modulated broadband changes (Brindley and Craggs, 1972, Crone et al., 2001, Edwards et al., 2009, Miller et al., 2009c, Hermes et al., 2010, Jacobs and Kahana, 2010), and more recently by decomposition of spectral changes to remove the rhythms (Miller et al., 2009d). These brain rhythms have long been known to fluctuate with behavior (Beck, 1891), but whether they reflect an active or passive agent in cortical computation has not been directly addressed until recently. Recent measurements have demonstrated that the phase of low-frequency rhythms modulates the amplitude of high frequency power in ECoG (Mormann et al., 2005, Canolty et al., 2006, Osipova et al., 2008, Penny et al., 2008, He et al., 2010). This finding implies that the physiological mechanisms underlying a particular brain rhythm are influencing neuronal population activity recorded at the cortical surface, and further investigation may therefore yield insight into large-scale information processing motifs in the brain. These previous studies have focused on phase modulation of broadband amplitudes on the timescale of minutes. The examination of modulation at finer temporal resolution may reveal how information is dynamically processed in the brain on the timescale at which neural circuits engage and disengage with transient stimuli.

With a single exception (He et al., 2010), previous reports of these types of nested oscillations have focused on coupling between the phase of a low frequency rhythm and a “high-gamma” range (Mormann et al., 2005, Canolty et al., 2006, Osipova et al., 2008, Penny et al., 2008, Cohen et al., 2009). Close inspection of the figures in these manuscripts indicates that this “high-gamma” may be

a reflection of broadband change, and not a band-limited γ-rhythm. It is important to draw a distinction between broad band activity and higher frequency γ-rhythm (>50Hz) amplitude changes as they may reflect distinct underlying physiologic phenomena. The γ-rhythm has been suggested to play a role in active computation in the brain by synchronization – associating distinct cortical sites coherently to facilitate computation (Singer, 1993, Fries et al., 2001, Womelsdorf et al., 2005, Womelsdorf et al., 2007, Siegel et al., 2008, Mitchell et al., 2009). In contrast to playing a specific computational role, the broadband power measured at an electrode reflects the average spike rate of the neurons that project to the local neuronal population of roughly $5*10^5$ neurons in the gray matter beneath each electrode (Manning et al., 2009, Miller et al., 2009b, Miller et al., 2010a). Any phenomena that are observed in the aggregate potential therefore reflect the general activity of this underlying population.

Universal functional properties are often attributed to band-limited rhythmic phenomena. In some cases, this might be biologically plausible – the θ rhythm, for example, may enable a central hippocampal mechanism to coordinate a distributed neocortical network during planning and memory retrieval (Mormann et al., 2005, Canolty et al., 2006, Tort et al., 2009). The α rhythm may reflect suppressive synchronization across visual cortex when there is no visual input at all (Osipova et al., 2008), and therefore not a major feature of our task (as described below), where the subjects' eyes were open throughout both visual search and ISI epochs. Emerging experimental results suggest that the α-rhythm may not emerge as a large scale brain feature in visual cortex until the signal is averaged over the larger spatial scales associated with EEG and MEG recordings (Edwards, 2010).

In this article, we lay out a general framework for examining modulation of local population activity by low frequency rhythms in the brain. A "phase-coupling palette" is constructed to visualize the

full range of coupling across a wide range of frequencies. We isolate particular frequency ranges, and demonstrate how trial-by-trial modulation can be quantified in a robust way using the "phase-coupling vector". These measures reveal numerous coupling motifs between low-frequency rhythms and broadband spectral change in human occipital cortex. This coupling changes dramatically on a trial-by-trial basis as individuals switch between engagement in a visual search task and fixation on a blank screen. Our findings suggest that rhythms have multiple influences, facilitating and suppressing the activity of cortical populations of neurons. Within a specific frequency range, these influences can be gyrally specific, releasing one area during visual engagement, while actively suppressing another.

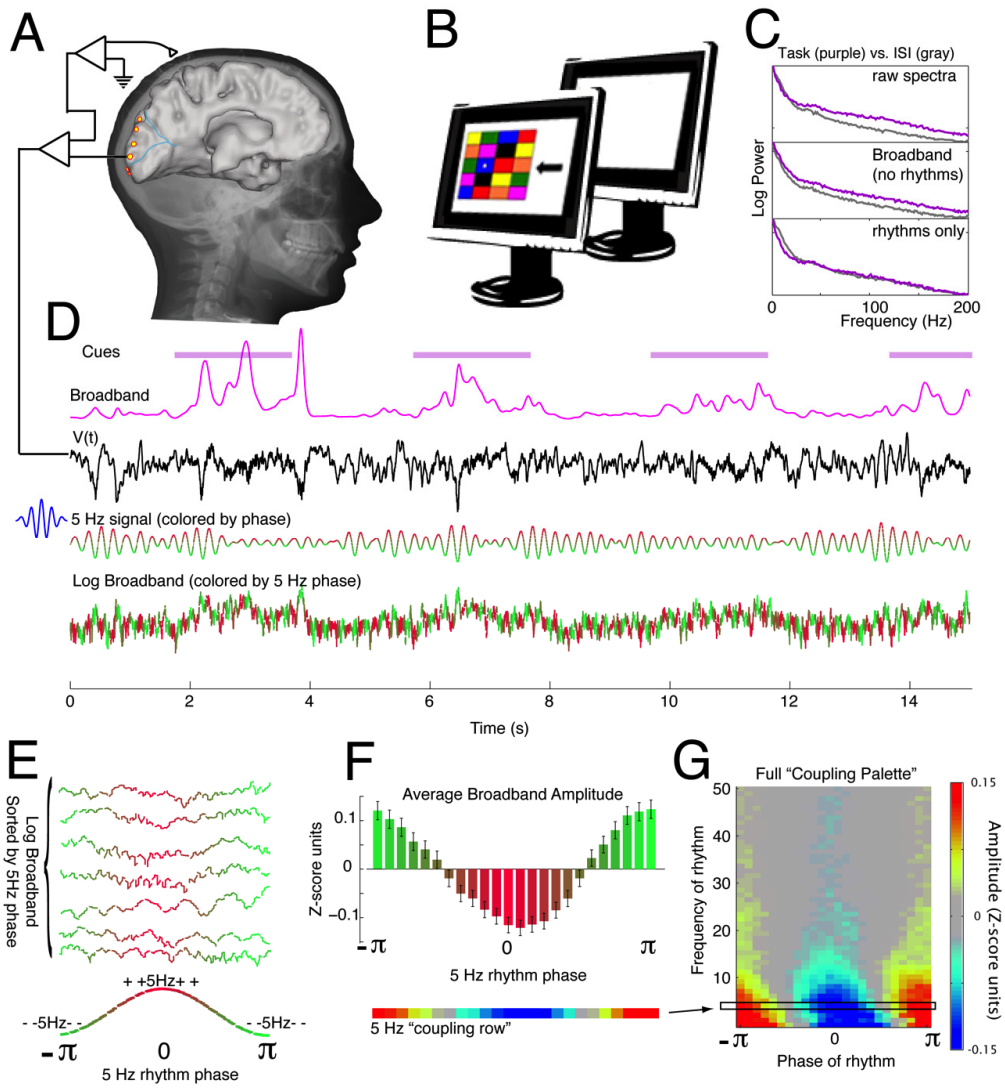


**Figure 1: Experimental approach. (A)** The electrocorticographic (ECoG) potential is measured from occipital lobe brain surface sites during participation in a visual search task (subject 4 shown here). **(B)** The visual search task consists of a 4-by-5 array of colored squares. Each cue consists of a star in one of the boxes (in this case a blue box), and an arrow. The subject states the color of the box in the direction of the arrow from the star ("green" would be the appropriate response in this case). Visual search cues are shown for 2 seconds, with blank inter-stimulus-interval (ISI) cues shown for intervening 2 seconds. **(C)** Power spectral changes during different portions of the experiment (top panel) may be appreciated and naively decoupled into broadband changes (middle panel, 2nd-4th PSCs omitted) and changes in brain rhythms (bottom panel, 2nd-4th PSCs only). **(D)** From the timeseries of the potential, dynamic, spectrally-broadband, fluctuations may be extracted (here shown smoothed). In this illustration, the 5 Hz portion of the signal is extracted using a 5Hz Morlet wavelet (here colored for phase – red denotes surface-positive, and green denotes surface-negative). The timeseries of the log of the broadband is shown, colored by coincident phase of the 5 Hz signal. **(E)** The timeseries of the log of the broadband is sorted by the coincident phase of the 5 Hz signal. **(F)** The average of the log-broadband amplitude (Z-score units, denoted $\chi_k$ in the methods) for each 5 Hz phase is shown, with errorbars denoting 3 times the standard error of the mean (3*SEM) for each phase. This can be appreciated in one dimension as the "5 Hz coupling row". **(G)** The process detailed in D-F is repeated at each frequency from 1-50 Hz, to obtain a full coupling palette, and to illustrate how the full range of low frequency rhythms modulates local brain activity (as captured by broadband spectral change).

# Methods

## Subjects

All 5 subjects in the study were epileptic patients at Harborview Hospital in Seattle, WA. Sub-dural grids and strips of platinum electrodes were clinically placed over frontal, parietal, temporal, and occipital cortex for extended clinical monitoring and localization of seizure foci. Each subject gave informed consent to participate in an Institutional Review Board approved experimental protocol. All patient data was anonymized according to IRB protocol, in accordance with HIPAA mandate.

## Recordings

Experiments were performed at the bedside, using Synamps2 amplifiers (Neuroscan, El Paso, TX) in parallel with clinical recording. Stimuli were presented with a monitor at the bedside using the general purpose BCI2000 stimulus and acquisition program (interacting with proprietary Neuroscan software), which also recorded the behavioral parameters and cortical data. Sub-dural platinum electrode arrays (Ad-Tech, Racine, WI) were arranged as combinations of 8x[4,6,8] rectangular fronto-tempero-parietal arrays and 1x[4,6,8] linear temporal and occipital strips. The electrodes had 4mm diameter (2.3mm exposed), 1 cm inter-electrode distance, and were embedded in silastic. The potentials were sampled at 1000 Hz, with respect to a scalp reference and ground (Fig. 1A). These signals had an instrument-imposed bandpass filter from 0.15 to 200 Hz.

## Visual search task

Subjects participated in a visual search task presented on a LCD monitor ~1m away, in which 2s visual search stimuli were interleaved with 2s inter-stimulus-intervals (ISIs) during which the screen was blank. Each visual search stimulus (e.g. Fig. 1B) consisted of three parts: 1) a 5-row by 4-column array of colored boxes (~1cm by 1cm), 2) a white star positioned in the center of one of these boxes, and 3) a black arrow (~2cm by 1cm) centered ~1.5cm to the right of the rightmost box

in the middle row. In each visual search stimulus, the star appeared randomly in one of the colored boxes, and the arrow pointed randomly in one of 4 cardinal directions ("right", "left", "up", or "down"). The subjects' task was to state the color of the box that was adjacent to the star in the direction of the arrow. Since fixation was not constrained, and eye position was not measured, we cannot know whether differential effects between different arrow directions were due to attention or a late visual microsaccade between the star and the arrow, or different box position. It seems unlikely that we are measuring "motor processing" in visual cortex during visual search, but we cannot exclude this possibility. Because the uncertainty about attention vs. gaze-shift-driven neural activity limits our ability to examine the functional subcomponent of visual processing, the present study is agnostic to these distinctions, and is focused on the generic relationship between brain rhythms and cortical visual processing.

## Electrode localization

Cortical surface mesh reconstructions were made using pre-operative structural MRI. Electrode positions were calculated with respect to the structural MRI from post-operative computed tomography (CT) using the CTMR package of Hermes, et. al., 2010 (Hermes et al., 2010). When the MRI or CT was of insufficient quality, hybrid techniques involving x-ray were employed to obtain cortical rendering and/or electrode position (Miller et al., 2010a).

## Signal processing

Complex signals $\tilde{V}(f,t) = r(f,t)e^{i\phi(f,t)}$ at discrete frequencies, $f$, were extracted from the raw potential using Morlet wavelets, and complex signals representing a range of frequencies $\tilde{V}(F,t) = r(F,t)e^{i\phi(F,t)}$ were generated using a band-pass and then the Hilbert transform. The log of the decoupled broadband amplitude, $\chi(t)$, was also extracted from the raw potential, using the approach outlined in (Miller et al., 2009d). The methods for pre-processing, and other pre-

established signal processing, are detailed in the methodological appendix. Synthetic data were generated to validate the signal processing approach, and the methods to do this are also detailed in the appendix.

## Broadband coupling to low frequency phase (illustrated in Fig. 1D-F)

The coupling was estimated by calculating the average log-broadband amplitude $\chi(t)$ as a function of the rhythm phase $\phi$ in small phase intervals, $\chi_k = \langle \chi(t) \rangle_{(k'+1/2)>\frac{\phi(t)}{\pi}\geq(k'-1/2)}$ ,

where $k' = k - K/2$ ( $K$ total intervals). For example, for K=24 (the number used in these analyses), then $\chi_{13}$ represents the mean log-broadband when the phase of the low frequency rhythm is in the interval between 0 and $\pi/12$. The center of each interval is denoted $\phi_k$, so $\phi_{13} = \pi/24$. To get a full picture of the strength and preferred phase of coupling across a range of frequencies, the wavelet-obtained rhythms at each frequency are used to build up a "palette" of $\chi_k$ at each frequency. This has an advantage in that ranges of coupling and distinct coupling to different rhythms are revealed, in many cases, as separate phenomena, because there are different preferred phases of coupling.

## The coupling vector and trial-by-trial statistics (illustrated in Fig. 2)

To condense the range of frequencies composing a given rhythm into one measure, the Hilbert transform was applied (as described above), with frequency range chosen based upon inspection of the palette. This allows for the calculation of a "coupling vector" by taking the dot product $Z_{\text{mod}} e^{i\phi_c} = \frac{1}{2K}\sum_k \chi_k e^{i\phi_k}$ . $Z_{\text{mod}}$ is the magnitude of coupling between phase of the rhythm and the log-broadband amplitude (because we z-score $\chi(t)$, $Z_{\text{mod}}$ is roughly the amount of variation in the z-score that correlates with the phase of the rhythm concerned), and $\phi_c$ is the preferred phase of this interaction. This can be calculated on a trial-by-trial basis, breaking up the data into smaller epochs (2s trials in our case) and calculating a coupling vector for each trial. To assess the distribution of

coupling for $N$ trials of a given type, one cannot simply compare the contribution of trial $n$ to the distribution of coupling values as $Z_{\text{mod}}(n)$ because if $\phi_c$ is not reproducible from trial-to-trial, then $\overline{Z_{\text{mod}}(n)}$ can be a large value even on trials in which the coupling preferred phase is opposite to that of the majority of other trials in the distribution. In other words, the fact that $\overline{Z_{\text{mod}}(n)}$ could be nonnegative would strongly bias the distribution of $\overline{Z_{\text{mod}}(n)}$ values so that the mean of the distribution can be significantly greater than zero even when there would be no underlying coupling of consistent phase. For this reason, the distribution of values $Z^q_{\text{mod}}(n) = Z_{\text{mod}}(n) * \cos\left(\phi(n) - \overline{\phi^q}\right)$ is used, where $\overline{\phi^q}$ is the preferred phase of the mean coupling vector for trials of type $q$: $\overline{Z^q_{\text{mod}}} e^{i\overline{\phi^q}} = \frac{1}{N}\sum_n Z_{\text{mod}}(n) e^{i\phi(n)}$. The quantity $\overline{Z^q_{\text{mod}}}$ can be negative or positive and can therefore have a distribution significantly overlapping with zero (indicating an absence of reliable phase modulation). For each type of trial, the distribution of coupling can be assessed using the distribution $Z^q_{\text{mod}}(n)$. We demonstrate the significance of these measures using error bars which represent 3 times the standard error of the mean. Note that if all trials are of type $q$, then the average coupling vector across trials is the same as the coupling vector of the full timeseries. This method has an advantage over the "large-time shift" bootstrapping approach (Penny et al., 2008) because the data may be segregated into smaller time trials, and statistics may be computed by comparing the distribution of values for trials of one behavioral state versus trials of a different behavioral state. It may also be used to compare discontinuous trials of one type (or all trials concatenated) versus 0. This allows us to examine significant shifts in phase amplitude coupling during different trial types (where $q$="ISI", vs $q$="right", etc.) and also to assess the significance of each independently versus zero. One might in principle look for shifts in the distribution of preferred phase, but this is only meaningful in the case that significant coupling versus zero has

been established independently for each of the two distributions. We defer examination of task-related shift in preferred phase to future studies.

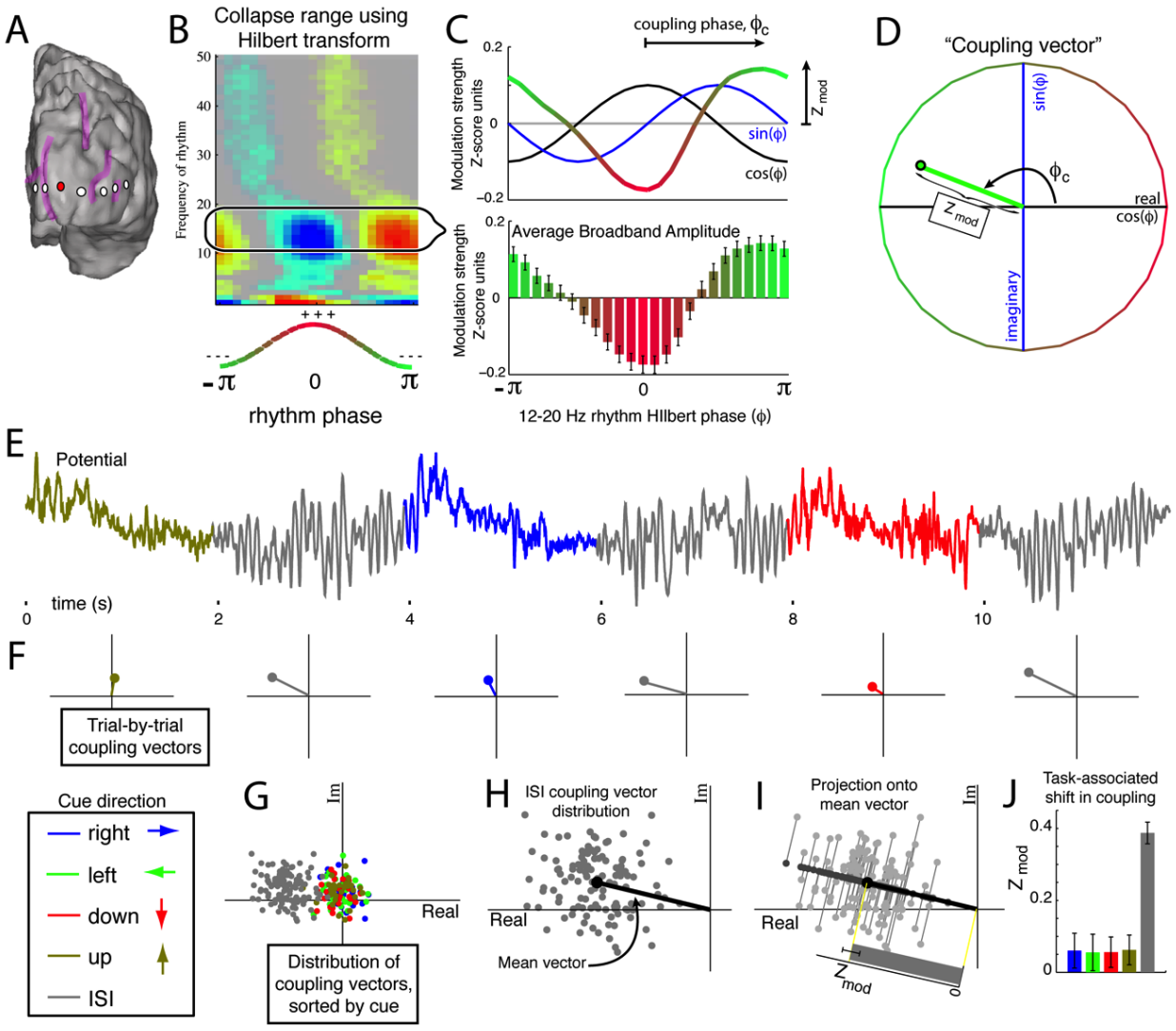


**Figure 2: The "coupling vector" and trial-by-trial characterization of modulation. (A)** A selected electrode (orange) on the Subject 5 cortical surface. **(B)** The coupling palette for this electrode. Phase-amplitude coupling across a range of low-β band frequencies (12-20 Hz), rather than at a single frequency, may be captured using the Hilbert transform rather than Morlet wavelets. **(C)** Coupling of broadband power to the Hilbert phase of the band-passed 12-20 Hz signal. The lower panel shows the mean amplitude (+/- 3*SEM) of broadband for each Hilbert phase (ϕ) of the 12-20 Hz signal. The dot-product of this mean with an exponential of the form $e^{i\phi}$ reveals the coupling phase and magnitude of the modulation ($Z_{mod}$ – the portion of the Z-score of broadband power modulation with the phase of the 12-20 Hz rhythm). This calculation can be appreciated visually by taking the dot-product of mean broadband power with $\sin(\phi)$ and $\cos(\phi)$ independently, since $e^{i\phi} = \cos(\phi) + i\sin(\phi)$. **(D)** The "coupling vector" reveals the magnitude, $Z_{mod}$, and phase, $\phi_c$,

of the modulation of broadband activity by the 12-20 Hz rhythm in the complex plane. **(E)** The potential trace can be broken up into cue periods of visual search in different directions (colors) plus ISI periods (gray). **(F)** From each cue period, a single trial coupling vector can be obtained. **(G)** Plotting the distribution of coupling vectors across all cues reveals stronger coupling during ISI periods than during active visual search. **(H)** For a given epoch type (in this case, ISI) a mean coupling vector (e.g. $\overline{Z_{\text{mod}}} * e^{i\bar{\varphi}}$) may be obtained. **(I)** The distribution of coupling values for each epoch can then be obtained by projecting their coupling vectors onto the epoch mean vector direction; for the $n^{th}$ trial, the magnitude of coupling contributing to the distribution of coupling values is $Z_{\text{mod}}(n) * \cos\left(\varphi(n) - \bar{\varphi}\right)$. Using the distribution of $Z_{\text{mod}}(n)$ alone biases the distribution to higher mean coupling values that wouldn't be appropriate if there is no reproducible phase coupling. **(J)** Coupling strength for each cue type, projected onto its own mean coupling vector. The error bars indicate 3*SEM. The error bars for visual search are typically larger than for ISI since there are 4 times more ISI cues than visual search cues in any particular direction. In this case, the coupling is strong and significant during ISI periods, and greatly reduced during all directions of visual search.

### Cross-rhythm interaction

We also calculated the interaction between the 4-8 Hilbert phase $\phi$(4-8Hz,t), and the 12-20 Hz analytic amplitude $_r$(12-20Hz,t). This was done in the exact same fashion as for the $\phi$ to $\chi$ comparison, replacing $\chi$ with $_r$(12-20Hz,t). There are many such inter-rhythm interactions [e.g. (Lakatos et al., 2005, Osipova et al., 2008, Cohen et al., 2009, Tort et al., 2009)], but we defer further explorations of these to future studies.

## Results

### Task-specific changes in the raw potential, the amplitude of rhythms, and in decoupled log-broadband spectral change between visual search and inter-stimulus interval epochs

*Averaged power spectra:* The averaged power spectral density (PSD) during visual engagement and ISI exhibits a general 1/f shape, with superimposed rhythms that deviate from this 1/f structure at particular frequencies. During behavior, these averaged PSDs most commonly reveal decreases in power in the classic θ (~4-8Hz), α (~8-12Hz),and β (~12-20Hz) rhythms during visual

engagement, and increases in power in the γ rhythm (30-50Hz), and in broadband change (Fig. 1C, 4H-I).

*Dynamic power spectra:* The dynamic spectra shown in Figs. 4 and 5 reveal that there are both broadband spectral changes, and corresponding increases and decreases in the θ/α/β/γ ranges associated with the onset of visual search stimuli.

*Decoupling the cortical power spectrum:* A principal component decomposition of the PSD clustered rhythmic, spectrally peaked, phenomena in the 2nd-4th principal components (Fig. 1C). Reconstruction of the PSD without these components revealed broadband spectral change, across the entire frequency domain, with an approximately 1/f structure. This broadband phenomenon is distinct from a higher γ-rhythm occurring as a peaked activity at 50Hz and above (see Fig. 4H-I).

*Extraction of time-varying broadband change:* A time-varying estimate of broadband spectral change was obtained by projecting the dynamic spectrum into the first principal spectral component (Fig. 1D). The broadband change approximates the time-varying amplitude function $A(t)$ in the power-law relationship: $P(t) \sim A(t)\frac{1}{f^{\chi}}$. In early visual areas of the occipital cortex (peri-calcarine and occipital pole), this phenomenon is augmented throughout the entire visual search task, and most strongly so at cue onset (Figs. 4 and 5). In other areas, such as portions of the lingual gyrus, this phenomenon is suppressed (Fig. 5H). This broadband measure is a robust correlate of local cortical activity (Manning et al., 2009, Miller et al., 2009b, Miller et al., 2009d, Miller et al., 2010a) and its modulation by the phase of low-frequency rhythms is the focus of this paper.

*Event-related potentials* The event-related potentials reveal characteristic voltage deflections at the onset and offset of visual stimuli. These were transient and non-specific, and present whether the corresponding broadband signal increased or decreased (Figs. 4 and 5).

*Trial-by-trial amplitude measures:* The average and 3*SEM amplitudes of epoch-averaged broadband change reveal both increases and decreases (Figs. 4 and 5) during visual search periods when compared with ISI epochs. Early visual areas show characteristic increases in power, while

other areas show decrease. As shown in Fig. 4, these trends cluster by gyral location. Amplitudes of the 12-20Hz amplitude (Figs. 4 and 5) also reveal both task-related increases and decreases in amplitude during visual search engagement, but these are not linked to broadband change in any simple way. There is task-related increase in the 4-8 Hz amplitude (Fig. 5) – although this phenomenon was not universal across subjects nor brain area.

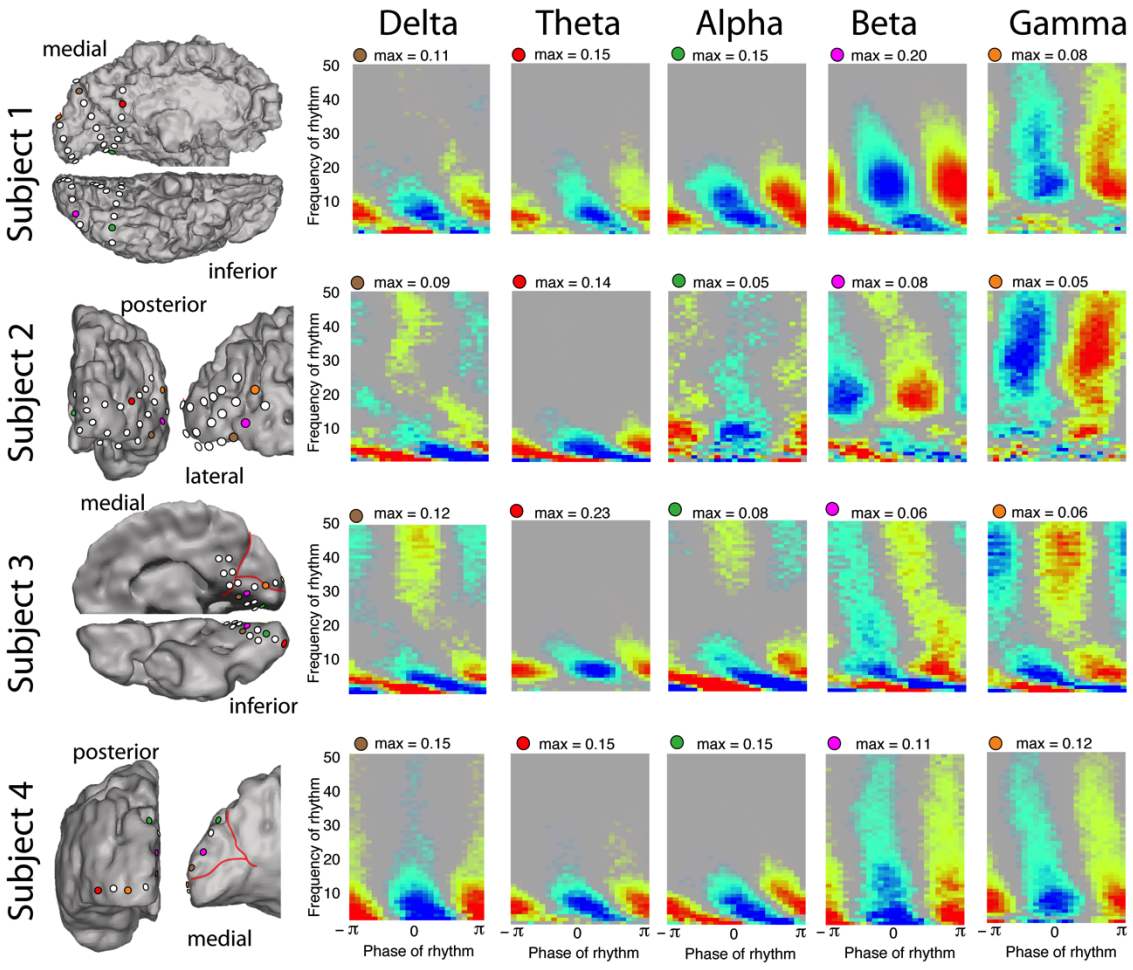


**Figure 3: Coupling to different rhythms in different subjects.** Each row represents the palettes from 5 different electrode sites in subjects 1-4, respectively (site location color coded on the rendered brain surface). The palettes illustrate that local cortical activity (as revealed by broadband spectral change) is modulated by the δ/θ/α/β/γ rhythms in each case. Note that at many electrodes we observe coincident modulation of broadband power by multiple rhythms with distinct phases of preferred coupling. In Subject 4, each of the palettes shown in the δ/θ/α coupling columns exhibit phase-amplitude coupling in all of those bands (δ/θ/α), and could each have been used to exemplify phase-amplitude coupling in any of the bands. All palettes for subject 5 are shown in Fig. 4, where coupling to δ/θ/α/β/γ rhythms can also be observed.

## There are numerous coupling motifs between low frequency rhythms and broadband spectral change

Figure 1 demonstrates that robust modulation of broadband power can be identified across a range of different rhythms by visualizing palettes of rhythm-to-broadband coupling. These palettes display the range of frequencies that are coupled, and the predominant phase of this coupling. Figure 3 shows a strong and significant modulation of broadband spectral change with the phase of low frequency rhythms in the δ/θ/α/β/γ ranges, and the relative magnitude of each change at different sites in occipital cortex. These modulatory rhythms often superimpose at the same cortical sites, and can often be appreciated as separate phenomena by the different preferred phase of coupling.

- δ (~1-3 Hz) most often has a preferred coupling phase of $-\pi/4$ to $-\pi/2$, although there are clear exceptions in subjects 4 and 5 (leftmost lower palette in Fig. 3, and panel D in Fig. 4) where the preferred phase is $\pi$.
- θ (~4-8Hz) has a preferred coupling phase of $\pi$ which appears robustly across subjects and electrodes. (Although Fig. 4G is a notable exception in this and other rhythm cases).
- α (~8-12Hz) most often has a preferred coupling phase of $\pi/2$ to $3\pi/4$, although this is not universal.
- β (~12-20Hz, "low-β" although particular range appears variable between sites) most often has a preferred coupling phase of $3\pi/4$. There are notable exceptions to this (Fig. 3 – row 4, column 2; Fig. 4G)
- "Canonical γ" (30-50Hz) coupling is observed in Figs. 2-4 with various preferred phases.

It is possible that, in some cases, the smooth, continuous, "diagonal bands" visible in the lower frequencies of the phase-coupling palettes (δ, θ, α bands) may not reflect a set of distinct couplings

between band-limited low-frequency rhythms and broadband power. Instead, they may reflect a process in which broadband power is elevated at a fixed time lag relative to the peak of the voltage trace, and this fixed time lag then appears as a continuously varying phase lag across different low-frequency bands.

## The amplitudes and phases of rhythms in adjacent cortical sites are correlated with one another

As shown in Fig. 4J, the phase coherence in the 12-20Hz range is strong and significant in adjacent sites throughout the 7-electrode strip for subject 5 (note that this is not simply a result of re-referencing, because 63 electrode sites contributed to the common average, not just the 7 shown). This coherence is significant throughout, but is less during visual search task – which might partially be a product of the lower rhythm amplitude in a noise-like background. The coherence is sustained better across neighboring electrodes on the same gyrus. The correlation in the time course of the amplitude of the rhythms in adjacent electrodes is also significant (Fig. 4K), and is significantly increased during visual search engagement in only 3 co-gyral electrodes (sites B-D).

## The broadband amplitude is significantly modulated by the phase of low frequency rhythms

When the potential time series is separated into behaviorally-relevant epochs (as described in Fig. 3), there is significant modulation during both visual search cues and inter-stimulus intervals. This is shown explicitly for a 4-8Hz band and a 12-20Hz band (Figs. 4 and 5).

## The modulation of broadband power by rhythm phase shows task-dependent increases and decreases

The 12-20Hz range simultaneously shows both increases and decreases in modulation with engagement in the visual search task, and these patterns cluster gyrally (Figs. 4, 5). The visual-

search induced modulation decreases are most often associated with "active" brain areas, where broadband power increases during visual search (Fig. 2).

## The phase of one rhythm can also modulate the amplitude of another, in a task-dependent manner

In each subject, modulation of the 12-20Hz amplitude by the 4-8Hz phase was observed, and changed during visual search in some cases (Figs. 5 and 6). Such inter-rhythm modulation appeared in at least one site in every subject, but was not present in most sites.

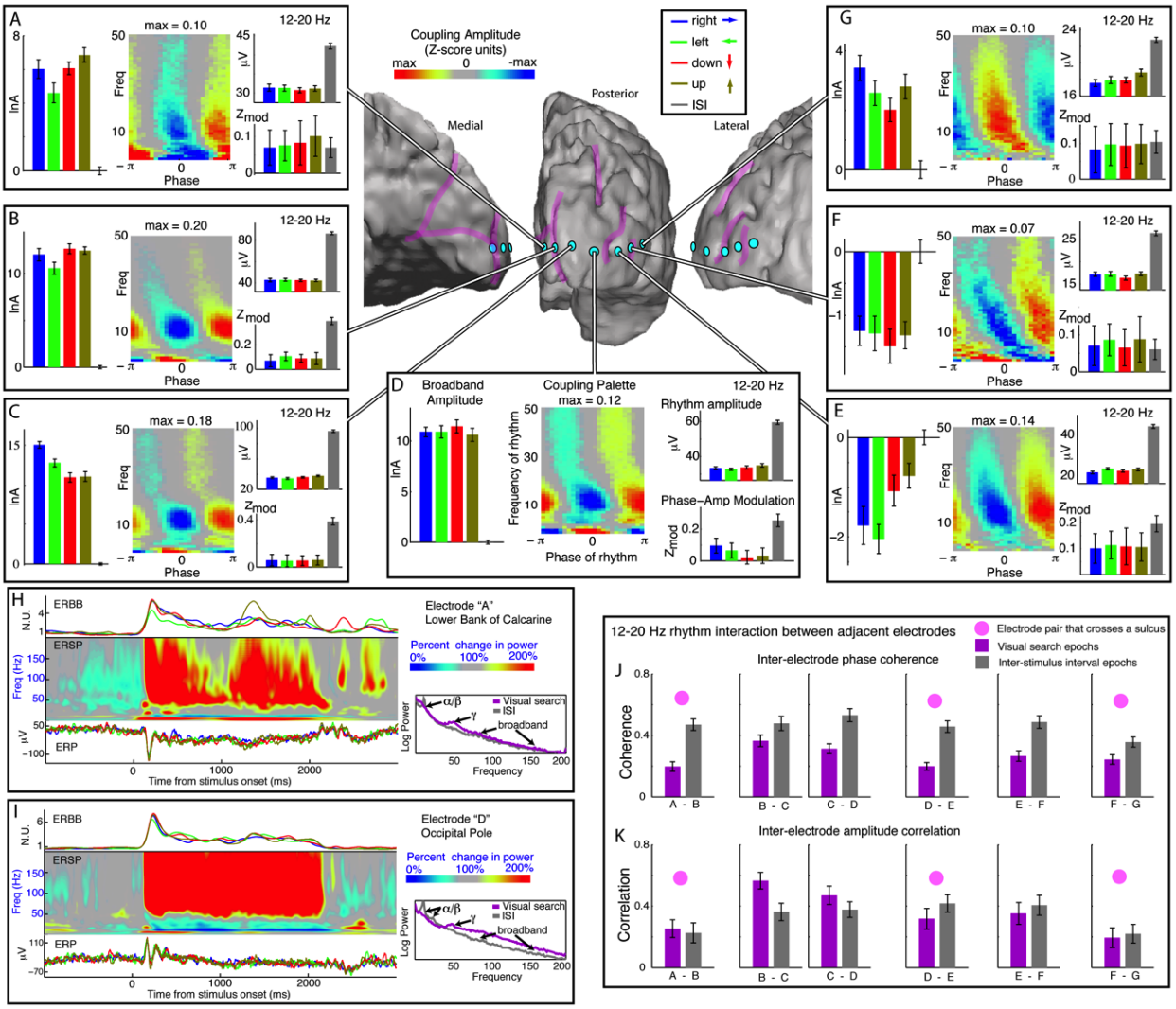

**Figure 4: Coupling across occipital cortex, in Subject 5, with a focus on the β-range (12-20 Hz). (A-G)** Each of 7 surface electrodes is shown on an electrode strip beginning in medial, peri-calcarine, occipital cortex, extending laterally around the occipital pole into the lateral occipital gyrus. The left-most series of bars in each panel is the log-broadband amplitude, in Z-score units, with the mean of ISI periods subtracted out. Errorbars represent 3*SEM. The right-most error bars, flanking the horizontal origin, represent the variation during ISI periods. The medial 4 and the most lateral electrodes (e.g. A-D, G) all show increased local cortical activity during visual search, while the 5$^{th}$ and 6$^{th}$ electrode sites show suppressed activity during visual search (these two share gyral location). The palettes show average coupling across all cues. All sites have strong and significant coupling to the 12-20 Hz (β) range. The upper-right axes within each panel show the amplitude of the 12-20 Hz rhythm during different cue types. There is a lower amplitude during visual search engagement in every case. The 12-20 Hz modulation of broadband amplitude, however, is selectively suppressed during task engagement in the B-D sites, which share common gyral location. **(H)** Dynamics of visual response from the electrode highlighted in panel A. On the Left: The upper trace is the average event-related broadband (ERBB) for each of the cue types. The middle plot is the average dynamic spectrum for all active sites combined called the "event related spectral perturbation" (ERSP). The lower plot is the event related potential (ERP) for each cue type. On the right, the changes in the mean spectrum during visual search (red) and ISI (blue) are shown. Note the so-called "event-related desynchronization" in the α/β rhythm range, and "event-related synchronization" in the γ–range (Pfurtscheller, 1999). Broadband change, though small, is present throughout – although it is covariant with the γ-rhythm change, it is a distinct entity. **(I)** Same analysis as in H, for the electrode highlighted in D. Broadband change is strong and robust, with α/β-ERD and γ-ERS. In this case, the broadband change is large compared with the γ-rhythm ERS, although both can still be seen. The change at this site was representative of all 3 occipital pole electrodes – sites B-D. **(J)** Inter-electrode phase coherence in the 12-20Hz range. **(K)** Inter-electrode amplitude correlation in the 12-20Hz range.

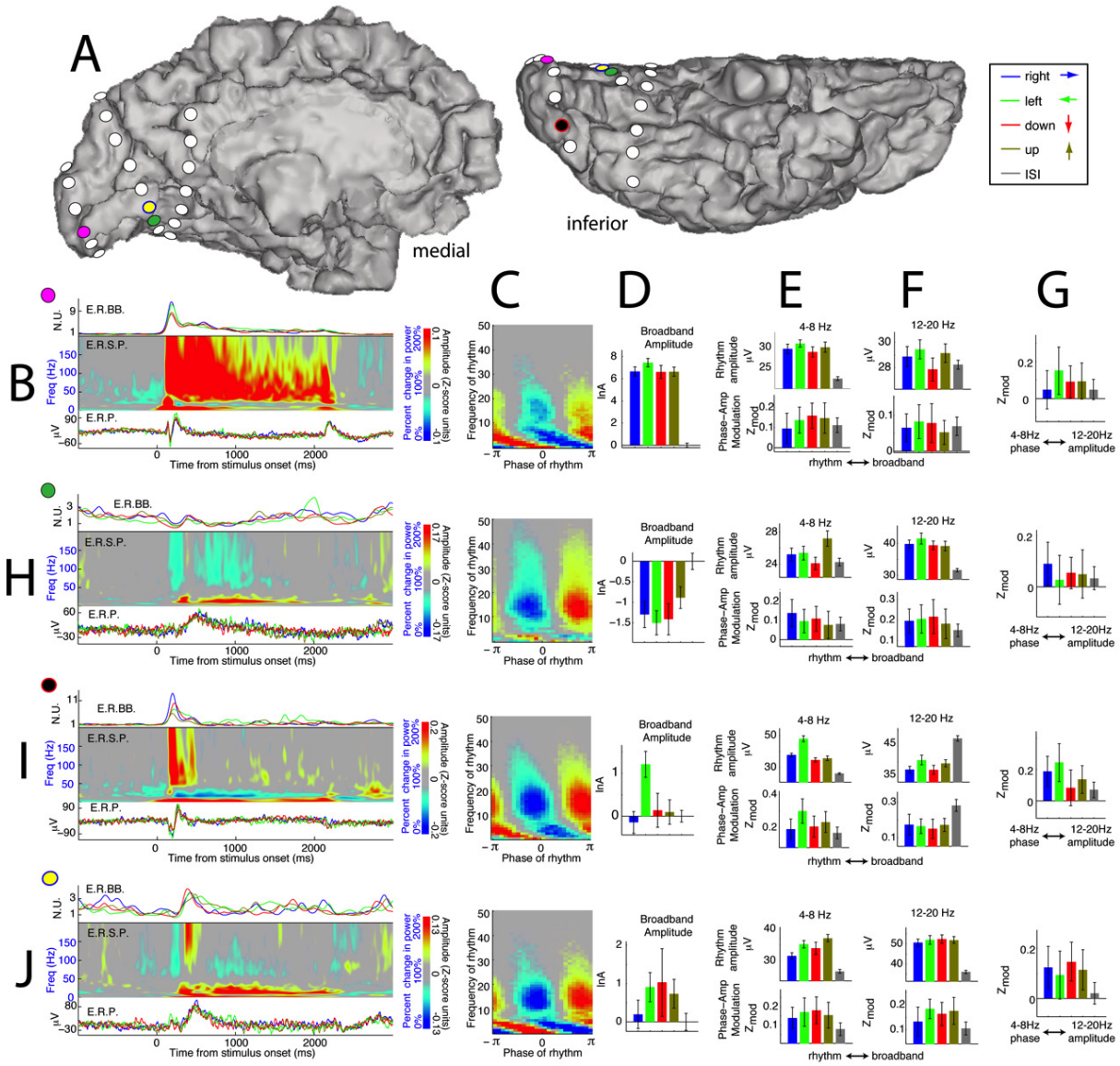


**Figure 5: The variety of dynamics of occipital visual response, and the different changes of rhythms: Phase modulation of cortical activity can both increase and decrease with task engagement. (A)** Dynamics are examined from 4 electrodes (color coded) in subject 1. **(B)** Pink electrode site dynamics – posterior lower bank of the calcarine sulcus. The three panels on the left show the average dynamics leading into the 2 second visual search cues (onset at time zero). The upper trace is the average event-related broadband (ERBB) for each of the cue types. The middle plot is the average dynamic spectrum for all active sites combined – the "event related spectral perturbation" (ERSP). The lower plot is the event related potential (ERP) for each cue type. **(C)** The coupling palette for the pink electrode site. Note the strong θ and β contributions. **(D)** Broadband activity during each of the different cue types. The log-broadband amplitude is shown, in Z-score units, with the mean of ISI periods subtracted out. Errorbars represent 3*SEM. The rightmost error bars, flanking the horizontal origin, represent the variation during ISI periods. **(E)** Upper panel: 4-8 Hz amplitude during each of the different cue types. Lower panel: The modulation of the broadband by the 4-8 Hz phase during each cue type. **(F)** As in E, for 12-20 Hz. **(G)** Interaction between rhythms, computed analogously to the rhythm-broadband interaction. The 4-8 Hz phase modulation of the 12-20 Hz amplitude is quantified, revealing a significant coupling during all but the "rightward" cue condition. **(H)** As in B-G, for the green electrode site – lingual gyrus. There is a suppression of broadband activity when engaged in visual

search, revealed by the broadband timeseries and mean broadband amplitude (but not by the ERP). Broadband amplitude changes couple to both the 4-8 Hz rhythm and the 12-20 Hz rhythm. There is a specific augmentation of the 12-20 rhythm amplitude and 12-20 Hz coupling to the broadband rhythm during engagement in the visual task. The interaction between the two rhythms is significant during the "rightward" cue. **(I)** As in B-G for the black electrode site – posterior lateral occipitotemporal gyrus. There is specific broadband power increase at time of cue onset – the bars show that this is only sustained for the "leftward" cue. There is task related increase in the 4-8 Hz rhythm amplitude and corresponding coupling. The 12-20Hz rhythm shows a task-related decrease in both amplitude and coupling during visual search. The rightmost plot demonstrates that there is significant modulation of the 12-20 Hz amplitude by the 4-8 Hz phase. **(J)** As in B-G for the yellow electrode site – anterior lower bank of the calcarine sulcus. Visual search cues show increase in broadband, 4-8 Hz, and 12-20 Hz amplitude. There is also a task-related increase in modulation of the broadband amplitude by 4-8 Hz and 12-20 Hz phase. In turn, the 12-20 Hz amplitude is modulated by the 4-8 Hz phase, specifically while engaged in the visual search cues, and not during the ISI cues.

## Simulated data supports signal processing approach

A heuristic model was used to create synthetic data with broadband 1/f properties and modulation by a rhythmic input (Figs. 7, 8). This synthetic data was naively separated by the data analysis methods used on cortical data. The resulting spectra, palette, and modulation measures clearly resemble those found from recorded brain signals. When a negative control was analyzed (Fig. 9), there is a complete lack of coupling structure.

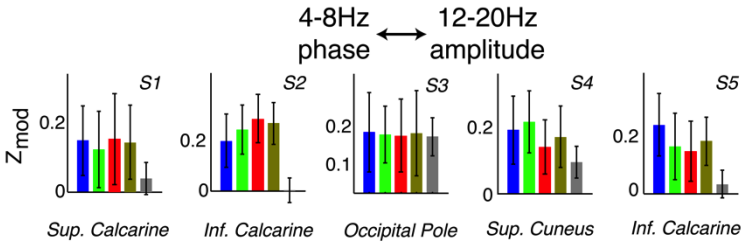


**Figure 6: The rhythms interact with one another.** Examples of 4-8 Hz phase modulation of 12-20 Hz amplitude in all 5 subjects (denoted S#). Note that there are examples of this kind of coupling in each subject, but most electrodes did not show significant phase-amplitude relationships between rhythms.

# Discussion

Our most significant and novel finding is that local cortical activity is dynamically modulated by the phase of different brain rhythms, tracking cognitive engagement on a second-to-second basis for specific cortical sites. In the occipital cortex this modulation was most pronounced in the θ (4-8Hz) and β (12-20Hz) ranges during periods of relative cognitive disengagement and dissolve during engagement in a visual search task. This relative increase and decrease of phase-amplitude modulation during visual search engagement suggests that rhythms can actively both suppress and facilitate sensory processing in the occipital cortex. Even though the spatial distribution of amplitude changes in rhythms can be widely distributed across the occipital lobe, the influence that they have on local cortical activity is gyrally specific.

## Implications of rhythmic modulation of broadband activity

From the perspective that broadband power reflects aggregate firing rate, the modulation of broad band activity by these lower frequency oscillations would indicate that these rhythms are influencing the instantaneous firing rate of many neurons simultaneously. This is consistent with coarse-graining of phenomena at the single-neuron scale, where the timing of individual action potentials is preferentially locked to a specific phase of ongoing local field potential oscillations ("spike-field coupling" – (Buzsaki and Draguhn, 2004)). Thus, ECoG rhythm-phase to broadband amplitude findings, such as those reported in this study, may reflect a population-averaged reflection of this spike-field coupling. Because these experimental results imply that rhythms are modulating the activity of whole neuronal populations, a distinction must be drawn between fluctuations in rhythmic modulation and amplitude in a rhythm. For example, in Fig. 4D there is a decrease in both the amplitude and the modulation associated with the 12-20Hz rhythm, but in Fig. 4G the decrease in 12-20Hz rhythm is not accompanied by a corresponding decrease in modulation.

## Technical considerations

The techniques presented here for characterizing and statistically testing phase and amplitude interactions in the cortical surface potential are performed in stages, each of which is non-trivial. We independently isolate a broadband signal and simultaneous brain rhythms; subsequently, we examine correlations between these two phenomena. In order to test whether our assumptions about the underlying mechanisms could be valid, we constructed a simulated signal that had task-related broadband change, and was modulated by rhythmic influence in a task dependent way (Fig. 8). Our analytic algorithms were able to naively uncover the broadband change as well as the rhythmic modulation. These phenomena are not induced by event-related potentials; the ERP dies out after 400ms, and is thus too transient to account for the robust amplitude modulation we observe. Furthermore, the ISI periods had smaller or no ERPs, and exhibited dramatically larger modulation. Sharp discontinuities in the timeseries can give artificial phase modulation at higher frequencies, so artifactual epochs had to be excluded from analysis. When the method was applied to task-modulated brown noise (Fig. 9), there was no coupling, suggesting that coupling is not a by-product of the method used for analysis.

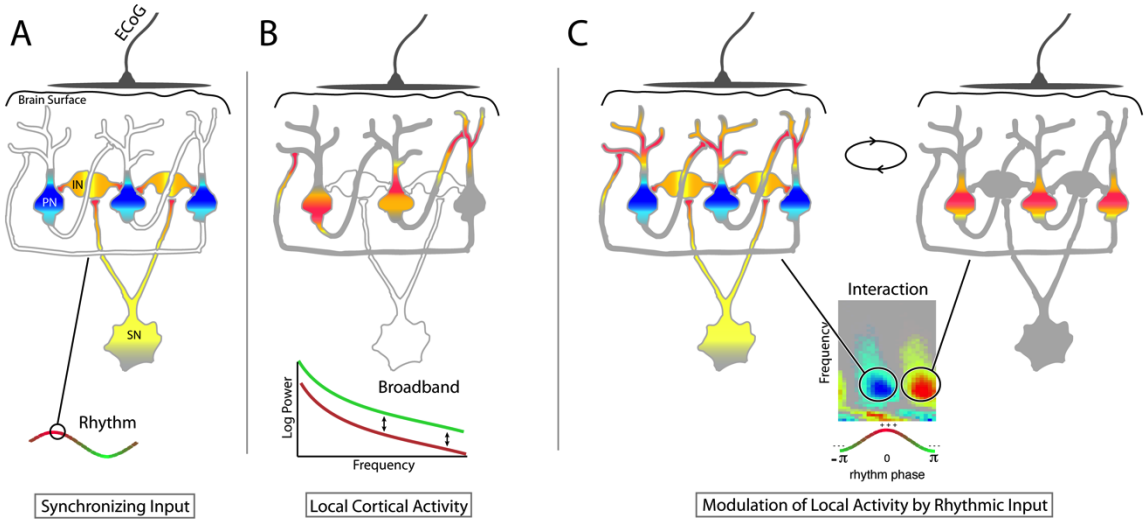


**Figure 7: Heuristic for inhibition through synchronization.** While there are many potential roles subserved by different rhythms, one potential role that we highlight is inhibition of population-scale processing by synchronization. This inhibitory function for rhythms is supported in cases where there is a clear, robust decrease in phase modulation of broadband by the rhythms' phase during visual task engagement (e.g. Fig. 4 B-E, Fig. 5 H). **(A)** Input from a "synchronizing neuron" (SN) projects diffusely to an inhibitory population of layer 4/5 neurons (IN) which in concert inhibit pyramidal neurons (PN) at their basal dendrites and soma. When averaged across the cortex immediately beneath an ECoG electrode, this is revealed by the presence of a rhythm. (yellow/orange/red – depolarization; light/dark blue – hyperpolarization). When present, the rhythm keeps the cortex in an idling, dynamically "ready", state – shut down, but rapidly able to shift to active computation. Blanket inhibition, could also prevent computation, but would not allow for easy transition to diverse and complex patterns of activity. **(B)** During active computation, the population of pyramidal neurons engages in a complex pattern of mutual excitation. Averaged across the population, these appear Poisson-distributed, and no special timescale emerges in the ECoG signal produced by this local, cortical-cortical interaction. **(C)** The synchronized influence of the rhythm forces cortical-cortical inputs to synchronize, effectively reducing their ability to perform computation. This modulation of local activity by rhythms is revealed at our ECoG scale by significant broadband modulation by low frequency phase.

## Suppression by synchronization

Existing studies of rhythm-broadband modulations have mainly focused on a facilitatory role (Womelsdorf et al., 2005, Canolty et al., 2006, Jensen and Colgin, 2007, Siegel et al., 2008, He et al., 2010), suggesting that the presence of a rhythm enables an active component of local cortical processing. While this may be the case for Theta-range modulations, including those observed here, the β-range changes we observe are more suggestive of an inhibitory process in which the rhythm actively modulates local occipital cortical activity during periods of task disengagement (Handel et al., 2005, Klimesch et al., 2007). In the setting of the γ-rhythm, it has been demonstrated that the influence of the rhythm facilitates cortical computation (Womelsdorf et al., 2007), particularly

during visual processing. These observations have been linked to the hypothesis that rhythms enhance spike transmission between synchronized areas – "communication through coherence" (Singer, 1993, Fries, 2005). This is consistent with the increase in power that we observe in γ-rhythms (Fig. 4H&I). We propose that rhythms may also play a role in suppressing local cortical computation, with the cortically suppressed (disengaged) state one in which widespread populations of cortical neurons are phase-coupled to the rhythm (Fig. 7). In this "suppression by synchronization" model, neurons from a distant "pacemaker" circuit project diffusely to populations of cortical pyramidal neurons, targeting their basal dendrites and somas with synchronized input. Whether the synchronized inputs are excitatory or inhibitory, the cortico-cortical inputs between pyramidal neurons will need to be stochastically resonant with the synchronized input to induce a downstream action potential (anti-aligned if the synchronizing input is inhibitory, aligned if it is excitatory). In this way, weak but synchronous input keeps the population in a "dynamically suppressed" state, where it can quickly transition into an engaged "processing state". An alternative model -- suppression by blanket inhibition, would be more metabolically expensive and would also not allow for easy transition from the suppressed state to a computing state because the targeted pyramidal population would have to overcome an effective hyperpolarization barrier. In the suppression-by-synchronization regime, one need only remove time-locking influence and the neuronal population can switch to an engaged and actively computing state. At this stage, identifying the anatomic locus of the synchronizing source will require further research. The thalamus, specifically the lateral pulvinar and lateral geniculate nucleus, is a compelling candidate because of its diffuse projection and known role in visual processing (Zhang et al., 2010). Additionally, it has been demonstrated that weak but synchronous thalamic input can drive cortical processing dramatically in the active feedforward state (Bruno and Sakmann, 2006). Whatever the case, this rhythmic modulatory influence acts over large cortical regions, and coherence is significantly decreased during visual engagement (Fig. 4J). Perhaps the

same is true for selective suppression of other cortical regions. During behavior, some rhythms might serve as "spotlights of utility" that, at baseline, actively suppress non-relevant cortical areas by synchronization. When the cortical area becomes functionally relevant the rhythm is withdrawn.

## Universal rhythmic motifs?

Although it is frequently treated as if a rhythm at a particular frequency has a universal functional property, a rhythm with a particular center frequency need not serve a single neural function in every state and location in which it is observed. The fact that we observe different preferred phases, and also conjugate task related changes in the same frequency ranges, in different cortical areas, suggests that there is unlikely to be a simple, universal, role for a particular band-limited rhythm. What we call "β" in the lateral occipital gyrus and what we call "β" at the occipital pole may in fact represent different phenomena, with different physiological origins, but with a common timescale and corresponding frequency range (Fig. 4). That said, the observation of significant changes in inter-electrode coherence between adjacent electrodes suggests a common etiology that selectively releases some cortical areas (e.g., sites A-D, G) but not others (sites E-F), in a gyrally-conserved way, during task engagement.

The fact that the phase-amplitude coupling motifs sometimes shift substantially in phase across subjects or electrodes might point to different types of physiologic phenomena which are revealed with different types of rhythmic coupling motifs. For example, a rhythm with one preferred phase might exert an excitatory influence via one class of channels, and a different rhythm might exert an inhibitory influence via a separate class of channels. The different timescales implied by the frequencies different rhythmic phenomena might reflect feedback loops involving different numbers of neurons, or slow vs. fast types of membrane channels. Some rhythms might reflect emergent properties of highly interconnected networks, while other rhythms of the same frequency-range but different cortical location, might reflect cortical-subcortical feedback loops.

The observed nesting of 12-20Hz amplitude in the 4-8 Hz phase demonstrates that, in some cases, the physiologic processes underlying these rhythms can interact with one another, and in a task-dependent manner (see, for example (Lakatos et al., 2005, Tort et al., 2009)).

## Emerging questions

This study is part of a continuing project to investigate the many phase-phase, phase-amplitude and amplitude-amplitude couplings both within and between electrodes on the cortical surface. Are there functionally relevant shifts in coupling phase across distinct behavioral states? Are these interactions present between cortical regions communicating over many centimeters? What rhythms play a role in different cognitive and sensorimotor processes? Can we measure a distant source of the rhythm at the same time as the nested oscillation, and is there in fact such a source? Is there a direct relationship between the phase of the coupling we observe and the spike-field coupling measured at the single-neuron scale? Answers to these questions will likely pave the way for a new understanding of large-scale information processing mechanisms in the human brain.

## Methodological appendix

**Signal pre-processing:** To reduce common artifact, the potential, $V_n^0(t)$, measured at each electrode $n$ was re-referenced with respect to the common average of all electrodes, $V_n(t) = V_n^0(t) - \frac{1}{N}\sum_{i=1}^{N} V_i^0(t)$, (channel label, $n$, henceforth dropped). Electrodes with significant artifact or epileptiform activity were rejected prior to common averaging. Epochs that appeared artifactual were rejected. Following re-referencing, only occipital electrodes were further examined; the remainder was discarded. Ambient line noise was rejected by notch filtering between 58-62Hz using a 3rd-order Butterworth filter (Porat, 1997).

**Power spectral densities:**

*Power spectral snapshots:* A set of epochs surrounding onset and middle of each visual search and ISI cue, $\tau_q$, were extracted from $V(t)$; each epoch was of duration $T$ =1s, $\left(\tau_q - \frac{1}{2}T\right) < t < \left(\tau_q + \frac{1}{2}T\right)$.The epochs were sorted according to cue type $q$, and labeled by their event markers $\tau_q$ [note times of onset, middle of both cues and ISI]. The power spectral density (PSD) of the epoch flanking time $\tau_q$ was calculated as $P(f,q) = \left| \frac{1}{\sqrt{T}} \sum_{t=-T/2}^{+T/2} V\left(\tau_q + t\right) H(t) e^{i2\pi ft} \right|^2$ with Hann window (Porat, 1997) $H(t) = \frac{1}{2}\left(1 + \cos\left(\frac{2\pi t}{T}\right)\right)$.

**Dynamic power spectral measures:** Time-frequency approximations (dynamic spectra) were made using both a wavelet and a Hilbert transform approach.

*Wavelet approach:*A Morlet wavelet (Goupillaud et al., 1984) of the form: $\psi(\tau,t) = \exp\frac{i2\pi t}{\tau}\exp\frac{-t^2}{2\tau^2}$ was convolved with the timeseries to get a time-frequency estimate for every $f = 1/\tau$:

$$\tilde{V}\left(1/\tau,t\right)=\sum_{t'=-5\tau/2}^{5\tau/2}V(t+t')\psi(t',\tau)$$

A total of 5 cycles ($5\tau$) was used to estimate the amplitude and phase of the signal at each frequency for every point in time. In this way a time-varying Fourier component $\tilde{V}\left(f,t\right)=r\left(f,t\right)e^{i\varphi\left(f,t\right)}$, with fixed uncertainty between the confidence in the estimate of the instantaneous amplitude and phase versus the confidence in temporal resolution is obtained at each Hz.

*Hilbert transform approach:* A complex signal to reflect the timecourse of a functionally-relevant frequency-range band was constructed as follows: The signal $V(t)$ was band-passed using a 3rd order Butterworth filter for a specific range, to obtain the "band-limited" potential, $V(F,t)$, where $F$ denotes the frequency range (e.g. for "alpha", $F\rightarrow$ [8-12Hz], etc.). A complex analytic signal, $\tilde{V}\left(F,t\right)=V\left(F,t\right)+iV^{IM}\left(F,t\right)$ was constructed using the Hilbert transform (e.g. such that the new signal satisfies the Cauchy-Riemann conditions for analyticity at all times)

*Discrete-Time Signal Processing.* For discussion of different approaches and illustration of nested ECoG measurements, see, for example, (Penny et al., 2008). This signal may also be expressed in polar notation: $\tilde{V}\left(F,t\right)=r\left(F,t\right)e^{i\phi\left(F,t\right)}$. The "analytic amplitude" of the range $F$ at time $t$ is $r(F,t)$ and the "phase" is $\phi(F,t)$. The interpretation of $\phi$ is intuitively difficult, but the most concrete understanding is that the rhythm captured by range $F$ is most surface-positive at $\phi=0$, and most surface-negative at $\phi=\pi$ or $-\pi$. Note that $\phi$ becomes poorly defined as $r\rightarrow 0$.

**Amplitude correlation and phase coherence of rhythms:** The relationships between complex rhythms $\tilde{V}_n\left(F,t\right)=r_n\left(F,t\right)e^{i\phi_n\left(F,t\right)}$ for trial $k$ (electrode $n$) were determined as follows. The inter-electrode amplitude correlation $R_{ab}(k)$ for the rhythm defined by range of frequencies $F$ between electrodes $a$ and $b$, during trial $k$ is: $R_{ab}\left(k\right)=\frac{1}{T_k}\sum_{t_k\in k}r_a^z\left(F,t_k\right)r_b^z\left(F,t_k\right)$

Where $t_k$ are the times of epoch $k$ ($t_k \in k$, total $T_k$ timepoints) and the z-score amplitude for the epoch is: $r_n^z(F,t_k) = \frac{r_n(F,t_k) - \langle r_n \rangle_{t_k \in k}}{\sigma_{r_n}\big|_{t_k \in k}}$, where $\langle r_n \rangle_{t_k \in k} = \frac{1}{T_k}\sum_{t_k \in k} r_n(F,t_k)$, and $\sigma_{r_n}\big|_{t_k \in k} = \left(\frac{1}{T_k}\sum_{t_k \in k}\left(r_n(F,t_k) - \langle r_n \rangle_{t_k \in k}\right)^2\right)^{1/2}$

The single trial inter-electrode phase coherence, $Q_{ab}(k)$, is: $Q_{ab}(k) = \left|\frac{1}{T_k}\sum_{t_k \in k} e^{i\left(\phi_a(F,t) - \phi_b(F,t)\right)}\right|$

**Stimulus-triggered average of time-frequency power estimate:** This time-frequency approximation can be used to calculate mean power in relation to the onset of visual stimuli:

$$\overline{P}^v(f,t_w) = \frac{1}{N_v}\sum_{\tau_v}\left(\frac{\left|\tilde{V}(f,t_w+\tau_v)\right|^2}{\frac{1}{N_{t'}}\sum_{t'}\left|\tilde{V}(f,t')\right|^2}\right)$$

Where $\tau_v$ denote onset times of visual search cues (total $N_v$), and $t'$ denote inter-stimulus times (total $N_{t'}$). The peristimulus time window of interest is denoted $t_w$; in our case, $-1s < t_w \le 3s$. These normalized maps of power as a function of time and frequency provide important information about characteristic spectral changes with local cortical function (also called "event-related spectral perturbations" – ERSPs (Makeig et al., 2002)). While ERSPs could be calculated independently for each condition (arrow direction) of the visual search task, for simplicity we calculate an ERSP collapsed across conditions.

**Decoupling the cortical spectrum to separate rhythmic activity away from broadband change:** The decoupling process is described and illustrated in detail in the main text and supplement to (Miller et al., 2009d). It was applied here as follows:

*Principal component decomposition of spectral change:* The samples of the PSD, $P(f,q)$, (total $N_q$), were normalized prior to decomposition. $\tilde{P}(f,q) = \ln\left(P(f,q)\right) - \ln\left(\frac{1}{N_q}\sum_q P(f,q)\right)$

The PCA method (Jolliffe, 2002) determines the eigenvalues $\lambda_k$ and eigenvectors $\vec{e}_k$ of the correlation matrix $C(f,f') = \sum_q \hat{P}(f,q)\hat{P}(f',q)$

These eigenvectors, $\hat{C}\,\vec{e}_k = \lambda_k\,\vec{e}_k$, the ``Principal Spectral Components" (PSCs), reveal which frequencies vary together, and are ordered by magnitude of corresponding eigenvalue: $\lambda_1 > \lambda_2 > \cdots > \lambda_{N_f}$ ( $N_f \equiv$ number of frequencies). If we define the rotation matrix $A(f,k) = (\vec{e}_1, \vec{e}_2, \cdots, \vec{e}_{N_f})$, then the projection, $W(k,q)$, of each individual original spectrum in the ensemble onto the new basis vector $k$ is $W(k,q) = \sum_f A(k,f)\hat{P}(f,q)$.

The inverse rotation matrix $\hat{A}^{-1}$, $\hat{A}^{-1}\hat{A} = \hat{I}$, allows us to compare and visualize specific subsets of PSC components with the original full spectrum in frequency space. The 2nd to 4th PSCs typically capture rhythmic power spectral phenomena, and power spectra can be reconstructed with and without this rhythmic influence: $\hat{P}_{\Xi}(f,q) = \sum_{k\in\Xi} A^{-1}(f,k)W(k,q)$.

If the 2nd to 4th PSCs are omitted, $\Xi \rightarrow \{1,5 \ldots N_f\}$, then PSDs can be reconstructed where changes in rhythmic spectral phenomena are mostly removed (although there may be residual variance in the decomposition, or some rhythmic influence in all cases). If $\Xi \rightarrow \{2\text{-}4\}$, then PSDs can be reconstructed where changes in rhythmic spectral phenomena are mostly isolated (Fig. 1C, 7).

*The timecourse of broadband spectral change:* The time-dependent, normalized, dynamic spectrum, $\hat{P}(f,q)$, can be obtained in parallel fashion to the spectral snapshots.

$P(f,t) = \dfrac{\left|\tilde{V}(f,t)\right|^2}{\frac{1}{N_t}\sum_t \left|\tilde{V}(f,t)\right|^2}$, and $\hat{P}(f,t) = \ln\left(P(f,t)\right) - \ln\left(\frac{1}{N_t}\sum_t P(f,t)\right)$.

The reflection of the 1st PSC ($\vec{e}_1$) in the dynamic spectrum can be estimated by projecting the dynamic spectrum onto it. $\ln A(t) = \sum_f e_1(f)\hat{P}(f,t)$

We call it $\ln A(t)$ here, because it approximates the logarithm of the timecourse of the coefficient of a power law in the cortical spectrum of the form $P(f,t) = A(t) f^{-\chi}$ (Miller et al., 2009b); it is smoothed with a Gaussian window of 50ms standard deviation, z-scored, and exponentiated to obtain the "broadband" traces of Fig. 1D, 4H-I, 5B&H-J (e.g. time varying estimates of the coefficient of the power law spectrum). The broadband power timecourses are robust estimates of behaviorally relevant local cortical activity (Miller et al., 2009d). Because the quantity $\ln A(t)$ is approximately log-normal distributed, we express it in z-score units, and, for notational brevity, denote it $\chi(t)$ in connection to the broadband power law it reflects.

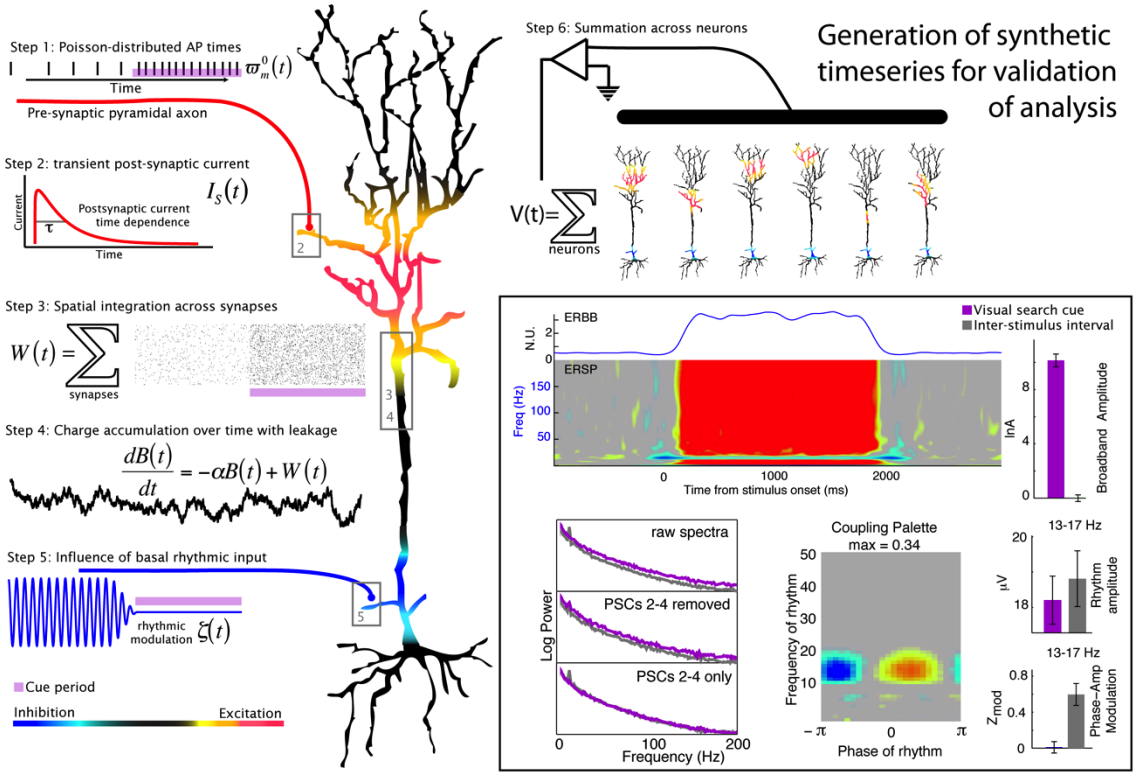


**Figure 8: Generation of a simulated timeseries and validation of signal processing technique.** The illustrated heuristic was used to generate a 1/f base, broadband, synthetic timeseries (e.g. (Miller et al., 2009b)) that is modulated by a 15 Hz rhythm (described in detail in the appendix). In the boxed region on the bottom right, the synthetic timeseries is analyzed in the same way as the physiological data. It demonstrates that the decoupling and phase-modulation estimation signal processing techniques described in this manuscript work for simulated data that were based on the mechanisms hypothesized for our physiological data (e.g., Fig 7).

**Synthetic data (Fig. 8):** The heuristic method illustrated in Fig. 7A-C was used to create simulated data by combining input signals whose properties are known. The synthetic data could then be analyzed to validate the methods developed for the cortical data. The process is an extension of the one used to illustrate broadband, power-law, spectral change in previous manuscripts (Bedard et al., 2006, Miller et al., 2009b, Miller et al., 2010a). Recent in-vivo simultaneous recordings have demonstrated a strong correlation between trans-membrane and local field potentials (Okun et al., 2010), suggesting that models like this, based upon a relationship between post-synaptic potentials and field potential, may provide useful insight. It is a construct that simulates the hypothesis of Fig. 7A-C, which is a mechanism for what role some (not all) rhythms might play in cortical processing. This heuristic is meant to synthetically generate data of known 1/f broadband structure with influence of nested oscillation. It is not meant to serve as an accurate physiological model, but rather as a means to validate our signal processing techniques on synthetic data that has approximately similar statistics as empirical data, but with known underlying structure.They are synthesized in the following steps:

***Step 1:*** Action potentials (AP – "spikes") with Poisson-distributed inter-spike intervals arrive from a pre-synaptic cortical pyramidal neuron. We model 6000 of these and assign a random synaptic weight on the interval -1 to 1 to each synapse. The instantaneous AP rate, $\varpi_m$ , is modulated as a function of task, so that the probability of an AP is higher during the simulated visual search time. This can be formalized as: $\varpi_m^0(t) = \begin{cases} 1 \ni \eta < \rho(t_k) \\ 0 \ni \eta > \rho(t_k) \end{cases}$

where $\eta$ is a random variable uniformly distributed on the interval [0, 1] and $\rho(t_k)$ is a variable threshold that corresponds to the mean population spike rate within the $k^{th}$ epoch (e.g. $\rho(t_k) =$ "firing rate" / "sampling rate"). The maximum firing rate was set to 40 spikes/s. During simulated ISI epochs, $\rho(t_k)$ was set to 25% of maximum firing rate, and during each simulated visual search

epoch the value of $\rho(t_k)$ was set to a value drawn from a uniform distribution on the range 55-100% of maximum firing rate.

***Step 2:*** Each AP produces stereotyped transient post-synaptic current with a sharp rise, and an exponential decay of timescale $\tau_S = (2\pi 75Hz)^{-1} = 2.1ms$ consistent with empirical measurement (Sabatini and Regehr, 1996). Following Lindén, et. al. (Lindén et al., 2010), the timecourse of the synaptic current induced by a single AP is: $I_S(t) = \eta \frac{t}{\tau_s} e^{1-t/\tau_S} \theta(t)$, where $\eta$, in this case, is a "synaptic strength" drawn randomly from a uniform distribution on the range [-1,1], $\tau_S$ is thetime constant of the synapse, and $\theta(t)$ is a step function (i.e. "Heavyside function"). The AP timeseries is convolved ( * denotes convolution operation) with the synaptic current shape, $I_S$. $\varpi_m = \varpi_m^0 * I_S$

***Step 3:*** Synaptic inputs from 6000 synapses, "$m$", are summed at each point in time: $W(t) = \sum_m \varpi_m(t)$ and charge integrates over time, perturbing the trans-membrane difference in charge concentration between the inside and outside of the neuron (Connor and Stevens, 1971).

***Step 4:*** Thetemporal integration and Ohmic leakage that produce the broadband $B(t)$ are governed by: $\frac{dB(t)}{dt} = -\alpha B(t) + W(t)$. The timecourse of $B(t)$ is determined iteratively. Note that, in more comprehensive and subtle simulations, the effect of rhythmic input (through back-propagation or otherwise), might be incorporated into this step.

***Step 5:*** A cortical rhythm $\zeta(t) = r_\zeta(t)\cos(2\pi f_0 t + \Delta(t_k))$, is simulated, with center frequency $f_0$ set to 15Hz. The amplitude $r_\zeta(t)$ is set to zero during simulated visual search epochs, and takes on a non-zero value drawn randomly from a uniform nonzero distribution during ISI epochs (determining the strength of the modulation). A different random phase shift, $\Delta(t_k)$, is also added to each epoch to prevent inter-trial coherence in the mean spectrogram. This rhythm contributes to the simulated

membrane potential of a neuron in two ways. Firstly, it multiplicatively modulates the broadband process: $V_{BB}(t) = \left(1 + \zeta(t)\right) B(t)$

Secondly, the rhythm contributes directly to the potential:

$V_{\zeta}(t) = A_{\zeta} r_{\zeta}(t) \cos\left(2\pi f_0 t + \Delta(t_k) + \phi_C\right)$, where $\phi_c$ is the coupling phase (which we set to $\pi/4$), and $A_{\zeta}$ is the overall amplitude of the rhythmic contribution, linked to match the variation in the underlying noise: $A_{\zeta} = A_{\zeta}^{0} \frac{\sigma_{\zeta(t)}}{\sigma_{V_{BB}(F,t)}}$ and $\sigma$ denotes the standard deviation over time, and $V_{BB}(F,t)$ is the band-pass filtered $V_{BB}(t)$ for $F = \{ f_0$ -2Hz to $f_0$ +2Hz $\}$. Then the simulation contribution to the potential from one neuron is $V_{BB}(t) + V_{\zeta}(t)$. In this simulation, we use this quantity to approximate the timecourse that gives rise to our measured potential.

***Step 6:*** Simulation is performed for the summation of 10 such model neurons. The broadband change is a stochastic process, different in each neuron although the timecourse of firing probability, $\rho(t_k)$, is the same at each synapse, and in each neuron. The timing and phase of the rhythm is also fixed across neurons (because it is 'synchronized'). The resulting timeseries was analyzed in the same manner as the cortical data were.

The inhibition through synchronization aspect of the model is forced into effect by having the firing rate, $\rho(t_k)$, constructed to be low when $r_{\zeta}(t)$ is non-zero, and $\rho(t_k)$ high as $r_{\zeta}(t) \to 0$. More sophistocated network simulations should exhibit this as an emergent property.

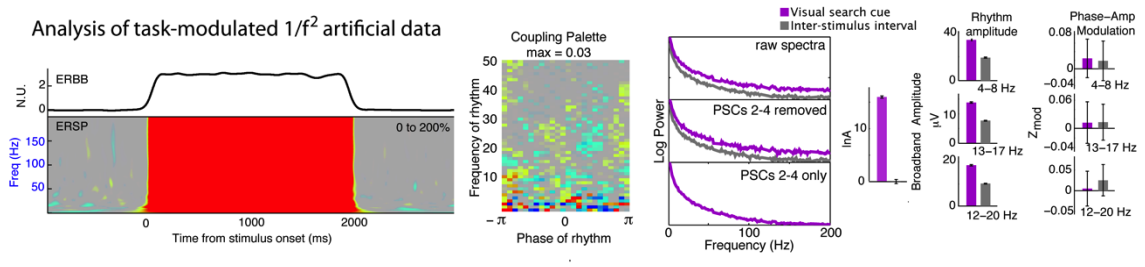


**Figure 9: Application of signal processing technique to colored noise.** When the signal processing methods were applied to task-modulated $P \sim f^{-2}$ colored noise as a negative control, there is no significant coupling.

**Negative control validation on brown noise (Fig. 9):** We tested the methods on pure brown noise that was generated by creating a timeseries with property $P(f) = f^{-2}$ by taking a random white noise variable $\eta$uniformly distributed on the interval [-.25, .25] during simulated ISI, and [1, 1] during simulated visual engagement. It was then temporally integrated to give it brown noise structure, and high-passed at 1Hz to avoid DC offset issues. Analysis was then performed in an identical manner as with data and the above simulation to demonstrate a negative control (Fig. 9).

# Chapter 4: Gamma oscillations in visual cortex are an idiosyncrasy of low-level stimulus features [7]

A striking feature of some field potential recordings in visual cortex is a rhythmic oscillation within the gamma band (30-80 Hz). These oscillationshave been proposed to underlie computations in perception, attention, and information transmission. Recent studies of cortical field potentials, including human electrocorticography (ECoG), have emphasized another signal within the gamma band,a non-oscillatory, broadband signal, spanning 80-200 Hz. It remains unclear under what conditions gamma oscillations are elicited in visual cortex, whether theyare necessary and ubiquitous in visual encoding, and what relationship they have to non-oscillatory, broadband field potentials. We demonstrate that ECoG responses in human visual cortex (V1/V2/V3) can include robust narrowband gamma oscillations, and that these oscillations are reliably elicited by some spatial contrast patterns (luminance gratings) but not by others (noise patterns and many natural images). The gamma oscillations can be conspicuous and robust, but because they are absent for many stimuli, which observers can see and recognize, the oscillations aren't necessaryfor seeing. In contrast, all visual stimuli induced broadband spectral changes in ECoG responses. Asynchronous neural signals in visual cortex, reflected in the broadband ECoG response, can support transmission of information for perception and recognition in the absence of pronounced gamma oscillations.

[7] This chapter will appear as a manuscript in Cerebral Cortex: Hermes D, Miller KJ, Wandell BA, Winawer J (in press). Stimulus specificity of gamma oscillations in human visual cortex. Cerebral Cortex, doi:10.1093/cercor/bhu091

## Introduction

Recordings of stimulus induced field potentials in visual cortex sometimes show a narrowband increase in spectral power within the gamma range typically peaking around 40-60 Hz (reviewed by (Fries et al., 2008)). This narrowband response has attracted a great deal of attention because of the suggestion that the oscillations play a key role in perception and cognition(Eckhorn et al., 1988, Gray et al., 1989, Gray, 1999, Fries et al., 2007), and because of the related hypothesis that the precise timing of these neural oscillations is critical for information transfer between remote cortical sites (Fries, 2005).

Some researchers have made vigorous counterarguments against the functional significance of these oscillations for perception (Shadlen and Movshon, 1999, Thiele and Stoner, 2003, Roelfsema et al., 2004). Recent studies in non-human primates show that the characteristics of narrowband gamma responses depend on the spatial structure of the visual stimulus. For example, the amplitude (Henrie and Shapley, 2005) and peak frequency (Ray and Maunsell, 2010) of the gamma oscillations increase with grating contrast. Large gamma oscillations can be recorded in response to a large grating stimulus, but the response amplitude is reduced when a perpendicular grating is superimposed to create a plaid pattern (Lima et al., 2010, Bartolo et al., 2011), when noise is superimposed on the grating (Zhou et al., 2008, Jia et al., 2011), when the grating is relatively small (Bauer et al., 1995, Gieselmann and Thiele, 2008, Jia et al., 2011, Ray and Maunsell, 2011, Jia et al., 2013b), or when natural movies are viewed rather than a grating (Kayser et al., 2003). Some researchers have argued that these stimulus-dependent variations in frequency and amplitude of the oscillatory gamma response preclude a role for oscillations in perceptual binding or communication (Ray and Maunsell, 2010).

Despite the clear stimulus dependencies of gamma oscillations, hypotheses about a fundamental role of oscillations for vision have not been rejected. Several reasons are offered. First, the fact that parameters of the gamma rhythm depend on stimulus properties might not preclude narrowband

gamma oscillations from playing an important role in information transfer (Bosman et al., 2012, Roberts et al., 2013). Second, the absence of gamma oscillations when viewing natural stimuli(Kayser et al., 2003), was explained as a consequence of motion signals in the stimuli masking gamma oscillations rather than the oscillations being sensitive to the spatial structure of the image. Finally, a recent study in non-human primates claims that gamma oscillations are elicited in macaque during free viewing of all static natural images (Brunet et al., 2013).

If narrowband gamma oscillations are essential for seeing and recognition (Melloni et al., 2007) and for feedforward information transfer (Bosman et al., 2012), then we expect these oscillations to be elicited by all static, visible stimuli, not just a restricted set – say stimuli with a periodic spatial or temporal structure. Moreover, it is important to analyze the data in using methods that distinguish narrowband gamma oscillations, which are indicated by a peak in the spectral response (Lopes da Silva, 2013), from broadband signals, which span the gamma range but do not have a distinct peak (Miller et al., 2009b). Recent reports have claimed that these two signals may originate from different neural circuits (Manning et al., 2009, Ray and Maunsell, 2011). Prior reports of gamma oscillations in human intracranial recordings did not always separate these two responses (Tallon-Baudry et al., 2005, Crone et al., 2011).

We specifically looked for narrowband gamma oscillations using intracranial recordings in human visual cortex, and we analyzed the dependence of these oscillations on the visual stimulus. We found that static grating stimuli elicited both narrowband gamma and broadband high frequency responses in a large area of visual cortex. The amplitude of the oscillations was large and the narrowband response could be measured on single trials. However, highly visible static noise patterns failed to elicit a narrowband response. Instead, these patterns produced a substantial broadband response. Only a small subset of face and house picture stimuli elicited narrowband oscillations, and these responses were present in only a restricted region within early visual areas. We could find no gamma oscillations on the fusiform or parahippocampal gyri, regions that appear

to be important for perceiving face and house stimuli (Allison et al., 1994a, Puce et al., 1995, Parvizi et al., 2012).

The amplitude of the narrowband oscillations depends substantially on the spatial structure of the image, so much so that many plainly visible stimuli do not give rise to narrowband responses. The cortical locations of the oscillations to face and house stimuli are not located in regions thought to be responsible for perception of these objects. We conclude that gamma oscillations do not play an essential role for seeing many types of visual stimuli.

## Materials and Methods

### Subject and procedure

ECoG data were measured from two subjects who were implanted with subdural electrodes (2.3 mm diameter, AdTech Medical Instrument Corp) for clinical purposes. All subjects gave informed consent to participate in the study and the study was approved by the Stanford University IRB. During ECoG measurements stimuli were shown on a 15 inch MacBook Pro laptop using Psych toolbox (http://psychtoolbox.org/). The laptop was placed 60 cm from the subject's eyes at chest level. Screen resolution was 1280x800 pixels (33x21 cm). In subject 1, an fMRI scan was performed for retinotopic mapping before the implantation of the electrodes and the same experiment was repeated during ECoG (data presented in (Winawer et al., 2013), see Figure S1).

### Stimuli and task

In experiment 1, the subjects viewed static images of gratings and noise patterns for 500 ms each, with 500 ms of zero-contrast (mean luminance) between successive stimuli. Stimuli came from 7 classes (30 exemplars per class, 25x25°), including high contrast vertical gratings (0.16, 0.33,0.65, or 1.3 duty cycles per degree square wave) and noise patterns (spectral power

distributions of $k/f^4$,$k/f^2$,and $k/f^0$). Subjects fixated on a dot in the center of the screen that alternated between red and green, changing colors at random times. Subject 1 pressed a button when the fixation dot changed color. Subject 2 fixated the dot but did not make manual responses because these responses were found to interfere with visual fixation.

In experiment 2, the subject viewed static images of faces or houses (50 each, 10x10°) in random order with a small amount of stationary (not moving) white noise superimposed on the image (70% gray-scale image + 30% noise in pixel intensities). Images were presented for durations ranging from 293 ms to 2625 ms, with a mean ISI of 1838 ms. Only stimuli with durations of at least 460 ms were included in analyses (n = 99). The subject indicated whether the image was a face or a house by pressing a button.

### ECoG recording

ECoG data were recorded at 3052/1528 Hz (subject 1/subject 2) from 118/96 electrodes through a 128-channel Tucker Davis Technologies recording system (http://www.tdt.com). To localize electrodes, a computed tomography (CT) scan was acquired after electrode implantation and co-registered with a preoperative structural MRI scan. Electrodes were localized from the CT scan and co-registered to the MRI (Hermes et al., 2010). Electrodes that showed large artifacts or showed epileptic activity, as determined by the patient's neurologist were excluded from analysis (7/35 electrodes were excluded in subject 1/subject 2 in experiment 1 and 13 electrodes were excluded in experiment 2). Off-line, data were re-referenced to the common average, low pass filtered and resampled at 1000Hz for computational purposes using the Matlab resample function. Line noise was removed at 60, 120 and 180 Hz using a 3rd order Butterworth filter. Results from the manuscript were unchanged if data were pair-wise re-referenced to a "silent" electrode rather than to the common average.

## ECoG analyses

### Time frequency analysis

To visualize spectral power changes during stimulus presentation, a time frequency analysis was performed around stimulus onset (-200 to 1000 ms) with a multitaper approach (Percival and Walden, 1993) using chronux (http://www.chronux.org/ (Mitra and Bokil, 2008)). A moving window of 200 ms (with overlap of 50 ms) and the use of five tapers result in a frequency resolution of 5 Hz, with a spectral smoothing of ± 15 Hz. To normalize the responses to baseline, the average spectrum from all inter trial intervals 250-500 ms after stimulus offset was computed and divided from every time bin. The base 10 log was then computed on this normalized power and plotted (Figures 1, 4).

### Spectral analysis

To quantify the responses, we calculated power spectra and separatedECoG responses into broadband and narrowband gamma band spectral power increases. To control for the influence of evoked activity on the spectrum, event related potentials (ERPs) were calculated per condition and the condition specific ERP was regressed from each trial. This procedure makes sure that the broadband increase is not due to a sharp edge in the ERP; the same pattern of results is obtained if this step is omitted. For each condition, the average power spectral density was calculated every 1 Hz by Welch's method (Welch, 1967) with a 500 ms window (0 – 500 ms after stimulus onset, and 0-500 ms after stimulus offset for the baseline) and a Hamming window to attenuate edge effects (Figure 2 and Figure S2). ECoG data are known to obey a power law and to capture broadband and narrowband gamma increases separately the following function (*F*) was fitted to the average log spectrum from 35 to 200Hz (leaving out 60Hz line noise and harmonics) from each condition:

$$P(x) = (\beta_{broadband} - nx) + \beta_{narrowband} G(x \mid \mu, \sigma).$$

With, $x = \log_{10}(frequency)$ and $G(x \mid \mu, \sigma) = e^{\frac{-(x-\mu)^2}{2\sigma^2}}$, with $10^{\sigma}$ = 1.1 Hz and 35 Hz < $10^{\mu}$< 80 Hz.

The slope of the log-log spectral power function ($n$) was fixed for each electrode by fitting it based on the average power spectrum of the baseline. To estimate whether broadband and gamma increases were significant, confidence intervals were calculated by a bootstrap procedure. For each condition C with $N_c$ trials, $N_c$ trials were drawn randomly with replacement and power spectra were averaged. The function $P$ is the average log power spectrum from these trials and the parameters β were fitted. This was repeated 100 times, resulting in a distribution of broadband and narrowband weights. Effects are reported as significant if the 95% overlapping confidence intervals were not overlapping with the 95% confidence interval from the baseline period, and are not further corrected for multiple comparisons across electrodes.

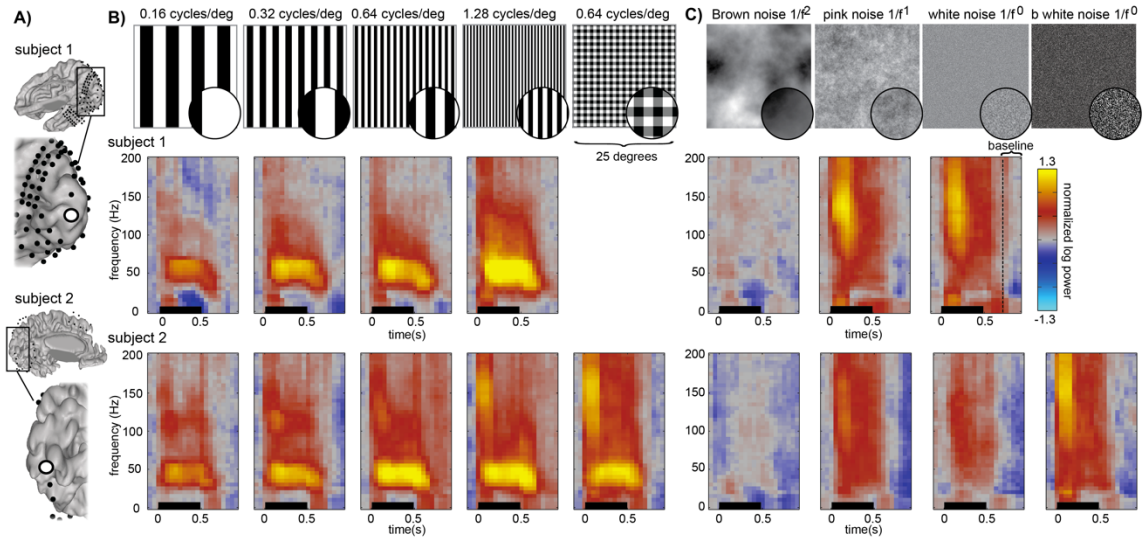


**Figure 1: Time-frequency power estimates in V1/V2 for gratings and noise stimuli. A)** ECoG electrode locations in subject 1 and 2. **B)** Grating stimuli were presented for 500 ms, insets in circles show a magnified portion of the stimuli for visibility. Time-frequency power estimates ("spectrograms") from an electrode in V1/V2 from subject 1 (top row) and subject 2 (bottom row). **C)** Noise patterns were presented for 500 ms. Spectrograms from the same early visual electrode in subject 1 (top row) and subject 2 (bottom row). All spectrograms are normalized with respect to the same baseline: the inter-stimulus interval between all trials (from 750-1000 ms after stimulus onset). Spectrograms are cut off at a maximum of +/- 1.3 $\log_{10}$ units. The multitaper approach results in a temporal smoothing of 200 ms and a frequency smoothing of +/- 15Hz. Spectrograms represent averages across all trials of a given type.

## Results

In one experiment, we measured responses to square wave gratings of different spatial frequencies and noise patterns with several amplitude spectra. In a second experiment, we measured responses to images of faces and houses. For all stimuli in both experiments, the spectral responses were modeled as the sum of three components: a baseline, a narrowband gamma signal, and a broadband signal (Winawer et al., 2013). Quantitatively modeling the responses enables us to test for stimulus specificity of both types of signals across several areas in visual cortex.

### Gratings, but not noise patterns, elicit narrowband gamma

Measurements were made in visual cortex in two subjects. To illustrate the principles, we first consider responses in two electrodes (one from each subject) located near the foveal representation at the V1/V2v border (Figure 1A). We then discuss a more extensive set of data.

The ECoG responses differ strikingly as a function of the spatial pattern in the stimuli. Here, we show the complete response spectrograms from both subjects to square wave gratings at several spatial frequencies (Figure 1B) and several types of noise patterns (Figure 1C). The power spectra are shown in Figure 2. In all cases, the square wave stimuli elicited robust narrowband gamma responses, peaking near 50 Hz (Figure 1B, 2A). This response duration is sustained for the entire stimulus duration (0.5 s). These ECoG oscillations are consistent with LFP recordings in animal and MEG and EEG recordings in human (Fries et al., 2008).

There is also a spectrally broadband response elevation. The broadband response spans a wide range of frequencies, from 50-200 Hz (upper limit due to the noise floor). This response begins slightly earlier in time (50-100 ms) than the narrowband response. It is larger at stimulus onset and then continues at a lower level for the stimulus duration. The amplitude of the broadband response increases as the fundamental spatial frequency of the grating stimuli rises from 0.16 to 1.28 cycles per degree.

The responses to the spatial noise patterns are very different from the responses to the gratings (Figure 1C, 2B). The noise stimuli produce a broadband elevation in spectral power, but there are no narrowband gamma oscillations. The broadband response to noise stimuli is similar to the broadband response to the gratings; the amplitude is largest at stimulus onset and then continues throughout the stimulus presentation but at a lower level (Figure 2C).

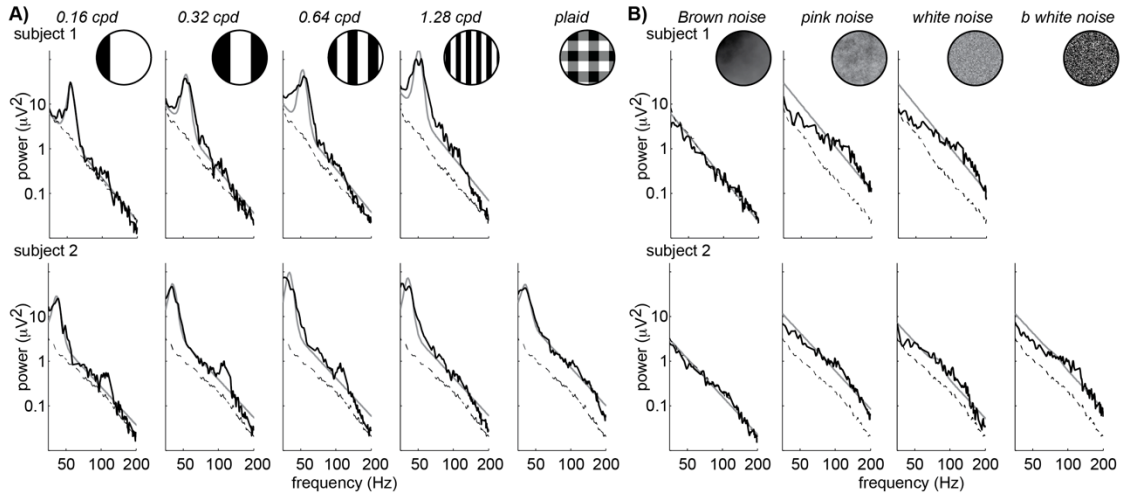


**Figure 2: Power spectra in V1/V2 for gratings and noise stimuli.** Power spectra to the grating stimuli for the same electrodes shown in Figure 1 on a log-log plot (top, subject 1; bottom, subject 2). The black line showsthe power spectrum from the grating stimuli **(A)** and noise stimuli **(B)**. The dashed line shows the power spectrum from the baseline periods. A line plus Gaussian (model) was fitted to the average power spectra of each condition (data) in log-log space, resulting in one weight for broadband and one weight for narrowband increases relative to baseline. The fit from this model is plotted in gray.

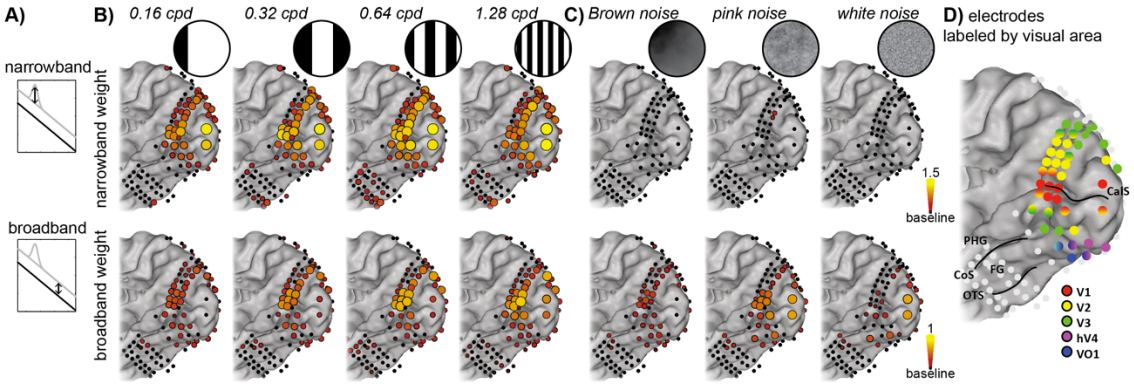


**Figure 3: Spatial distribution of narrowband (gamma) and broadband weights.A)** Spectral power changes during visual stimulation compared to baseline were separated in increases in narrowband gamma rhythms and broadband increases by fitting a power law shape with a Gaussian. **B)** Spatial distribution of narrowband gamma (top) and broadband weights (bottom) in subject 1 during grating stimuli. **C)** Spatial distribution of narrowband gamma (top) and broadband weights (bottom) in subject 1 during noise stimuli. Electrodes that showed a significant increase compared to baseline are plotted in color on the rendered brain surface ($p<0.05$ uncorrected). **D)** ECoG electrodes labeled by visual field mapping experiment (Winawer et al., 2013). CalS = Calcarine sulcus, PHG = parahippocampal gyrus, CoS = collateral sulcus, FG = fusiform gyrus, OTS = occipital temporal sulcus.

The response pattern in the foveal V1/V2 electrodes in the two subjects shown in Figures 1 and 2 is replicable across more than 30 other cortical locations (Figure 3). Across visual sites, the response is well approximated as a mixture of a narrowband gamma oscillation and a broadband response. To summarize the measurements, we modeled the power spectrum as the weighted sum of two components in log-power by log-frequency plot: (1) a straight line from 35 Hz to 200 Hz (broadband) and (2) a Gaussian centered between 35 Hz and 80 Hz (gamma band oscillation) (Equation 1). This allowed us to visualize the spatial distribution of the two signal components across the electrode arrays.

Nearly all electrodes (33/34) in visual areas V1/V2/V3 show a significant narrowband gamma response to at least one of the square wave gratings (Figure 3B, top). Most (31/34) also have a significant broadband response (Figure 3B). For the noise patterns, however,

only two electrodes on V1/V2/V3 have measurable gamma responses (Figure 3C, top, pink noise condition). These two electrodes were not located near the foveal representation.

Most V1/V2/V3 electrodes (28/34) have a significant broadband response to at least one of the three types of noise stimuli (Fig 3C, bottom). Broadband responses in the fovea are larger for white and pink noise than for Brown noise patterns, consistent with the observation that foveal V1/V2/V3 is less sensitive to low spatial frequencies (Wandell, 1995), which dominate the Brown noise stimuli. Peripheral electrodes show the opposite pattern: a larger broadband response to the Brown noise stimuli than the white noise stimuli. This spatial pattern is consistent with the fact that the periphery is more sensitive to low spatial frequencies. The ventral occipital-temporal electrodes responded occasionally, but weakly, to both grating and noise stimuli.

## The spatial distribution of broadband and narrowband responses to object stimuli differ

Next, we measured responses to face and house picture stimuli (subject 1; Figure 4). During the ECoG recording, the subject correctly indicated for each image whether it was a face or a house (n = 99, mean reaction time +/- sd: 682+/-160ms for faces and 726+/-202ms for houses). There was little narrowband gamma evoked in electrodes near the foveal representation in V1/V2. Spectrograms from the V1/V2 electrode with the strongest narrowband gamma response are shown in Figure 4B. In foveal V1/V2, 0 of 2 electrodes showed significant narrowband gamma responses for faces, 1 of 2 for houses (Figure 4C). Narrowband gamma responses were not observed in the fusiform nor parahippocampal

gyri. Some weak but significant gamma oscillations were observed in peripheral V1/V2/V3, in cortical regions that represent the visual field position at the stimulus edge.

The spatial pattern of broadband responses is quite different from the pattern of narrowband responses (Figure 4C). The distribution of this activity is similar to the pattern observed in functional MRI experiments. The largest response is near the occipital pole (in the 2 electrodes on foveal V1/V2). This is expected because these stimuli subtended a relatively small visual angle (10° diameter). In addition, significant broadband responses were measured on the fusiform gyrus for face stimuli and on the parahippocampal gyrus for house stimuli, consistent with the location of face- and place-selective regions of ventral temporal cortex (Allison et al., 1994a, Puce et al., 1995, Kanwisher et al., 1997, Aguirre et al., 1998, Epstein and Kanwisher, 1998).

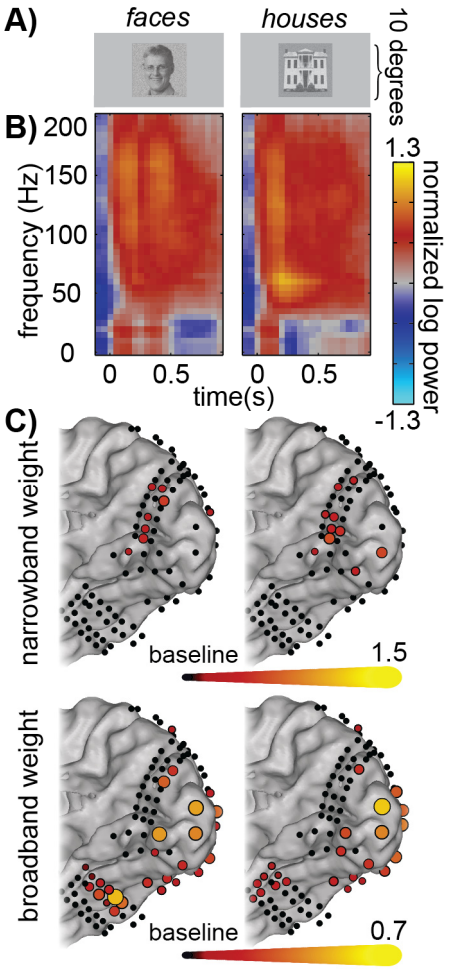


**Figure 4: Spectral power changes during face and house viewing. A)** Examples of face and house stimuli presented during experiment 2. **B)** Spectrograms from an early visual electrode in subject 1 (Figure 1A) while seeing faces (left) and houses (right). **C)** Spatial distribution of significant increases in narrowband and broadband weights ($p<0.05$ uncorrected). Early visual areas show little or no narrowband gamma increases while viewing faces (top left) and houses (top right), but large increases in broadband power (bottom). The fusiform gyrus and parahippocampal gyrus show significant broadband increases, but no gamma increases, while viewing faces and houses respectively.

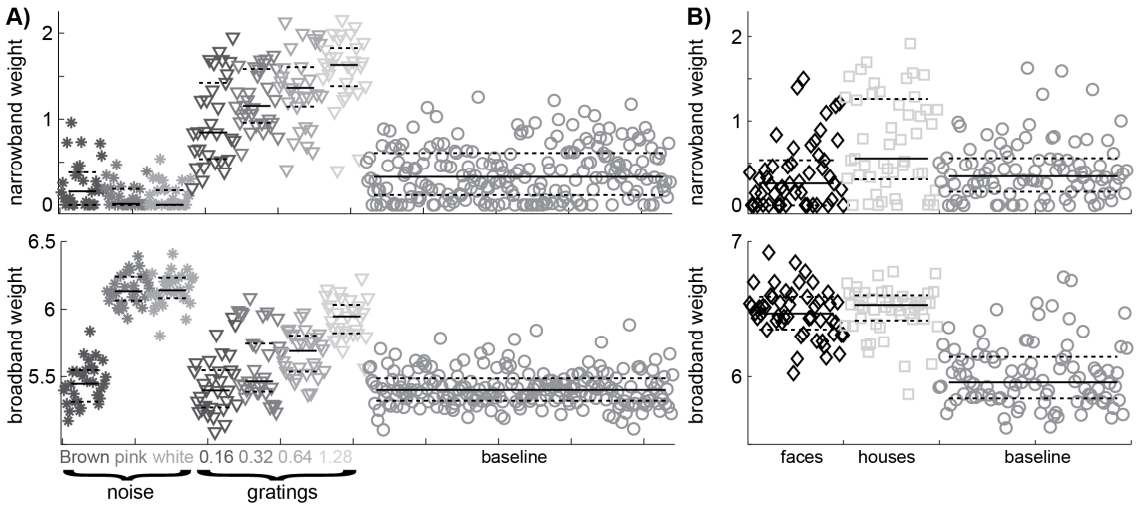


**Figure 5: Narrowband (gamma) and broadband power in individual trials.A)** Increases in narrowband gamma (top row) and broadband (bottom row) in a V1/V2 electrode in subject 1 during all individual trials of experiment 1. Horizontal bars indicate the median (solid) and quartiles (dotted) for each condition. **B)** The same for experiment 2. This electrode shows increased gamma oscillations for only some face and house stimuli, it shows a broadband increase for almost all stimuli.

## Individual trial analysis

Noise patterns did not elicit reliable gamma oscillations on single trials; but gratings did. For an electrode on the boundary of foveal V1/V2, the narrowband gamma responses to noise stimuli were beyond the 50% confidence interval defined by the baseline period response for only 4 of 90 trials (Figure 5A, top). For the highest spatial frequency grating stimuli, the narrowband gamma responses were beyond the 50% confidence interval of the baseline periods on 28 of 30 trials (Figure 5A, top).

A broadband response was measured on nearly every trial with stimuli containing relatively high spatial frequency patterns (pink and white noise patterns; gratings of 1.3 cpd) (Figure 5A, bottom). The relative insensitivity of a foveal V1/V2 electrode to very low spatial frequencies (0.16 cpd grating and brown noise patterns) is expected (Wandell, 1995).

For face and house stimuli, the narrowband gamma responses were mostly in the baseline range (Figure 5B, top). For a few trials, however, narrowband gamma responses exceeded baseline. The broadband responses to faces and houses were reliably outside the baseline range (Figure 5B, bottom).

## Discussion

Narrowband gamma responses to certain stimuli can be reliably measured with ECoG in human visual cortex. In this general sense, there is agreement between ECoG and MEG/EEG in human, and LFP measurements in cat and macaque (reviewed by (Fries et al., 2008)). When present, the ECoG narrowband oscillations are substantially (~1.5 $\log_{10}$ units) above baseline and they can be observed on individual trials.

However, many types of static, visible stimuli fail to elicit narrowband gamma oscillations. Three different types of noise patterns fail to elicit narrowband gamma oscillations. Many pictures of faces and houses tested do not elicit gamma oscillations.

The broadband response amplitude and position is in much better agreement with excitations expected from visible stimuli. With the exception of spatial frequency inappropriate stimuli (low frequencies in the fovea and high frequencies in the periphery), all the stimuli used in this study produce a general (broadband) response that spanned all frequencies from ~80 Hz up to the noise floor. The broadband responses to face and house stimuli were clearly present in ventral occipital regions that are thought to be important for recognizing these images.

## Gamma oscillations are stimulus specific

The failure to observe narrowband gamma responses to certain classes of stimuli cannot be explained by the experimental setting or signal contamination. In electrodes where grating stimuli generate clear narrowband gamma as well as broadband responses, other types of stimuli in the same visual field positions produce robust single trial broadband responses in the absence of gamma oscillations. It is unlikely that the stimuli that did not elicit gamma rhythms were not perceived, because all stimuli were large (at least 10 x 10 deg), had an abrupt onset during central fixation, and remained on the screen for at least 500 ms, sufficiently long to allow for conscious perception (Dehaene and Changeux, 2011). Moreover the grating stimuli (which reliably elicited gamma oscillations) and the noise stimuli (which did not) were randomly interleaved and presented at a rapid rate (1 stimulus per second), ruling out the possibility that the subjects' attentional state differed between the stimulus classes. Finally, the behavioral performance during the face and house experiment showed that the subject correctly labeled all stimuli (n = 99 trials) as a face or a house.

A previous report showed that in macaque LFP recordings, narrowband gamma oscillations are observed in response to high contrast gratings but not low contrast gratings (Henrie and Shapley, 2005). In our experiments, the noise stimuli and the gratings had the same luminance range, and the binary white noise stimuli and the gratings had the same luminance variance. Hence the absence of gamma oscillations in response to the noise patterns is not a result of low spatial contrast. Some spatial patterns do not elicit gamma oscillations.

The lack of narrowband oscillations to the noise patterns cannot be due to a lack of coherent spatial structure or recognizable content in the images. Images containing faces and houses with moderate white noise superimposed did not lead to consistent gamma band oscillations in the expected locations in visual cortex, despite the fact that the subject attended to and accurately classified the images as faces or houses.

Exactly which stimulus features are necessary to elicit gamma oscillations is unclear. As we show, noise patterns do not have the necessary features. It appears that gratings and bars reliably elicit gamma oscillations in humans (Figures 1, 2, 3, 5, and (Hoogenboom et al., 2006)) as well as animals (Gray et al., 1989, Gray and Singer, 1989). Important features of the oscillation such as its peak frequency and amplitude depend on specific stimulus features such as color (Swettenham et al., 2013), contrast (Henrie and Shapley, 2005, Ray and Maunsell, 2010), spatial area (Bauer et al., 1995, Gieselmann and Thiele, 2008, Jia et al., 2011, Ray and Maunsell, 2011, Jia et al., 2013b), noise masking (Zhou et al., 2008, Jia and Kohn, 2011, Jia et al., 2013a), and the number of orientations (Lima et al., 2010, Bartolo et al., 2011).

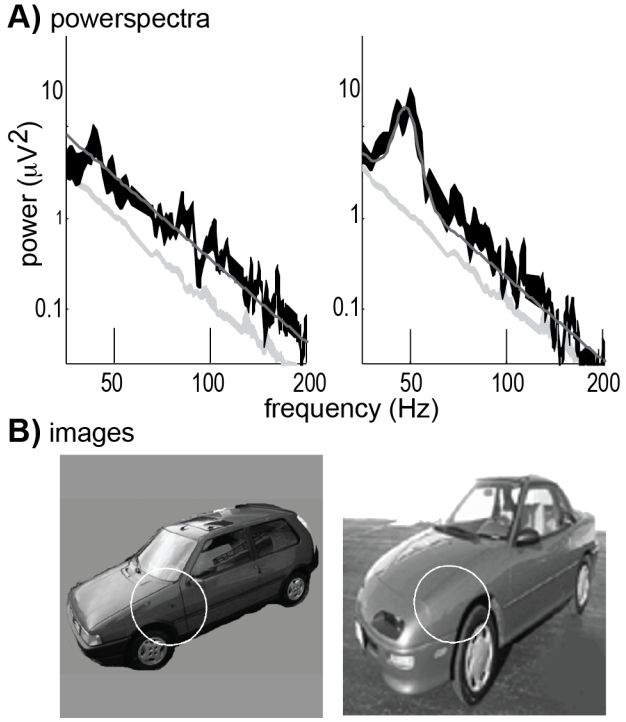


**Figure 6: Two example stimuli that induced different levels of narrowband gamma power in V1. A)** Power spectra from a foveal V1 electrode for two example stimuli (from a set of 72 stimuli, see Supplemental Figure S3) that were shown to a separate subject in a prior study (Parvizi et al., 2012). Each stimulus was shown 6 times in random order.The 95% confidence intervals are shown in black and the baseline periods are shown in light gray. The baseline is identical for all images. The model fits (power law plus Gaussian) are plotted as a dark gray line. **B)** The two images with the population Receptive Field (pRF) from the measured electrode indicated by a white circle (two standard deviations of the pRF Gaussian). The pRF models were obtained from a prior study (Winawer et al., 2013). The car image on the left elicited only a broadband response but no clear gamma oscillation. The car image on the right elicited both a broadband response and a large gamma oscillation.

A recent ECoG measurement in macaque showed that gamma oscillations were elicited during the free viewing of natural images (Brunet et al., 2013). The gamma response was present for several of the images shown and in the mean response across all images. In a re-analysis of a dataset used for another study (Parvizi et al., 2012, Jacques et al., 2013), we quantified the narrowband gamma response to 72 images of faces, houses, limbs, and cars (Figure S3). It is likely that our results are consistent with those of Brunet et al (2013) in one sense: some natural images elicit narrowband gamma oscillations in visual cortex. Consequently, the mean across all stimuli is above zero.

However, many images do not elicit significant gamma oscillationsin V1 (32 and 33 of 72 images for two V1 electrodes). The lack of gamma oscillations observed for nearly half the stimuli is unlikely to be due to measurements artifacts, as nearly all stimuli elicited a significant broadband response (69 and 68 of 72 images for the same two electrodes).

Figure 6 shows two example images, one that produces a large gamma oscillation and one that does not. These images were viewed 6 times each and the amplitude of the broadband and narrowband responses was reliable across the repetitions, but different between stimuli. All of the images contained recognizable objects or scenes; the fact that many failed to elicit clear gamma oscillations indicates that this response depends on the spatial structure of the image, and is not likely to be necessary for perception, attention, or recognition. We cannot rule out the possibility that for stimuli near detection or recognition threshold, the presence or absence of gamma oscillations will modulate an observer's judgments. However, since very large differences in the gamma response can be observed across different stimuli, it is unlikely that the gamma amplitudeis the principal determinant of stimulus detection or recognition.

We conclude that narrowband gamma oscillations are stimulus specific.Principles of information transfer that are governed by gamma oscillations, such as increased coherence between sites for attended stimuli (Womelsdorf et al., 2007), may hold for specific stimulus patterns that produce gamma oscillations, but are not likely to hold generally across different types of stimuli.

Predicting which stimuli will elicit a narrowband gamma response and predicting the parameters of that response will require a more complete model. There has been some progress modeling the local neural circuits that give rise to gamma oscillations in neocortex. For example, in vitro measurements show that gamma oscillations can be driven by the interactions between principal cells and interneurons (Llinas et al., 1991, Whittington et al., 1995, Cunningham et al., 2004), and computational models have been developed to capture these interactions (Wang, 2010). One possibility is that regularized

spatial patterns projected to visual cortex might be traded for a regularized 'reverberation' timescale in recurrent feedback between principal cell and interneuron synaptic connections, reflected by the frequency of gamma oscillations (20-25ms for feedback corresponding to a 40-50Hz oscillation). More work is needed to define the stimulus-driven inputs that set up the conditions to produce these oscillations.

### Broadband spectral power elevation is observed for all visual stimuli tested

The stimulus features that give rise to the broadband ECoG signals in visual cortex, unlike the features which give rise to gamma oscillations, are qualitatively well-matched to expectations from other functional measurements, such as fMRI and single unit measurements in animals. All stimuli with spatial contrast patterns induced robust broadband signals across V1/V2/V3, with the exception of stimuli confined to very low spatial frequencies that only elicited broadband signals in more peripheral electrodes, and stimuli dominated by high frequencies, which only elicited in broadband signals in more foveal electrodes. Furthermore, broadband ECoG responses to faces and houses arise in the same regions known to be activated in fMRI measurements (Puce et al., 1995, Kanwisher et al., 1997, Aguirre et al., 1998, Epstein and Kanwisher, 1998).

Although human MEG and EEG recordings sometimes show narrowband oscillations (Hoogenboom et al., 2006, Vidal et al., 2006, Muthukumaraswamy et al., 2009, Scheeringa et al., 2011, van Pelt and Fries, 2013), human ECoG measurements typically show an increase in broadband amplitude (for a review see (Crone et al., 2011) and for recordings in early visual cortex see (Harvey et al., 2013, Winawer et al., 2013)). Although these broadband responses often extend into the gamma range, they should not be considered oscillations, as the spectra are not peaked (Ray and Maunsell, 2011, Lopes da Silva, 2013).

A previous human ECoG study reported gamma oscillations in visual cortex (Tallon-Baudry et al., 2005), but from analyses and figures these narrowband responses are often not separable from broadband responses. Because broadband increases can span frequencies in which oscillations are typically observed (30-80 Hz) (Miller et al., 2009b, Harvey et al., 2013, Winawer et al., 2013), decomposing the signal into two frequency bins (e.g. 50-80 Hz and 100-200 Hz) may not adequately separate the two responses. We fit a model to the spectrum to differentiate between these two phenomena; other methods have also been developed to separate narrowband and broadband changes in the ECoG power spectrum (Miller et al., 2009d, Winawer et al., 2013).

### Implications for theories of brain function

Only certain stimuli, such as gratings, reliably produce neural responses that drive resonant (narrowband) gamma oscillations in visual cortex circuits. However, all the stimuli used in this study produce a general (broadband) response. Gamma oscillations and broadband responses do not just differ in the frequency range in which they occur; they also differ in that one has a narrow peak and one does not, reflecting different underlying circuit properties (Manning et al., 2009, Miller et al., 2009b, Ray and Maunsell, 2011). Understanding the relationship between the stimulus and the two responses is likely to clarify fundamental aspects of the circuitry in visual cortex.

For certain stimuli, the power in gamma oscillations is poorly matched to the amplitude of multi-unit activity, in that stimulus manipulations which increase one signal decrease the other (Bartolo et al., 2011, Ray and Maunsell, 2011). Spectrally broadband signals, in contrast, are likely better matched to the total neural activity in nearby regions, reflecting the rate of either input (Miller et al., 2009b) or output (Ray and Maunsell, 2011) action

potentials. Hence when a large spectral peak is observed in a field potential recording, it does not imply that there is a large underlying neural response; it may be a relatively small response that is highly synchronized. In contrast, a large broadband response is more likely to indicate a large neural response. It is likely that perceptual phenomena and other physiological measures such as the BOLD signal will depend in different ways on these circuits.

Broadband and narrowband gamma signals thus indicate different neurophysiological processes. Gamma oscillations may serve a function of information transfer, but only for certain types of visual stimuli that produce a gamma oscillation. Theories about the role of gamma oscillations in visual information processing that do not incorporate stimulus properties are at best incomplete.

# Chapter 5: Decoding the inferior temporal cortex at the speed of perception

Most brain-computer interface classification experiments from electrical potential recordings have been focused on the identification of classes of stimuli or behavior where the timing of experimental parameters is known or pre-designated. Real world experience, however, is spontaneous, and to this end we describe an experiment predicting the occurrence, timing, and types of visual stimuli perceived by human subjects. Electrocorticographic arrays were placed on the subtemporal cortical surface of 7 epilepsy patients. Simple, luminance and contrast matched, grayscale faces and houses were displayed rapidly, in random sequence. We develop a novel template-projection method, where event-averaged broadband timecourse and event-averaged raw potential from training periods were used as filters for testing periods. We found that they contribute independently to classifiability and prediction of the stimuli. If both broadband and raw potential features were used, and the timing of testing stimuli was defined ahead of time, 97% of stimuli could accurately be classified as face or house. When the spontaneous testing data stream was examined, 96% of all stimuli were captured spontaneously (more than 90% in every subject), with approximately 20ms error. Only 4% of the spontaneous predictions were incorrect (i.e. predicted stimuli at the wrong time, or as the wrong class).

## Introduction

Different measurements from the brain contain information about different processes. For the decoding of neural activity it is necessary to understand whether different information can be gained from these different types of responses. Functional MRI (fMRI) measures a combination of blood flow, blood volume and blood oxygenation and single unit recordings measure the firing in individual neurons. Local field potentials (LFP) measure the signal from a large number of neurons, and are therefore a complex combination of signals from different origin (Buzsaki et al., 2012). This study investigated how different parts of the local field potential contribute to the decoding of visual stimuli.

A neuronal population in early visual cortex processes different classes of visual information within the same spatial location of the visual field (Wandell, 1995). Higher order inferotemporal visual areas instead represent different classes of visual stimuli with distinct cortical surface regions: category specific areas in the human temporal lobe have been established unambiguously at the several millimeter to centimeter scale, using functional imaging and field potentials (Puce et al., 1995, Kanwisher et al., 1997, Aguirre et al., 1998, Epstein and Kanwisher, 1998). They have also been demonstrated at the single unit level in epileptic human patients (Kreiman et al., 2000) and non-human primates (Kiani et al., 2007).

The first measurements of category specific responses in inferior temporal cortex were shown using event related potentials (ERPs) (Allison et al., 1994a, Allison et al., 1994b) and fMRI (Puce et al., 1995, Kanwisher et al., 1997, Aguirre et al., 1998, Epstein and Kanwisher, 1998). When relating these two signals however, little overlap was found between the ERP and the fMRI response (Huettel et al., 2004). In contrast, high frequency broadband increases matched well with the category specific fMRI responses in the inferior temporal cortex (Engell et al., 2012). The ERP and broadband signals show distinct, and partially overlapping responses to faces (Engell and

McCarthy, 2011), and broadband responses are more specific for face identity (Engell and McCarthy, 2014). The N200 ERP may thus simply reflect an initial response that occurs in all occasions of the correct object with the correct features (a face), but not carry much specific information. It thus remains unknown whether the ERPs provide a useful signal about the processing of category specific stimuli in inferior temporal cortex in addition to broadband responses.

Even though the ERP may not correlate well with the fMRI signal, and may contain less object specific information, EEG and MEG recordings have shown that using the ERP, single trial object categories could be classified with 90% accuracy (Simanova et al., 2010, van de Nieuwenhuijzen et al., 2013). Previous ECoG work in humans that used the raw potential (filtered between 1-100 Hz) to identify 5 different object categories, could decode the individual trial object category with an accuracy of 58-82% (Liu et al., 2009). An optimal 'neural decoder' however requires two additional steps. First, previous studies decoded which stimulus was shown, when the onset was known and a decoder should also be able to identify whether and when a stimulus was present. Second, when seeing a face or a house, humans can easily identify the category with >90%, and a neural decoder should be able to reach similar performance.

This paper shows a method that allows for a direct comparison between the information from broadband and ERP signals for the use of online decoding from the brain. Using ECoG, we measured from several inferior temporal visual areas simultaneously and attempted to spontaneously identify visual stimuli and assign them to one of two classes, faces or houses. Rather than examine fluctuations in the raw potential, we employed a new technique for extracting broadband temporal power spectral estimates which recently has been shown to capture robust local neuronal population activity (Miller et al., 2009b, Miller et al., 2009d), and demonstrate that it can be used to capture, with high temporal fidelity, the cortical responses to spontaneous face or house visual stimuli. We extract the site-specific ERP and investigate whether the ERP adds any

additional information about the stimulus category or onset. Using these techniques, we can decode with >90% correct whether, when and which stimulus was shown, therefore reaching levels of performance on the same scale as behavior.

# Methods

## Subjects

All 7 subjects in the study were epileptic patients at Harborview Hospital in Seattle, WA. Sub-dural grids and strips of platinum electrodes were clinically placed over frontal, parietal, temporal, and occipital cortex for extended clinical monitoring and localization of seizure foci. Each subject gave informed consent to participate in an Institutional Review Board approved experimental protocol. All patient data was anonymized according to IRB protocol, in accordance with HIPAA mandate.

## Recordings

Experiments were performed at the bedside, using Synamps2 amplifiers (Neuroscan, El Paso, TX) in parallel with clinical recording. Stimuli were presented with a monitor at the bedside using the general purpose BCI2000 stimulus and acquisition program (interacting with proprietary Neuroscan software), which also recorded the behavioral parameters and cortical data. Sub-dural platinum electrode arrays (Ad-Tech, Racine, WI) were arranged as combinations of 8x[4,6,8] rectangular fronto-tempero-parietal arrays and 1x[4,6,8] linear temporal and occipital strips. The electrodes had 4mm diameter (2.3mm exposed), 1 cm inter-electrode distance, and were embedded in silastic. The potentials were sampled at 1000 Hz, with respect to a scalp reference and ground, then subjected to an instrument-imposed bandpass filter from 0.15 to 200 Hz.

## Face-House visualization task

Subjects performed a basic face and house stimulus discrimination task. Subjects were presented with simple, grayscale, pictures of faces and houses (luminance and contrast matched) that were displayed in random order for 400ms each, with 400ms inter-stimulus interval between. 10cm-

wide pictures were displayed at ~1m from the patients, while they were seated at the bedside (figure 1). There were 3 experimental runs with each patient, with 50 house pictures and 50 face pictures in each run. In order to maintain fixation on the stimuli, patients were asked to report a simple target (an upside-down house), which appeared once during each run. There were no errors in reporting the target house in each run.

## Electrode localization

Electrode location relative to gyral surface anatomy was determined by projection of the post-implant CT to the pre-operative axial T1 using normalized mutual information in SPM (Wells et al., 1996, Ashburner and Friston, 2005). Cortical surface mesh reconstructions were made using pre-operative structural MRI. Electrode positions were calculated with respect to the structural MRI from post-operative computed tomography (CT) using the CTMR package of Hermes, et. al., 2010 (Hermes et al., 2010) and rendered on the freesurfer extracted surface (Dale et al., 1999). When the MRI or CT was of insufficient quality, hybrid techniques were employed to obtain cortical rendering and/or electrode position (Miller et al., 2010a).

## Signal processing

Lateral frontoparietal electrode grids were discarded from analysis, and only strip electrodes were further considered. To reduce common artifact, the potential, $V_n^0(t)$, measured at each electrode $n$ was re-referenced with respect to the common average of all $N$ electrodes, $V_n(t) = V_n^0(t) - \frac{1}{N}\sum_{i=1}^{N} V_i^0(t)$, (electrode label, $n$, dropped for the time being). Electrodes with significant artifact or epileptiform activity were rejected prior to common averaging. Ambient line noise was rejected by notch filtering between 58-62Hz using a 3rd-order Butterworth filter (Porat, 1997).

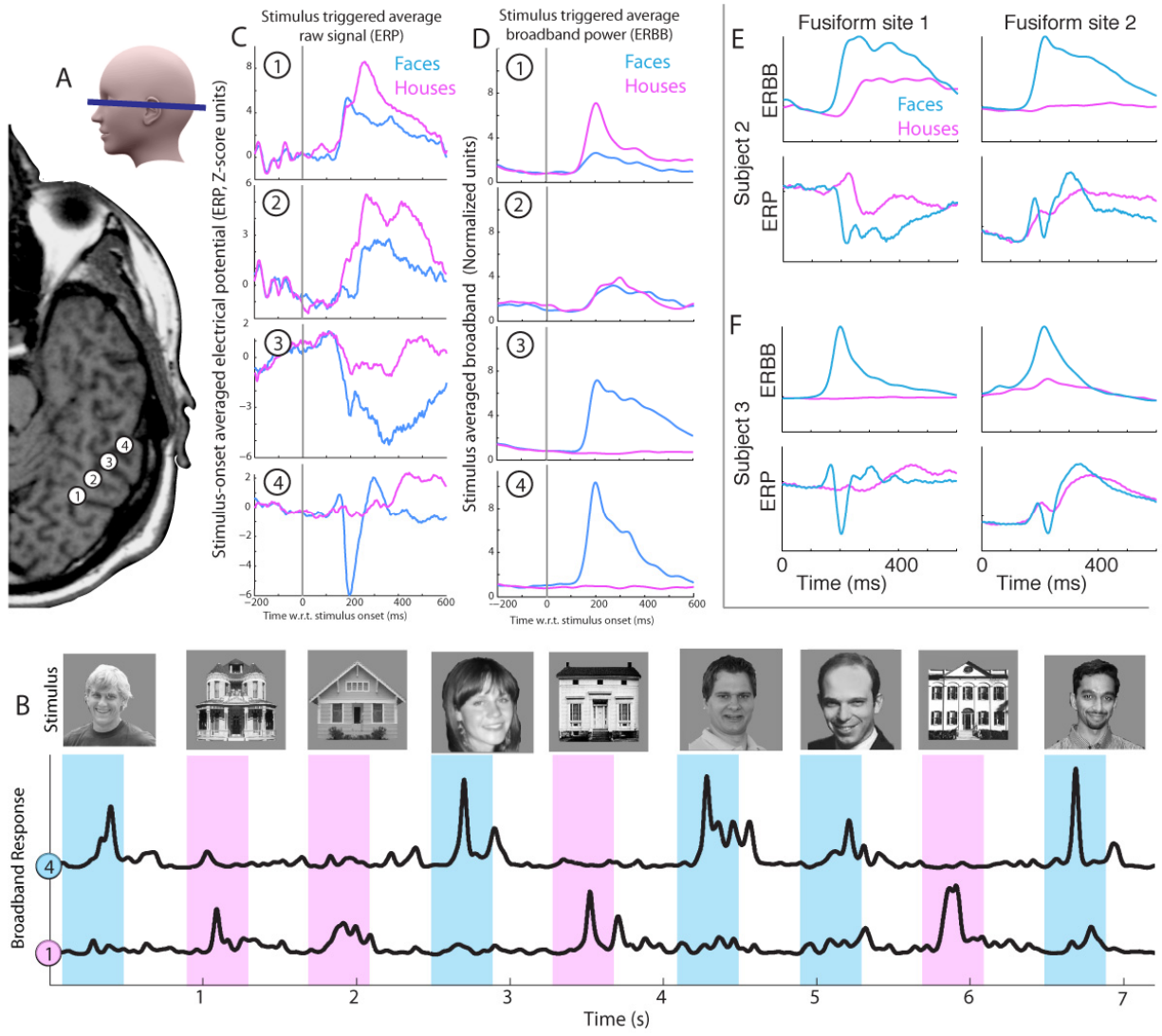


**Figure 1: The basic face and house discrimination task, and the polymorphic nature of the electrophysiologic response. (A)** Sub-dural electrocorticographic (ECoG) electrode strips were placed through burrholes in the skull, onto to ventral temporal brain surface. 4 adjacent sites are shown for subject 1. **(B)** Simple luminance and contrast matched grayscale faces and houses that were displayed in random order for 400ms each (blue=faces; pink=houses), with 400ms blank gray screen inter-stimulus interval between each picture. Subjects were asked to report a simple target (an upside-down house, which was rejected from analyses). From the raw potential, the timecourse of broadband spectral change can be extracted from each brain site (here sites 1&4 from (A)). **(C)** The averaged raw potential (ERP) following face (blue) and house (pink) stimuli, at the sites in (A). **(D)** The averaged broadband following different stimuli (ERBB), reflecting the averaged neuronal population activity as a function of time. **(E-F)** ERBB and ERP for 2 fusiform sites in subjects 2 and 3. Note that the responses are highly polymorphic for the event related potentials, and that there are ERP face-selective sites that do not have the classic N200 shape.

## Power spectral densities

*Power spectral snapshots:* A set of epochs surrounding the middle of each face or house visual stimulus and each ISI period, $\tau_q$, were extracted from $V(t)$; each epoch was of duration $T$=1s, $\left(\tau_q - \frac{1}{2}T\right) < t < \left(\tau_q + \frac{1}{2}T\right).\tau_q$. The power spectral density (PSD) of the epoch flanking time $\tau_q$ was calculated as $P(f,q) = \left| \frac{1}{\sqrt{T}} \sum_{t=-T/2}^{+T/2} V(\tau_q + t) H(t) e^{i2\pi ft} \right|^2$ with Hann window (Porat, 1997) $H(t) = \frac{1}{2}\left(1 + \cos\left(\frac{2\pi t}{T}\right)\right)$.

*Wavelet approach:* A Morlet wavelet (Goupillaud et al., 1984) of the form: $\psi(\tau,t) = \exp\frac{i2\pi t}{\tau}\exp\frac{-t^2}{2\tau^2}$ was convolved with the timeseries to get a time-frequency estimate for every $f = 1/\tau$:

$$\tilde{V}(1/\tau,t) = \sum_{t'=-5\tau/2}^{5\tau/2} V(t+t')\psi(t',\tau)$$

A total of 5 cycles ($5\tau$) was used to estimate the amplitude and phase of the signal at each frequency for every point in time. In this way a time-varying Fourier component $\tilde{V}(f,t) = r(f,t)e^{i\phi(f,t)}$, with fixed uncertainty between the confidence in the estimate of the instantaneous amplitude and phase versus the confidence in temporal resolution is obtained at each Hz.

## Decoupling the cortical spectrum to separate rhythmic activity away from broadband change

The decoupling process is described and illustrated in detail in the main text and supplement to (Miller et al., 2009d), and illustrated for this context in (Miller et al., 2014). It was applied here as follows:

*Principal component decomposition of spectral change:* The samples of the PSD, $P(f,q)$, (total $N_q$), were normalized prior to decomposition: $\hat{P}(f,q) = \ln(P(f,q)) - \ln\left(\frac{1}{N_q}\sum_q P(f,q)\right)$. A PCA

method was used to determine the eigenvalues $\lambda_k$ and eigenvectors $\vec{e}_k$ of the correlation matrix: $C(f,f') = \sum_q \hat{P}(f,q)\hat{P}(f',q)$. These eigenvectors, $\hat{C}\,\vec{e}_k = \lambda_k\,\vec{e}_k$, the ``Principal Spectral Components" (PSCs), reveal which frequencies vary together, and are ordered by magnitude of corresponding eigenvalue: $\lambda_1 > \lambda_2 > \cdots > \lambda_{N_f}$ ($N_f \equiv$ number of frequencies). If we define the rotation matrix $A(f,k) = (\vec{e}_1, \vec{e}_2, \cdots, \vec{e}_{N_f})$, then the projection, $W(k,q)$, of each individual original spectrum in the ensemble onto the new basis vector $k$ is $W(k,q) = \sum_f A(k,f)\hat{P}(f,q)$.

*The timecourse of broadband spectral change:* The time-dependent, normalized, dynamic spectrum, $\hat{P}(f,q)$, can be obtained in parallel fashion to the spectral snapshots.

$P(f,t) = \frac{\left|\tilde{V}(f,t)\right|^2}{\frac{1}{N_t}\sum_t \left|\tilde{V}(f,t)\right|^2}$, and $\hat{P}(f,t) = \ln(P(f,t)) - \ln\left(\frac{1}{N_t}\sum_t P(f,t)\right)$. The reflection of the 1st PSC ($\vec{e}_1$) in the dynamic spectrum can be estimated by projecting the dynamic spectrum onto it: $\ln A(t) = \sum_f e_1(f)\hat{P}(f,t)$. We call it $\ln A(t)$ here, because it approximates the logarithm of the timecourse of the coefficient of a power law in the cortical spectrum of the form $P(f,t) = A(t)f^{-\chi}$ (Miller et al., 2009b). The "broadband timecourse" for electrode $n$ is obtained by smoothing $\ln A(t)$ with a Gaussian filter of standard deviation 80ms and then z-scoring, exponentiating, and subtracting 1: $B_n(t) = \exp\left(\ln A_n^Z(t)\right) - 1$. The broadband power timecourse is meant to function as a time-varying estimate of a multiplicative factor in the population firing rate (Miller et al., 2009b, Miller et al., 2009d, Miller et al., 2014).

## Classification

### Cross-folding

Prior to further analysis, the data were then divided into thirds temporally. Subsequent analyses were then performed in a 3-fold fashion. In each fold, two thirds of the data were assigned to a "training" set, and the remaining third was assigned to a "testing" set. In this way, all data could be used for both testing as well as training, but never at the same time (to maximize use without simultaneously testing and training on the same data).

### Template projection technique

*Stimulus triggered averaged raw potential and broadband template:* In each electrode $n$, stimulus triggered averages of the **training data** were obtained for the common-averaged electric potential for the face ($S \to F$, face) and house ($S \to H$, house) stimuli independently ($\tau_{k_s}$ denotes the $k^{th}$ of $N_S$ total instances of stimulus type $S$):

$$\langle V_n(t') \rangle_S^0 = \frac{1}{N_S} \sum_{k_s=1}^{N_S} V_n\left(\tau_{k_s} + t'\right).$$

This quantity is only calculated on the peri-stimulus interval $-199 < t' \le 400$ ms (where $t'$ denotes time with respect to stimulus start). It is then re-centered by subtracting the average potential peri-stimulus baseline on the interval $-199 < t' \le 50$, to obtain $\langle V_n(t') \rangle_S$:

$$\langle V_n(t') \rangle_S = \langle V_n(t') \rangle_S^0 - \frac{1}{250} \sum_{t''=-199}^{50} \langle V_n(t'') \rangle_S^0$$

We perform the same averaging over the **training data** for the broadband signal to obtain $\langle B_n(t') \rangle_S$.

### Projection of templates into pre-defined times of stimuli onset

$\langle V_n(t') \rangle_S$ and $\langle B_n(t') \rangle_S$ were generated from the **training period**.

**Training feature points** were obtained by back-projecting $\langle V_n(t') \rangle_S$ and $\langle B_n(t') \rangle_S$ into the **training period** to obtain a set of training feature points, $\Gamma_{n,S}^V(q)$ and $\Gamma_{n,S}^B(q)$ for each event $q$ at time $\tau_q$:

$\Gamma^{V}_{n,S}(q) = \sum_{t'=-199}^{400} \langle V_n(t') \rangle_S \left( V_n(\tau_q + t') - \overline{V^b_n(\tau_q)} \right)$, where $\overline{V^b_n(\tau_q)}$ represents an "instantaneous" baseline surrounding time $\tau_q$: $\overline{V^b_n(\tau_q)} = \sum_{t=-199}^{50} V_n(t + \tau_q)$. $\Gamma^{B}_{n,S}(q)$ were obtained in the same fashion. The event types were face picture stimulus onset, house picture stimulus onset, or randomly chosen points during the ISI (4 during each ISI period, at least 100ms from stimulus offset/onset and 50ms from one another, notated as $S \to o$).

**Testing feature points** $\Gamma^{V}_{n,S}(p)$ and $\Gamma^{B}_{n,S}(p)$ were similarly obtained by projecting $\langle V_n(t') \rangle_S$ and $\langle B_n(t') \rangle_S$ into the **testing period** for pre-defined times of face or house picture stimuli onset events, $p$, at times $\tau_p$.

### Projection of templates into continuous data stream

In order to quantify how well the averaged raw potential $\langle V_n(t') \rangle_S$ is represented in the voltage timeseries of the **testing data** at time $t$, it is directly projected onto the continuous timeseries: $\Gamma^{V}_{n,S}(t) = \sum_{t'=-199}^{400} \langle V_n(t') \rangle_S \left( V_n(t + t') - \overline{V^{\tau}_n(t)} \right)$, where $\overline{V^{\tau}_n(t)}$ was obtained in the same fashion as above. The same projection is performed for the broadband template $\langle B_n(t') \rangle_S$, to obtain $\Gamma^{B}_{n,S}(t)$.

### Generation of a feature space

The full feature space for classification, consisting of the union of projections of the stimulus triggered average raw potentials ($V$) or broadband ($B$) across all electrodes ($n$), for faces ($F$) and houses ($H$) independently, is the combination of $\Gamma^{V}_{n,F}$, $\Gamma^{V}_{n,H}$, $\Gamma^{B}_{n,F}$, and $\Gamma^{B}_{n,H}$. For notational brevity, we can combine the notation to denote each feature as $\Gamma_m$, where $m$ represents a unique combination of on electrode $n$, $V$ or $B$, and $F$ or $H$. Many of these features will not be particularly informative about when and how the brain is processing these visual stimuli. Therefore, features were individually downselected by independently assessing their squared cross-correlation between events of the paired stimulus type and events drawn from the ISI during

the **training period**, and rejecting those which fell beneath the pre-defined threshold $r_m^2 < 0.05$. For example, for projections of the face event-related feature, $\Gamma_{n,F}$ ($V/B$ label dropped here) we can denote the average of face stimuli as

$r_{n,F}^2 = \frac{\left(\overline{\Gamma_{n,F}(q=F)} - \overline{\Gamma_{n,F}(q=o)}\right)^2}{\sigma_{n,Fo}^2} \frac{N_F * N_o}{N_{Fo}^2}$, where $\sigma_{n,Fo}$ is the standard deviation of the joint distribution for face and ISI events $\Gamma_{n,F}(q=F,o)$, $N_F$ is the number of face events, $N_o$ is the number of ISI events, and $N_{Fo} = N_F + N_o$. In this study, we consider feature spaces consisting of projections of all types, and also downselect to assess the utility of $B(t)$ and $V(t)$ independently.

### Classifier type and feature space

We begin with the feature set of training points ($q$, drawn from only the training period), $\Gamma_m(q)$, where each $m$ is a dimension in the feature space, and represents a particular combination of electrode, broadband or raw potential timeseries, and face or house template. For the sake of simplicity, Fisher linear discriminant analysis (LDA) was used for classification (Bishop, 1995). This characterizes the full distribution and the **training period** sub-distributions $\Gamma_m(q \to F)$, $\Gamma_m(q \to H)$, $\Gamma_m(q \to o)$, by their means and covariances only (i.e. as if they are normally distributed). LDA assumes that the covariances of the sub-distributions are the same. Given these training distributions, data from the testing set can be assigned a posterior probability of belonging to each distribution.

### Classification of discrete events (where onset time is designated)

We began with the case where we identify the timing of testing visual stimuli, and attempt to classify whether a face or a house picture was shown. Only the face and house **training point distributions** were used. For each **testing point**, $p$, the assigned class was whichever posterior probability $\Pr\{\Gamma(p)|q \to F\}$, or $\Pr\{\Gamma(p)|q \to F\}$, was higher.

### Classification of continuous data

For the prediction of type and timing of visual stimulus from continuous signal, first the face, house, and ISI **training point distributions** were characterized. Then, the LDA posterior probability that a face or house stimulus has been shown at any point in time can be measured as $\Pr\{\Gamma(t)|q \to F\}$ or $\Pr\{\Gamma(t)|q \to H\}$. We then smooth each of these posterior probabilities with a σ=80ms Gaussian filter. From this, we assign predicted times for stimuli onset as follows: The posterior probability must be a local maximum. There must be at least with at least 320ms between any point and the nearest assigned point (of either stimulus type – the larger posterior probability 'wins').

## Results

ECoG signals were measured in seven subjects from electrodes implanted on the inferior temporal visual areas for the purpose of epilepsy monitoring. Subjects looked at simple pictures of faces and houses (similar to those in figure 1). We attempted to spontaneously identify visual stimuli and assign them to one of two classes, faces or houses.

### Signal features used for classification: the event related broadband (ERBB) and event related potential (ERP)

To test whether the ERBB and ERP provide useful information to decode the whether, when and which class of stimulus was presented, we extracted the ERBB and ERP for every electrode. Some electrodes show a classical face specific N200, as described before stimuli (Allison et al., 1994a, Allison et al., 1994b). Other electrodes show every differently shaped face specific ERPs (figure 1).

### Decoding single trial stimulus class when the onset of a stimulus is known

To decode the single trial stimulus class when the onset of a stimulus is known, template ERBB and ERP responses were calculated from the training data. Training data for the classifier consisted of 2/3 of the data and testing data consisted of the other 1/3, and we used 3 fold cross validation. Figure 2 shows a simple example of template ERBB responses for a face and a house specific site. Even in a simple two-dimensional subspace of the full feature space, a simple line serves as a good classification boundary between the two classes of stimuli. Using either the ERP or the ERBB feature, stimuli could be robustly and reliably categorized in all cases. The average prediction using the ERBB alone was 97% across all 7 subjects (figure 3). Using the ERP alone, it was 90%, and using a combination of the two features, 97% of stimuli could accurately be classified as face or house (Figure 3). The overall best prediction was thus reached with the ERBB or a combination of the ERBB and the ERP.

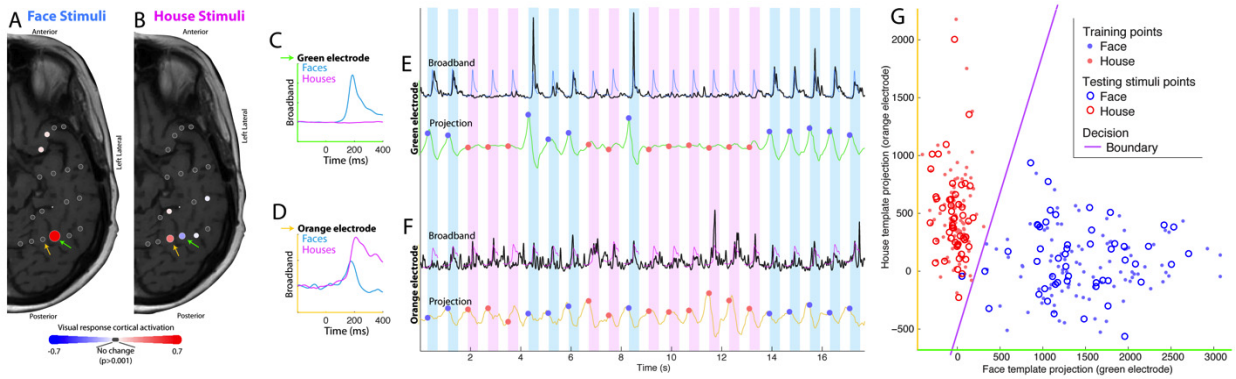


**Figure 2: Discrete point classification, subject 3. (A)** Squared cross-correlation values at each electrode **training feature points** were obtained by back-projecting the event triggered broadband, $\langle B_n(t')\rangle_F$, into the training data and comparing projected face, $\Gamma^B_{n,F}(q \to F)$, and ISI, $\Gamma^B_{n,F}(q \to o)$, points. These $r_n^2$ values are scaled by color, and plotted on an axial MRI slice. as shown in the colored bar beneath. The electrodes meeting acceptance criteria $r_n^2 > 0.05$ were selected as features for classification for the face template. **(B)** As in (A), but for house stimuli from the training period. **(C)** Event triggered broadband for face, $\langle B_1(t')\rangle_F$, and house, $\langle B_1(t')\rangle_H$, from the electrode noted with a green arrow in A/B.**(D)** As in (C), but from the electrode noted with an orange arrow. (**E)** Projection of event-triggered face template from (C) into **testing data**:The top black trace shows a portion of the broadband timecourse from the electrode noted with a green arrow, during the testing period, $B_1(t)$. The $\langle B_1(t')\rangle_F$ face template is shown in light blue at each stimulus time, irrespective of class, at event testing times $\tau_p$. The result of projecting the face template $\langle B_1(t')\rangle_F$ to $B_1(t)$is shown in the green trace, $\Gamma^B_{1,F}(t)$, with testing points at defined face stimulus times, $\Gamma^B_{1,F}(p \to F)$, shown in blue circles, and defined house stimulus times, $\Gamma^B_{1,F}(p \to H)$, shown with red circles. **(F)** As with (E),, but for the orange-arrow electrode, $B_2(t)$, and using the house template from (D), $\langle B_2(t')\rangle_H$. **(G)** The subspace $\Gamma^B_{1,F}$ vs $\Gamma^B_{2,H}$, is used to illustrate discrete classification approach. Here the back-projected training points $\Gamma^B_{n,S}(q)$ are shown with dots (blue for $q \to F$ and red for $q \to H$), along with the testing feature points $\Gamma^B_{n,S}(p)$ shown with circles. One may see that a simple decision line (purple) in this subspace would result in only 1 error.

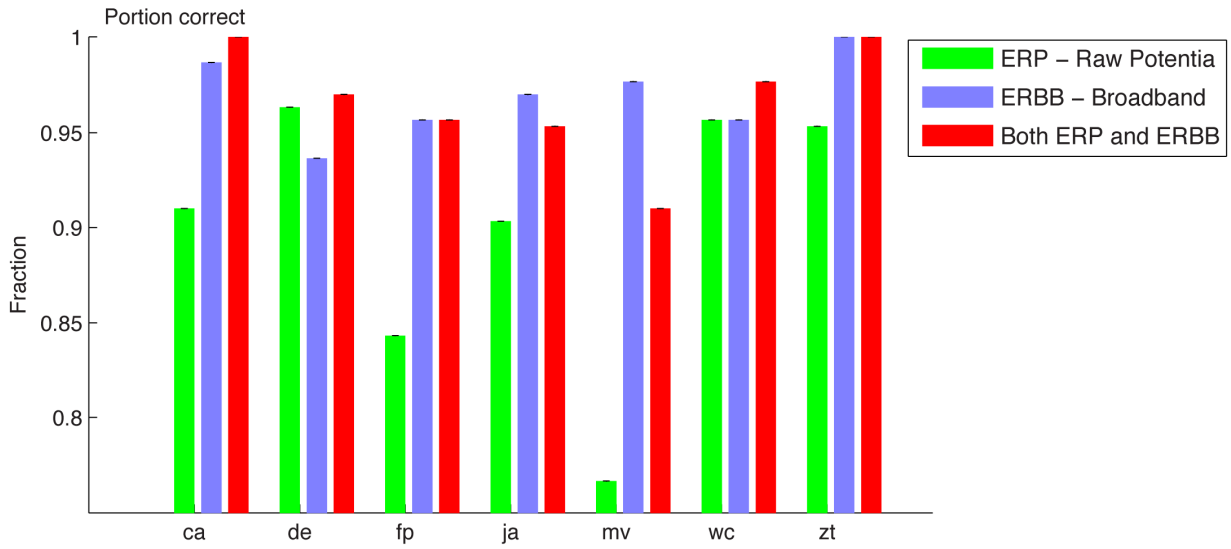


**Figure 3: Classification accuracy for pre-defined timepoints, using ERP, ERBB, or both template types.** In some subjects, 100% accuracy was reached, and all were above 90% when both raw potential and broadband templates were used.

## Decoding stimulus class and onset in a spontaneous data stream

More important than the classification of stimuli where the timing is pre-designated is whether we could decode the single trial stimulus class and onset time from a continuous data stream. The mechanism we used first to attempt this is shown in figure 4, where template responses from a training period were run through a testing period of data. The result of plotting the projection timeseries trajectory in a 2-dimensional subspace, $\Gamma^{B}(t)$, can be seen alongside training points $\Gamma^{B}_{n,S}(q)$. Even in this 2-dimensional subspace projection, the furthest excursions of $\Gamma^{B}(t)$ into the face or house training clouds, $\Gamma^{B}_{n,S}(q)$, were generally the times of predicted stimulus onset.

Figure 5 shows a similar example to figure 4, but when the ERP is used to predict the onset and class of a stimulus, and is illustrated for a three dimensional subspace of the full feature space. Similarly, figure 6 shows how a combination between ERP and ERBB projections can be used to predict the onset timing and class of stimuli more than either independently. Figure 7 shows that spontaneous classification of onset time and stimulus class was robust: the average prediction accuracy was 92% using the ERBB, 92% when using the ERP, and 96% of all stimuli were captured spontaneously when using a combination if both. Furthermore, timing of stimulus onset could be

predicted with approximately 20ms error when the ERP or a combination between the ERP and ERBB was used. The number of incorrect predictions was overall the least (4%) when a combination between the ERP and ERBB was used (i.e. predicted stimuli were at the wrong time >160ms, or as the wrong class). Taken together, the overall best prediction was reached by a combination of ERBB and ERP projections.

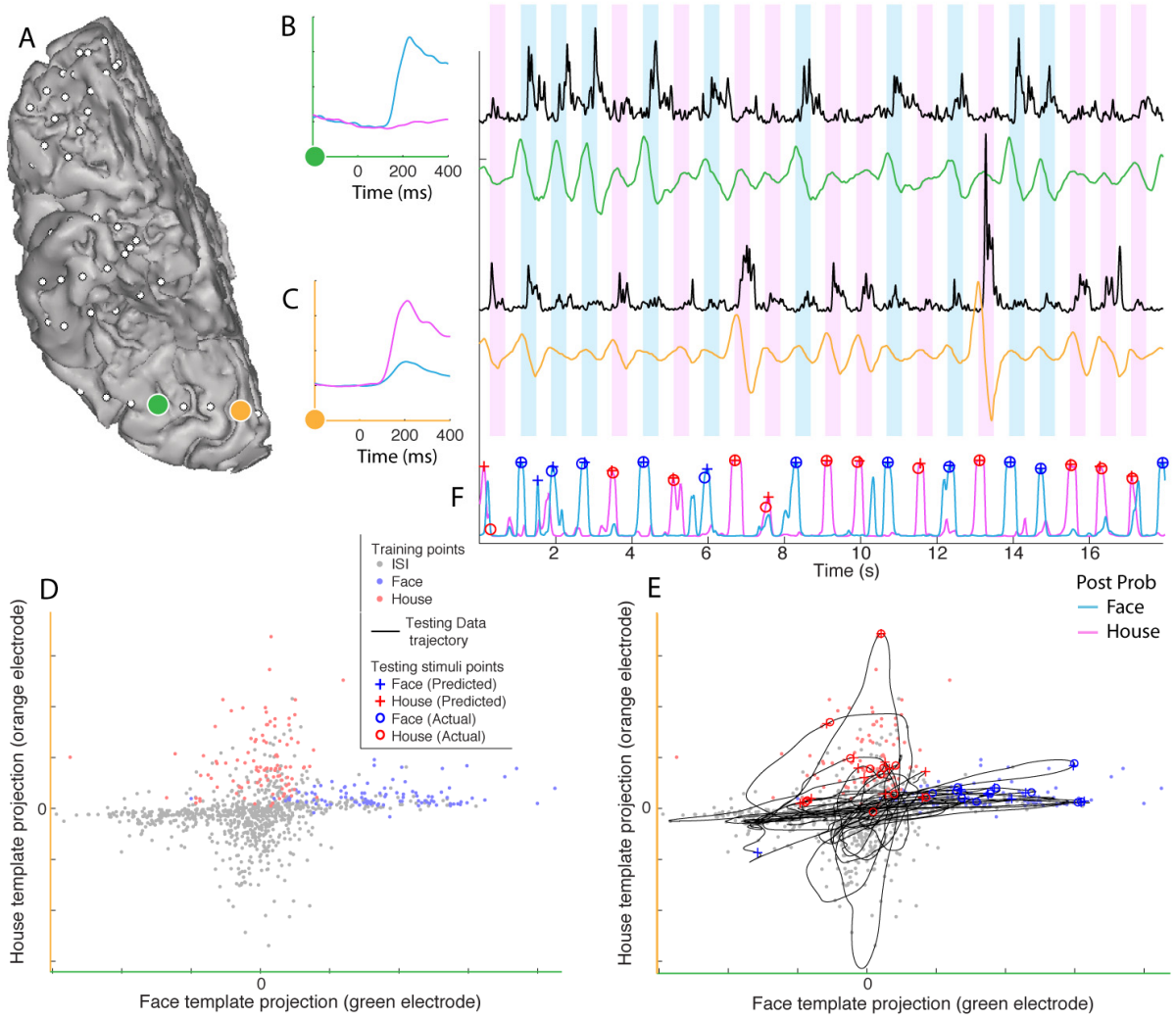


**Figure 4: Illustration of two electrodes and the continuous classifier using 2 broadband features (subject 2). (A)** Two cortical sites on the fusiform (green) and lingual (orange) gyri are examined., 3 cm from one another. **(B)** Broadband **training** templates from the green electrode for faces (blue, $\langle B_1(t')\rangle_F$) and houses (green, $\langle B_1(t')\rangle_H$) are shown on the axes to the left. **Testing** timecourse of green electrode broadband spectral change, $B_1(t)$, is shown to the right in black, with the projection of the face template $\langle B_1(t')\rangle_F$ into $B_1(t)$ to produce $\Gamma_F^{B_1}(t)$ shown in the green trace beneath.**(C)** As in B, but for the orange electrode site, using projections of a house template $\langle B_2(t')\rangle_H$ to produce $\Gamma_H^{B_2}(t)$. **(D)** The classification feature subspace defined by the templates on the left in (B-C), with training points $\Gamma_{n,S}^{B}(q)$ for face, house, and ISI eventsat times $\tau_q$ shown. **(E)**The same subspace as D, but with the trajectory of $\Gamma_F^{B_1}(t)$ vs $\Gamma_H^{B_2}(t)$from (B-C) shown as well, in black. The predicted (plus sign) and actual (open circle) face (blue) and house (red) onsets from this testing time are shown on this trajectory. Predictions based upon entire broadband feature space, not limited to this subspace. **(F)** The trajectory of the face onset posterior probability from the classifier $\Pr\{\Gamma(t)|q\to F\}$ (blue) is shown alongside $\Pr\{\Gamma(t)|q\to H\}$ (pink), with predicted and actual times shown.

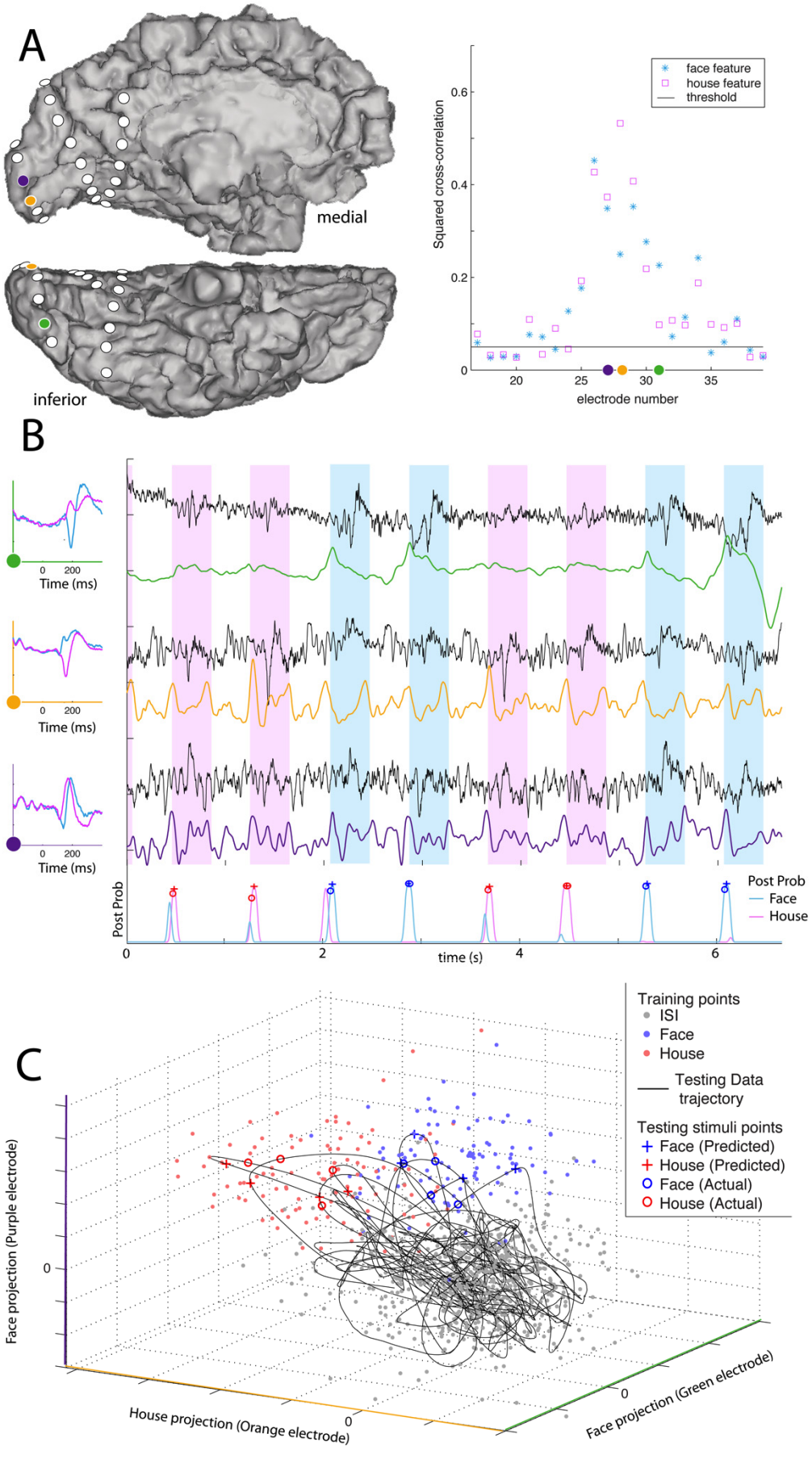
A
medial
inferior
face feature
house feature
threshold
Squared cross-correlation
0.6
0.4
0.2
0
20
25
30
35
electrode number
B
0
200
Time (ms)
Post Prob
Face
House
0
2
4
6
time (s)
C
Training points
ISI
Face
House
Testing Data
trajectory
Testing stimuli points
Face (Predicted)
House (Predicted)
Face (Actual)
House (Actual)
Face projection (Purple electrode)
House projection (Orange electrode)
Face projection (Green electrode)

**Figure 5: Illustration of three electrodes and the continuous classifier using 3 ERP template to voltage timeseries projections** (subject 4)**. (A)** Three cortical sites are shown for illustration (purple, orange, and green). The axes on the right show the $r^2_{n,F}$ (blue asterick) and $r^2_{n,H}$ (pink box) for ERP-voltage **training** projections show that these purple/orange/green sites are highly selective during the training period. **(B)** Averaged face and house ERPs, $\langle V_n(t')\rangle_F \& \langle V_n(t')\rangle_H$, from each site are shown on the left axes. These are projected into the raw voltage traces ($V_n(t)$, black) to obtain continuous projection weight traces ($\Gamma^V_{n,F/H}$; green – face projection from green electrode, orange – house projection from orange electrode, and purple – face projection purple electrode). These are fed into a feature space (in C) to obtain posterior probability of a face, $\Pr\{\Gamma(t)|q \to F\}$ (blue), or house stimulus, $\Pr\{\Gamma(t)|q \to F\}$ (pink), having been presented (bottom axis).**(C)** A 3-dimensional subspace (from the sites in A and B) is illustrated, with training points from the training period shown with dots, and the subspace trajectory of the brain state, $\Gamma(t)$, shown with a black line. Predicted and actual timing and type of stimulus are shown along this trajectory.

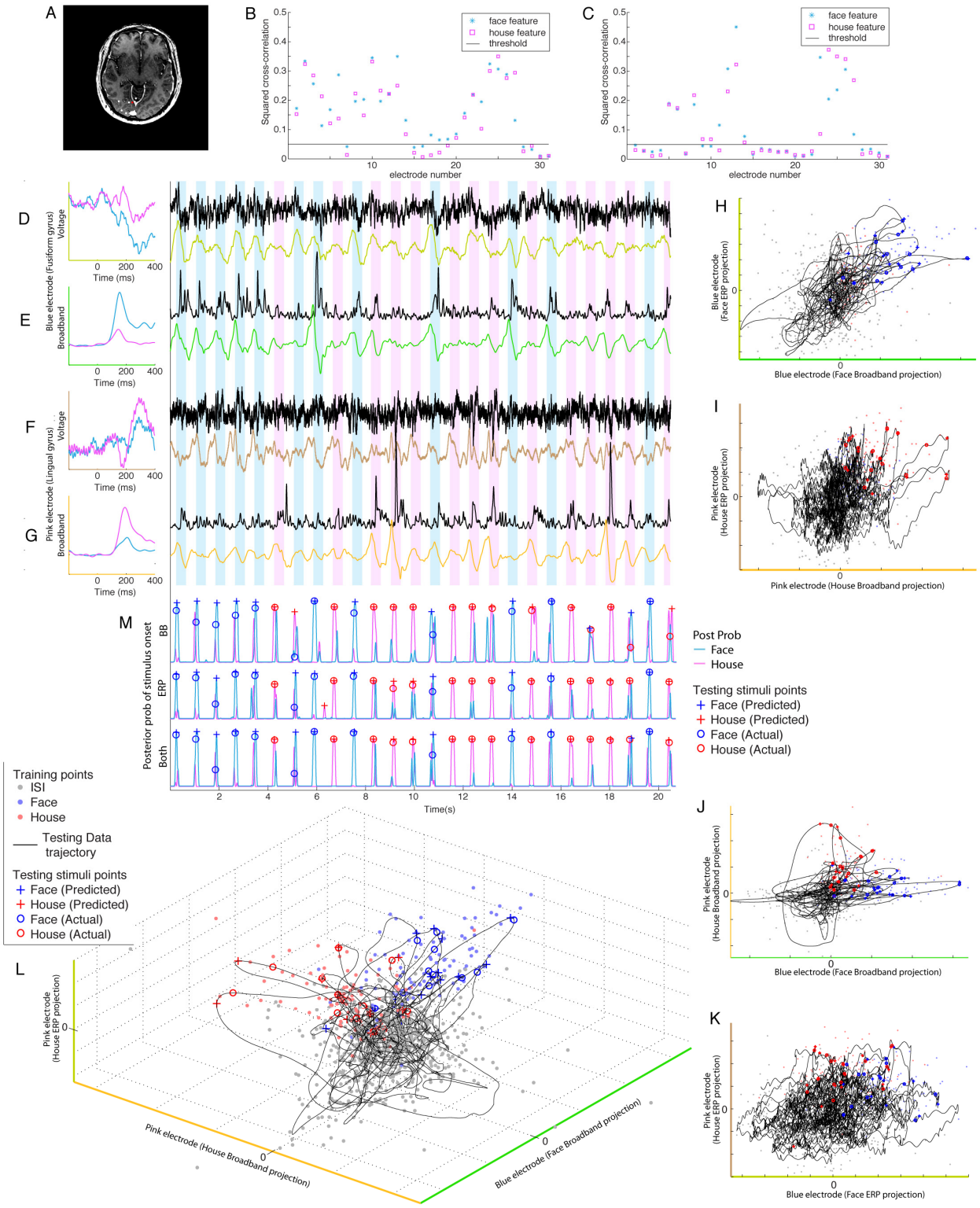
A
B
face feature
house feature
threshold
Squared cross-correlation
electrode number
C
face feature
house feature
threshold
Squared cross-correlation
electrode number
D
Blue electrode (Fusiform gyrus) Voltage
Time (ms)
E
Blue electrode (Fusiform gyrus) Broadband
Time (ms)
F
Pink electrode (Lingual gyrus) Voltage
Time (ms)
G
Pink electrode (Lingual gyrus) Broadband
Time (ms)
H
Blue electrode (Face ERP projection)
Blue electrode (Face Broadband projection)
I
Pink electrode (House ERP projection)
Pink electrode (House Broadband projection)
M
Posterior prob of stimulus onset
BB
ERP
Both
Time(s)
Post Prob
Face
House
Testing stimuli points
Face (Predicted)
House (Predicted)
Face (Actual)
House (Actual)
Training points
ISI
Face
House
Testing Data trajectory
Testing stimuli points
Face (Predicted)
House (Predicted)
Face (Actual)
House (Actual)
J
Pink electrode (House Broadband projection)
Blue electrode (Face Broadband projection)
L
Pink electrode (House ERP projection)
Pink electrode (House Broadband projection)
Blue electrode (Face Broadband projection)
K
Pink electrode (House ERP projection)
Blue electrode (Face ERP projection)

**Figure 6: A combined ERBB-broadband and ERP-voltage projection feature space for classification** (subject 5). **(A)** Two cortical sites (red and blue dots) are examined. **(B)** The axes on the right show the $r^2_{n,F}$ (blue asterick) and $r^2_{n,H}$ (pink box) for ERP-voltage **training** projections show that these purple/orange/green sites are highly selective during the training period. **(C)** $r^2_n$ for ERBB-Broadband **training** projections. **(D)** Averaged face and house ERPs from the blue site are shown on the left axes (olive green). The face-ERP are projected into the raw voltage trace (black) to obtain continuous a projection weight trace (olive green trace). **(E)** As in (D), but for ERBB-broadband in the blue site (neon green). **(F&G)** As in (D&E), except for the red electrode site in (A), using house ERP (brown) and ERBB (burned orange) templates. **(H)** Blue electrode, face ERP vs ERBB subspace projections. **(I)** Red electrode house ERP vs ERBB subspace projections. **(J)** ERBB projection subspace (blue-electrode face-template projection vs red-electrode house-template projection). **(K)** As in (J), for ERP projection subspace. **(L)** A 3-d subspace projection (features from D,E,G). **(M)** Posterior probability of a face, $\Pr\left\{\Gamma_m(t)|q\to F\right\}$ (blue), or house stimulus, $\Pr\left\{\Gamma_m(t)|q\to F\right\}$ (pink), having been presented (where $m\to$ ERP, ERBB or both features for the projection space).

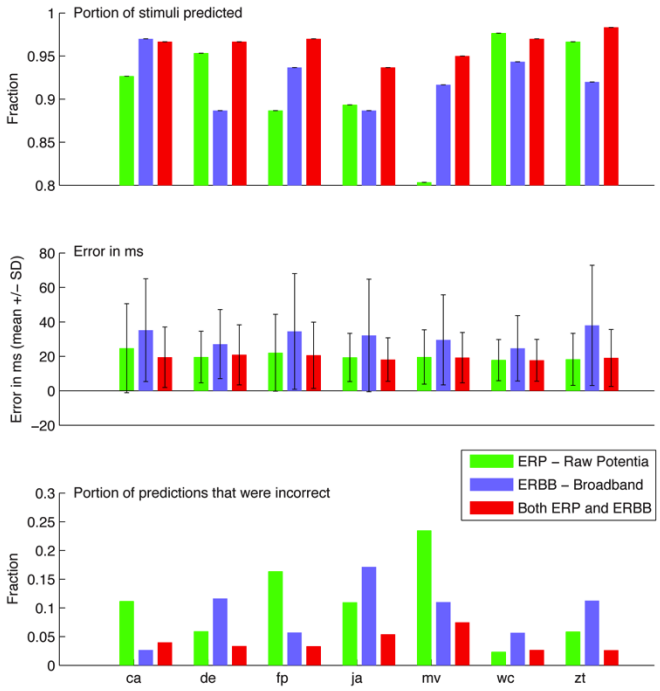


**Figure 7: Continuous / spontaneous prediction results.** When all features were used, more than 90% of all stimuli were captured spontaneously in every subject, with approximately 15-20ms error. Fewer than 10% of predictions were incorrect (i.e. predicted stimuli at the wrong time, or as the wrong class).

## Discussion

This study investigated how different parts of the local field potential recorded from inferior temporal cortex contribute to the decoding of visual stimuli. We compared the information contained in two different measurements: the ERP and broadband activity. In predicting the class of each stimulus when the onset of the stimulus is known, broadband activity is most informative. However, when we predict from a continuous stream of data whether, when and which stimulus appeared a combination of the broadband and ERP resulted in the best accuracy.

To predict the appearance onset, and class of a visual stimulus, we developed a template projection techniques. This technique was necessary to capture some aspects of the neural responses that has previously been impossible. First, the ERP in face-selective fusiform gyral sites is classically associated with a negative peak at ~200ms ("N200"). Our data show that the actual shape of face-selective fusiform ERPs can vary widely, even at fusiform sites 1cm from one another. The template projection technique captures these diverse response patterns, allowing them to be used for classification. Second, broadband responses show variability in the pattern of the response in every individual trial. The template provides a superposition of the single trial characteristic shape and a probability density function for different shapes. With this template, the template projection method offers a robust prediction in spite of the variability across single trials.

### The ERP and broadband give different information about visual stimuli

We found that the broadband signal or the raw potential (ERP) could both classify the onset and category of the stimulus relatively well, but the combination of both features generally increased the decoding accuracy specifically in the continuous data. Different signals have different properties that reflect different brain signals and can thus provide distinct information about a stimulus. For example, single-cell responses are less categorical than the responses in a population of neurons (Kiani et al., 2007). Previous recordings in macaque have similarly shown that using multi-unit activity and the raw LFP in combination can increase decoding accuracy (Hung et al., 2005).

Broadband changes in the electrical potential reflect an estimate of the average local neuronal population activity (Manning et al., 2009, Miller et al., 2009b, Ray and Maunsell, 2011). As demonstrated previously (Miller et al., 2014), broadband responses within the fusiform and parahippocampal gyri track the presentation of faces and houses on a single stimulus basis with high temporal fidelity. Event-related averaged traces of both the broadband (ERBB) and the raw potential (ERP) can be obtained from category-selective inferior temporal regions. Conversely, the ERBB is a generic correlate of population firing rate, and while, the width and latency may be different in adjacent cortical sites, cortical activation is associated with transient increases in this broadband, that do not have complicated forms.

The form and of the ERP was much more variable across different cites and the neural origin of the ERP is less well studies. The ERP is generally thought of as an initial response in ventral temporal cortex that occurs in all occasions of the correct object with the correct features (a face) (Engell and McCarthy, 2014). In our data, the accurate timing of the ERP improved the decoding of stimuli from a continuous stream of data beyond using the broadband response by itself.

### Decoding the onset of a visual stimulus from a continuous stream of data

Previous studies have addressed when the brain has information available about the visual stimulus, when the onset of a stimulus is known (Hung et al., 2005, Kiani et al., 2007, Liu et al., 2009, Simanova et al., 2010, van de Nieuwenhuijzen et al., 2013). These studies have shown that the stimulus class can be predicted within 100 ms after stimulus onset. People can also saccade towards a scene containing an animal or face within 140 ms (Kirchner and Thorpe, 2006, Crouzet et al., 2010). These fast eye movement can also be made just based upon the Fourier spectrum of the images of different classes (Honey et al., 2008), and are likely to depend on low level visual features. Our results show that some electrodes in early visual cortex already display some stimulus-selective responses (e.g. figure 5, purple site).

In a more natural environment, stimuli arrive in a continuous flow. Before a completely natural environment (e.g. movie) can be decoded, decoding has to be established in a well-controlled environment. The linear discriminant analysis we used assumes that the same probability of one class of stimuli is the same in the training set as in the testing set. However, no information was added regarding the total number of stimuli and that was still accurately predicted. Also, it was assumed that the mimimal separation between two stimuli was 320 ms. With these constraints, we reliably predicted whether and when a stimulus was presented with an accuracy of 20 ms.

In conclusion, this study presents a method for decoding a continuous stream of visual images with an accuracy that matches human behavior. This sets the groundwork for classifying visual information from a natural environment.

# Chapter 6: Context immediately influences the physiology of perception

Inferior temporal brain areas are known to have sub-regions that are specialized for processing specific categories of stimuli. To examine this physiology, 11 human subjects with electrocorticographic (ECoG) electrodes previously placed on the inferior temporal brain surface were shown simple pictures of faces and houses (with blank screen in between) for 400ms at a time. A real-time correlate of local neural population activity, broadband spectral change, was extracted from the ECoG power spectrum to characterize single trial response dynamics. Robust category-specific responses to each type of stimulus were found, where face-picture selectivesites were consistently found on the fusiform gyrus and house-selective sites were found on the lingual and parahippocampal gyri. Approximately half of the category-selective sites showed greater total activity for novel than for repeated stimulus class. In approximately half of the face-selective sites (and none of the house-selective sites), latency to peak activity was faster for novel than repeat stimuli. These observations suggest that aspects of inferotemporal cortical physiology are especially tuned to sequential context, with an emphasis on novelty during perception.

## Introduction

Human inferior temporal cortex is known to have anatomically distinct sub-domains, each of which is specialized for processing a semantically distinct category of objects encountered in the outside world. The most well-known of these is the fusiform "face" locus on the lateral occipitotemporal gyrus, which is specific for processing faces. Metabolic activity and neuronal firing rate selectively increase while viewing faces (Kanwisher et al., 1997, Kreiman et al., 2000, Grill-Spector et al., 2004), and focal lesion or electrical stimulation selectively impairs face recognition (Meadows, 1974, Damasio et al., 1982, Parvizi et al., 2012). This relationship is hard-wired, and insult to the pre-experiential neonatal fusiform area produces permanent prosopagnosia (Farah et al., 2000). On the parahippocampal and lingual regions of the medial occipitotemporal gyrus are selectively metabolically active when viewing "places" (buildings, houses, landmarks, etc), and focal damage to these "place regions" results in the specific inability to distinguish between buildings and landmarks, leaving face recognition relatively preserved(McCarthy et al., 1996). Electrical stimulation of these regions produces topographic hallucinations (Penfield and Perot, 1963, Megevand et al., 2014). Presentation of visual stimuli belonging to various semantic categories,while measuring task-related blood-oxygen-level-dependent (BOLD) changes in functional MRI has delineated a robust patchwork of distinct inferior temporal regions for processing different classes of stimuli, of which faces and places are just two (Ishai et al., 1999, Malach et al., 2002, Spiridon and Kanwisher, 2002, Grill-Spector et al., 2004, Peelen and Downing, 2005).

Examination of the class-specific fMRI hemodynamic responses in these regions shows that repeated presentation of the same visual stimulus is associated with less metabolic expenditure (Koutstaal et al., 2001, Schacter et al., 2004, Grill-Spector et al., 2006). It has been postulated that this repetition suppression reflects a type of adaptation, and that repeated stimuli (or repeated

class of stimulus) results in faster processing of each stimulus, with less overall neuronal population activity (Grill-Spector et al., 2006, James and Gauthier, 2006). These BOLD changes are intrinsically smeared over metabolic timescales of order several seconds (Kim et al., 1997, Yang et al., 2000). However, perception of individual objects occurs on the timescale of several hundreds of milliseconds. In order to understand the inferotemporal response to repeated or novel stimuli, we measured human electrocortiocographic (ECoG) responses while subjects were shown simple pictures of faces and houses. Time-resolved broadband ECoG change has emerged as a surrogate to approximate mean firing rate of a neural population with a temporal resolution of approximately 20-40ms (Miller et al., 2009d, Miller et al., 2010b, Miller et al., 2012b, Miller et al., 2014). This timescale is propitious, because the speeds of perception, decision, and action are all of this order or slower.

We used these recordings to ask: What are the what are the physiological properties that underlie repetition suppression? How do the dynamics of inferior temporal processing change for repeat processing of the same stimulus class? Is the magnitude of neural population activity actually not as strong? Is the process slower to occur or is it more drawn out? On what timescales are these repetition adaptations happening? If present, are these universal properties of class-specific inferotemporal processing, or are they limited to a subset of class-specific sites? We found that the magnitude and latency of the single trial neuronal population response to a single visual stimulus depends on whether the same or different stimulus class was just seen. These inferotemporal cortical responses show that semantic context is sustained in time. Because this is a within-class (rather than image specific) repetition phenomenon, it implies that semantic category assignment influences the dynamics of cortical processing in these regions of the brain.

## Experimental Setting and Methods

### Subjects

Cortical surface potentials were measured during simple visual tasks in 18 patients who underwent craniotomy and placement of intracranial sub-dural electrode arrays to localize seizure foci prior to surgical resection for medically refractory epilepsy. Of these, 11 had at least one face- or house-selective site (as described below), and were included in this study. The location of the electrodes and duration of implantation was determined by clinical criteria only, with no consideration for this study. The arrays were typically placed for 5-7 days, with experiments on day 3-5 following surgery. Experiments were performed at Harborview Hospital in Seattle, USA. Subjects gave informed consent for participation, in a manner approved by the University of Washington Institutional Review Board.

### Recordings

The platinum electrode arrays (Ad-Tech, Racine, WI) were configured as linear strips or grids. The electrodes had 4 mm diameter (2.3 mm exposed), 1 cm inter-electrode distance, and were embedded in silastic. They were implanted through burrholes or large craniotomies of patients undergoing electrophysiologic monitoring for seizure localization (Fig. 1A,C). ECoG signals were split into two identical sets. One set was fed into the clinical EEG system (XLTEK, Oakville, Ontario, Canada) and the other set was recorded with Synamps2 (Neuroscan, El Paso, TX) biosignal amplifiers. ECoG signals were then acquired from the Neuroscan system using the general-purpose BCI2000 software package (Schalk et al., 2004). The potentials were sampled at 1000 Hz, and then band-pass filtered from 0.3 Hz to 200 Hz.

## Task

Subjects performed a basic target detection task. Subjects were presented with simple, grayscale, pictures of faces and houses (luminance and contrast matched) that were displayed in random order for 400ms each, with 400ms inter-stimulus interval between. 10cm-wide pictures were displayed at ~1m from the patients, while they were seated at the bedside (figure 1). There were 3 experimental runs with each patient, with 50 different house pictures and 50 different face pictures in each run. In order to maintain fixation on the stimuli, patients were asked to report a simple target (an upside-down house), which appeared once during each run. All subjects were able to correctly report the target house in each run.

## Electrode localization

Electrode location relative to gyral surface anatomy was determined by projection of the post-implant CT to the pre-operative axial T1. The CT was co-registered to T1 Axial MRI using normalized mutual information in SPM, and then resliced into the MRI space (Wells et al., 1996, Ashburner and Friston, 2005). Electrodes were then identified in this mutual space on each axial slice so that their positions were known with respect to gyral anatomy from MRI. The inferotemporal sites included in the study were those where the electrode was localized to one of the following gyri: Temporal pole, Parahippocampal portion of the medial occipito-temporal gyrus, Inferior temporal gyrus, Middle temporal gyrus, Fusiform gyrus (Lateral occipito-temporal gyrus), Lingual portion of the medial occipito-temporal gyrus, Inferior occipital gyrus (Destrieux et al., 2010).

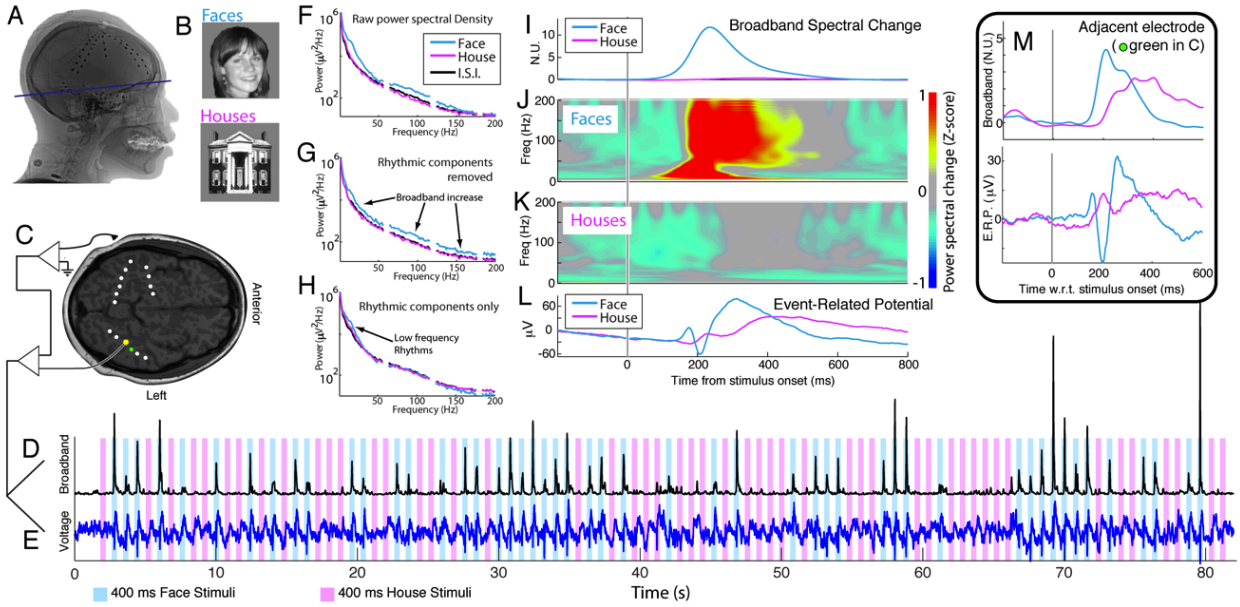


**Figure 1:** The multiple physiologic aspects of electrocorticographic measurement of category-specific subtemporal visual response (subject 1). **(A)** Sub-dural electrocorticographic (ECoG) electrode strips were placed through burrholes in the skull, and can be seen here in the frontal, parietal, and temporal regions. **(B)** Simple pictures of faces and houses were shown for 400ms at a time, interleaved in random order with 400ms inter-stimulus intervals. **(C)** The temporal ECoG electrodes can be seen in situ with their anatomic relationship to gyri on an axial MRI of the inferior temporal cortex. **(D)** A real-time extraction of broadband spectral change (black trace) from the raw potential at an electrode on the occipitotemporal gyrus (yellow in C) is seen for an ~80 second period. There is a dramatic and robust response to face stimuli (shown during times of blue background), and not house stimuli (shown during times of pink background). **(E)** The raw potential (voltage timeseries, blue trace) is also seen from the yellow electrode in C. It exhibits a face-specific deflection, classically named the "N-200" for the surface-negative trough at 200ms after the stimulus is delivered. **(F)** The averaged power spectral density (PSD) of the voltage timeseries, for segments of time during face picture presentations (blue), house picture presentations (pink), and inter-stimulus intervals (black). **(G)** The PSDs from individual trials can be decomposed using "singular value decomposition" into principal spectral components (PSCs) which reveal underlying motifs. When the 2nd-4th PSCs are removed and the averaged PSDs are re-constituted, face-specific broadband spectral change across all frequencies is revealed. **(H)** When the averaged PSDs are reconstructed using only the 2nd-4th PSCs, power spectral change is observed specifically in the 4-20Hz range of the θ/α/β rhythms. **(I)** Stimulus-triggered-average broadband timeseries in response to face (blue) and house (pink) stimuli, revealing a robust face-selective response. **(J)** Face stimulus-triggered-average dynamic spectra (spectrogram), showing the low frequency spectral changes associated with the raw potential deflection, as well as strong, sustained, broadband spectral change. **(K)** House stimulus-triggered-average dynamic spectra, without significant change. **(L)** Stimulus-triggered-average raw voltage timeseries (the "Event-related potential" - ERP) in response to face and house stimuli, revealing the classic N200 response to face stimuli. **(M)** The average broadband timeseries and ERP in a neighboring electrode, demonstrating that the N200 response in the ERP does not guarantee face selectivity in the aggregate neuronal response that the broadband measure captures.

## Spectral analysis, decomposition, and calculation of the broadband trace

After visual rejection of artifactual or epileptiform electrodes, the scalp-referenced ECoG potentials were re-referenced with respect to the common average reference across all remaining electrodes (Fig1C,E). From each electrode, samples of power spectral density (PSD) were calculated from 1 second epochs centered at the midpoint of each picture presentation or inter-stimulus interval. Individual PSDs were normalized in two steps: each spectral sample was element-wise divided by the average across the ensemble, at each frequency, and then the log was taken. A matrix from the inner product of these PSDs was then diagonalized via a singular value decomposition was then applied to identify motifs of movement-related change in the PSD. The eigenvectors (principal spectral components – "PSCs") from this decomposition reveal motifs in change in the PSD during cortical processing, and are ordered according to magnitude of the corresponding eigenvalue. Reconstruction of the PSDs corresponding to times of different stimulus display and ISI, without the $2^{nd}$-$4^{th}$ PSCs, reveals broadband spectral increases for specific visual stimuli (Fig 1G) (Miller et al., 2009d).

Continuous time-frequency approximations (dynamic spectra) were calculated using complex Morlet wavelets, which were then normalized by division of the mean power at each frequency and then taking the log. The timecourse of broadband spectral change was obtained by projecting the $1^{st}$ PSC to this normalized dynamic spectrum (excepting 5Hz notches at 60Hz harmonics), smoothing with a Gaussian envelope (SD 80ms), z-scoring, and then exponentiating (normalized units – "N.U."). There is a power law in the cortical PSD of the form, which is revealed by broadband fluctuations in the PSD across all frequencies (separate from the classic θ, α, and β rhythmic motifs) (Miller et al., 2009b, Miller et al., 2009d), and appears to directly correlate with multiplicative changes in local neuronal population firing rate (Manning et al., 2009, Miller et al., 2010a). This process for isolating the broadband is illustrated in (Miller et al., 2014).

## Single Trial Characterization

Single trial total integrated broadband power (Total Activity – "TA") is the average of the broadband timeseries from 100-400ms into each stimulus or 100-400ms into each ISI, and was used for trial-to-trial characterization of response magnitude (in N.U.). Latency to peak activity (in ms) is the time from stimulus onset until the highest peak of the broadband timeseries for the 800ms period from stimulus onset to stimulus onset (including the ISI). The response duration (in ms) is the sum of the broadband timeseries over the 800ms period from stimulus onset to stimulus onset, divided by the magnitude of the highest peak of the broadband timeseries in that interval.

## Statistical descriptions

Throughout the manuscript, individual distributions are compared using unpaired t-tests. For examination of visual as well as category-specific response, TA was compared for face-vs-ISI and house-vs-ISI, as well as face-vs-house stimuli. These were corrected for multiple comparisons using the Bonferroni-Holm method, adjusted for the total number of subtemporal sites. Within these category specific sites (19 for faces, 17 for houses), the tests for effect of novel vs repeat stimulus class were not corrected for multiple comparisons (across cortical sites). For total activity and latency, novel vs repeat stimulus effects were present, with the same direction of effect across sites and subjects, at much higher levels than the ~1-2 cases which might be expected at the $p<0.05$ chance threshold. The selectivity effect size for face-vs-house (cross-correlation) was quantified with a squared cross-correlation value, and only cortical sites that were robustly category-specific were further examined (at $r^2>0.08$ threshold, chosen subjectively).

# Results

## Electrocorticographic (ECoG) responses to simple face and house picture stimuli

Electric potentials were measured from sub-temporal ECoG sites, while patients performed a simple task watching pictures of faces and houses, interleaved with inter-stimulus intervals (ISI) of equal length (400ms, Fig 1B, C, E). From a face-specific inferior temporal electrode site, spectral changes associated with face picture presentations show changes in low frequency rhythms, as well as strong, sustained, broadband spectral change (Fig 1F, J). Using a principal component type decomposition of the power spectral density, this broadband is shown to extend across all frequencies, and to be separable from low frequency rhythmic elements (Fig 1G, H). This broadband change is primarily captured by the 1st principal spectral component (Miller et al., 2009d), and when projected to the dynamic power spectral density, it specifically captures the dynamics for processing of individual categories of visual stimuli with robust temporal fidelity (Fig 1D, I). As in previous studies, we observe a classic face-specific ERP from the lateral occipitotemporal (fusiform) gyrus that is characterized by an initially surface-positive deflection that starts 125-150ms after face picture onset, followed first by a negative deflection that peaks at ~200ms, and then a positive deflection that returns to baseline 400-500ms post stimulus onset (Fig. 1L, M). It is classically named the "N200" for the surface-negative trough at 200ms. Interestingly, comparison with the broadband timecourse reveals that this face-specific N200 does not guarantee face selectivity in the aggregate neuronal response that the broadband measure captures (Fig. 1M).

Eleven of the eighteen patients tested had at least one sub-temporal face or house selective site, and only these patients were included in the study. Of 258 total sub-temporal electrodes, 19 were face-selective ($p<0.05$ for both faces-vs-ISI and faces-vs-houses, after multiple comparison correction, with $r^2>.08$ for faces-vs-houses), 17 were house-selective (by the same criteria), and 23 were visually responsive to both stimuli ($p>0.05$ vs rest for both, with with $r^2<.08$ for faces-vs-

houses). Face-selective sites (mean |x|=34mm, SD11mm; mean y=-55, SD19mm) were consistently lateral (p=0.010) and anterior (p=0.003) to house-selective sites (mean |x|=23mm, SD13mm; mean y=72, SD10mm; distances are with respect to midpoint of anterior commisure).

The sub-temporal cortex was hand parcellated into 7 gyral domains: Of 47 *temporal pole* sites, 1 was face-selective and 1 was visually responsive but non-selective; 1 of 21 *middle temporal gyrus* sites was visually responsive but non-selective; There were 50 total *inferior temporal gyrus* sites, 3 of which were visually responsive but non-selective, and 1 that was house-selective; The *inferior occipital gyrus* was covered by 8 total electrodes, 1 of which was face-selective, 1 of which was house-selective, and 1 of which was visually responsive but non-selective; Amongst 39 sites on the *parahippocampal* portion of the medial occipitotemporal gyrus, only was 1 house-selective; Of 44 sites on the *lingual* portion of the medial occipitotemporal gyrus, 9 were house-selective (1 was face-selective), and 10 were visually responsive but non-selective; The *fusiform* portion of the lateral occipitotemporal gyrus, 49 total electrodes, 7 of which were visually responsive but non-selective, 16 face-selective electrodes, and 5 house-selective electrodes.

## Novel stimulus class augments total population activity

As illustrated in figures 2 and 3, there is a significant effect of novelty on the category-specific response magnitude for both face- and house-selective cortical sites. The aggregate neuronal activity, revealed by single trial total integrated broadband power between 100-400ms post stimulus onset, was used to compare repeated within-class stimuli (e.g. a face following previous face or house following house) versus novel stimulus class (e.g. face following house or vice-versa). What we discovered was a robust  but not universal property of category-selective sites. In 10 of 19 face-selective cortical sites, there was significantly less cortical activity for repeat stimulus class (face following face) than there was for novel stimulus class (face following house).

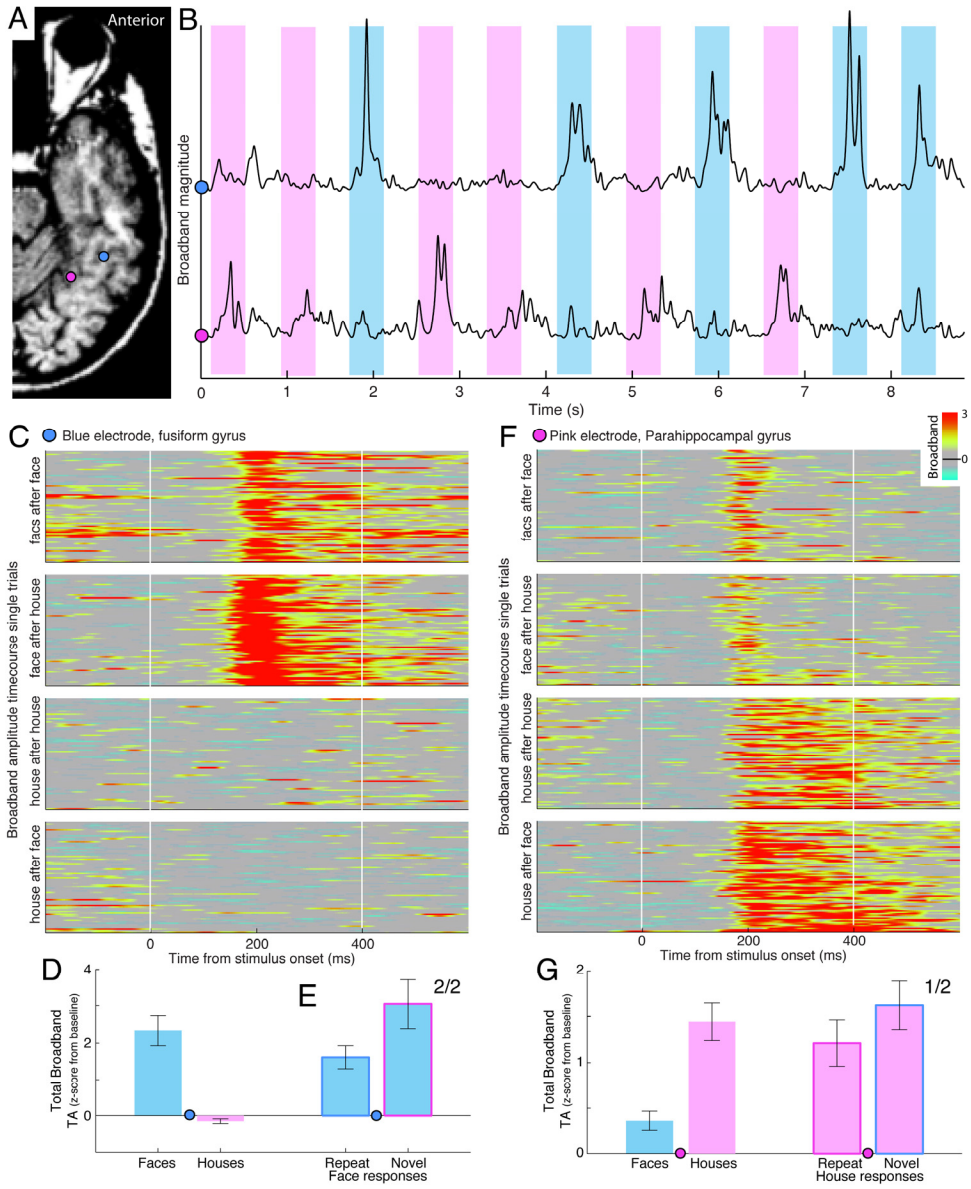


**Figure 2:** Novelty effect in the category-specific response magnitude. **(A)** A medial, parahippocampal, electrode (pink) and a lateral, fusiform, electrode (blue) are shown in situ. **(B)** Broadband timeseries (BB) from the sites in (A), with 400ms face picture presentation times shown in blue, and 400ms house presentations in pink. Note that the upper trace, from the blue site, is face stimulus selective, and the lower, from the pink site, is house selective. **(C)** All broadband stimulus responses from the fusiform site in (A), sorted by prior stimulus. The four clusters, from top to bottom are faces following faces, faces following houses, houses following houses, and houses following faces. Vertical white lines indicate stimulus onset and offset (colorscale truncated at N.U.=3). The novelty effect is visible by eye when comparing the top two rasters. **(D)** Averaged fusiform site broadband responses from 100-400ms following each stimulus for all face stimuli (blue bar on left) compared with all house stimuli (pink bar on right). Errorbars denote 3*SEM. Faces significant vs houses as well as ISI ($p<10^{-6}$, after correction, for each). **(E)** Face responses, sorted as novel (following previous house, right bar / pink outline) or repeat (following previous face, left bar / blue outline). The novelty effect is strong and significant ($p<10^{-6}$, uncorrected). The "2/2" indicates there are two face-selective sites for this patient, and both show the novelty effect (at least $p<.05$). **(F)** As in (C), for the parahippocampal electrode. **(G)** As in (D and E), house responses significant vs faces and ISI ($p<10^{-120}$ for both after correction). The repetition effect is similar for the house-specific site ($p=10^{-3}$, uncorrected). Note that there are two house-selective sites, but only one shows significant class-specific novelty effect.

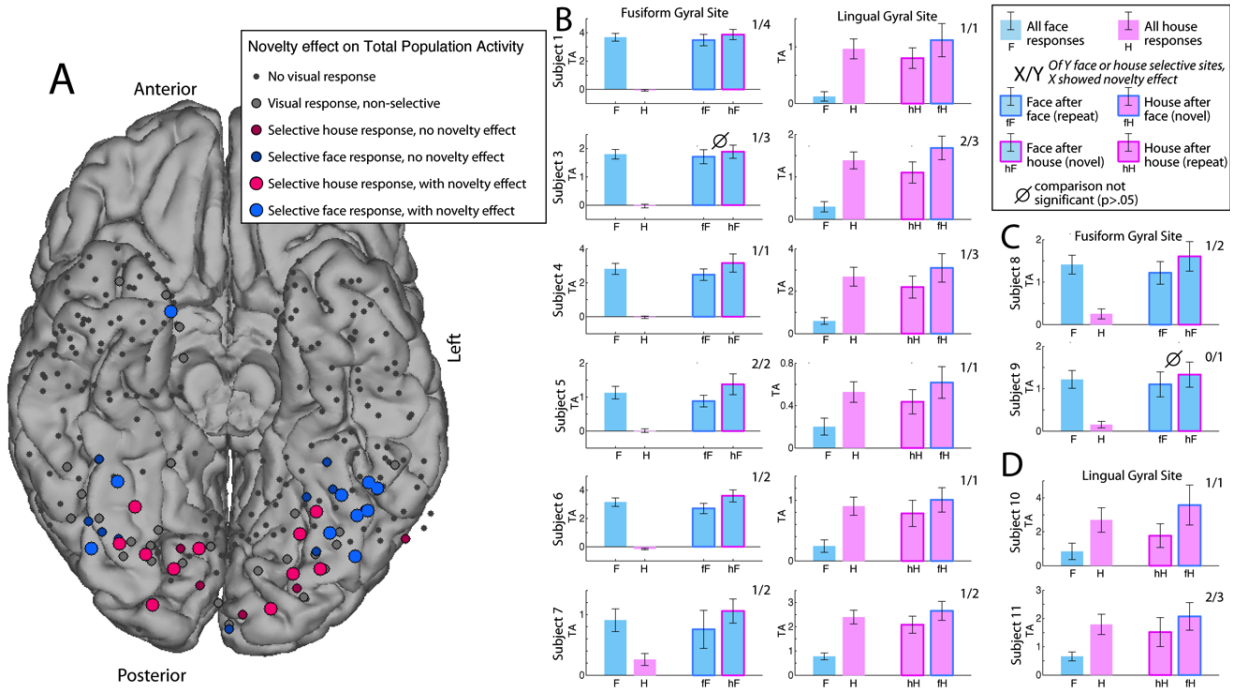


**Figure 3:** Novelty effect on total activity, across subjects. **(A)** Subdural electrode sites and broadband responses, all subjects: electrode positions in millimeters from anterior commissure are plotted on the underside of a template brain (MNI atlas - so underlying anatomy does not necessarily reflect the gyrus that plotted electrode was actually recorded from. Nearly all face or house responsive sites were on the posterior inferotemporal surface, and non-selective (face vs house) electrodes were intermingled amongst category selective sites. While there was a general organization of faces lateral to houses, there was not a robust spatial relationship between sites with a novelty effect verses those without. **(B)** Single site examples of face and house selective sites with significant novelty effect (subjects 1, 3-7). As in the bottom of figure 2, the two columns on the left show an example face-selective site from the fusiform gyrus, and the two columns on the right show an example house-selective lingual gyral site. Bar plots show broadband responses, clustered by stimulus type (F=all Faces; H=all Houses; fH=Houses that follow faces, and so forth; TA=Total broadband response Activity; error bars indicate 3*SEM). To the top right of the axes, the number pair separated by a forward slash indicates the number of sites that had the novelty effect out of the total number of selective sites for each type. The circle-slash indicates that the category selective site did not have a significant novelty effect. **(C)** Face-selective fusiform gyral site (as in the left column of (B)) for subjects 8 and 9, where

For the 17 house-selective cortical sites, 11 showed less cortical activity for repeat stimulus class (house following house) than for novel stimulus class (house following face). There was a single site that met significance criteria for an effect in the opposite direction (a house-selective site in subject 11). There was no significant spatial clustering of sites that exhibited the novelty effect. These results are unchanged if the whole 400ms stimulus onset to end time is used, or if the full 800ms is used from stimulus onset through the following ISI to the onset of the next stimulus, is used in place of the 100-400ms post-stimulus (data not shown).

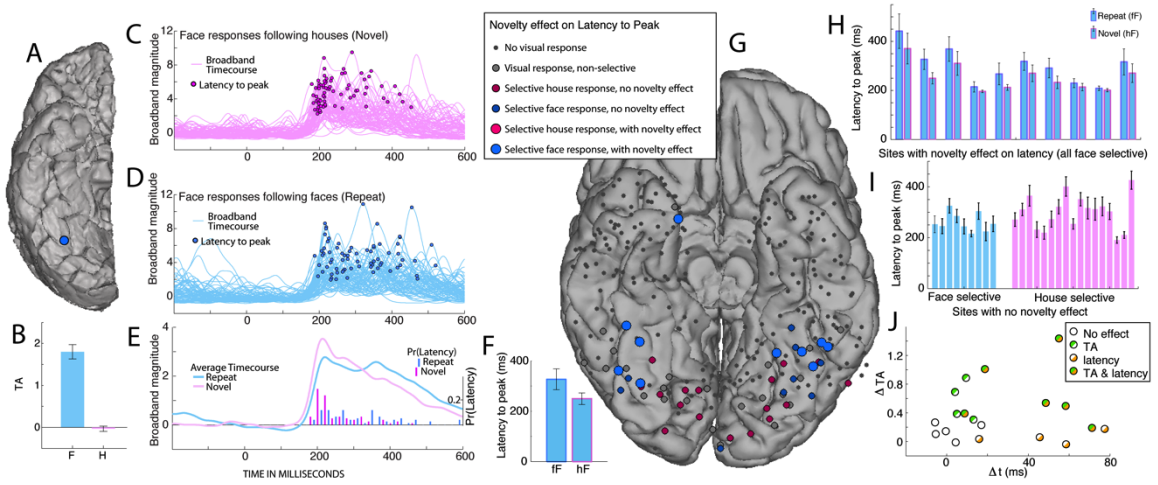


**Figure 4:** Effect of previous stimulus on response timing. **(A)** A fusiform site in subject 3 is examined (B-F). **(B)** This site is face selective, but it does not show novelty effect on total activity. **(C)** Single trial responses to face stimuli that follow previous house stimuli. The time of peak activity from each single trial is shown with a pink dot. **(D)** Responses to repeated face stimuli. Peak response times shown with blue dot. **(E)** Averaged broadband timecourse for faces following houses (novel - pink trace) and faces (repeat - blue trace). Beneath, the probability densities of peak times are shown with pink bars for faces following faces and blue bars for faces following faces (bin width 20ms). The novel responses are significantly quicker. **(F)** Average latencies of time to peak activity for repeat and novel class of stimuli (error bars represent 3*SEM), showing increase in latency for repeat stimulus class when compared with novel stimulus class ($p=3*10^{-6}$, uncorrected). **(G)** Topology of time to peak effect, all subjects (template brain - MNI atlas). There were novelty effects on latency to peak for 10 of the 19 face-selective sites, but none for the house-selective sites. **(H)** The latencies to peak for the 10 face-selective sites with significant effect. **(I)** The average latencies of grouped face responses for the remaining 9 face-selective electrodes that did not have are shown with blue bars (error bars indicate 3*SEM). The mean latencies to peak for all 17 house-selective sites are shown with pink bars (none showed the novelty effect). **(J)** The increase in TA for novel vs repeated stimuli are plotted against the increase in latency to peak for all face-selective cortical sites, with coloring to indicate significant effect of previous stimulus for total activity or latency to peak. There is no simple correlation between the two. (TA = total activity)

## Repeat stimulus class lengthens latency to peak activity

We measured how the class of previous stimulus affected the time to peak activity in the broadband response. Interestingly, there was a large discrepancy by stimulus class: in house-selective sites, there was no effect of previous class, but 10 of 19 face-selective sites showed longer latency-to-peak time if the face stimulus followed a face than if it followed a house (figure 4, $p<0.05$, uncorrected). The mean difference between novel and repeat stimulus class responses in these 10 sites was 46ms (SD=24ms; range 8 to 77ms, figure 4H).

There was no straightforward explanation for why face-selective sites showed a latency effect and house-selective sites did not. Only 6 of these 10 sites were amongst the 10 face-selective sites with significant effect for total activity (with no correlation between magnitude of repetition effect between total activity and latency, as seen in figure 4J). There was no significant difference ($p=0.14$) between latencies to peak for face selective sites (mean latency 269ms, SD 52, range 205 to 406) compared with house selective sites (mean latency 299ms, SD 66, range 191 to 426), as shown in figures 4H&I. There was also no significant difference ($p=0.30$) in the standard errors of latency for face-selective vs house-selective sites.

## Duration of response is occasionally affected by prior stimulus class

A third parameter, the single trial response duration, was estimated by dividing the total integrated activity from each trial by the peak activity in that trial. The average single trial response durations within the 36 category specific sites ranged from 61-170ms (mean 117, SD 25, kurtosis 2.9). Of these 36, 5 showed longer response duration for novel than repeat class of stimulus ($p<.05$, uncorrected, 4 house-selective), and 2 showed longer response duration for repeat than novel stimulus class ($p<.05$, uncorrected, both face-selective). Unlike the case for total activity and latency to peak, the effect is not robust in one direction, and appears to be a rare event. As such, it should be subject to correction for multiple comparisons. If multiple comparison correction is applied, only 3

of these sites remain significant (each by large margin, but these have no common thread). There was no statistical difference in average response duration for face selective vs house selective sites (p=0.84). The response duration of the stimulus-averaged broadband timeseries is much longer than the average of single-trial response durations, because the average broadband timeseries is more reflective of the probability distribution of peak responses than it is a scaling of the typical single trial timecourse (an example of this can be seen by inspection of figure 4 C-E). Further description of response duration is deferred to other studies.

## Discussion

Broadband spectral changes in cortical potentials are increasingly interpreted as reflections of the averaged local neuronal population firing rate (Manning et al., 2009, Miller et al., 2009b, Miller et al., 2009d, Miller et al., 2010a, Ray and Maunsell, 2011). In electrocorticography, the estimated coefficient $A(t)$ in a power law relation of the form $P(f,t) \sim A(t) f^{-\chi}$ has been shown to interact with rhythmic brain phenomena and also to correlate with behavior at a timescale of order 20-40ms (Miller et al., 2009d, Miller et al., 2010b, Miller et al., 2012b). Spatially, task-related broadband spectral increase overlaps with the regions of largest fMRI-BOLD change (Conner et al., 2011, Hermes et al., 2012, Miller et al., 2012b). With these robust spatial and temporal properties, the electrocorticographic broadband timecourse provides a unique window into single-event physiology of neuronal populations from multiple areas of the human brain, simultaneously. In this study, it allows us to understand fluctuations in percept-to-percept brain dynamics from inferotemporal cortex. We examine how the context stimuli are processed in (e.g. by preceding stimulus type) affects the physiologic mechanisms of perception.

When presented with simple face or house pictures, responses were robust: anatomically distinct loci were revealed for face-selectivity on the fusiform gyrus and house-selectivity on the

medial occipitotemporal gyrus (Figs 1-3). Interestingly, "place" loci of house stimulus selectivity were more frequently found on the baso-lateral lingual portion of the lateral occipitotemporal gyrus rather than the classically described parahippocampal portion (Aguirre et al., 1998). The use of repeat class of stimulus, but not repeat of individual stimuli, suggests that the same cortical processing stream is repetitively engaged, but that observed effects cannot be explained by low level features in each picture. In this setting, we examined the effect of novel versus repeat stimulus class on total neuronal activity, latency to peak activity, and duration of activity in class-selective inferotemporal sites. Approximately half of the category-selective sites showed greater total activity for novel than for repeated stimulus class (Figs 2-3). In approximately half of the face-selective sites (and none of the house-selective sites), latency to peak activity was faster for novel stimuli (Fig 4). While there were a few sites with an effect of repeat stimulus on duration of response, there was no consistent trend or motif.

Increase in total activity and shortened latency to peak with novel stimulus class are clearly common effects, seen across many subjects, but they are not a universal propery of these cortical regions: within each subject, a subset of cortical sites exhibit each effect, but an equal amount do not. Furthermore, the two main effects did not correlate with one another (Fig 4J). This may imply that different category-selective regions are differentially optimized for novelty, and that one effect cannot serve as an explanation for the other.

Decreased neuronal activity in response to repetitions of the same stimulus has been found across nearly all spatial and temporal scales in the human brain (Kandel and Schwartz, 2000). In category-specific inferotemporal cortex, repeated presentation faces, houses, and other familiar stimuli is associated with less metabolic expenditure (Koutstaal et al., 2001, Schacter et al., 2004, Grill-Spector et al., 2006). Our findings suggest that at least some of this adaptation effect happens dynamically with individual percepts, and in less than a second. This is too fast for synaptic depression, facilitation, or long-term depression, which have all been suggested as mechanistic

explanations (Grill-Spector et al., 2006). One proposed explanation is an 'accumulation model' (James and Gauthier, 2006), which predicts that less information needs to be accumulated for repeated stimuli and they will thus be processed faster. Either the latency or duration of the responses to repeated stimuli should thus be shorter. Our results show that this is not the case. In contrast with this model, we found that in many inferotemporal face-selective sites, the time to peak is actually increased for repeated stimuli, and no effects were found for the response duration. While most sources ascribe adaptation as a generic property of these regions (Schacter et al., 2004), we find instead that, within individual subjects, it is only present in a subset of category-selective fusiform and lingual/parahippocampal gyral sites.

In many face-selective fusiform sites, the time to peak processing of a face stimulus was found to be faster if preceded by a house stimulus, but the converse was never observed: it is unclear why this timing effect should be seen in the case of face-specific cortex, but not the house-selective sites. One might posit that the difference in significance between faces and houses in latency to peak could be explained by more drawn out responses, and more variable times to peak within the prolonged responses. However, there were no differences between the response durations for face-selective and house-selective sites. Recordings from neurons in MT and V1 of the non-human primate, have shown that repetition effects may not be the same for different cortical areas (Kohn and Movshon, 2004). Perhaps the differing microlaminar structure between the fusiform and lingual/parahippocampal gyri reveals structural optimization of the fusiform gyrus for higher temporal fidelity in the processing of faces.

This work illustrates the unique role of large-scale field potential measurement as a tool to characterize single event physiology. The ~20-40ms resolution obtained by our approximation of broadband spectral change is used to probe cortical physiology on the same timescales as that of cognition and behavior. The fMRI BOLD response, a temporally-smeared reflection of metabolic demand, cannot resolve cortical responses on these timescales, and requires averaging over many

trials to overcome signal-to-noise issues. The timing of action potentials in single neurons in these cortical regions is stochastic and Poisson distributed (Dayan and Abbott, 2001a, Kiani et al., 2005, Kiani et al., 2007, Lehky et al., 2011), and so averaging over units or averaging over trials is necessary to determine the timing of responses. Because broadband reflects averaged neuronal population activity, the single trial response is robust, and context-specific physiology can be resolved without averaging, on the sub-second timescale where conscious perception occurs. These findings illustrate that the physiology of object perception is directly influenced by the novelty of the context in which an object is observed.

# Chapter 7: Ventral temporal cortex is a locus of visual object perception

Neural responses in ventral temporal cortex are influenced by bottom up and top down information. Increasing levels of noise degrade the bottom up information in a stimulus and may leave room for top down influences revealed by a perceptual decision. We tested whether neuronal population activity in ventral temporal cortex could predict the stimulus or subjects choice with increasing noise in the stimulus. Subjects looked at images of faces and houses that were degraded with different levels of noise. Using ECoG recordings in seven human subjects, we tested whether we could predict the stimulus category using the broadband responses in ventral temporal cortex. At low levels of noise, the stimulus category was accurately predicted, at high levels of noise, the prediction degraded. In the four subjects that had a good task performance, we subsequently tested whether we could predict their choice rather than the stimulus. At low levels of noise, the stimulus type was better predicted than the subjects' choice. In contrast, at high levels of noise, when the subjects performed at chance level, the subjects' choice was predicted above chance, while the stimulus type could not be decoded. These results show that the physiology in ventral temporal cortex is driven by both bottom up and top down information. With decreasing bottom up information (increasing noise) the influence of higher order cognition on these areas during perception is revealed.

## Introduction

Visual perception is the process of putting together simple visual features into a larger construct that can be related to a general concept encountered in the external environment (Wandell, 1995). For example, a spherical shape with circumferential surface lines can quickly be identified as a ball, and associated with human interaction during sport. This act of perception involves a synthesis of two processes: Low level, "bottom-up," integration of simple features into increasingly complex amalgams; High level, "top-down," assignment of the amalgam to a conceptual framework, where memories, expectations, and context designate a larger meaning.

In the process of taking action under limited visual evidence, the relative influence of top-down dynamics in perception may vary. Consider driving in the rain and coming to a dark intersection: the rain increases the level of noise in the visual environment, limiting the bottom up visual information available to neuronal populations at every level in the visual stream. To compensate, higher cognitive functions, such as expectancy about which direction to turn based upon the previous turn or remembrance of driving the route in the past, may directly influence the visual perception of a partially obscured road sign.

There are many anatomic stages in the visual stream that build from basic photoreceptor inputs in order to synthesize complex scenes, and then assign contextual structure to external agents. Behavioral decisions can reveal the perception of this contextual structure. Identifying where the relative locus of object perception within the visual stream requires quantification of both bottom-up and top-down processing within specific cortical sites.

Although object perception is likely to be distributed amongst different anatomical stages, we specifically examined whether in ventral temporal cortex might be a locus of visual object perception.Human ventral temporal neuronal population responses were measured with implanted electrocorticographic (ECoG) electrodes during a face and house picture decision task in which visual evidence was parametrically degraded (Heekeren et al., 2004)(Figure 1). Robust neurometric

functions revealed decreasing magnitude and increasing delay in neuronal population activity as image noise increased for both face-selective fusiform gyral sites and house-selective lingual gyral sites. Interestingly, the shape of these neurometric functions was robust whether subjects correctly perceived the stimulus or not. We constructed a basic classifier using ventral temporal responses from a simple localizer experiment that had no element of class-specific perception, and applied it to the cortical responses in the noise-masked task. At low levels of stimulus noise, the predicted stimulus type was correlated more closely with the stimulus type than subjects' choice, but the converse was observed at high noise level, where predicted stimulus type was more correlated with the subjects' choice than stimulus type. Ventral temporal cortex must therefore be an active locus of perception, where bottom-up and top-down information converge.

## Methods

### Subjects

All 7 subjects in the study were epileptic patients at Harborview Hospital in Seattle, WA. Sub-dural grids and strips of platinum electrodes were clinically placed over frontal, parietal, temporal, and occipital cortex for extended clinical monitoring and localization of seizure foci. Each subject gave informed consent to participate in an Institutional Review Board approved experimental protocol. All patient data was anonymized according to IRB protocol, in accordance with HIPAA mandate. In order to be included in the study, a patient must have had at least one inferior temporal face-selective site identified on the localizer task, and must have fully completed the task. They performed the tasks at the hospital bedside, with 10cm-wide pictures were displayed on a bedside monitor at ~1m from the patients, indicating task choice using a separate keyboard.

### "Localizer task"

Subjects performed a basic face and house observation task. Subjects were presented with simple, grayscale, pictures of whole-field faces and houses that were displayed in random order for 400ms

each, with 400ms inter-stimulus interval (blank screen) between (figure 1B). There were 3 experimental runs with each patient, with 50 house pictures and 50 face pictures in each run. In order to maintain fixation on the stimuli, patients were asked to report a simple target (an upside-down house), which appeared once during each run. There were no errors in reporting the target house in each run.

### "Noisy-task"

Subjects also performed a face-identification task using phase-scrambled close-up pictures of faces and houses. These stimuli were generously shared by the Ungerleider laboratory at the NIH, and were originally used for a study described in their 2004 manuscript (Heekeren et al., 2004). Using the face database from MPI for Biological Cybernetics, Germany, a set of 38 images of faces and houses were chosen. Fast Fourier transforms (FFT) of these images were computed, producing 38 magnitude and 38 phase matrices. For each stimulus and each noise level, a new phase matrix was constructed by combining the original phase matrix with a random noise matrix (ranging from 0 to 100% noise, in 5% increments). These new phase matrices were combined with the average of the original magnitude matrix, and an inverse FFT was performed to produce stimuli that had identical frequency power spectra, but with graded amounts of noise.

Stimuli were randomly interleaved, and each picture was shown for 1 second, with no inter-stimulus interval. 5 blocks of 105 stimuli each were shown (each balanced for total number of faces and houses, and the total balanced for amount of noise). Because the clinical environment is prone to frequent interruption, any interrupted block was stopped and restarted from the beginning. Subjects were instructed that half of the stimuli were faces and half were houses, and were instructed to press the button "f" if they believed the picture to be of a face. A total of 630 stimuli were shown to each patient, 15 of each type at each 5% noise increment. There was neither incentive nor encouragement to respond faster (primarily due to the constraints of the clinical environment). Many subjects would make a choice as the stimuli switched, so key presses within

the first 200ms of any given stimulus were assigned to the previous stimulus. Because of a technical issue, key press data were not recorded in three cases (subjects 1, 2, 5), although they were verified by the examiner, in each case, to be performing the task carefully.

## Recordings

Experiments were performed at the bedside, using Synamps2 amplifiers (Neuroscan, El Paso, TX) in parallel with clinical recording. Stimuli were presented with a monitor at the bedside using the general purpose BCI2000 stimulus and acquisition program (interacting with proprietary Neuroscan software), which also recorded the behavioral parameters and cortical data. Sub-dural platinum electrode arrays (Ad-Tech, Racine, WI) were arranged as combinations of 8x[4,6,8] rectangular fronto-tempero-parietal arrays and 1x[4,6,8] linear temporal and occipital strips. The electrodes had 4mm diameter (2.3mm exposed), 1 cm inter-electrode distance, and were embedded in silastic. The potentials were sampled at 1000 Hz, with respect to a scalp reference and ground, and had an instrument-imposed bandpass filter from 0.15 to 200 Hz.

## Electrode localization

Electrode location relative to gyral surface anatomy was determined by projection of the post-implant CT to the pre-operative axial T1 because the clinical protocol axial T1. The CT was then interpolated and resliced into the T1 axial MRI. Electrodes were then identified in this mutual space on each axial slice so that their positions were known with respect to gyral anatomy from MRI (chapter 6). The ventral temporal sites were those where the electrode was localized to one of the following gyri: Temporal pole, Parahippocampal portion of the medial occipito-temporal gyrus, Inferior temporal gyrus, Middle temporal gyrus, Fusiform gyrus (Lateral occipito-temporal gyrus), Lingual portion of the medial occipito-temporal gyrus, Inferior occipital gyrus (Destrieux et al., 2010).

In come cases, cortical surface mesh reconstructions were made for display using pre-operative structural MRI. Electrode positions were calculated with respect to the structural MRI

from post-operative computed tomography (CT) using the CTMR package and Freesurfer (Dale et al., 1999, Hermes et al., 2010).

## Signal processing

Lateral frontoparietal electrode grids were discarded from analysis, and only inferotemporal strip electrodes were further considered. Electrodes with significant artifact or epileptiform activity were rejected. The electrical potential was then re-referenced with respect to the common average. Ambient line noise was rejected by notch filtering between 58-62, 118-120, and 178-182 Hz using 3rd-order Butterworth filters (Porat, 1997).

### Decoupling the cortical spectrum to isolate broadband spectral change

The decoupling process to extract the timecourse of broadband spectral change is described in full detail and illustrated in previous manuscripts (Miller et al., 2009d, Miller et al., 2014). From each electrode, discrete samples of power spectral density (PSD) were calculated from 1 second epochs centered at each stimulus or ISI period. Individual PSDs were normalized with element-wise division by the average power at each frequency, and then the log was taken. An inner product matrix of these normalized PSDs was then diagonalized with a singular value decomposition was then applied to identify motifs of movement-related change in the PSD. The eigenvectors ("PSCs") from this decomposition reveal motifs in change in the PSD during cortical processing. Continuous time-frequency power approximations (dynamic spectra) were calculated using complex Morlet wavelets. These dynamic spectra were then normalized is the same way as the discrete spectra, and projected onto the 1st PSC. This raw timeseries was smoothed with an 80ms Gaussian envelope (SD 80ms), z-scored, and then exponentiated to obtain the "Broadband timecourse," which has been shown to reflect a power law in the cortical PSD and directly correlate with local neuronal population firing rate (Manning et al., 2009, Miller et al., 2009b, Miller et al., 2010a).

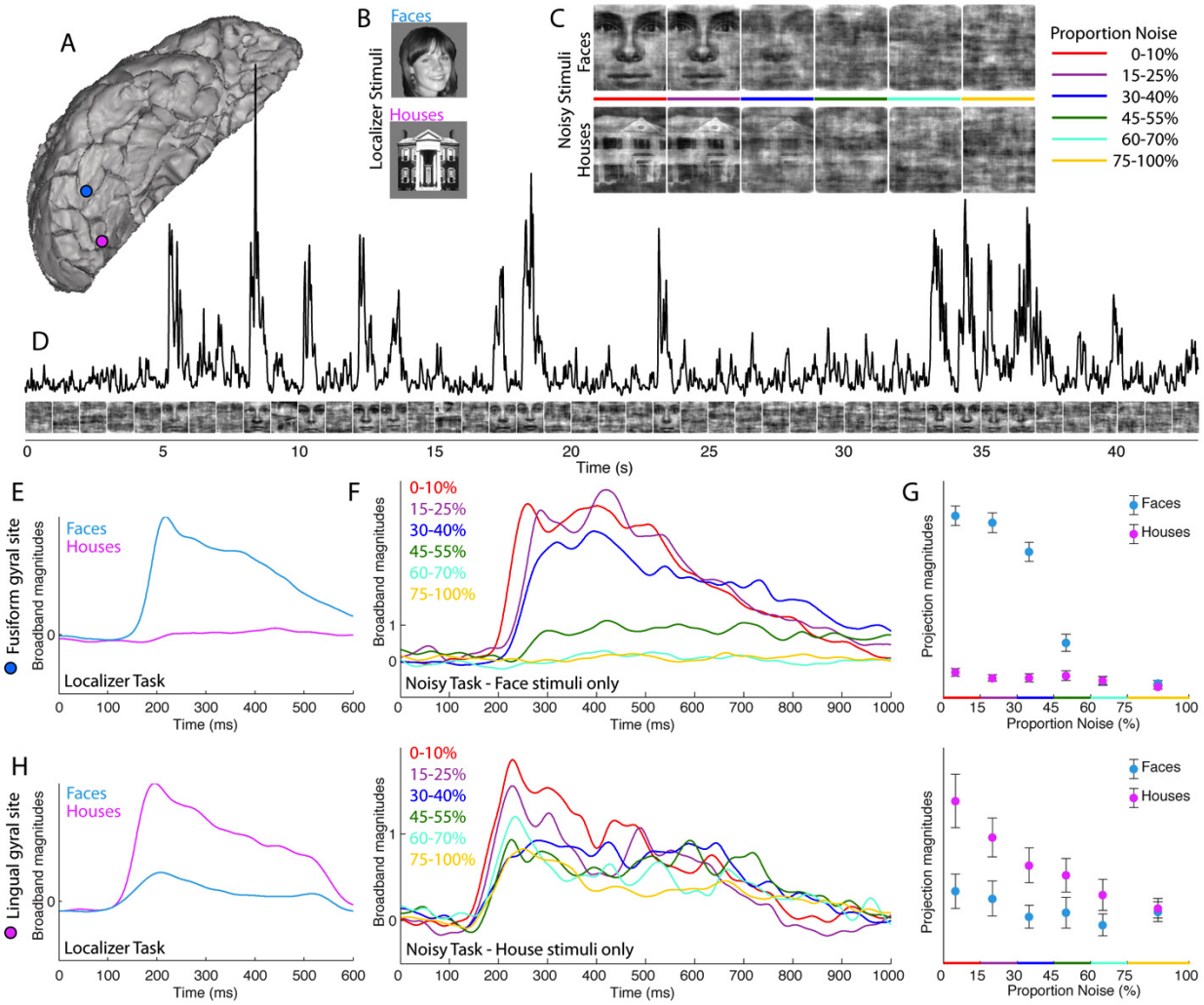


**Figure 1: Experimental setting and response magnitude**. **(A)** Inferior temporal ECoG electrodes were examined during presentation of face and house stimuli. Blue site – fusiform gyrus; pink site – lingual gyrus (Subject 1). **(B)** Localizer task: Subjects were first presented with simple, grayscale, pictures of whole-field faces and houses that were displayed in random order for 400ms each, with 400ms inter-stimulus interval (blank screen) between. **(C)** Noisy-task: Subjects also performed a face-identification task with 1s presentation of phase-scrambled close-up pictures of faces and houses. Stimuli ranged from 0 to 100% noise in 5% increments, and subjects pressed a key when they believed a face was shown. **(D)** The timecourse of broadband spectral change in the electrical potential, a reflection of averaged neuronal population activity, was compared with individual stimuli. In this case, the broadband timecourse from the blue electrode in (A) is shown above the corresponding stimuli from the noisy task **(E)** Projection templates are generated by averaging the broadband response in the blue electrode site (fusiform gyrus) to face and house stimuli in the localizer task. **(F)** Averaged broadband timecourses in response to face stimuli in the noisy task illustrates the graded response in neuronal population activity as stimulus noise is increased. **(G)** The face projection template, generated from the localizer task, is projected to individual trials from the noisy task, revealing a robust neurometric function, with decreasing neuronal activity as image noise is increased. **(H)** As in E-G, but for the pink electrode site in (A) (lingual gyrus), using a house-template for the axes on the far right.

### Template projection technique

The projection templates used were from stimulus triggered averaged raw potential and broadband template (Localizer task only): In each electrode, $n$, stimulus triggered average templates of the cortical response to stimuli were obtained from the voltage timeseries (usually called the Event-related potential – "ERP", $\langle V_n(t')\rangle_S$), and the broadband timeseries (Event-related broadband – "ERBB", $\langle B_n(t')\rangle_S$). These were calculated for face ($S \to F$, face) and house ($S \to H$, house) stimuli independently ($\tau_{k_s}$ denotes the $k^{th}$ of $N_S$ total instances of stimulus type $S$):

$$\langle V_n(t')\rangle_S = \frac{1}{N_S}\sum_{k_s=1}^{N_S} V_n\left(\tau_{k_s} + t'\right).$$

This is only calculated on the peri-stimulus interval $0 < t' \le 600$ ms (where $t'$ denotes time with respect to stimulus start). We perform the same averaging for the broadband signal to obtain $\langle B_n(t')\rangle_S$. Note that templates were obtained only from the localizer task.

### Projection of templates into localizer task

$\langle V_n(t')\rangle_S$ and $\langle B_n(t')\rangle_S$ were back-projected into the localizer task data to obtain a set of localizer feature points, $\Gamma^V_{n,S}(q)$ and $\Gamma^B_{n,S}(q)$ for stimulus presentationat time $\tau_q$:

$\Gamma^V_{n,S}(q) = \sum_{t'=0}^{600}\langle V_n(t')\rangle_S\left(V_n\left(\tau_q + t'\right) - \overline{V_n^b\left(\tau_q\right)}\right)$, where $\overline{V_n^b\left(\tau_q\right)}$represents an "instantaneous" baseline: $\overline{V_n^b\left(\tau_q\right)} = \sum_{t=1}^{100} V_n\left(t + \tau_q\right)$. $\Gamma^B_{n,S}(q)$ were obtained in the same fashion for the broadband timeseries. The event types were face picture stimulus onset, house picture stimulus onset, or ISI onset (notated as $S \to o$).

### Projection of templates into noisy task

In order to quantify the single trial response in the noisy task, the projection templates (generated from the localizer task) were applied to each stimulus presentation, scanning through a 0 to 300 ms delay with respect to each stimulus onset: $\Gamma^B_{n,S}\left(t_p\right) = \sum_{t'=1}^{600}\langle B_n(t')\rangle_S\left(B_n\left(t_p + t'\right) - \overline{B_n^b\left(t_p\right)}\right)$,

where $t_p$ ranges over the 0-300ms interval, and $\overline{B_n^b(t_p)}$ is the instantaneous baseline obtained for each timepoint. For each such trial, the "Projection magnitude" is $\Gamma_{n,S}^B(p) = \max\left(\Gamma_{n,S}^B(t_p)\right)$, and the time of this maximum value – the "Projection latency" – is denoted $L_{n,S}^B(p)$. These magnitudes, $\Gamma_{n,S}^B(p)$, for $n \rightarrow$ most face- and house- selective electrodes for $S \rightarrow F$ and $S \rightarrow H$ are illustrated in each neurometric function, and associated with latency profiles, $L_{n,S}^B(p)$. Similar projections were performed for the voltage timeseries to obtain $\Gamma_{n,S}^V(p)$ and $L_{n,S}^V(p)$.

## Classification of noisy task trials

A simple classifier was generated and trained on the localizer task only, and then applied to the noisy task to predict whether a given stimulus was a face or a house picture.

## Generation of a feature space

The full feature space for classification, consisting of the union of projections of the stimulus triggered average raw potentials ($V$) or broadband ($B$) across all electrodes ($n$), for face ($F$) and house ($H$) templates independently, is the combination of $\Gamma_{n,F}^V$, $\Gamma_{n,H}^V$, $\Gamma_{n,F}^B$, and $\Gamma_{n,H}^B$. For brevity, we can combine the notation to denote each feature as $\Gamma_m$, where $m$ represents a unique combination of one electrode $n$, $V$ or $B$, and $F$ or $H$. Each feature was scaled with division by its mean, $\Gamma_m \rightarrow \Gamma_m / \overline{\Gamma_m}$, for the localizer and noisy tasks independently. Many of these features will not be particularly informative about when and how the brain is processing these visual stimuli. Therefore, features were downselected by independently assessing the squared cross-correlation between face or house vs ISI, as well as face vs house from the localizer task, and rejecting those which fell beneath the pre-defined threshold $r_m^2 < 0.10$. For example, the comparison of face and house stimuli is:

$r_m^2 = \frac{\left(\overline{\Gamma_m(q=F)} - \overline{\Gamma_m(q=H)}\right)^2}{\sigma_m^2} \frac{N_F * N_H}{N_{FH}^2}$, where $\sigma_m$ is the standard deviation of the joint distribution for face and house stimuli $\Gamma_m(q=F\,\&\,H)$, $N_F$ is the number of face events, $N_H$ is the number of house events, and $N_{FH} = N_F + N_H$.

### Classification

For the sake of simplicity, Fisher linear discriminant analysis (LDA) was used for classification. From the localizer task, this characterizes the full distribution and the sub-distributions $\Gamma_m(q \to F)$, $\Gamma_m(q \to H)$, by their means and covariances only (i.e. as if they are normally distributed). LDA assumes that the covariances of the sub-distributions are the same. Given the feature space of the training distribution (localizer task), single trials ($p$) from the noisy task can be assigned a posterior probability of belonging to the face- or house- distribution: $\Pr\{\Gamma_m(t)|q \to F\}$ or $\Pr\{\Gamma_m(t)|q \to H\}$. The higher posterior probability is the one that is chosen.

## Results

### Cortical response to basic face and house stimuli

Subjects were first presented with simple, grayscale, pictures of whole-field faces and houses that were displayed in random order. As demonstrated previously (Miller et al., 2014)(chapter 5 and chapter 6), broadband responses within the fusiform and lingual gyri track the presentation of faces and houses on a single stimulus basis with high temporal fidelity. Event-related averaged traces of both the broadband (ERBB) and the raw potential (ERP) were obtained from category-selective inferior temporal regions (although the broadband response may be category selective when the event-related potential is not (chapter 5). While the event related potential in face-selective fusiform gyral sites is classically associated with a negative peak at ~200ms ("N200"), the actual shape of face-selective fusiform ERPs can vary widely, even at fusiform sites 1cm from one another (chapter 5). Conversely, the ERBB is a generic correlate of population firing rate, and while, the

width and latency may be different in adjacent cortical sites, general fast-rise→slow-fall shape is preserved. The ERBB may be interpreted as a combination of the individual trial response shape and a probability density function for the distribution of latencies.

The templates generated in response to robust, wide-field, pictures of faces and houses were then used to both characterize single trial responses that could be applied to a more sophisticated setting. Furthermore, the basic localizer task was used to identify category-selective cortical sites, and generate a multidimensional feature space within which the distributed ventral temporal response could be characterized in a straightforward manner.

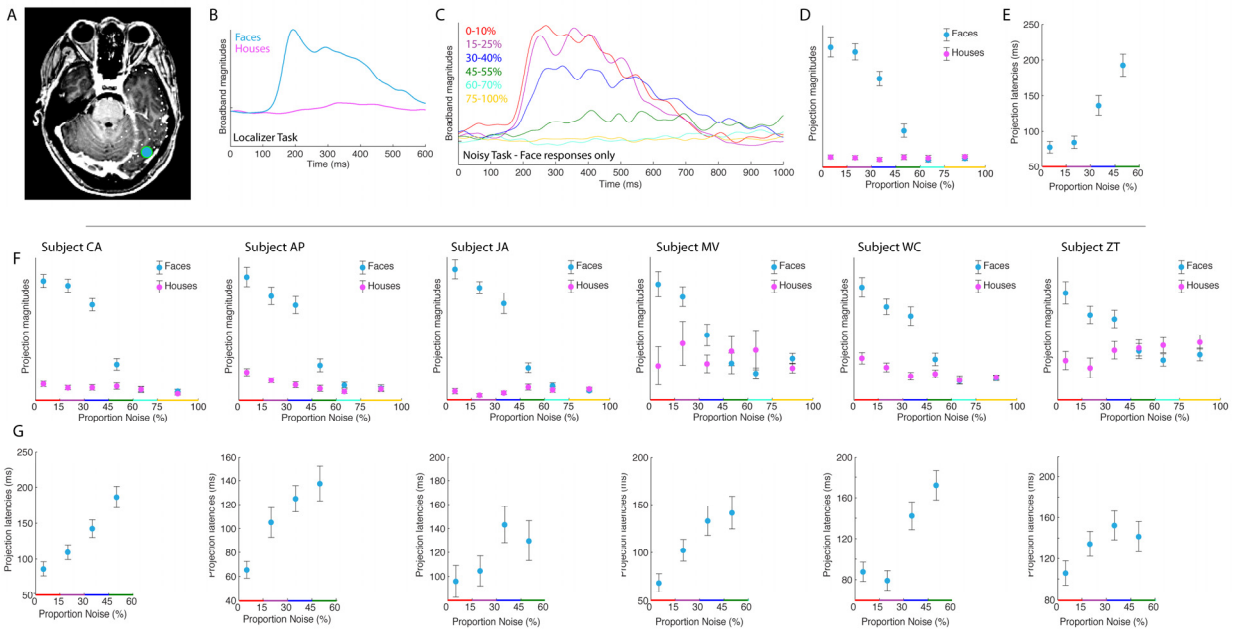


**Figure 2: Neuronal population responses are delayed with increasing stimulus noise. (A)** The most face-selective electrode in subject 2 is shown in blue. **(B-D)** As in figure 1E-G, for the site in (A). **(E)** Projection latencies as a function of stimulus noise for the site in (A). For the higher noise levels, no latency is included because the neuronal activity is not large enough for the measure to be meaningful. **(F)** Neurometric functions for the remaining 6 subjects in the most face-selective site (all were on fusiform gyrus). **(G)** Corresponding projection latencies for the 6 subjects.

## Responses to noisy stimuli in face and house selective sites

After identification of projection templates and salient electrodes from the localizer task, subjects then performed a face-identification task with 1s presentation of randomly interleaved phase-scrambled close-up pictures of faces and houses ("Noisy task" - stimuli from (Heekeren et al., 2004)). Stimuli ranged from 0 to 100% noise in 5% increments (later divided in six bins: 0-10%, 15-25%, 30-40%, 45-55%, 60-70% and 75-100%), and subjects were instructed to press a key when they believed a face was shown. Averaged broadband timecourses in response to both face and house stimuli reveal a decremented, graded, response in neuronal population activity as stimulus noise is increased. Projection templates, generated from the localizer task, were projected to individual trials from the noisy task, evaluated by sliding the projection template through several hundred milliseconds following stimulus onset and calculating the dot product at each point to obtain the projection magnitude (maximum dot product) and associated latency (between stimulus onset and maximum). A robust neurometric function reveals decreasing neuronal activity as image noise is increased in both face-selective fusiform gyral sites and house-selective lingual gyral sites. Similarly, latency profiles reveal parametrically delayed responses with image noise increase. This was true independent of perception: within correct choices only, the neurometric and latency profile shapes were conserved (figure 3).

## Decoding stimuli and subject responses from inferior temporal cortex

We subsequently applied a simple classifier to test whether the broadband responses could be used to predict the stimulus type or the subject's choice (figure 4). In the 4 subjects where choice response was recorded, task performance was quite high at low levels of noise, but descended to chance above ~50% noise. A simple decoder was constructed from a choice-free localizer task, and applied to the noisy task. The decoder prediction was correlated more closely with the stimulus that the subjects' choice at low noise, but dropped to chance at high noise levels. At high levels of noise, the classifier predicted subjects' choice above chance, and was correlated with the subjects' choice rather than the stimulus type.

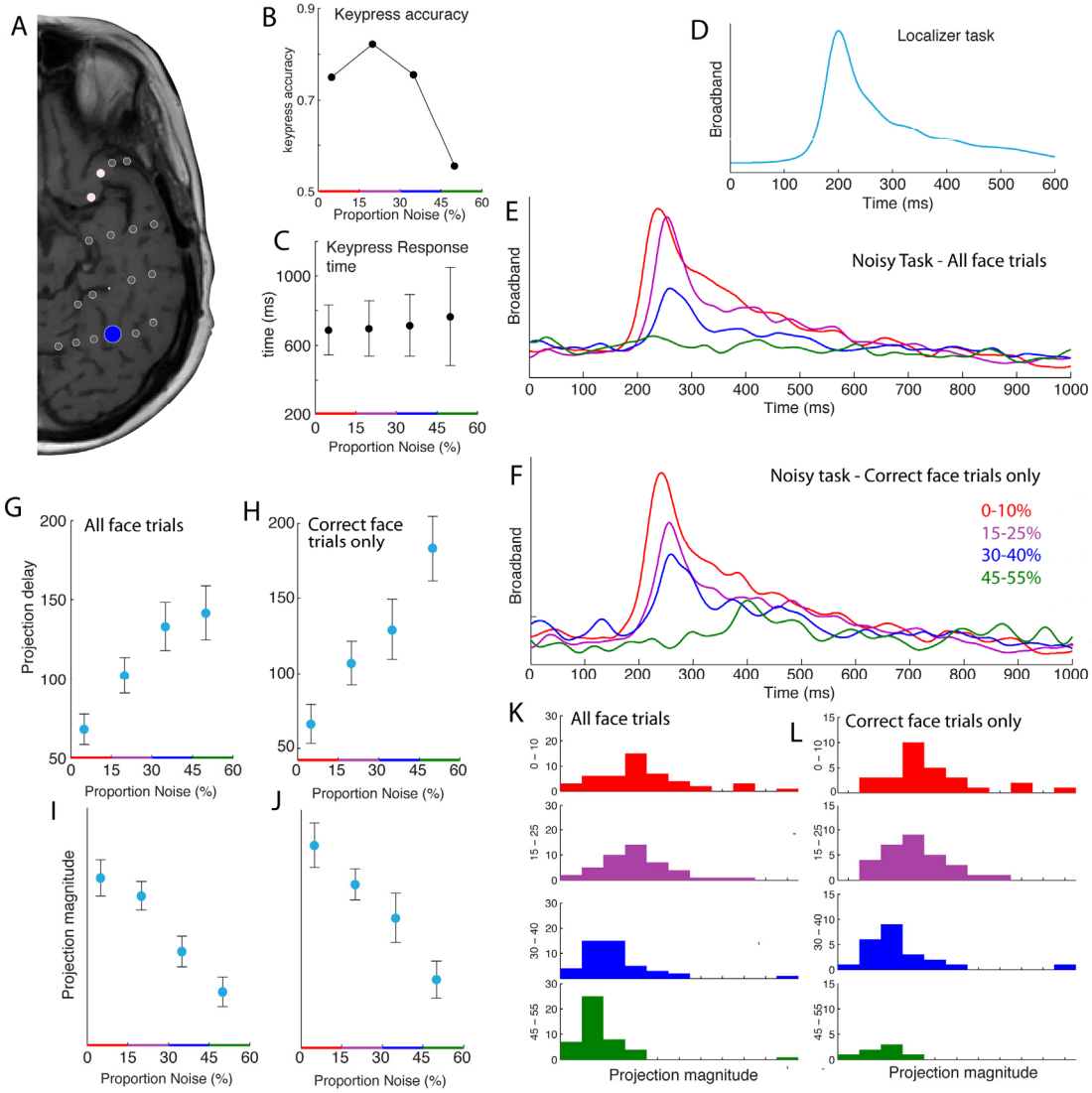


**Figure 3: The graded nature of the neuronal population response with noise is independent of perception. (A)** The most face-selective electrode in subject 3 is shown in blue. **(B)** Subject accuracy, sorted by noise level. The fact that the accuracies in this subject were the same at low noise levels implies that the smaller, delayed, cortical activity with added noise (e.g. in the 15-25% noise group), does not necessarily correspond to worse performance. **(C)** Key press response times, sorted by noise level (note: there was no incentive to respond faster, and stimuli were shown for a fixed period). **(D)** Localizer-task projection template for faces. **(E)** Averaged broadband timecourses in response to all face stimuli in the noisy task. **(F)** As in (E), but for correct keypress trials only. **(G)** Projection latencies as a function of stimulus noise. **(H)** As in (G), but for correct trials only. This shows that the increasing delay observed with increasing noise cannot be explained by an averaging of correctly and incorrectly perceived face stimuli. **(I)** Neurometric function – projection magnitudes of the face-template into all noisy task data. **(J)** As in (I), but for correct keypress trials only. **(K)** Histogram of projection magnitudes of all face stimuli in the noisy task, sorted by noise level. Note that each distribution is unimodal. This indicates that the decremented average traces (E), and projection magnitudes (I) with noise are not due to the averaging of an all-or-nothing response, but are instead graded with stimulus noise. **(L)** As in (K), but for correct trials only. This indicates that the graded effect is a function of the noise in the stimulus and not whether a face

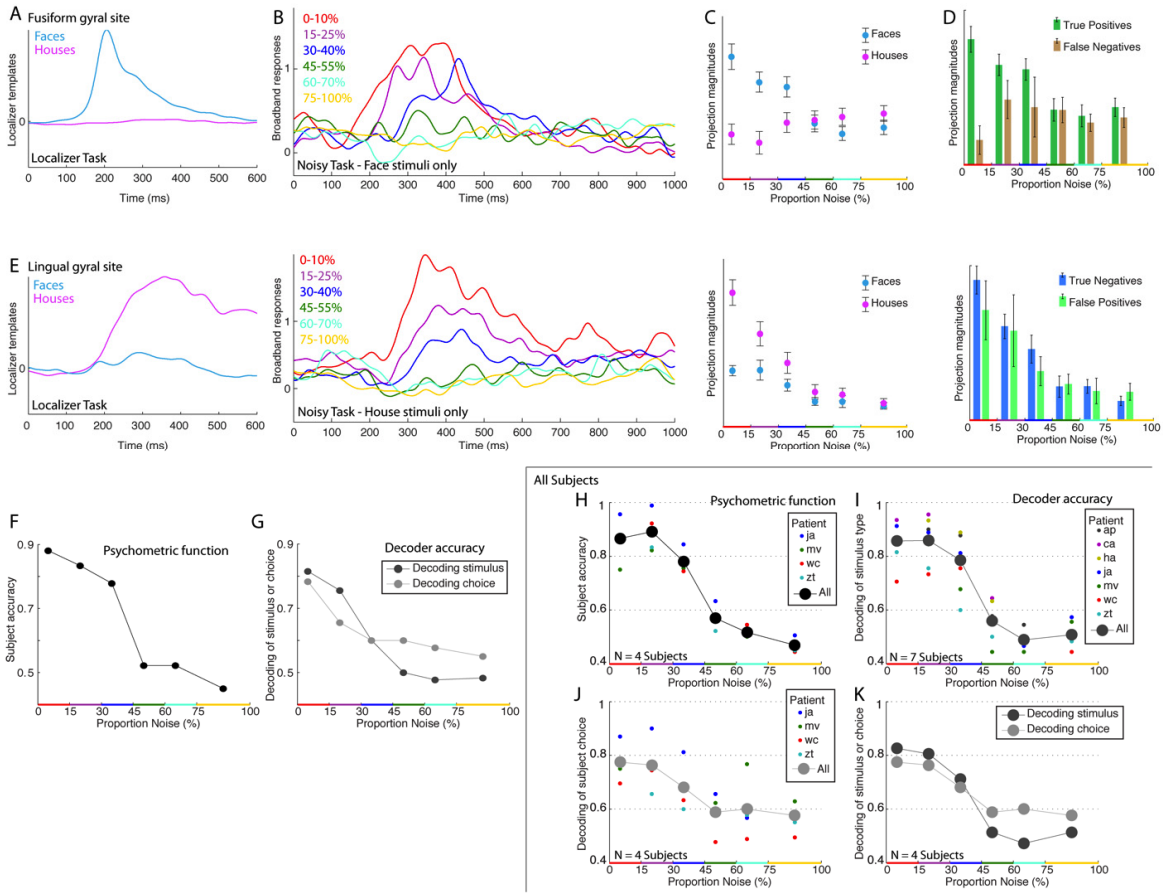


**Figure 4: Decoding stimuli and subject responses from inferior temporal cortex.** (A-G) are from subject 4, with (A-D) measured at a single face-selective fusiform gyral site, and (E) measured at a single house-selective lingual gyral site. **(A-C)** As in figure 1E-G. **(D)** Template projection magnitudes for face stimulus trials, sorted by keypress (true positives) or lack thereof (false negatives). **(E)** As in (A-D), but for a lingual gyral electrode and house picture responses. **(F)** Psychometric function – subject choice accuracy as a function of stimulus noise. **(G)** Decoder accuracy in predicting stimulus type (dark gray) or subject choice (light gray). Note that the decoder (classifier) is generated on a simple localizer task that does not itself have a choice component. **(H)** Psychometric function for all subjects where response was recorded (N=4 subjects). **(I)** Decoder accuracy in predicting stimulus type (N=7 subjects). **(J)** Decoder prediction compared with subject choice. **(K)** Decoder accuracy for stimulus compared with subject choice.

## Discussion

This study investigated whether low-level information is represented in the ventral temporal cortex, and we found a robust, parametric relationship between stimulus noise and neuronal population response (Figures 1&2). This held true whether all trials were examined, or correct choices only (Figure 3). A classifier, trained on a choice-free task, was applied to noise-masked data: At low levels of noise, the stimulus category was accurately predicted, and this prediction accuracy gradually declined to chance with increasing levels of noise (Figure 4). Therefore, the ventral temporal cortex processes the "bottom-up" aspect of visual object perception.

The predictions of this classifier could also be compared with subjects' choice. At low levels of noise, the stimulus type was better predicted than the subjects' choice. Training a classifier in one experimental paradigm, and testing it in another, was extremely useful in this setting. The classifier was trained on an independent dataset of images from the same class, but of much different quality. Using a choice-free paradigm to train the classifier meant that "choice-related" changes in the cortical state did *not* confound the classification of stimulus nor choice. Instead, the perception of the stimulus was the quantity that was classified. At high levels of noise, when the subjects performed at chance level and stimulus type could not be decoded, the subjects' choice was predicted above chance (Figure 4). Ventral temporal cortex must also subserve the "top-down" assignment of visual inputs to distinct semantic category

One must conclude that the inferotemporal cortex represents a confluence of the modes of processing. At low levels of noise, bottom up information drives the neuronal population activity. With decreasing bottom up information (increasing noise) the influence of higher order cognition on these areas is revealed. The ventral temporal cortex must therefore be a locus of visual object perception.

While this role for the ventral temporal cortex has been proposed before, the simultaneous demonstration of top-down and bottom-up processing during single trials firmly establishes it.

Much as earlier visual regions project into ventral temporal regions, so must association areas as well, providing contextual influences such as attention, expectation, and working memory. Top down influences may influence neural responses in such a way that they provide more information about the stimulus to improve perception (Gilbert and Li, 2013). We show that at the highest levels of noise, when the subjects' performance was at chance, neural responses in inferior temporal cortex could decode perception while viewing pure noise.

# Chapter 8: Closing Remarks

I began the thesis by asking which portions of the ECoG signal are needed to understand ventral temporal physiology, and explored broadband spectral change, cortical oscillations, and stimulus-locked potential deflections (ERPs). Similar to other work in motor and language regions, my colleagues and I found that continuous approximations of broadband spectral change reflect of neuronal population activity at timescales <50ms throughout the ventral visual stream. The connection between neuronal population firing rate and broadband spectral change implies that the broadband timecourse has a number of unique properties that make it ideal to study the physiology of perception. The first is that the interpretation of the broadband ECoG change is straightforward: it may be loosely thought of as a realtime cross-sectional raster across the inputs to the neuronal population beneath the electrode. Because of the intrinsic averaging, ECoG changes are robust on a single-event scale (e.g. faster than most perceptions, decisions, and behaviors), so the effect of *immediate context*, rather than *average context*, may be examined. Second, ECoG sits in a type of "Goldilocks zone" of experimental scales (with the drawback that placement is stochastic because of the clinical setting, and even common placement areas are surveyed very sparsely). By intrinsically averaging across a population, ECoG is not limited by stochastic responses in the same way that single unit studies are. Because the spatial scale of cortical columns is not drastically smaller than the exposed electrode surface, 'local' physiology correlated with a particular brain function is not drowned by the uncorrelated cortex surrounding it, as would be the case for EEG or MEG. The BOLD signal of fMRI cannot probe the same temporal scales, and must be averaged to obtain meaning: as a metabolic derivative of neuronal activity, it has intrinsically poor temporal fidelity and a low signal-to-noise ratio. The experiments performed and analyses developed in this thesis were tailored to capitalize on the unique properties of the ECoG scale and signal properties.

In contrast to these broadband changes, gamma oscillations, which have been billed as a generic marker of visual processing and inter-areal interaction, were shown to be related to specific low-level features of visual stimuli, and absent during viewing of many easily identifiable natural images. Gamma rhythms likely reveal a particular aspect of circuit physiology where pyramidal neurons interact with one another laterally and recurrently. Because of retinotopy, macroscale linear regularity (e.g. gratings) produces larger scale spatial synchronization across a population of neurons at some point early in the visual stream. Taken in this light, stimuli producing gamma rhythms then represent a clever way of isolating (and 'tagging') a particular circuit motif in the physiology by choice of stimulus. Perhaps existing experimental findings should be re-examined in this light.

Lower frequency rhythms in the α and β range were shown to actively phase-entrain population firing, and selective release the entrainment during visual task engagement. This is important, as it suggests that the role of these rhythms in the ventral stream is not one of organizing or performing computations for actively processing complex visual stimuli, but rather seem to play a role in the function of 'disengaged cortex'. Instead, we proposed a "suppression by synchronization" model, where neurons from a distinct pacemaker circuit project diffusely to populations of cortical pyramidal neurons, targeting their basal dendrites and somas with synchronized input, forcing recurrent inputs between pyramidal neurons to be stochastically aligned with the rhythm if they are to induce a downstream action potential. In this way, weak but synchronous input keeps the population in a "dynamically suppressed" state, where it can quickly transition into an engaged "processing state". One need only remove time-locking influence and the neuronal population can switch to an engaged and actively computing state. While this hypothesis has yet to gain traction, my hope is that it will be read and considered by others in the field, and tested for validity at some point.

With the knowledge of what aspects of the ECoG signal to employ, and how to interpret them, we turned to the central concern of the thesis: the relationship between ventral temporal cortex, and the formation of a percept. If the act of perception has occurred in or prior to these regions, then both high level features, such as visual object category, and low level features, such as timing in the perceptual stream should be able to be decoded from the spontaneous stream of ECoG data. The robust nature of neurophysiologic responses in two distinct subregions of the ventral temporal cortex, fusiform and parahippocampal/lingual gyri, and two categories of stimuli, faces and places, has been clearly demonstrated in a variety of settings. In order to make the experimental setting as straightforward as possible, we showed subjects simple, wide-field, grayscale pictures of faces and houses. As expected, robust category-specific responses to each type of stimulus were found, where face-picture selective sites were consistently found on the fusiform gyrus and house-selective sites were found on the lingual and parahippocampal gyri. If we designated the time of stimulus onset, we were able to decode face vs house stimuli with near-perfect accuracy (it is likely that some of the individuals lapsed attention at approximately the error rate that we report). Several groups had shown robust classification in this same manner (although not with the same accuracy). However, we wanted to do something that (to our knowledge) had not been done before: decode the perceptual content and timing from the spontaneous stream of ECoG data. Using a method for projecting averaged responses as sliding templates for prediction, we were able to predict the timing of stimulus onset, and class of stimulus with >95% accuracy, to ~20ms temporal precision, while tolerating <5% false predictions (a 600ms measurement lag is required in the process). I feel that this is result is game-changing: it illustrates that, from a sparse sampling of the ventral temporal brain surface, the human perceptual experience can be decoded at essentially the same timescale that decisions and behaviors will be made in response to these very perceptions. From the perspective of cognitive neuroscience, this shows that the perceptual process for simple visual stimuli is physiologically robust in category-selective ventral temporal regions.

From the perspective of neural engineering, this represents a perceptual type-and-timing decoder that has near-perfect accuracy (at least in this 2-class setting).

Examination of the magnitude and latency of broadband responses in the simple face-house stimulus stream (which did not have a choice component) reveals that there is trial-to-trial variability. Because of the simplicity in the task (simple grayscale images, randomly interleaved, with fixed 400ms stimulus&ISI timing interval), the first (and most trivial) explanation for this might be that the variability is explained by stochasticity in these neuronal populations combined with noise in the ECoG measurement. However, closer examination would reveal that the experimental context was actually changing dynamically. Each simple face or house was being viewed in the context of having seen either a face or a house less than a second earlier. In other words, each image could be parameterized as either a face or a house, but it could also be parameterized as novel or repeated. Even in a series of randomly interleaved grayscale faces and houses, there is perceptual context. A face following a prior face is viewed in a different context than a face that follows a house, and we isolated face- and house- selective ventral temporal loci to see if this sequence-context might be reflected in the single-trial broadband responses. Approximately half of the category-selective sites showed greater total broadband activity for novel than for repeated stimulus class. In approximately half of the face-selective sites (and none of the house-selective sites), latency to peak activity was faster for novel than repeat stimuli (with no correlation between the total activity and latency effects). These observations suggest that some aspect of ventral temporal physiology is tuned to sequential context, with an emphasis on perceptual novelty.

Finding evidence that perception is reflected in the ventral temporal neuronal populations does not definitively establish that those populations are themselves loci for the perceptual process. This act of forming a visual percept implies low level, “bottom-up,” integration of simple features into increasingly complex amalgams, combined with high level, “top-down,” assignment of the

amalgam to a conceptual framework, where memories, expectations, and context designate a larger meaning. If we were to establish that the ventral temporal cortex is itself a locus for this perception, we should see clear evidence that both bottom-up and top-down phenomena are simultaneously represented in the same neuronal populations, and are, to some degree, independent of one another. We used a set of phase-scrambled 'noisy' pictures of faces and houses, and asked subjects to report when they saw a face. We found that robust neurometric functions revealed decreasing neuronal population activity as image noise increased in both face-selective fusiform gyral sites and house-selective lingual gyral sites. Interestingly, the shape of these neurometric functions was robust whether subjects correctly perceived the stimulus or not. The distributions within each noise grouping were unimodal and graded. This shows, definitively, that low-level (bottom-up) features are represented independent of top-down influence (perception and choice). In order to test whether the converse is true, we constructed a basic classifier using ventral temporal responses from the simple localizer experiment where there was no decision element. We applied this classifier to the noisy stimulus decision task, and assessed whether it predicted the stimulus and/or the subjects' choice. At low levels of noise, the stimulus category was accurately predicted, at high levels of noise, the prediction degraded to chance. The decoder correlated more with the stimulus than the subjects' choice at low noise levels. However, at high noise levels, where the bottom-up evidence for one class of stimuli or the other was poor, the prediction correlated above chance with the subjects' choice, revealing top-down influence on these ventral temporal neuronal populations. These results show that the physiology in ventral temporal cortex is driven by both bottom up and top down information and must be locus of human perception. Although this conclusion may have been anticipated from experiments in other settings, the ability to quantify physiologic response or to predict choice on a single-stimulus basis would not have been possible.

As this work continues beyond this thesis, my next steps in exploring the ventral temporal cortex will address two basic questions:

How does bias influence the physiology of perception?

Does multi-sensory integration change how visual stimuli are processed and perceived?

# Acknowledgments

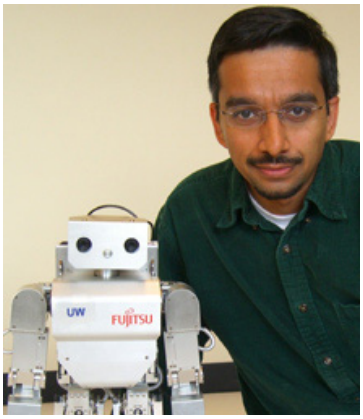


Thanks to Raj, Jeff, and Marcel

None of this could have been done without the generous participation of the patients and staff at Harborview Hospital in Seattle, WA.

I was fortunate to be able to work with Raj Rao, Jeff Ojemann, Marcel den Nijs, Eb Fetz, Gerv Schalk, Chris Honey, Brian Wandell, John Winawer,Kurt Weaver, Vinitha Rangarajan, Brett Foster,Kalanit Grill Spector, Gagan Wig, Franco Pestilli, Tim Blakeley, and Adam Hebb, during the creation of this work. I am grateful to David Heeger,Jaan Aru, Miah Wander, Lise Johnson Bharathi Jagadeesh, Geoff Boynton, and Nathan Witthoft for helpful discussion, and the Ungerleider Laboratory at the National Institute of Health in Bethesda, MD for sharing their stimuli.

This work was financially supported by the generous contribution of National Aeronautics and Space Administration Graduate Student Research Program, National Institute of General Medical Sciences Medical Scientist Training Program, National Science Foundation 0622252 & 0642848,and NIH R01-NS065186.

**References**


Afraz SR, Kiani R, Esteky H (Microstimulation of inferotemporal cortex influences face categorization. Nature 442:692-695.2006).

Aguirre GK, Zarahn E, D'Esposito M (An area within human ventral cortex sensitive to "building" stimuli: evidence and implications. Neuron 21:373-383.1998).

Allison T, Ginter H, McCarthy G, Nobre AC, Puce A, Luby M, Spencer DD (Face recognition in human extrastriate cortex. Journal of neurophysiology 71:821-825.1994a).

Allison T, McCarthy G, Nobre A, Puce A, Belger A (Human extrastriate visual cortex and the perception of faces, words, numbers, and colors. Cereb Cortex 4:544-554.1994b).

Allison T, Puce A, Spencer DD, McCarthy G (Electrophysiological studies of human face perception. I: Potentials generated in occipitotemporal cortex by face and non-face stimuli. Cerebral cortex 9:415-430.1999).

Aoki F, Fetz EE, Shupe L, Lettich E, Ojemann GA (Increased gamma-range activity in human sensorimotor cortex during performance of visuomotor tasks. Clin Neurophysiol 110:524-537.1999).

Ashburner J, Friston KJ (Unified segmentation. Neuroimage 26:839-851.2005).

Bartolo MJ, Gieselmann MA, Vuksanovic V, Hunter D, Sun L, Chen X, Delicato LS, Thiele A (Stimulus-induced dissociation of neuronal firing rates and local field potential gamma power and its relationship to the resonance blood oxygen level-dependent signal in macaque primary visual cortex. Eur J Neurosci 34:1857-1870.2011).

Barton JJ, Press DZ, Keenan JP, O'Connor M (Lesions of the fusiform face area impair perception of facial configuration in prosopagnosia. Neurology 58:71-78.2002).

Bates JA (Electrical activity of the cortex accompanying movement. J Physiol 113:240-257.1951).

Bauer R, Brosch M, Eckhorn R (Different rules of spatial summation from beyond the receptive field for spike rates and oscillation amplitudes in cat visual cortex. Brain research 669:291-297.1995).

Beck A (Mapping of localization in brain and cortex by means of electric phenomena. Polska Akademica Umiejetnosci 2:186-232.1891).

Bedard C, Kroger H, Destexhe A (Does the 1/f Frequency Scaling of Brain Signals Reflect Self-Organized Critical States? Physical Review Letters 97:118102.2006).

Bentin S, Taylor MJ, Rousselet GA, Itier RJ, Caldara R, Schyns PG, Jacques C, Rossion B (Controlling interstimulus perceptual variance does not abolish N170 face sensitivity. Nature neuroscience 10:801-802; author reply 802-803.2007).

Bishop CM (1995) Neural networks for pattern recognition: Oxford university press.

Bosman CA, Schoffelen JM, Brunet N, Oostenveld R, Bastos AM, Womelsdorf T, Rubehn B, Stieglitz T, De Weerd P, Fries P (Attentional stimulus selection through selective synchronization between monkey visual areas. Neuron 75:875-888.2012).

Brindley GS, Craggs MD (The electrical activity in the motor cortex that accompanies voluntary movement. Proceedings of the Physiological Society 28P.1972).

Brunet N, Bosman CA, Roberts M, Oostenveld R, Womelsdorf T, De Weerd P, Fries P (Visual Cortical Gamma-Band Activity During Free Viewing of Natural Images. Cereb Cortex.2013).

Bruno RM, Sakmann B (Cortex is driven by weak but synchronously active thalamocortical synapses. Science 312:1622.2006).

Buckner RL, Andrews-Hanna JR, Schacter DL (Anatomy, Function, and Relevance to Disease. Annals of the New York Academy of Sciences 1124:1-38.2008).

Bullock TH, McClune MC, Enright JT (Are the electroencephalograms mainly rhythmic? Assessment of periodicity in wide-band time series. Neuroscience 121:233-252.2003).

Buzsaki G, Anastassiou CA, Koch C (The origin of extracellular fields and currents--EEG, ECoG, LFP and spikes. Nature reviews Neuroscience 13:407-420.2012).

Buzsaki G, Draguhn A (Neuronal oscillations in cortical networks. Science 304:1926-1929.2004).
Buzsaki G, Leung LW, Vanderwolf CH (Cellular bases of hippocampal EEG in the behaving rat. Brain Res 287:139-171.1983).
Canolty RT, Edwards E, Dalal SS, Soltani M, Nagarajan SS, Kirsch HE, Berger MS, Barbaro NM, Knight RT (High gamma power is phase-locked to theta oscillations in human neocortex. Science 313:1626.2006).
Canolty RT, Soltani M, Dalal SS, Edwards E, Dronkers NF, Nagarajan SS, Kirsch HE, Barbaro NM, Knight RT (Spatiotemporal dynamics of word processing in the human brain. Front Neurosci 1:185-196.2007).
Chong SC, Jo S, Park KM, Joo EY, Lee MJ, Hong SC, Hong SB (Interaction between the electrical stimulation of a face-selective area and the perception of face stimuli. NeuroImage 77:70-76.2013).
Clare Kelly AM, Uddin LQ, Biswal BB, Castellanos FX, Milham MP (Competition between functional brain networks mediates behavioral variability. Neuroimage 39:527-537.2008).
Cohen MX, Elger CE, Fell J (Oscillatory Activity and Phase–Amplitude Coupling in the Human Medial Frontal Cortex during Decision Making. Journal of Cognitive Neuroscience 21:390-402.2009).
Conner CR, Ellmore TM, Pieters TA, DiSano MA, Tandon N (Variability of the relationship between electrophysiology and BOLD-fMRI across cortical regions in humans. J Neurosci 31:12855-12865.2011).
Connor JA, Stevens CF (Inward and delayed outward membrane currents in isolated neural somata under voltage clamp. The Journal of Physiology 213:1.1971).
Crone NE, Hao L, Hart Jr J, Boatman D, Lesser RP, Irizarry R, Gordon B (Electrocorticographic gamma activity during word production in spoken and sign language. Neurology 57:2045.2001).
Crone NE, Korzeniewska A, Franaszczuk PJ (Cortical gamma responses: searching high and low. International journal of psychophysiology : official journal of the International Organization of Psychophysiology 79:9-15.2011).
Crone NE, Miglioretti DL, Gordon B, Lesser RP (Functional mapping of human sensorimotor cortex with electrocorticographic spectral analysis. II. Event-related synchronization in the gamma band. Brain 121 ( Pt 12):2301-2315.1998a).
Crone NE, Miglioretti DL, Gordon B, Sieracki JM, Wilson MT, Uematsu S, Lesser RP (Functional mapping of human sensorimotor cortex with electrocorticographic spectral analysis. I. Alpha and beta event-related desynchronization. Brain 121 ( Pt 12):2271-2299.1998b).
Crouzet SM, Kirchner H, Thorpe SJ (Fast saccades toward faces: face detection in just 100 ms. Journal of vision 10:16 11-17.2010).
Cunningham MO, Davies CH, Buhl EH, Kopell N, Whittington MA (Gamma oscillations induced by kainate receptor activation in the entorhinal cortex in vitro. J Neurosci 23:9761-9769.2003).
Cunningham MO, Whittington MA, Bibbig A, Roopun A, LeBeau FE, Vogt A, Monyer H, Buhl EH, Traub RD (A role for fast rhythmic bursting neurons in cortical gamma oscillations in vitro. Proceedings of the National Academy of Sciences of the United States of America 101:7152-7157.2004).
Dale AM, Fischl B, Sereno MI (Cortical surface-based analysis. I. Segmentation and surface reconstruction. Neuroimage 9:179-194.1999).
Damasio A, Damasio H, van Hoessen G (Prosopagnosia: anatomic basis and behavioral mechanisms. Neurology 32:331–341.1982).
Dayan P, Abbott LF (2001a) Theoretical neuroscience. Cambridge, MA: MIT Press.
Dayan P, Abbott LF (2001b) Theoretical neuroscience : computational and mathematical modeling of neural systems. Cambridge, Mass.: Massachusetts Institute of Technology Press.

Dehaene S, Changeux JP (Experimental and theoretical approaches to conscious processing. Neuron 70:200-227.2011).
Destrieux C, Fischl B, Dale A, Halgren E (Automatic parcellation of human cortical gyri and sulci using standard anatomical nomenclature. NeuroImage 53:1-15.2010).
Eckhorn R, Bauer R, Jordan W, Brosch M, Kruse W, Munk M, Reitboeck HJ (Coherent oscillations: a mechanism of feature linking in the visual cortex? Multiple electrode and correlation analyses in the cat. Biol Cybern 60:121-130.1988).
Edwards E, Nagarajan SS, Dalal SS, Canolty RT, Kirsch HE, Barbaro NM, Knight RT (Spatiotemporal imaging of cortical activation during verb generation and picture naming. Neuroimage 50:291-301.2010).
Edwards E, Soltani M, Kim W, Dalal SS, Nagarajan SS, Berger MS, Knight RT (Comparison of time-frequency responses and the event-related potential to auditory speech stimuli in human cortex. Journal of neurophysiology 102:377.2009).
Edwards EE (2010) Presentation of visual cortex power spectra to K.J. Miller, Seattle, WA, USA.
Engell AD, Huettel S, McCarthy G (The fMRI BOLD signal tracks electrophysiological spectral perturbations, not event-related potentials. NeuroImage 59:2600-2606.2012).
Engell AD, McCarthy G (The Relationship of Gamma Oscillations and Face-Specific ERPs Recorded Subdurally from Occipitotemporal Cortex. Cereb Cortex 21:1213-1221.2011).
Engell AD, McCarthy G (Repetition Suppression of Face-Selective Evoked and Induced EEG Recorded From Human Cortex. Human brain mapping doi 10.1002/hbm.22467.2014).
Epstein R, Kanwisher N (A cortical representation of the local visual environment. Nature 392:598-601.1998).
Farah MJ, Rabinowitz C, Quinn GE, Liu GT (Early commitment of neural substrates for face recognition. Cogn Neuropsychol 17:117-123.2000).
Foster BL, Dastjerdi M, Parvizi J (Neural populations in human posteromedial cortex display opposing responses during memory and numerical processing. Proc Natl Acad Sci U S A 109:15514-15519.2012).
Fries P (A mechanism for cognitive dynamics: neuronal communication through neuronal coherence. Trends Cogn Sci 9:474-480.2005).
Fries P, Nikolic D, Singer W (The gamma cycle. Trends Neurosci 30:309-316.2007).
Fries P, Reynolds JH, Rorie AE, Desimone R (Modulation of oscillatory neuronal synchronization by selective visual attention. Science 291:1560.2001).
Fries P, Scheeringa R, Oostenveld R (Finding gamma. Neuron 58:303-305.2008).
Friston KJ, Holmes AP, Worsley KJ, Poline JB, Frith CD, Frackowiak RSJ (Statistical parametric maps in functional imaging: a general linear approach. Human brain mapping 2:189-210.1995).
Gauthier I, Anderson AW, Tarr MJ, Skudlarski P, Gore JC (Levels of categorization in visual recognition studied using functional magnetic resonance imaging. Curr Biol 7:645-651.1997).
Gauthier I, Curby KM, Skudlarski P, Epstein RA (Individual differences in FFA activity suggest independent processing at different spatial scales. Cogn Affect Behav Neurosci 5:222-234.2005).
Gieselmann MA, Thiele A (Comparison of spatial integration and surround suppression characteristics in spiking activity and the local field potential in macaque V1. Eur J Neurosci 28:447-459.2008).
Gilbert CD, Li W (Top-down influences on visual processing. Nature reviews Neuroscience 14:350-363.2013).
Goupillaud P, Grossmann A, Morlet J (Cycle-octave and related transforms in seismic signal analysis. Geoexploration 23:85-102.1984).
Gray CM (The temporal correlation hypothesis of visual feature integration: still alive and well. Neuron 24:31-47, 111-125.1999).

Gray CM, Konig P, Engel AK, Singer W (Oscillatory responses in cat visual cortex exhibit inter-columnar synchronization which reflects global stimulus properties. Nature 338:334-337.1989).

Gray CM, Singer W (Stimulus-specific neuronal oscillations in orientation columns of cat visual cortex. Proceedings of the National Academy of Sciences of the United States of America 86:1698-1702.1989).

Grill-Spector K, Henson R, Martin A (Repetition and the brain: neural models of stimulus-specific effects. Trends Cogn Sci 10:14-23.2006).

Grill-Spector K, Knouf N, Kanwisher N (The fusiform face area subserves face perception, not generic within-category identification. Nat Neurosci 7:555-562.2004).

Gunduz A, Brunner P, Daitch A, Leuthardt EC, Ritaccio AL, Pesaran B, Schalk G (Neural correlates of visual-spatial attention in electrocorticographic signals in humans. Front Hum Neurosci 5:89.2011).

Handel BF, Haarmeier T, Jensen O (Alpha Oscillations Correlate with the Successful Inhibition of Unattended Stimuli. J Cogn Neurosci.2005).

Harvey BM, Vansteensel MJ, Ferrier CH, Petridou N, Zuiderbaan W, Aarnoutse EJ, Bleichner MG, Dijkerman HC, van Zandvoort MJ, Leijten FS, Ramsey NF, Dumoulin SO (Frequency specific spatial interactions in human electrocorticography: V1 alpha oscillations reflect surround suppression. NeuroImage 65:424-432.2013).

He BJ, Zempel JM, Snyder AZ, Raichle ME (The Temporal Structures and Functional Significance of Scale-free Brain Activity. Neuron 66:353-369.2010).

Heekeren HR, Marrett S, Bandettini PA, Ungerleider LG (A general mechanism for perceptual decision-making in the human brain. Nature 431:859-862.2004).

Henrie JA, Shapley R (LFP power spectra in V1 cortex: the graded effect of stimulus contrast. Journal of neurophysiology 94:479-490.2005).

Hermes D, Miller KJ, Noordmans HJ, Vansteensel MJ, Ramsey NF (Automated electrocorticographic electrode localization on individually rendered brain surfaces. Journal of neuroscience methods 185:293-298.2010).

Hermes D, Miller KJ, Vansteensel MJ, Aarnoutse EJ, Leijten FS, Ramsey NF (Neurophysiologic correlates of fMRI in human motor cortex. Hum Brain Mapp epub.2012).

Hermes D, Miller KJ, Vansteensel MJ, Edwards E, Ferrier CH, Bleichner MG, van Rijen PC, Aarnoutse EJ, Ramsey NF (Cortical theta wanes for language. Neuroimage 85 Pt 2:738-748.2014).

Honey C, Kirchner H, VanRullen R (Faces in the cloud: Fourier power spectrum biases ultrarapid face detection. Journal of vision 8:9 1-13.2008).

Hoogenboom N, Schoffelen JM, Oostenveld R, Parkes LM, Fries P (Localizing human visual gamma-band activity in frequency, time and space. NeuroImage 29:764-773.2006).

Huettel SA, McKeown MJ, Song AW, Hart S, Spencer DD, Allison T, McCarthy G (Linking hemodynamic and electrophysiological measures of brain activity: evidence from functional MRI and intracranial field potentials. Cereb Cortex 14:165-173.2004).

Hung CP, Kreiman G, Poggio T, DiCarlo JJ (Fast readout of object identity from macaque inferior temporal cortex. Science 310:863-866.2005).

Ishai A, Ungerleider LG, Martin A, Haxby JV (The representation of objects in the human occipital and temporal cortex. Journal of cognitive neuroscience 12 Suppl 2:35-51.2000).

Ishai A, Ungerleider LG, Martin A, Schouten JL, Haxby JV (Distributed representation of objects in the human ventral visual pathway. Proceedings of the National Academy of Sciences of the United States of America 96:9379-9384.1999).

Itier RJ, Taylor MJ (N170 or N1? Spatiotemporal differences between object and face processing using ERPs. Cereb Cortex 14:132-142.2004).

Izard V, Dehaene-Lambertz G, Dehaene S (Distinct cerebral pathways for object identity and number in human infants. PLoS biology 6:e11.2008).

Jacobs J, Kahana MJ (Neural representations of individual stimuli in humans revealed by gamma-band electrocorticographic activity. J Neurosci 29:10203-10214.2009).
Jacobs J, Kahana MJ (Direct brain recordings fuel advances in cognitive electrophysiology. Trends Cogn Sci 14:162-171.2010).
Jacques C, Witthoft N, Weiner KS, Foster BL, Miller KJ, Hermes D, Parvizi J, Grill-Spector K (Electrocorticography of category-selectivity in human ventral temporal cortex: spatial organization, responses to single images, and coupling with fMR. Journal of vision 13:495.2013).
James TW, Gauthier I (Repetition-induced changes in BOLD response reflect accumulation of neural activity. Hum Brain Mapp 27:37-46.2006).
Jasper H, Penfield W (Electrocorticograms in man: effect of voluntary movement upon the electrical activity of the precentral gyrus. European Archives of Psychiatry and Clinical Neuroscience 183:163-174.1949).
Jasper HH (Electrical activity of the brain. Annual Review of Physiology 3:377-398.1941).
Jasper HH, Andrews HL (Brain potentials and voluntary muscle activity in man. Journal of Neurophysiology 1:87.1938).
Jensen O, Colgin LL (Cross-frequency coupling between neuronal oscillations. Trends Cogn Sci 11:267-269.2007).
Jia X, Kohn A (Gamma rhythms in the brain. PLoS biology 9:e1001045.2011).
Jia X, Smith MA, Kohn A (Stimulus selectivity and spatial coherence of gamma components of the local field potential. The Journal of neuroscience : the official journal of the Society for Neuroscience 31:9390-9403.2011).
Jia X, Tanabe S, Kohn A (gamma and the coordination of spiking activity in early visual cortex. Neuron 77:762-774.2013a).
Jia X, Xing D, Kohn A (No consistent relationship between gamma power and peak frequency in macaque primary visual cortex. The Journal of neuroscience : the official journal of the Society for Neuroscience 33:17-25.2013b).
Jolliffe IT (2002) Principal component analysis: Springer verlag.
Joseph JE (Functional neuroimaging studies of category specificity in object recognition: a critical review and meta-analysis. Cogn Affect Behav Neurosci 1:119-136.2001).
Kandel E, Schwartz J (2000) Principles of Neural Science: McGraw-Hill.
Kannurpatti SS, Biswal BB (Negative Functional Response to Sensory Stimulation and Its Origins. Journal of Cerebral Blood Flow & Metabolism 24:703-712.2004).
Kanwisher N, McDermott J, Chun MM (The fusiform face area: a module in human extrastriate cortex specialized for face perception. The Journal of neuroscience : the official journal of the Society for Neuroscience 17:4302-4311.1997).
Katzner S, Nauhaus I, Benucci A, Bonin V, Ringach DL, Carandini M (Local Origin of Field Potentials in Visual Cortex. Neuron 61:35-41.2009).
Kayser C, Salazar RF, Konig P (Responses to natural scenes in cat V1. Journal of neurophysiology 90:1910-1920.2003).
Kiani R, Esteky H, Mirpour K, Tanaka K (Object category structure in response patterns of neuronal population in monkey inferior temporal cortex. J Neurophysiol 97:4296-4309.2007).
Kiani R, Esteky H, Tanaka K (Differences in onset latency of macaque inferotemporal neural responses to primate and non-primate faces. Journal of neurophysiology 94:1587-1596.2005).
Kim SG, Richter W, Ugurbil K (Limitations of temporal resolution in functional MRI. Magn Reson Med 37:631-636.1997).
Kirchner H, Thorpe SJ (Ultra-rapid object detection with saccadic eye movements: visual processing speed revisited. Vision Res 46:1762-1776.2006).

Klimesch W, Sauseng P, Hanslmayr S (EEG alpha oscillations: the inhibition-timing hypothesis. Brain Res Rev 53:63-88.2007).
Koch C, Rapp M, Segev I (A brief history of time (constants). Cereb Cortex 6:93-101.1996).
Kohn A, Movshon JA (Adaptation changes the direction tuning of macaque MT neurons. Nat Neurosci 7:764-772.2004).
Koutstaal W, Wagner AD, Rotte M, Maril A, Buckner RL, Schacter DL (Perceptual specificity in visual object priming: functional magnetic resonance imaging evidence for a laterality difference in fusiform cortex. Neuropsychologia 39:184-199.2001).
Kreiman G, Koch C, Fried I (Category-specific visual responses of single neurons in the human medial temporal lobe. Nature neuroscience 3:946-953.2000).
Lakatos P, Shah AS, Knuth KH, Ulbert I, Karmos G, Schroeder CE (An oscillatory hierarchy controlling neuronal excitability and stimulus processing in the auditory cortex. Journal of neurophysiology 94:1904.2005).
Landis T, Cummings JL, Christen L, Bogen JE, Imhof HG (Are unilateral right posterior cerebral lesions sufficient to cause prosopagnosia? Clinical and radiological findings in six additional patients. Cortex 22:243-252.1986).
Lehky SR, Kiani R, Esteky H, Tanaka K (Statistics of visual responses in primate inferotemporal cortex to object stimuli. Journal of neurophysiology 106:1097-1117.2011).
Lima B, Singer W, Chen NH, Neuenschwander S (Synchronization dynamics in response to plaid stimuli in monkey V1. Cereb Cortex 20:1556-1573.2010).
Lindén H, Pettersen KH, Einevoll GT (Intrinsic dendritic filtering gives low-pass power spectra of local field potentials. Journal of Computational Neuroscience 1-22.2010).
Liu H, Agam Y, Madsen JR, Kreiman G (Timing, timing, timing: fast decoding of object information from intracranial field potentials in human visual cortex. Neuron 62:281-290.2009).
Liu J, Harris A, Kanwisher N (Stages of processing in face perception: an MEG study. Nature neuroscience 5:910-916.2002).
Llinas RR, Grace AA, Yarom Y (In vitro neurons in mammalian cortical layer 4 exhibit intrinsic oscillatory activity in the 10- to 50-Hz frequency range. Proceedings of the National Academy of Sciences of the United States of America 88:897-901.1991).
Lopes da Silva F (EEG and MEG: Relevance to Neuroscience. Neuron 80:1112-1128.2013).
Luhmann CC, Chun MM, Yi DJ, Lee D, Wang XJ (Neural Dissociation of Delay and Uncertainty in Intertemporal Choice. Journal of Neuroscience 28:14459.2008).
Makeig S, Westerfield M, Jung TP, Enghoff S, Townsend J, Courchesne E, Sejnowski TJ (Dynamic brain sources of visual evoked responses. Science 295:690-694.2002).
Malach R, Levy I, Hasson U (The topography of high-order human object areas. Trends Cogn Sci 6:176-184.2002).
Manning JR, Jacobs J, Fried I, Kahana MJ (Broadband shifts in local field potential power spectra are correlated with single-neuron spiking in humans. Journal of Neuroscience 29:13613.2009).
Marois R, Leung HC, Gore JC (A stimulus-driven approach to object identity and location processing in the human brain. Neuron 25:717-728.2000).
McCarthy G, Puce A, Belger A, Allison T (Electrophysiological studies of human face perception. II: Response properties of face-specific potentials generated in occipitotemporal cortex. Cereb Cortex 9:431-444.1999).
McCarthy RA, Evans JJ, Hodges JR (Topographic amnesia: spatial memory disorder, perceptual dysfunction, or category specific semantic memory impairment? J Neurol Neurosurg Psychiatry 60:318-325.1996).
McGugin RW, Gatenby JC, Gore JC, Gauthier I (High-resolution imaging of expertise reveals reliable object selectivity in the fusiform face area related to perceptual performance. Proceedings of the National Academy of Sciences of the United States of America 109:17063-17068.2012).

Meadows JC (The anatomical basis of prosopagnosia. Journal of neurology, neurosurgery, and psychiatry 37:489-501.1974).
Megevand P, Groppe DM, Goldfinger MS, Hwang ST, Kingsley PB, Davidesco I, Mehta AD (Seeing scenes: topographic visual hallucinations evoked by direct electrical stimulation of the parahippocampal place area. The Journal of neuroscience : the official journal of the Society for Neuroscience 34:5399-5405.2014).
Melloni L, Molina C, Pena M, Torres D, Singer W, Rodriguez E (Synchronization of neural activity across cortical areas correlates with conscious perception. The Journal of neuroscience : the official journal of the Society for Neuroscience 27:2858-2865.2007).
Mesgarani N, Chang EF (Selective cortical representation of attended speaker in multi-talker speech perception. Nature 485:233-236.2012).
Miller FR, Stavraky GW, Woonton GA (Effects of eserine, acetylcholine and atropine on the electrocorticogram. Journal of Neurophysiology 3:131.1940).
Miller KJ, Abel TJ, Hebb AO, Ojemann JG (Rapid online language mapping with electrocorticography. Journal of Neurosurgery: Pediatrics 7.2011).
Miller KJ, denNijs M, Shenoy P, Miller JW, Rao RP, Ojemann JG (Real-time functional brain mapping using electrocorticography. NeuroImage 37:504-507.2007a).
Miller KJ, Foster BL, Honey CJ (Does rhythmic entrainment represent a generalized mechanism for organizing computation in the brain? Front Comput Neurosci 6:85.2012a).
Miller KJ, Hebb AO, Hermes D, den Nijs M, Ojemann JG, Rao RPN (Brain surface electrode co-registration using MRI and x-ray. IEEE, Engineering in Medicine and Biology Society in print.2010a).
Miller KJ, Hermes D, Honey CJ, Hebb AO, Ramsey NF, Knight RT, Ojemann JG, Fetz EE (Human motor cortical activity is selectively phase-entrained on underlying rhythms. PLoS computational biology 8:e1002655.2012b).
Miller KJ, Hermes D, Schalk G, Ramsey NF, Jagadeesh B, den Nijs M, Ojemann JG, Rao RP (Detection of spontaneous class-specific visual stimuli with high temporal accuracy in human electrocorticography. IEEE Eng Med Biol Soc 2009:6465-6468.2009a).
Miller KJ, Honey CJ, Hermes D, Rao RP, denNijs M, Ojemann JG (Broadband changes in the cortical surface potential track activation of functionally diverse neuronal populations. NeuroImage 85 Pt 2:711-720.2014).
Miller KJ, Leuthardt EC, Schalk G, Rao RP, Anderson NR, Moran DW, Miller JW, Ojemann JG (Spectral changes in cortical surface potentials during motor movement. Journal of Neuroscience 27:2424-2432.2007b).
Miller KJ, Schalk G, Fetz EE, Den Nijs M, Ojemann JG, Rao RPN (Cortical activity during motor execution, motor imagery, and imagery-based online feedback. Proceedings of the National Academy of Sciences 108:4430-4435.2010b).
Miller KJ, Shenoy P, den Nijs M, Sorensen LB, Rao RN, Ojemann JG (Beyond the gamma band: the role of high-frequency features in movement classification. IEEE transactions on bio-medical engineering 55:1634.2008).
Miller KJ, Sorensen LB, Ojemann JG, den Nijs M (Power-law scaling in the brain surface electric potential. PLoS Comput Biol 5:e1000609.2009b).
Miller KJ, Weaver KE, Ojemann JG (Direct electrophysiological measurement of human default network areas. Proceedings of the National Academy of Sciences 106:12174.2009c).
Miller KJ, Zanos S, Fetz EE, den Nijs M, Ojemann JG (Decoupling the Cortical Power Spectrum Reveals Real-Time Representation of Individual Finger Movements in Humans. Journal of Neuroscience 29:3132.2009d).
Mitchell JF, Sundberg KA, Reynolds JH (Spatial attention decorrelates intrinsic activity fluctuations in macaque area V4. Neuron 63:879-888.2009).
Mitra P, Bokil H (2008) Observed brain dynamics. New York: Oxford University Press.

Mitzdorf U (Current Source-Density Method and Application in Cat Cerebral-Cortex - Investigation of Evoked-Potentials and Eeg Phenomena. Physiological Reviews 65:37-100.1985).
Mollazadeh M, Aggarwal V, Thakor NV, Law AJ, Davidson A, Schieber MH (Coherency between Spike and LFP Activity in M1 during Hand Movements. Neural Engineering, 2009 NER '09 4th International IEEE/EMBS Conference on 506-509.2009).
Mormann F, Fell J, Axmacher N, Weber B, Lehnertz K, Elger CE, Fernández G (Phase/amplitude reset and theta-gamma interaction in the human medial temporal lobe during a continuous word recognition memory task. Hippocampus 15:890-900.2005).
Murthy VN, Fetz EE (Coherent 25- to 35-Hz oscillations in the sensorimotor cortex of awake behaving monkeys. Proc Natl Acad Sci U S A 89:5670-5674.1992).
Muthukumaraswamy SD, Edden RA, Jones DK, Swettenham JB, Singh KD (Resting GABA concentration predicts peak gamma frequency and fMRI amplitude in response to visual stimulation in humans. Proceedings of the National Academy of Sciences of the United States of America 106:8356-8361.2009).
Niessing J, Ebisch B, Schmidt KE, Niessing M, Singer W, Galuske RAW (2005) Hemodynamic Signals Correlate Tightly with Synchronized Gamma Oscillations. vol. 309, pp 948-951: American Association for the Advancement of Science.
Nunez PL, Cutillo BA (1995) Neocortical dynamics and human EEG rhythms. New York: Oxford University Press.
O'Keefe J, Recce ML (Phase relationship between hippocampal place units and the EEG theta rhythm. Hippocampus 3:317-330.1993).
Okeefe J, Nadel L (The Hippocampus as a Cognitive Map. Behavioral and Brain Sciences 2:520-528.1979).
Okun M, Naim A, Lampl I (2009) Intracellular recordings in awake rodent unveil the relation between local field potential and neuronal firing. In: Society for Neuroscience Chicago, IL, USA.
Okun M, Naim A, Lampl I (The subthreshold relation between cortical local field potential and neuronal firing unveiled by intracellular recordings in awake rats. Journal of Neuroscience 30:4440.2010).
Oram MW (Contrast induced changes in response latency depend on stimulus specificity. J Physiol Paris 104:167-175.2010).
Osipova D, Hermes D, Jensen O (Gamma power is phase-locked to posterior alpha activity. PLoS One 3:e3990.2008).
Parvizi J, Jacques C, Foster BL, Witthoft N, Rangarajan V, Weiner KS, Grill-Spector K (Electrical stimulation of human fusiform face-selective regions distorts face perception. Journal of Neuroscience 32:14915-14920.2012).
Pascalis O, Scott LS, Kelly DJ, Shannon RW, Nicholson E, Coleman M, Nelson CA (Plasticity of face processing in infancy. Proc Natl Acad Sci U S A 102:5297-5300.2005).
Peelen MV, Downing PE (Within-subject reproducibility of category-specific visual activation with functional MRI. Hum Brain Mapp 25:402-408.2005).
Pei X, Barbour DL, Leuthardt EC, Schalk G (Decoding vowels and consonants in spoken and imagined words using electrocorticographic signals in humans. J Neural Eng 8:046028.2011).
Penfield W (Mechanisms of voluntary movement. Brain 77:1.1954).
Penfield W, Perot P (The Brain's Record of Auditory and Visual Experience. A Final Summary and Discussion. Brain 86:595-696.1963).
Penny WD, Duzel E, Miller KJ, Ojemann JG (Testing for nested oscillation. Journal of neuroscience methods 174:50-61.2008).
Percival DB, Walden A (1993) Spectral analysis for physical applications, multitaper and conventional univariate techniques. Cambrigde, UK: Cambridge UP.

Pfurtscheller G (1999) Event-Related Desynchronization (ERD) and Event Related Synchronization (ERS). Baltimore: Williams and Wilkins.
Philiastides MG, Ratcliff R, Sajda P (Neural representation of task difficulty and decision making during perceptual categorization: a timing diagram. The Journal of neuroscience : the official journal of the Society for Neuroscience 26:8965-8975.2006).
Philiastides MG, Sajda P (Temporal characterization of the neural correlates of perceptual decision making in the human brain. Cereb Cortex 16:509-518.2006).
Porat B (1997) A course in digital signal processing: Wiley.
Puce A, Allison T, Gore JC, McCarthy G (Face-sensitive regions in human extrastriate cortex studied by functional MRI. Journal of neurophysiology 74:1192-1199.1995).
Puce A, Allison T, McCarthy G (Electrophysiological studies of human face perception. III: Effects of top-down processing on face-specific potentials. Cereb Cortex 9:445-458.1999).
Puce A, Allison T, Spencer SS, Spencer DD, McCarthy G (Comparison of Cortical Activation Evoked by Faces Measured by Intracranial Field Potentials and Functional MRI: Two Case Studies. Human brain mapping 5:298–305.1997).
Ray S, Maunsell JH (Differences in gamma frequencies across visual cortex restrict their possible use in computation. Neuron 67:885-896.2010).
Ray S, Maunsell JH (Different origins of gamma rhythm and high-gamma activity in macaque visual cortex. PLoS Biol 9:e1000610.2011).
Ritaccio A, Brunner P, Crone NE, Gunduz A, Hirsch LJ, Kanwisher N, Litt B, Miller K, Moran D, Parvizi J, Ramsey N, Richner TJ, Tandon N, Williams J, Schalk G (Proceedings of the Fourth International Workshop on Advances in Electrocorticography. Epilepsy Behav 29:259-268.2013).
Roberts MJ, Lowet E, Brunet NM, Ter Wal M, Tiesinga P, Fries P, De Weerd P (Robust gamma coherence between macaque V1 and V2 by dynamic frequency matching. Neuron 78:523-536.2013).
Roelfsema PR, Lamme VA, Spekreijse H (Synchrony and covariation of firing rates in the primary visual cortex during contour grouping. Nature neuroscience 7:982-991.2004).
Rotstein HG, Pervouchine DD, Acker CD, Gillies MJ, White JA, Buhl EH, Whittington MA, Kopell N (Slow and fast inhibition and an H-current interact to create a theta rhythm in a model of CA1 interneuron network. J Neurophysiol 94:1509-1518.2005).
Sabatini BL, Regehr WG (Timing of neurotransmission at fast synapses in the mammalian brain. Nature 384:170-172.1996).
Schacter DL, Dobbins IG, Schnyer DM (Specificity of priming: a cognitive neuroscience perspective. Nat Rev Neurosci 5:853-862.2004).
Schalk G, McFarland DJ, Hinterberger T, Birbaumer N, Wolpaw JR (BCI2000: a general-purpose brain-computer interface (BCI) system. IEEE Trans Biomed Eng 51:1034-1043.2004).
Scheeringa R, Fries P, Petersson KM, Oostenveld R, Grothe I, Norris DG, Hagoort P, Bastiaansen MC (Neuronal dynamics underlying high- and low-frequency EEG oscillations contribute independently to the human BOLD signal. Neuron 69:572-583.2011).
Scheffer-Teixeira R, Belchior H, Leao RN, Ribeiro S, Tort AB (On high-frequency field oscillations (>100 Hz) and the spectral leakage of spiking activity. J Neurosci 33:1535-1539.2013).
Sederberg PB, Kahana MJ, Howard MW, Donner EJ, Madsen JR (Theta and gamma oscillations during encoding predict subsequent recall. J Neurosci 23:10809-10814.2003).
Sergent J, Villemure JG (Prosopagnosia in a right hemispherectomized patient. Brain 112 ( Pt 4):975-995.1989).
Shadlen MN, Movshon JA (Synchrony unbound: a critical evaluation of the temporal binding hypothesis. Neuron 24:67-77, 111-125.1999).
Siegel M, Donner TH, Oostenveld R, Fries P, Engel AK (Neuronal synchronization along the dorsal visual pathway reflects the focus of spatial attention. Neuron 60:709-719.2008).

Siegel M, Engel AK, Donner TH (Cortical network dynamics of perceptual decision-making in the human brain. Front Hum Neurosci 5:21.2011).
Sigeti D, Horsthemke W (High-Frequency Power Spectra for Systems Subject to Noise. Physical Review A 35:2276-2282.1987).
Simanova I, van Gerven M, Oostenveld R, Hagoort P (Identifying object categories from event-related EEG: toward decoding of conceptual representations. PloS one 5:e14465.2010).
Singer W (Synchronization of cortical activity and its putative role in information processing and learning. Annual Review of Physiology 55:349-374.1993).
Sohal VS, Zhang F, Yizhar O, Deisseroth K (Parvalbumin neurons and gamma rhythms enhance cortical circuit performance. Nature 459:698-702.2009).
Spiridon M, Kanwisher N (How distributed is visual category information in human occipito-temporal cortex? An fMRI study. Neuron 35:1157-1165.2002).
Steriade M (Grouping of brain rhythms in corticothalamic systems. Neuroscience 137:1087-1106.2006).
Swann N, Tandon N, Canolty R, Ellmore TM, McEvoy LK, Dreyer S, DiSano M, Aron AR (Intracranial EEG reveals a time- and frequency-specific role for the right inferior frontal gyrus and primary motor cortex in stopping initiated responses. J Neurosci 29:12675-12685.2009).
Swettenham JB, Muthukumaraswamy SD, Singh KD (BOLD Responses in Human Primary Visual Cortex are Insensitive to Substantial Changes in Neural Activity. Front Hum Neurosci 7:76.2013).
Tallon-Baudry C, Bertrand O, Henaff MA, Isnard J, Fischer C (Attention modulates gamma-band oscillations differently in the human lateral occipital cortex and fusiform gyrus. Cereb Cortex 15:654-662.2005).
Tarr MJ, Gauthier I (FFA: a flexible fusiform area for subordinate-level visual processing automatized by expertise. Nat Neurosci 3:764-769.2000).
Thiele A, Stoner G (Neuronal synchrony does not correlate with motion coherence in cortical area MT. Nature 421:366-370.2003).
Thierry G, Martin CD, Downing P, Pegna AJ (Controlling for interstimulus perceptual variance abolishes N170 face selectivity. Nature neuroscience 10:505-511.2007).
Tiesinga P, Fellous JM, Sejnowski TJ (Regulation of spike timing in visual cortical circuits. Nat Rev Neurosci 9:97-107.2008).
Tort ABL, Komorowski RW, Manns JR, Kopell NJ, Eichenbaum H (Theta–gamma coupling increases during the learning of item–context associations. Proceedings of the National Academy of Sciences 106:20942.2009).
Traub RD, Kopell N, Bibbig A, Buhl EH, LeBeau FEN, Whittington MA (Gap junctions between interneuron dendrites can enhance synchrony of gamma oscillations in distributed networks. Journal of Neuroscience 21:9478-9486.2001).
van de Nieuwenhuijzen ME, Backus AR, Bahramisharif A, Doeller CF, Jensen O, van Gerven MA (MEG-based decoding of the spatiotemporal dynamics of visual category perception. NeuroImage 83:1063-1073.2013).
van Pelt S, Fries P (Visual stimulus eccentricity affects human gamma peak frequency. NeuroImage 78:439-447.2013).
Vidal JR, Chaumon M, O'Regan JK, Tallon-Baudry C (Visual grouping and the focusing of attention induce gamma-band oscillations at different frequencies in human magnetoencephalogram signals. Journal of cognitive neuroscience 18:1850-1862.2006).
Vidal JR, Ossandon T, Jerbi K, Dalal SS, Minotti L, Ryvlin P, Kahane P, Lachaux JP (Category-Specific Visual Responses: An Intracranial Study Comparing Gamma, Beta, Alpha, and ERP Response Selectivity. Front Hum Neurosci 4:195.2010).
Volgushev M, Chistiakova M, Singer W (Modification of discharge patterns of neocortical neurons by induced oscillations of the membrane potential. Neuroscience 83:15-25.1998).

Wandell BA (1995) Foundations of vision. Sunderland, Mass.: Sinauer Associates.
Wang XJ (Neurophysiological and computational principles of cortical rhythms in cognition. Physiological reviews 90:1195-1268.2010).
Weissman DH, Roberts KC, Visscher KM, Woldorff MG (The neural bases of momentary lapses in attention. Nature Neuroscience 9:971-978.2006).
Welch P (The use of fast Fourier transform for the estimation of power spectra: A method based on time averaging over short, modified periodograms. IEEE Trans Audio Electroacoustics 15:70-73.1967).
Wells WM, 3rd, Viola P, Atsumi H, Nakajima S, Kikinis R (Multi-modal volume registration by maximization of mutual information. Med Image Anal 1:35-51.1996).
Whittingstall K, Logothetis NK (Frequency-band coupling in surface EEG reflects spiking activity in monkey visual cortex. Neuron 64:281-289.2009).
Whittington MA, Traub RD, Jefferys JG (Synchronized oscillations in interneuron networks driven by metabotropic glutamate receptor activation. Nature 373:612-615.1995).
Winawer J, Kay KN, Foster BL, Rauschecker AM, Parvizi J, Wandell BA (Asynchronous broadband signals are the principal source of the BOLD response in human visual cortex. Current biology : CB 23:1145-1153.2013).
Wise RG, Ide K, Poulin MJ, Tracey I (Resting fluctuations in arterial carbon dioxide induce significant low frequency variations in BOLD signal. Neuroimage 21:1652-1664.2004).
Womelsdorf T, Fries P, Mitra PP, Desimone R (Gamma-band synchronization in visual cortex predicts speed of change detection. Nature 439:733-736.2005).
Womelsdorf T, Fries P, Mitra PP, Desimone R (Gamma-band synchronization in visual cortex predicts speed of change detection. Nature 439:733-736.2006).
Womelsdorf T, Schoffelen JM, Oostenveld R, Singer W, Desimone R, Engel AK, Fries P (Modulation of neuronal interactions through neuronal synchronization. Science 316:1609.2007).
Xu Y, Liu J, Kanwisher N (The M170 is selective for faces, not for expertise. Neuropsychologia 43:588-597.2005).
Yamamoto Y, Hughson RL (Extracting Fractal Components from Time-Series. Physica D 68:250-264.1993).
Yang Y, Engelien W, Pan H, Xu S, Silbersweig DA, Stern E (A CBF-based event-related brain activation paradigm: characterization of impulse-response function and comparison to BOLD. Neuroimage 12:287-297.2000).
Ylinen A, Bragin A, Nadasdy Z, Jando G, Szabo I, Sik A, Buzsaki G (Sharp wave-associated high-frequency oscillation (200 Hz) in the intact hippocampus: network and intracellular mechanisms. J Neurosci 15:30-46.1995).
Yoshiura T, Zhong J, Shibata DK, Kwok WE, Shrier DA, Numaguchi Y (Functional MRI study of auditory and visual oddball tasks. Neuroreport 10:1683-1688.1999).
Zhang D, Snyder AZ, Shimony JS, Fox MD, Raichle ME (Noninvasive functional and structural connectivity mapping of the human thalamocortical system. Cereb Cortex 20:1187-1194.2010).
Zhou Z, Bernard MR, Bonds AB (Deconstruction of spatial integrity in visual stimulus detected by modulation of synchronized activity in cat visual cortex. The Journal of neuroscience : the official journal of the Society for Neuroscience 28:3759-3768.2008).